THE UNIVERSITY OF QUEENSLAND

AUSTRALIA

The mechanisms of extracellular electron transfer

Christy Ann Grobbler

Bachelor of Science (Hon I)

The University of Queensland, Brisbane, Australia

A thesis submitted for the degree of Doctor of Philosophy at

The University of Queensland in 2015

School of Chemical Engineering

Advanced Water Management Centre

Abstract

In bioelectrochemical systems (BESs) microbial activity facilitates electricity generation and product synthesis. Using the microbial process of extracellular electron transfer (EET) *Shewanella* and *Geobacter* species can respire using a solid terminal electron acceptor, such as an anode in BES. Study of these microorganisms and how they behave at the molecular level is important for shining light on geomicrobial processes and development of BES. Through the use of molecular and electrochemical techniques, this PhD thesis will focus on the molecular mechanisms employed by bacterial biofilms on the anode of a BES, specifically *Shewanella oneidensis* MR-1 and *Geobacter sulfurreducens* DL-1. The physiology of these microorganisms appears to be directly associated with the operational conditions of the BES. The application of electrochemical and molecular studies enables the comparison and understanding of the cellular response to the BES operation, in particular on how they respond to changes in the anode potential. Quantitative proteomics from low biomass, biofilm samples is not well documented. The first objective of this thesis was to show the successful use of SWATH-MS for quantitative proteomic analysis of a microbial electrochemically active biofilm of *Shewanella oneidensis* MR-1. After growth at different potentials (+0.5 V, 0.0 V & -0.4 V vs. Ag/AgCl), biofilm proteins were extracted from anodes for proteomic assessment. SWATH-MS analysis identified 704 proteins, and quantitative comparison was made of those associated with tricarboxcylic acid (TCA) cycle. Metabolic differences detected between the biofilms suggested a branching of the *S. oneidensis* TCA cycle when grown at the different electrode potentials. In addition, the higher abundance of enzymes involved in the TCA cycle at higher potential indicated an increase in metabolic activity. This objective demonstrated SWATH-MS as a suitable method for studying differences between biomass limited biofilm samples. Subsequently, SWATH-MS and electrochemical methods were used to characterize anodic biofilms of *S. oneidensis* MR-1 and *G. sulfurreducens* DL-1. Experiments were conducted at the different electrode potentials of +0.5 V, 0.0 V and -0.4 V or at +0.1 V and +0.6 V for *S. oneidensis* and *G. sulfurreducens* respectively. SWATH-MS analysis revealed different strategies of adaption to changes in potential for both microorganisms, with *S. oneidensis* showing an increase in the relative abundance of its EET cytochromes with increased potential. In addition, these findings support the model that *S. oneidensis* nanowires are extensions of the outer membrane. Conversely, the majority of EET cytochromes quantified for *G. sulfurreducens* showed little or no significant change in relative abundance in response to electrode

potential. These results suggest *S. oneidensis* has greater adaptability in its regulation of EET cytochromes compared to *G. sulfurreducens.* Proteomic, bioelectrochemical and UV-HPLC methods, confirm the involvement and dominance of mediated electron transfer in biofilms of *S. oneidensis* respiring with an electrode. Furthermore, the relative higher abundance of a riboflavin biosynthesis protein, suggested the involvement of flavins in the EET of biofilms of *G. sulfurreducens*. Biofilms of *G. sulfurreducens* grown at the highly oxidative potential of +0.6 V, showed indications of oxidative stress, with lower current production, lower bioelectrochemical signals, and the presence of certain cellular protection mechanisms. Furthermore, similarities between the species were detected, with an increase in the relative abundance of TCA cycle proteins observed with higher rates of EET. In summary, this PhD thesis provides evidence that SWATH-MS is a reliable method to observe changes in the relative abundance of proteins in anodic biofilms of *S. oneidensis* and *G. sulfurreducens.* Furthermore, it provides insight into regulation of EET proteins, the physiological response to electrode potential, and how these differ between species of dissimilatory metal respiring bacteria.

Declaration by author

This thesis is composed of my original work, and contains no material previously published or written by another person except where due reference has been made in the text. I have clearly stated the contribution by others to jointly-authored works that I have included in my thesis.

I have clearly stated the contribution of others to my thesis as a whole, including statistical assistance, survey design, data analysis, significant technical procedures, professional editorial advice, and any other original research work used or reported in my thesis. The content of my thesis is the result of work I have carried out since the commencement of my research higher degree candidature and does not include a substantial part of work that has been submitted to qualify for the award of any other degree or diploma in any university or other tertiary institution. I have clearly stated which parts of my thesis, if any, have been submitted to qualify for another award.

I acknowledge that an electronic copy of my thesis must be lodged with the University Library and, subject to the policy and procedures of The University of Queensland, the thesis be made available for research and study in accordance with the Copyright Act 1968 unless a period of embargo has been approved by the Dean of the Graduate School.

I acknowledge that copyright of all material contained in my thesis resides with the copyright holder(s) of that material. Where appropriate I have obtained copyright permission from the copyright holder to reproduce material in this thesis.

Publications during candidature

Peer-reviewed papers:

Grobbler, C.; Virdis, B.; Nouwens, A.; Harnisch, F.; Rabaey, K.; Bond, P.L. Use of SWATH mass spectrometry for quantitative proteomic investigation of *Shewanella oneidensis* MR-1 biofilms grown on graphite cloth electrodes. *SYST APPL MICROBIOL*. 2014, DOI: 10.1016/j.syapm.2014.11.007

Conference presentations:

Grobbler, C.; Virdis, B.; Nouwens, A.; Harnisch, F.; Rabaey, K.; Bond, P.L. Effect of the anodic potential in the extracellular electron transfer capability of *Shewanella oneidensis* MR-1. *Australian Society for Microbiology 2012 Annual Scientific Meeting*, 1 to 4 July 2012. Brisbane (Australia). (*Poster presentation*)

Grobbler, C.; Virdis, B.; Nouwens, A.; Harnisch, F.; Rabaey, K.; Bond, P.L. Molecular mechanisms of extracellular electron transfer. *The University of Queensland Postgraduate Engineering Conference*. 3rd of June 2013. Brisbane (Australia) (*Oral presentation*)

Grobbler, C.; Virdis, B.; Nouwens, A.; Harnisch, F.; Rabaey, K.; Bond, P.L. Effect of the anodic potential in the extracellular electron transfer capability of *Shewanella oneidensis* MR-1. *4th International Microbial Fuel Cell Conference.* 1 to 4 September 2013. Cairns (Australia). (*Oral presentation*)

Grobbler, C.; Virdis, B.; Nouwens, A.; Harnisch, F.; Rabaey, K.; Bond, P.L. Quantitative proteomic analysis from biomass limited electroactive biofilms of *Shewanella oneidensis* MR-1 through SWATH-MS. *15th ISME International Symposium on Microbial Ecology.* 24 to 29 August 2014. Seoul (South Korea). (*Oral presentation*)

Publications included in this thesis

Grobbler, C.; Virdis, B.; Nouwens, A.; Harnisch, F.; Rabaey, K.; Bond, P.L. Use of SWATH mass spectrometry for quantitative proteomic investigation of *Shewanella oneidensis* MR-1 biofilms grown on graphite cloth electrodes. *SYST APPL MICROBIOL*. 2014, DOI: 10.1016/j.syapm.2014.11.007

This paper has been modified and included as part of sections 4.1.1 and 5.1. The original paper is attached as Appendix A.

Contributor	Statement of contribution
Christy Grobbler (Candidate)	Designed experiments (60%) Conducted experiments (100%) Performed SWATH data analysis (95%) Wrote the paper (100%)
Bernardino Virdis	Designed experiments (20%) Edited paper (20%)
Amanda Nouwens	Operation of mass spectrometer (100%) Assisted with SWATH data analysis (5%) Edited the paper (5%)
Falk Harnisch	Designed experiments (5%) Edited the paper (10%)
Korneel Rabaey	Designed experiments (5%) Edited the paper (5%)
Philip L. Bond	Designed experiments (10%) Edited the paper (60%)

Contributions by others to the thesis

This thesis includes the reporting of some important contributions made by other researchers that I have collaborated with throughout the duration of my PhD. These contributions are acknowledged as follows:

- Prof. Korneel Rabaey (Ghent University) and Dr. Bernardino Virdis (AWMC, UQ), who assisted with the set up and design of the bioelectrochemical systems and experiments.
- Dr. Amanda Nouwens, from the School of Chemical and Molecular Biosciences (SCMB, UQ) for assistance with proteomic procedures and the operation of the mass spectrometer, as well as initial interpretation of proteomic spectra.

Statement of parts of the thesis submitted to qualify for the award of another degree

None.

Acknowledgements

My PhD has been a long and rewarding journey and one that could have never been completed on my own. First, I would like to thank my principle advisor Dr. Phil Bond who has guided me through both my honours and PhD research projects. No matter what the problem or question, I could always come knocking and be greeted with a smile. I thank you greatly for your time, your incredible patience and the continual support through both the ups and downs of my PhD.

I would like to express my sincere appreciation to my advisory team, Dr. Bernardino Virdis, Dr. Falk Harnisch, Dr. Amanda Nouwens and Prof. Korneel Rabaey for your valued advice, knowledge and insightful suggestions. Thank you to Dr. Damien Batstone, Dr. Stefano Freguia and Dr. Jens Kroemer for their constructive criticism and guidance as advisors for my milestone evaluations. Thank you to the ASL team, in particular Beatrice and Nathan for their analytical expertise.

Thank you to my office neighbours, Katrin S, Katrin D, Libertus, Frauke and Ludovic. Each of you made my PhD experience that much brighter, I have thoroughly enjoyed working next to you. Also, I would like to thank the lovely Vivenne and Susan, for their friendship and all their administrative help throughout my PhD. Thank you to my ladies Inka & Elena (Team ICE), words cannot express how much you have supported me over the past four years. Your friendship, encouragement and our weekly get-togethers helped me hang in there during the toughest of times. I would like to thank all members of the AWMC both past and present, many of whom I have shared the PhD path. I thoroughly enjoyed working with such an amazing team that was always accepting, friendly, professional and fun.

I would like to thank my family who have followed me throughout every part of my PhD journey, I could never have made it this far without them. The biggest heartfelt thanks goes to my Mum and Dad who have always encouraged my pursuit of further education. Thank you for believing in me, for your never ending encouragement and support, and for instilling in me the belief that I ought to finish everything that I start. Thank you to my grandparents Minnie, Gaga and Gran for inspiring me, encouraging me and believing in me. Finally, I would like to thank my partner Justin Todhunter for his encouragement, his strength and for sticking by me.

Keywords

bioelectrochemical system, biofilm, proteomics, shewanella oneidensis mr1, swath-ms, geobacter sulfurreducens dl1, bioelectrochemsitry

Australian and New Zealand Standard Research Classifications (ANZSRC)

ANZSRC code: 060501 Bacteriology, 40%
ANZSRC code: 060109 Proteomics and Intermolecular Interactions 40%
ANZSRC code: 090703 Environmental Technologies, 20%

Fields of Research (FoR) Classification

FoR code: 0605, Microbiology, 70%
FoR code: 0907, Environmental Engineering, 30%

Table of Contents

List of Figures

List of Tables

Abbreviations

DMRB	Dissimilatory metal respiring bacteria
EET	Extracellular electron transfer
DET	Direct electron transfer
MET	Mediated electron transfer
CV	Cyclic voltammetry
CA	Chronoamperometry
Ag/AgCl	Silver/ silver chloride reference electrode
BES	Bioelectrochemical system
MFC	Microbial fuel cell
TCA	Tricarboxylic acid cycle
ETC	Electron transport chain
NADH	Nicotinamide adenine dinucleotide
NADP	Nicotinamide adenine dinucleotide phosphate
NAD	Nicotinamide adenine dinucleotide
OMC	Outer membrane cytochrome
SHE	Standard hydrogen electrode
SCE	Saturated calomel electrode
FADH	Flavin adenine dinucleotide
ATP	Adenosine triphosphate
IDA	Information dependant acquisition
ºC	Degrees Celsius
µl	Microliters
ml	Millilitres
V	Volt
mV	Millivolt
Fe	Iron
Mn	Manganese
J_{max}	Maximum current density
HPLC	High performance Liquid Chromatography
UV-HPLC	High performance liquid chromatography-UV
RT-qPCR	Reverse transcription quantitative polymerase chain reaction

1. Introduction

Bioelectrochemical systems (BESs) can facilitate multiple functions, from electricity generation, to product production [1]. Microbial activity is used to drive these systems; hence, the study of the microorganisms involved is imperative to the development and enhancement of BES. Using microorganisms to drive processes has several advantages over the use of purified enzymes, as micrograms are able to self-regenerate, adapt their abundance to the environment, are flexible in substrate use and have greater adaptability [1]. However, one limitation is that microorganisms can only transfer a fraction of the total electrons available from the electron donor, as a portion of electrons needs to be retained for growth and maintenance. Hence, they cannot be considered as 'true' catalysts [1]. However, they do improve the overall performance of a bioelectrochemical system by decreasing the overpotential at both anode [2, 3] and cathode [4]. Dissimilatory metal reducing bacteria (DMRB) are typically studied in BES as they can use different solid metal oxides as a final electron acceptor during the metabolism of carbon or hydrogen [2, 3]. One type of BES called a microbial fuel cell (MFC) uses bacterial activities to generate electricity. It is the underlying principle of extracellular electron transfer (EET) that provides bacteria with the ability to drive a BES and generate a current, which can then be used as a potential source of power.

Improved methods for the production of renewable energy are required. This ability to generate electricity through MFC has attracted attention as a promising alternative to unsustainable energy sources. In recent years, the understanding of sustainable electricity generation and microbial electron transfer has improved. The integration of both would aid in the development this new exciting technology. Elucidating the electron transfer and associated metabolic pathways of model organisms, with the objective to improve the process performance by fine-tuning the molecular potential of the microorganisms is crucially important to achieve this. With current research exploring this area, BES power generation may be improved. This literature review will explore the current research within the field of BESs and the principle of EET.

2. Literature Review

2.2 Microbial Electron Transfer

Respiration is a mechanism used by microorganisms for energy transformation. It is where the synthesis of ATP takes place, known as oxidative phosphorylation, driven by a series of oxidation-reduction reactions. Heterotrophic respiration consists of three components; glycolysis, the tricarboxylic acid (TCA) cycle and the electron transport chain (ETC). Glycolysis is the process whereby glucose is broken down to form pyruvate, NADH and ATP through substrate-level phosphorylation. Pyruvate may be oxidized through the TCA cycle, to produce reducing equivalents such as $FADH_2$ and NADH, ATP, and the regeneration of oxaloacetate [4]. During respiration the NADH and $FADH_2$ can be oxidized and the electrons flow through ETC to an electron acceptor, whilst generating a proton gradient [4, 5]. The proton gradient then drives the enzyme ATP synthase to generate ATP, an important energy rich molecule and the primary currency of energy in cells [5].

The ETC typically includes a series of proteins or electron carriers that are often associated with the cell membrane and the periplasmic space [5]. During aerobic conditions, microorganisms may use oxygen as the terminal electron acceptor to provide a high level of energy gain. In the absence of oxygen or other soluble electron acceptors, microorganisms are forced to use alternative terminal electron acceptors in the process of anaerobic respiration. Soluble electron acceptors are those found in solution and include oxygen, nitrate, nitrite, sulfate, iron and fumarate[3]. Microorganisms can also use insoluble electron acceptors, which can be minerals in the environment (including iron oxides (Fe^{3+}), manganese oxides (Mn^{2+}) and polysulfides [3]) or an electrode (anode) in a BES [1].

2.2.1 Extracellular Electron Transfer

Microbial metal reduction is an important activity for carbon cycling [6-9] in many anaerobic environments. Bacteria active in EET include most notably the *Shewanella* species [10-12], *Geobacter* species [1, 13, 14], *Pseudomonas aeruginosa* [15-17] the oxygenic phototrophic cyanobacterium *Synechocystis PCC6803* and the thermophilic fermentative bacterium *Pelotomaculum thermopropionioum* [10]. There are two broadly described mechanisms these microorganisms use to carry out EET. These are most commonly referred to as direct electron transfer (DET) and mediated electron transfer (MET). MET is where a mobile molecule facilitates the EET and DET is where the organism makes direct contact with the electron acceptor for EET (Figure 2.1). These two pathways are not mutually exclusive as *Shewanella oneidensis* can use these simultaneously to facilitate EET [18-20].

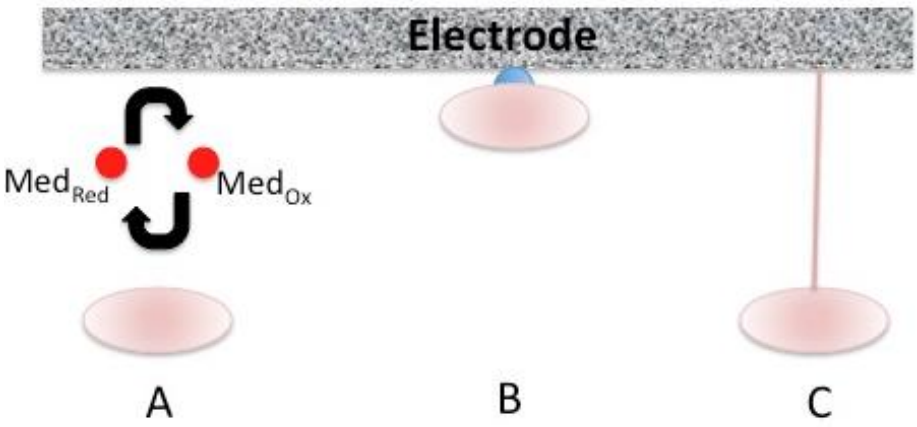

Figure 2.1: A simple representation of the different mechanisms of electron transfer between a microorganism and an insoluble electron acceptor. A) Mediated electron transfer via redox active mediators. B) Direct electron transfer via membrane bound protein. C) Long-range electron transfer.

2.2.1.1 Direct Electron Transfer

Here we define DET as ‘not requiring the diffusion of a mobile component to and from the cell for electron transport’ [1]. There are two major mechanisms for DET referred to in the literature. One is where the microorganism establishes physical contact with the electrode to transfer electrons through outer membrane cytochromes [21, 22], the second is through the use of appendages produced by the microorganism, often referred to as nanowires [1, 10, 14]. Both *Shewanella oneidensis* and *Geobacter sulfurreducens* are key microorganisms for the study of DET.

2.2.1.1.1 Outer Membrane Cytochromes

During *S. oneidensis* respiration, electrons are transferred from the reduced menaquinone pool in the inner membrane via CymA to a trans membrane protein complex consisting of cytochromes MtrA, MtrB, MtrC, and OmcA (Figure 2.2) [23]. MtrC and OmcA are assumed to be key proteins for DET found exposed on the outer membrane of the cell [24-26], that mediate electron transfer from the cell to the insoluble electron acceptor.

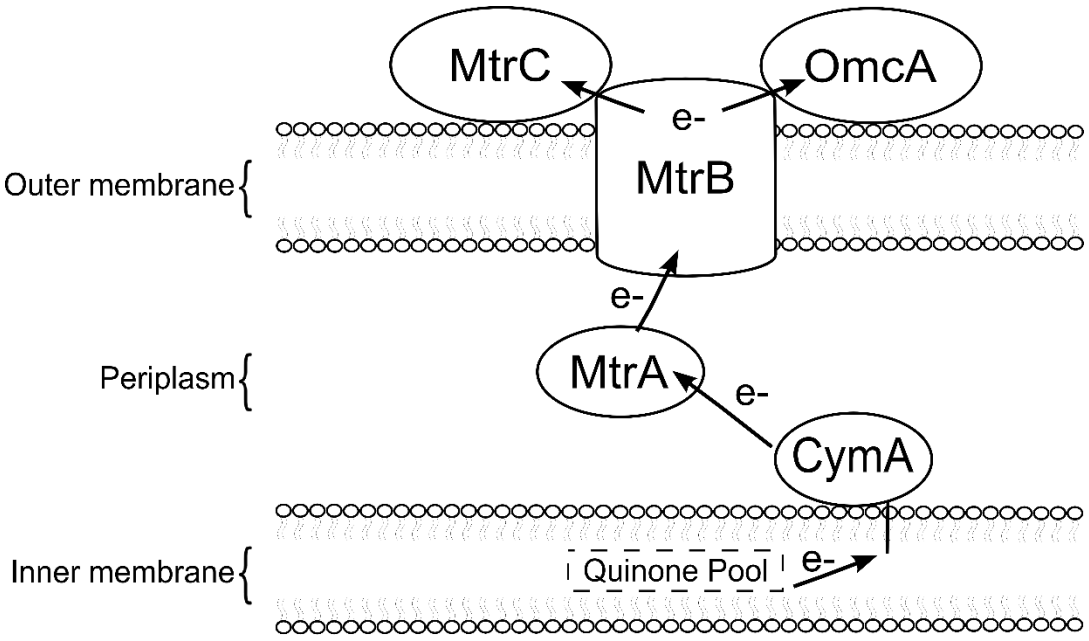

Figure 2.2: Cytochromes involved in the extracellular electron transfer process in *Shewanella* [27].

In comparison, *G. sulfurreducens* has been shown to have a dependency on membrane bound cytochromes similar to that of *S. oneidensis* [1, 28]. However, they differ in that they rely solely on DET for EET [29]. The important proteins involved in *G. sulfurreducens* EET to Fe(III) oxides and other electron acceptors are located on the outside of the cell [30, 31]. These include OmcS and OmcE that are loosely attached to the surface of the cell [32], and are believed to act as intermediates to direct electrons to type IV pili, which are postulated to be conductive and transfer electrons directly to metal oxides [31] (Figure 2.3). OmcS are also associated with *G. sulfurreducens* nanowires. In addition, the presence of a porin-cytochrome (Pcc) protein complex has recently been discovered. Composed of three proteins; a porin like outer membrane protein, a periplasmic cytochrome and an outer membrane cytochrome, the Pcc complex is thought to be responsible for facilitating electron transfer to the outside of the cell [33] . Furthermore, the outer membrane cytochrome OmcZ, has been found to be localised at the biofilm-electrode interface of current producing cells of *G. sulfurreducens* [34] and is proposed to act as an electrochemical gate, permitting the transfer of electrons from the electroactive biofilm to the electrode [34]. There is a large body of experimental evidence implicating these cell surface cytochromes as key components in mediating extracellular reduction of Fe(III) oxides. However, In Fe(III) oxide reduction OmcS is essential [28] where as OmcZ is not [35] and the opposite is reported on growth with an

electrode [35, 36]. These findings, along with the discovery that expression of the gene *omcZ* downregulates *omcS* expression [37], indicate that these two cytochromes play key roles in EET under different conditions.

It is suggested that the outer membrane cytochrome (OMC) model for Fe(III) reduction has limitations. *Geobacter* and *Desulfuromonas* species contain abundant *c*-type cytochromes, however phylogenetically related species *Pleobacter* has no *c*-type cytochromes and produce pili, yet maintains the capability to reduce insoluble Fe(III) oxide [38]. However, the intermediary electron transfer proteins may not be universal in all organisms, thereby explaining inconsistencies in cytochrome content detected in Fe(III) reducers [14]. It is suggested that the function of pili is to complete the circuit between the intermediate electron carriers and Fe(III) oxide [14].

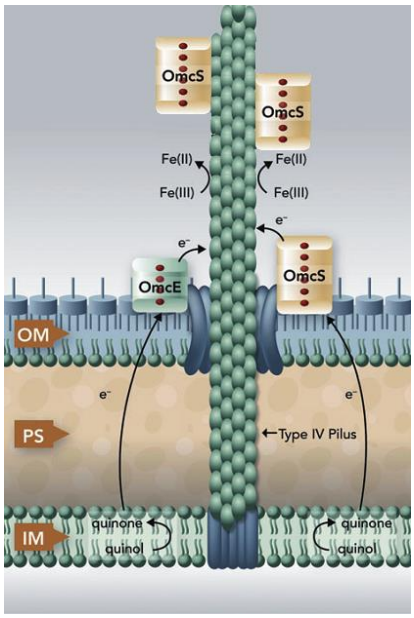

Figure 2.3: Schematic representation of the roles of OmcE and OmcS in *Geobacter sulfurreducens* in direct extracellular reduction of Fe(III) oxides, modified to show OmcS along the pilin length [31].

2.2.1.1.2 Nanowires

Pili are suggested to play a role in EET through contributing to microbial DET and MET (Figure 2.1C) as electrically conductive pili known as “nanowires” [14] and also play an important role in cell attachment and biofilm formation [24]. Both *S. oneidensis* and *G. sulfurreducens* have been studied extensively for their use of nanowires and it has been established that they are important to both in their ability to perform EET [10, 14]. Furthermore, nanowires are shown to facilitate EET between different microorganisms within a community [10, 39].

G. sulfurreducens are shown to produce pili during growth on the insoluble electron acceptor Fe(III) oxide but not on soluble Fe(III) [14]. Deletion of the *G. sulfurreducens pilA* gene which encodes for a pilin subunit, inhibited the microorganisms ability to produce pilin and to reduce the insoluble electron acceptor Fe(III) oxide [14]. Replacement with a functional *PilA* gene in *trans* restored pili assembly and Fe(III) oxide reduction, indicating the necessity of functional pili to reduce insoluble Fe(III) [14]. These results indicated a more direct role of pili in electron transfer to Fe(III) oxides. This was confirmed through measuring the electrical conductivity through the pili using atomic force microscopy, revealing that the pili of *G. sulfurreducens* are highly conductive. In addition, *Geobacter* pili are often intertwined, suggesting they are used for cell to cell electron transfer. Furthermore, these results indicate that the pili are the electrical connection between the cell surface and the Fe(III) oxides, contradicting the concept that OMCs are responsible for electron transfer to Fe(III) oxide. It is suggested that the function of pili is to complete the circuit between the intermediate electron carriers and the Fe(III) oxide [14].

The resistivity and the conductivity of *S. oneidensis* nanowires are found to be electrically conductive along micrometre length scales, with EET rates of up to 10^9 electrons/s at 100 mV of applied bias and a resistivity of 1 Ω.cm [40]. In addition, nanowires from mutants lacking the *c*-type cytochromes MtrC and OmcA (ΔMtrC/ΔOmcA) were nonconductive, indicating the requirement of cytochromes for conduction along *S. oneidensis* nanowires [40]. In contrast, *Geobacter* nanowires are presumed to be conductive not through OMCs, but through the amino acid sequence and the tertiary structure of the assembled pilus [14]. A strain of *G. sulfurreducens* that produced non-conductive pili (strain Aro-5) was constructed by modification of the amino acid sequence of the pilin protein PilA [41]. Each

of the five aromatic amino acids of PilA in strain Aro-5 were substituted with alanine which significantly decreased the pilin conductivity and diminished the ability of the strain to reduce Fe(III), thereby demonstrating the importance of pili conductivity for the capacity of *G. sulfurreducens* to perform long range EET [41].

Furthermore, another study revealed periodic 3.2-Å spacing in conductive wild type pilin of *G. sulfurreducens* which was associated with the spacing between aromatic amino acids [42]. This spacing was not detected in the nonconductive pilin of strain Aro-5, which does not contain the aromatic amino acids essential for conductivity [41]. The metal-like conductivity of wild type *G. sulfurreducens* pilin is said to be due to the overlapping of π-orbitals of aromatic amino acids [42]. To date, experimental results support the metal-like conductivity model of *G. sulfurreducens* pilin based nanowires in which the aromatic amino acids play a key role in electron transfer [41, 42].

It is now known that *S. oneidensis* nanowires can sustain current over distances of 0.5 microns [40]. However, the identity of the charge localisation sites and their organisation along the nanowire are unknown. To determine these details, one study used predicted redox cofactor separation distances [40] to explain the results from the previous study [43]. It was discovered that the currents require a multi-step hopping transport mechanism with charge localising sites separated by under 1 nm. This supports the understanding that charge localising sites need to be closely packed and reorganisation energy is to be kept small to permit charge transfer over long distances at rates described in the study by El-Naggar *et al*. [37]. In their study, the identity of the redox separation sites was not addressed, though it was previously proposed that the *c*-type cytochrome MtrC is accountable for the detected currents [40, 44]. Until recently, *S. oneidensis* nanowires were initially thought to be pilin based appendages that transfer electrons either by metallic-like conductivity [14, 44] or through electron tunnelling or hopping via closely linked cytochromes [43] . However, it has been discovered that *S. oneidensis* nanowires are extensions of the outer membrane and periplasm, containing the OMCs responsible for EET [45]. Through labelling *S. oneidensis* cells with a membrane selective stain, they were able to view in real-time the formation of these membrane extensions. This discovery provides reasoning to explain why *S. oneidensis* nanowires lacking the OMCs OmcA and MtrC were found to lose conductivity [40]. In addition, it supports the multi-step hopping transport mechanism and the proposition that the cytochrome MtrC is responsible for current production along the nanowire. However,

the details behind the conductivity of *Shewanella* nanowires is still unclear, and further study is needed to fully understand the mechanism.

2.2.1.2 Mediated Electron Transfer

The MET process employs soluble redox mediators or electron shuttles to reversibly transport electrons between cells and the electrode [1, 19]. This enables cells to transfer electrons without direct contact with the insoluble electron acceptor (Figure 2.1A). Two examples of mediators produced by microorganisms found in BESs include phenazines [17] and flavins [18, 19, 26]. When transferring electrons to the anode, mediators work by shuttling electrons while in their reduced state to the electrode where they are oxidized and then diffuse back to the inner or outer membrane of the cell where they take up electrons and are converted back to their reduced form [24]. In principle, mediators are not consumed, they catalyse the electron transfer within the system [46].

A key BES study on *Shewanella* strains MR-1 and MR-4 detected production of redox-active molecules riboflavin and riboflavin-5'-phosphate in the supernatants of biofilm bioreactors [18]. Riboflavin was found to be an important soluble redox electron shuttle, contributing to 70% of the external electron transfer activity. Additionally, a layer of flavins was found adsorbed to electrodes, even after the soluble components were removed [18]. This demonstrated that many environmentally relevant surfaces exposed to *Shewanella* may be coated by flavins which can affect interactions that occur with bacterial surface proteins. In environments with a high metal content, this means flavin electrode shuttling, metal chelation and surface binding could act together to promote respiration and metal oxide reduction phenotypes.

Pseudomonas aeruginosa is known to produce four electrochemically active compounds called phenazines [21]. These include pyocyanin [47], 1-hydroxyphenazine, phenazine-1-carboxylic acid and phenazine-1-carboxamide [47, 48]. Quorum sensing plays a regulatory role in current generation by *Pseudomonas aeruginosa* PA12 in BESs by regulating the production of phenazines, which are involved in MET [49]. The RetS protein negatively regulates the GacS/GacA system which controls quorum sensing in *P. aeruginosa* [50]**.** A

retS mutant was found to generate significantly higher current than wild type *P. aeruginosa* under anaerobic conditions due to the increase in phenazine production, thereby directly linking quorum sensing activity to current generation in BESs [49]. Furthermore, it has been shown that co-cultures of *Enterobacter aerogenes* and *Pseudomonas aeruginosa* PA14 in a BES had a 14 fold increased current density compared to each culture individually [21]. In co-culture *E. aerogenes* ferments glucose to 2,3-butanediol, which is consumed by *P. aeruginosa*. It is thought the utilisation of this intermediate, rather than consumption of glucose, led to an increase in pyocyanin production by *P. aeruginosa*. Furthermore, pure cultures of *E. aerogenes* have an increased current density when supplemented with pyocyanin as an electron mediator. Thus, a mutualistic relationship between the two organisms was occurring and resulted in increased respiratory activity. It was found that the concentration of phenazines produced by *P. aeruginosa* in co-culture with *E. aerogenes* was higher compared to a pure culture of *P. aeruginosa* grown with 2,3-butanediol [21]. Initially, it was suggested the reason behind, the higher concentration of phenazines in co-culture was the result of a higher cell density of *P. aeruginosa* due to the greater availability of multiple substrates. However, a recent study has shed greater light on the subject revealing an increase in phenazine pyocyanin when *P. aeruginosa* was grown with common fermentation products from co-habitant bacteria, in particular 2,3-butanediol compared to glucose [51]. Furthermore, it was discovered that the transcription regulator responsible for controlling quorum sensing (LasI LasR) was upregulated during growth on 2,3-butanediol, subsequently leading to higher phenazine concentration [51].

The highly efficient, current producing microorganism, *G. sulfurreducens* has previously been reported to perform EET without the use of mediators [52]. Replacement of the medium within BESs containing current producing *G. sulfurreducens* biofilm did not significantly affect the ability to produce current [52], suggesting the cells in contact with the electrode are responsible for current production without assistance from exogenous mediators. Based on the discovery that flavins have a high affinity for outer membrane c-type cytochromes of *S. oneidensis* [53], a study found that *G. sulfurreducens* has the ability to secrete flavins [54]. In addition, the mediators riboflavin and riboflavin-5'-phosphate were found to bind to the outer membrane cytochromes of *G. sulfurreducens* thereby functioning as redox cofactors [54]. This finding explains why replacement of medium surrounding a current producing biofilm of *G. sulfurreducens* did not affect its current production [52], as the flavins are largely not free within the media, but bound to the cytochromes of cells within the biofilm.

In contrast, an experiment performed on anodic *S. oneidensis* MR-1 biofilms demonstrated that replacement of medium containing mediators with fresh medium resulted in an 80% decrease in current production [18]. In summary, these results indicate the importance of the mediators riboflavin & riboflavin-5'-phosphate for both *G. sulfurreducens* and *S. oneidensis* EET.

2.3 Bioelectrochemical Systems

BESs can be used to produce valuable chemicals, desalinate water [55, 56], recover energy during wastewater treatment [57, 58], sequestrate or fix CO_2 [59, 60], for bioremediation [61-63], as biosensors [61, 64] and computing devises [65]. BESs use microorganisms to catalyse an oxidation reaction at the anode and/or a reduction reaction at the cathode to carry out these processes [46] (Figure 2.4). If electrical power is harvested from a BES, it is referred to as a microbial fuel cell (MFC). In these systems, electrons produced by bacteria from a carbon source (e.g. glucose or lactate) are transferred to the anode and flow to the cathode, which are separated by a membrane [1]. The two electrodes are linked by a conductive material including a resistor or are operated under a load (i.e. the lead to the formation of potential and a current flow) [66]. The protons and cations produced during electron flow migrate through the membrane into the cathode chamber where they can be used to accept electrons [66]. In BESs the anode can be used as the terminal electron accepter for microbial EET. For the electron transfer to be thermodynamically favourable, the anode must have a more positive potential than the microbial electron donor or the mediator that is used [67]. Theoretically, microorganisms must possess electron transfer molecules that can use the potential provided by an anode, and are thereby capable of donating the electrons [67]. If not, the microorganism will only be able to capture a fraction of the free energy provided and the remaining will be wasted [67].

The field of BESs encompasses multiple disciplines from microbiology to electrochemistry, material science and engineering. Research targeted at improving the performance of BESs requires the integration of these disciplines to improve both the performance and feasibility of these systems. Variations in reactor design such as electrode material, modification of electrode surfaces and operation can greatly impact BES performance. For example, many

types of materials have been used as electrodes in BESs including carbon paper [68], reticulated vitreous carbon [69] as well as graphite rods, felt and brushes [68-70]. To highlight the importance of electrode material, one study screened a range of anode materials (including graphite foil, carbon paper, graphite felt, carbon felt and carbon cloth) in a BES with *S. oneidensis* [71]. By monitoring current production, they discovered the best working electrode was activated carbon cloth and attributed good anode performance to the high surface area of the material available for MET. In addition, several electrode surface modification techniques have been shown to improve BES performance. This has been done, for example, by immobilising electron transfer mediators (such as neutral red and methylene blue) to the electrode [72-75], by physical modification of the electrodes with carbon nanotubes [76, 77] or through chemical treatment [78, 79].

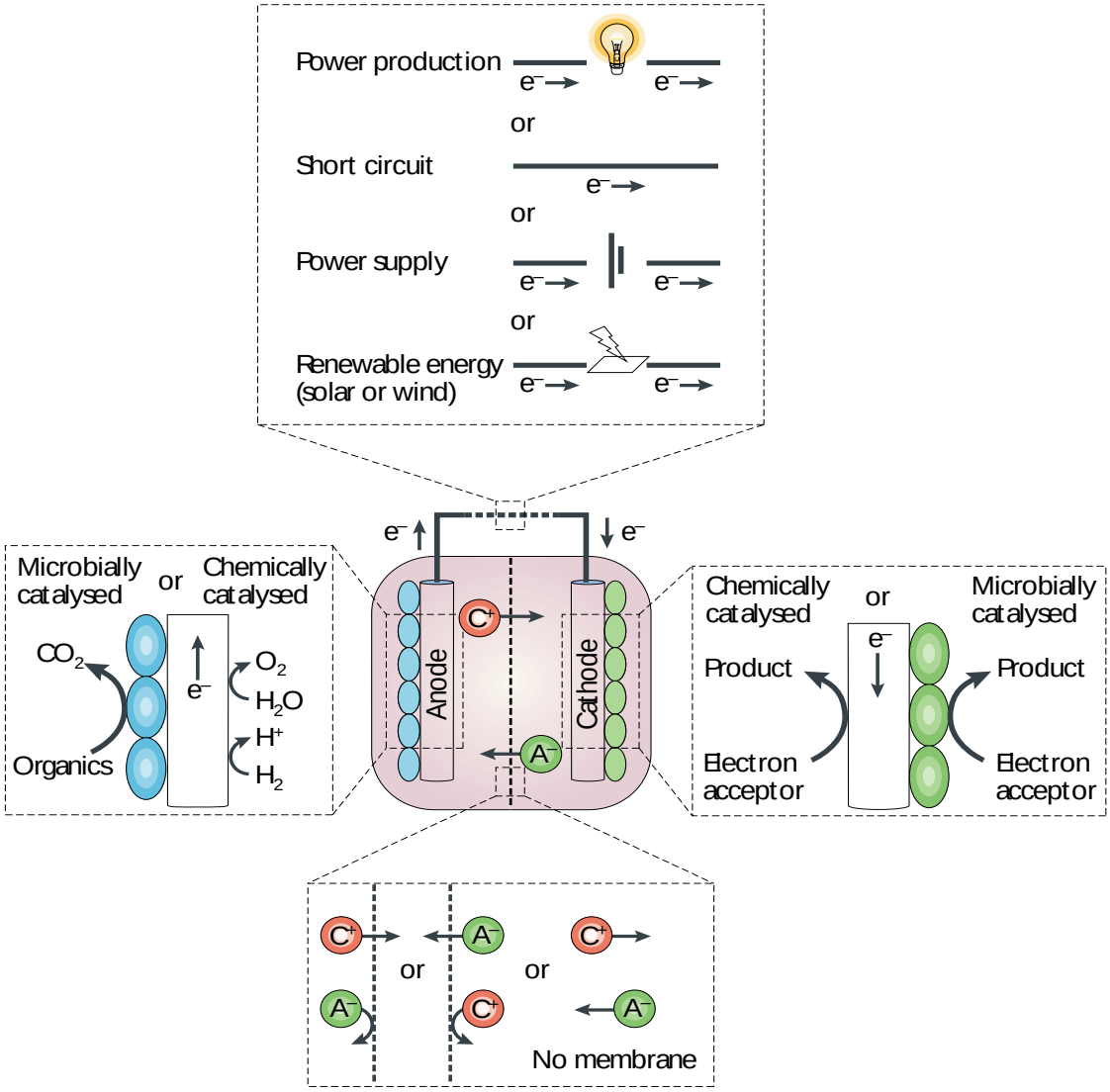

Figure 2.4: Demonstration of the many variations that make up bioelectrochemical systems [1] and how both anode and cathode reactions can be either chemically or microbially catalysed.

2.4 Biofilms

Biofilms are microbial colonies encased within extracellular polymeric substances (EPS) which act as an adhesive to attach to a surface [5, 80]. Bacteria form biofilms on electrodes of BESs, allowing significant exchange capabilities and opportunities for EET [81]. The environmental conditions and physiological responses of biofilms to their environment are not homogenous. The distribution of solutes such as electron acceptors, electron donors, cofactors and metabolic products is dependent on the result of its concurrent production,

consumption and diffusion [82]. The resulting chemical gradients that develop can overlap and intercept causing unique environmental niches.

The EPS surrounding a biofilm community can cause the diffusion coefficient into the biofilm to be lowered, consequently the substrate supply within a biofilm may become rate limiting [46]. Furthermore, the electron transfer rate from bacteria to the electrode may become limiting due to the transfer mechanism employed by the bacterial community under certain conditions, this effect is in addition to transport limitations expected in thicker biofilms [46]. Technological advances for identifying such physiological activities and limitations at the molecular level would be important for providing and increased understanding of the behaviour of bacteria within biofilms.

2.5 Microorganisms commonly associated with BESs

The microbes associated with anodes in BESs mostly consist of fermenters and dissimilatory metal reducing bacteria (DMRB). DMRB are able to survive through using different solid metal oxides [3] for the metabolism of carbohydrates, organic substances, or hydrogen [2, 3]. Fermenters include *Enterobacter aerogenes* [21, 83, 84] and *Brevibacillus* sp. [17]. DMRB include Pseudomonas *aeruginosa* [83, 84], *Geobacter sulfurreducens* [84, 85] and *Shewanella oneidensis* MR-1 [85, 86].

2.5.1 Shewanella

S. oneidensis MR-1 was isolated from anaerobic sediments in lake Oneida in New York, USA and has the ability to reduce iron and manganese as well as a wide array of other electron acceptors [87, 88]. *Shewanella* species has been found abundant in many environments where the reduction of Mn and/or Fe is high, however, they are insignificant or absent in environments where Mn and/or Fe are reduction is not so important [2]. It is suggested that this is due to the ecological competitiveness of the *Shewanellae*, as it has some advantage and out competes other species in the presence of Mn and/or Fe [2].

As mentioned previously, *S. oneidensis* MR-1 facilitates electron transfer across the cytoplasmic membrane to external electron acceptors through the use of its metal respiratory system (Mtr) [23, 89]. This system consists of MtrA; a decahaem *c*-type cytochrome periplasmic electron carrier (PEC) [90, 91], MtrC and OmcA; outer membrane decahaem *c*-type cytochromes [92], MtrB; a non-haem containing integral outer-membrane protein which functions to localise OmcA and MtrC [93], and finally CymA; a membrane anchored *c*-type cytochrome ([23, 94]). In addition, a small periplasmic *c*-type cytochrome (CctA) has been associated with Mtr reduction in both *Shewanella frigidmarina* and *S. oneidensis* MR-1, however specifics of its role are yet to be described [95, 96].

A great deal of research has been invested into the *Shewanella* species to discover the proteins involved in EET. One study defined the roles of MtrA, MtrC and their paralogues in respiration [26]. It was found that some periplasmic electron carrier components and terminal reductases can provide partial compensation of electron transfer in the absence of primary components, MtrA, MtrB, MtrC, CymA & OmcA (Figure 2.5).

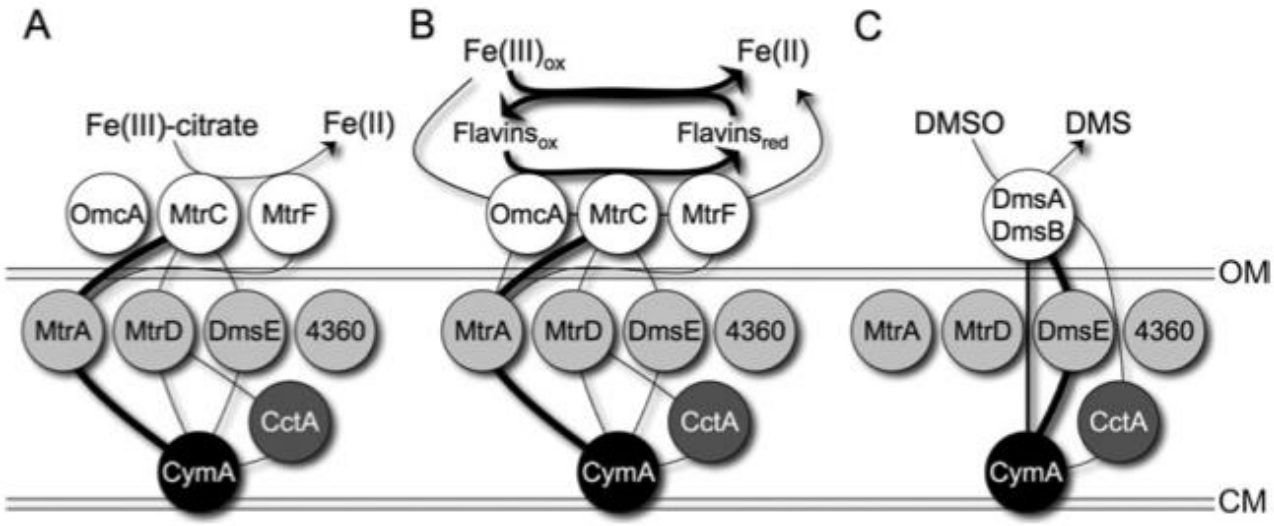

Figure 2.5: Electron transfer maps of *S. oneidensis* MR-1 depicting both primary pathways (thick lines) and pathways observed in the absence of primary proteins (thin lines) [26]. Shows electron flow from CymA to A) ferric citrate, B) flavins and iron oxide and C) DMSO.

Cyclic Voltammetry (CV) is an electrochemical technique whereby the potential of an electrode being studied is altered (relative to a fixed reference electrode) over time between two designated potentials at a set scan rate, and the resulting current is measured [97].

Using CV it was discovered that the OMCs of *S. oneidensis* are reversibly regulated by electrode potential [98]. A CV redox wave revealed a signature peak related to OmcA/MtrC when poised at 0 V (vs. SCE) but not at -0.24 V, indicating electrode-attached cells expressed cytochromes OmcA & MtrC at the cell cell-electrode interface at the high potential but not at the low potential. At -0.24V a CV analysis showed MET was present, and the presence of flavins was confirmed by HPLC, but was absent at the higher potential. A multi-step chronoamperometry (CA) experiment was performed (Figure 2.6) to investigate why no MET occurred at 0 V. After switching the electrode from -0.24V to 0 V, decreased flavin levels and increased OmcA and MtrC CV signals were recorded. It was suggested that the higher abundance of the OMC OmcA was possibly be impeding contact between flavins and the electrode by forming an insulating barrier. The study demonstrates unusual behaviour where a lower poised potential induced higher current production. A more recent study demonstrated similar behaviour, where current production was found to increase with potential to a certain limit, and was then found to decrease with further increases in potential [99]. This finding was attributed to the more oxidising potentials causing damage to the electroactive biofilm, there by affecting the EET mechanism and current production [99].

Another study also investigated the effect of electrode potential on the anodic current production using *Shewanella putrefaciens* NCTC [100]. They found that both current density and biomass on the electrode increased with electrode potential. Furthermore, cyclic voltammetry revealed DET to be the most dominant method of EET, with MET only playing a minor role across all potentials studied.

Electrochemical analysis has revealed that electroactive bacterial EET is directly associated with the operation of the BES [98, 100]. However, further study is needed to reveal the mechanism by which the conditions of the electrode regulate cytochrome expression. Furthermore, bioelectrochemical studies such as those described above give little insight into the other molecular changes that may occur at different electrode potentials. Further study using molecular techniques is required to understand what is causing these electrochemical variations at the molecular level. For example, protein expression changes through a range of applied potentials could be used to reveal changes in cell physiology and activities relevant to the organisms EET capabilities.

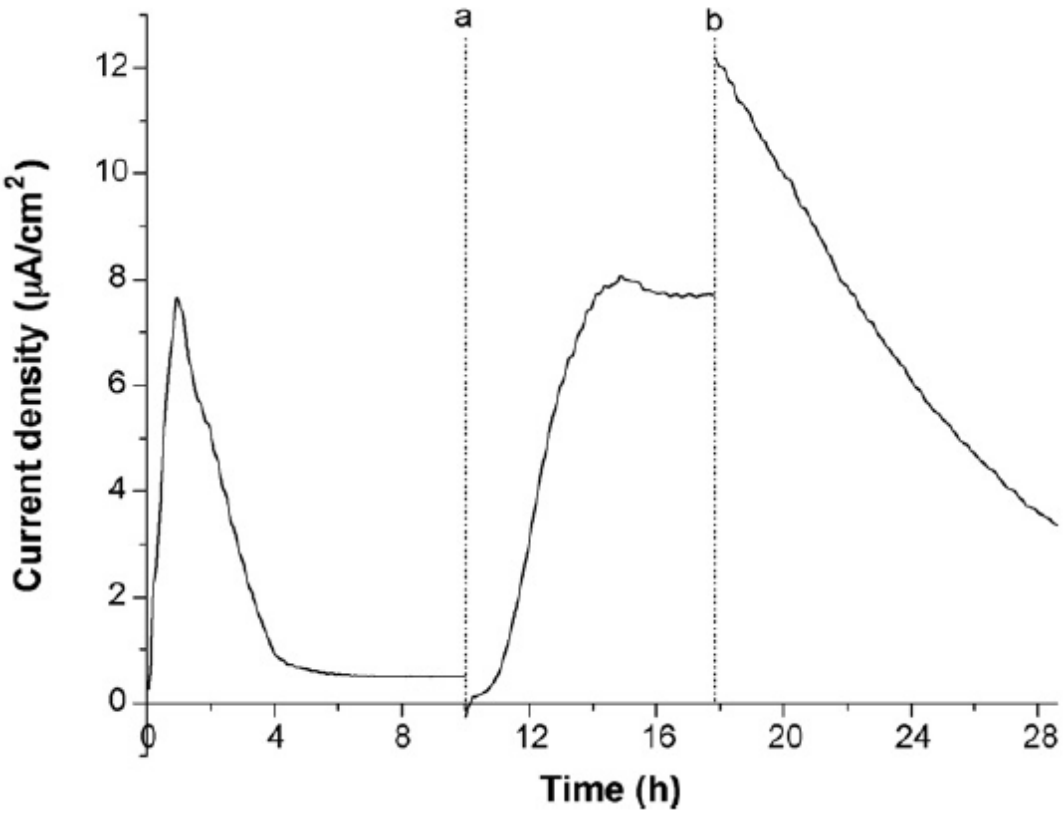

Figure 2.6: Chronoamperometric plot of multi-step chronoamperometry of *S. oneidensis* [98]. a) When the potential is switched from 0 V to -0.24 V, and b) when the potential is returned to 0 V.

The *Shewanella* metal reduction system (MtrABC, CymA & OmcA) plays an important role in EET and is the focus of many molecular studies. A genomic study discovered that genes encoding the proteins MtrA, MtrB, CymA and OmcA were up regulated when grown in conditions of anaerobic respiration compared to aerobic respiration [101]. Another genomic study compared gene expression of *S. oneidensis* grown using either an electrode as a solid terminal electron acceptor, or oxygen, or iron(III) citrate as a soluble terminal electron acceptor. The study revealed changes in the expression of many genes thought to be involved in respiration with an electrode [102]. The genes for proteins known to be participate in EET (*mtrA, mtrB, mtrC, omcA and cctA*) were up regulated in cultures using the anode compared to those using iron (III) citrate or oxygen. In another study, a proteomic investigation discovered the increased abundance of unique c-type cytochromes when cultures of *S. oneidensis* were grown using a soluble (iron (III) citrate) as opposed to growth when using an insoluble electron acceptor (Manganese (IV) oxide) [103].

Most previous studies that combine both molecular and electrochemical techniques to investigate the physiology and response to current production, have done this at a single potential [24, 26, 102, 104]. Consequently, there is a lack of detail of and understanding of how *S. oneidensis* physiology may change in relation to electron transfer in changed redox conditions. Recently a study used both quantitative reverse transcription polymerase chain reaction (RT-qPCR) and chronoamperometry combined with cyclic voltammetry to monitor both the protein turnover and stress response of *S. oneidensis* anodic biofilms at different applied electrode potentials [99]. The current production (rate of EET) was found to increase linearly between the applied potentials of 3 and +397 mV (SHE) as expected. However, the current production was then found to drop at the higher potentials +597 and +797 mV. They discovered that the stress response of *S. oneidensis* biofilms was not affected by the rate of EET and suggests a direct relationship between protein degradation and current production. This is the first study to observe how electrode potential affects the physiology of anodic biofilms of *S. oneidensis* at the molecular level.

2.5.2 Geobacter

Geobacteracea are often found to be the most dominant bacterial species in MFCs using a sediment mixed culture inoculum [105-107]. *Geobacter* is an important Fe^{3+} reducer, which can use H_2 or alternative organic electron donors, including toluene [5]. This holds great environmental significance as accidental spills or leakage of toluene from hydrocarbon storage tanks can often cause contamination of ferric-rich aquifers, making *Geobacter* a prospective natural agent for decontamination of such an environment [5]. *Geobacter sulfurreducens* is a commonly studied model organism for bioremediation purposes [5], and aspects of metal reduction and energy production have been investigated [108]. *Geobacter* spp. are frequently found as the most dominant microorganisms to colonize the anodes of BESs from an aquatic sediment inoculum [109-111] and frequently dominate microbial fuel cells set up for high current production under strictly anoxic conditions [112, 113].

DET occurs when the electrons are transferred from the respiratory chain in the cell to extracellular electron acceptor via several outer membrane cytochromes [23]. The in situ

technique of surface-enhanced resonance Raman (SERS) spectroscopy has been used in combination with cyclic-voltammetry (CV) to characterise OMCs within *G. sulfurreducens* biofilms. Using SERS, they were able to reveal the redox coordination and spin states of the heme iron within the OMC as well as the nature of its axial ligand, hence offering important structural information, which would potentially support information gathered from CV data [114]. They discovered that two bis (histadine) coordinated heme cytochrome redox couples are involved in the DET between bacteria and the electrode. In addition, they found that both cytochromes were equal distance to the electrode suggesting that both were either involved in two parallel electron transfer pathways or one electron relay with two parallel exit sites. This study provided important structural and functional information about the OMCs of *G. sulfurreducens* involved in DET.

It is demonstrated that *G. sulfurreducens* biofilms change the way they transfer electrons in response to changes in applied electrode potential [115]. Potentials of 0.1V, 0.4 V and 0.6 V (Ag/AgCl) were applied to a biofilm of *G. sulfurreducens* attached to an electrode and the differences were observed. Cyclic voltammograms comparing the applied potentials of 0.1V to 0.4V were very similar, however, two very different redox waves were seen between 0.1V and 0.6V (Figure 2.7). This suggests the existence of two potential EET domains responsible for electron transfer at different potentials. A reversible redox couple was evident at the lower potential (Figure 2.7a), while a more energetic signal transferring higher current was noticeable at the higher potential (Figure 2.7b). These findings suggest an increase in *G. sulfurreducens* ability to transfer electrons at higher potential. Furthermore, identification of these distinct redox domains dependent on the applied potential, not only shows that cells may have alternative pathways to exchange electrons, but also that cells may sense differences in potential at the cell-electrode interface. In addition, it was noted that the electrode cell density and current density was related to the applied potential, with the highest amount of cells found on the electrode set at 0.6V. This was suggested to be a result of the higher potential providing a more energetically productive environment leading to faster population growth. As a result, the biofilm produces higher current either due to the increased number of attached cell or an increased cell capacity for transferring electrodes. The results implicate that *G. sulfurreducens* can reversibly adapt to changes in electron potential by changing their electron transfer mechanism. The study also demonstrates that electrode potential is an important variable to optimize for energy generation from an electroactive biofilm. Only electrochemical methods were used to study these differences,

hence more specific molecular methods are needed to identify the cells physiological response to potential change. Furthermore, the biofilms studied were grown at a constant potential. A study that focuses on biofilms grown under different electrode potentials would provide insight into how potential affects the cells cytochromes and hence EET.

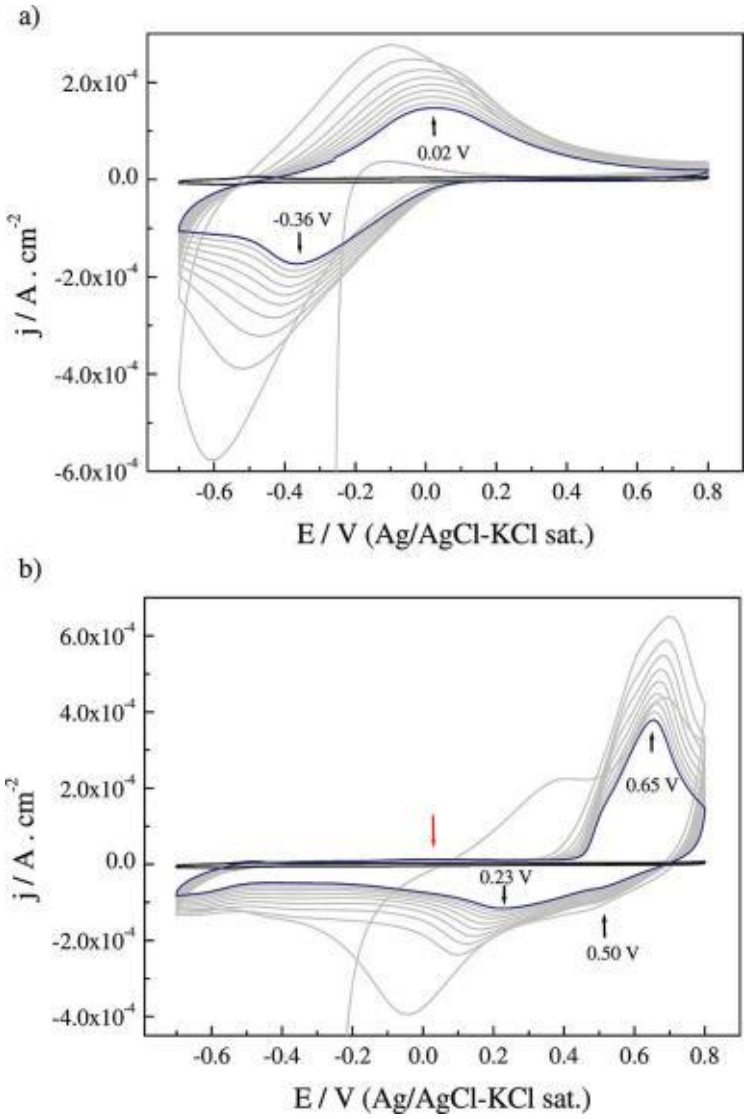

Figure 2.7: Cyclic voltammograms of graphite electrodes after 18hrs in fumarate limited conditions with polarization at a) 0.1 V and b) 0.6 V [115].

3. Research objectives

Shewanella and *Geobacter* species are intensively studied for extracellular respiration in BESs and there is much interest in the EET mechanisms of these organisms. There has been many bioelectrochemical and molecular research studies performed on these microorganisms with the aim to gain a deeper understanding of their EET mechanisms. However, to date no one has attempted to assess the EET ability of these electroactive biofilms at differing electrode potentials through the use of quantitative proteomics. This novel approach first requires proof that such a method can be performed on the biomass limited biofilm samples of *S. oneidensis* MR-1. Secondly, studies are required to determine how these microorganisms respond in terms of EET capability, as well as physiologically. The knowledge gaps mentioned above will be addressed by the following research questions of this PhD.

3.1. Research objective 1: To determine the suitability of SWATH mass spectrometry as a novel quantitative proteomic method on low biomass biofilm samples of Shewanella oneidensis MR-1

In order to determine the appropriate method for quantitative proteomic analysis of the biofilm samples it is important to address the common shortcomings of current experimental methods. The main pitfalls encountered when working with low biomass electrode samples are:

- BESs are often operated at a small scale for convenience and to simplify operation. This becomes problematic for proteomic studies that require adequate biomass for protein extraction and subsequent steps involved for MS and quantitative purposes.
- Quantitative proteomic labelling techniques such as tandem mass tags and isobaric tags for relative and absolute quantitation often require a minimum amount of protein sample for affective labelling to occur. In addition the extensive labelling procedure can often result in gradual loss of protein throughout each step of sample preparation.

- Fractionation of protein sample is often needed with standard LC-MS/MS techniques to gain a greater resolution of proteins identified within a sample. This is an extra preparation step that can contribute to additional protein losses.

Consequently, these shortfalls can limit the outcomes of proteomic investigations of electroactive biofilms in BESs. SWATH-MS is a recently developed approach that provides extensive label-free quantitation of the measurable peptide ions in a sample [116]. The approach rapidly acquires high resolution Q-TOF mass spectrometer data through repeated analysis of sequential isolation windows (swaths) throughout the chromatographic elution range [117]. Of the few reports on the use of SWATH-MS for bacterial proteomics, to our knowledge this is the first to use the method on low biomass electrode biofilms.

Here the proteome of *S. oneidensis* was compared to detect functional differences while growing on an anodic electrode at different potentials. As hypothesised, successful quantitative proteomic analysis of the anodic *Shewanella* biofilm samples using SWATH-MS without the need for fractionation, labelling or other procedures that can contribute to protein losses is shown. Furthermore, the high numbers of identifications and quantitative data obtained from this study suggest that this procedure is very well suited for proteomic studies of low biomass biofilms.

The experiments, results and discussion discussed in this research objective are described in the publication: Grobbler, C., Virdis, B., Nouwens, A., Harnisch, F., Rabaey, K., Bond, P. L., Use of SWATH mass spectrometry for quantitative proteomic investigation of *Shewanella oneidensis* MR-1 biofilms grown on graphite cloth electrodes. Systematic and Applied Microbiology 2014.

3.2 Research objective 2: To use of different electrode potentials to examine the extracellular electron capabilities of Shewanella oneidensis MR-1

It is unclear under which conditions certain EET mechanisms are exploited and whether multiple mechanisms are used simultaneously. As *Shewanella* has modularity in electron transfer proteins and the ability to utilise mediators and nanowires, there is the likelihood that electron transfer mechanisms could differ and be fine-tuned to different redox potentials. A change in anode potential will alter the energy conservation opportunity for organisms using it as an electron acceptor. Hence, we hypothesise that different anode potentials will select for particular proteins within the electron transport pathway of *S. oneidensis*.

Study of both electrochemical and molecular detail will examine how different applied electrical potentials affect the extracellular electron transfer mechanisms of the cell, and thus provide detailed knowledge of the cell components that are important for the various mechanisms. This approach was used in this study for understanding details of EET by identifying the molecular mechanisms employed by biofilms of *Shewanella oneidensis* MR-1 at different applied potentials, and by determining the physiological response. Additionally, the investigative approach here will utilise the proteomic method SWATH-MS developed in the previous study (section 5.1), which has been successfully used for quantitative proteomic analysis of anode grown S. *oneidensis* biofilm.

3.3 Research Objective 3: To study the effect of applied electrode potential on the extracellular electron transfer capability of Geobacter sulfurreducens DL-1

The objective of this research question is to study the effects that applied electrode potential has on protein abundances of cells of *G. sulfurreducens* DL-1 within a biofilm community attached to an anode of a BES. Furthermore, answering this question would allow the comparison of responses between different species of DMRB by comparing data obtained from research question 2 (section 3.2). This is accomplished by using the SWATH-MS method determined in research question 1 (section 3.1) and through using similar bioelectrochemical techniques established in both research questions 1 and 2 (section 3.1 and 3.2). We hypothesise that different anode potentials will select for particular proteins within the electron transport pathway of *G. sulfurreducens*. In addition, it would be expected to see differences in responses between the two microorganisms as they come from completely different evolutionary lineages with *Shewanella* belonging to the phylum γ-proteobacteria [3] and *Geobacter* belonging to δ-proteobacteria [118].

4. Research methods

4.1 Culturing and media

4.1.1 Culturing Shewanella oneidensis MR-1

Shewanella oneidensis MR-1 was first grown in 20 ml of LB overnight at 30 ˚C in a 50 ml falcon tube while shaking at 200 rpm. The LB culture (3 ml) was used as an inoculum for 300 ml of defined minimal medium [119] that included lactate as the electron donor, a vitamin solution and oxygen and the electron acceptor. The culture was grown at 30 ˚C shaking at 200 rpm for 24 hours and then the cell density was adjusted to an OD600 of 0.6-0.7 and 5 ml was used as inoculum for each of the BES experiments that followed.

4.1.2 Culturing Geobacter sulfurreducens DL-1

Active cultures *Geobacter sulfurreducens* DL-1 was maintained in 50 ml NBAF anaerobic medium with acetate (10 mM) as the electron donor and fumarate (40 mM) as the electron acceptor.

Using an active culture as an inoculum, *G. sulfurreducens* was grown anaerobically in 3 x 100 ml of NBAF medium described above. After 5 days of growth at 30 ºC the cultures were pelleted by centrifuging for 10 minutes at 5000 rpm. Spent medium was removed and pellets were combined and suspended in 40 ml of fresh medium without fumarate. The OD600 was noted to ensure a consistent inoculum and 10 ml of the culture suspension was used as the inoculum for each BES replicate.

4.2 Reactor design and operation

4.2.1 Single working electrode reactor

4.2.1.1 Setup and operation

Single cell BESs (250 ml volume) were prepared using a three-electrode configuration (Figure 4.1). Plain carbon cloth (Fuel Cell Store, USA) was used as the working electrode (2.0cm x 6.0cm), titanium wire was used as the counter electrode and Ag/AgCl reference electrode in 3M KCl, +210 mV vs SHE (BASi, USA) was used in all BES experiments. The electrodes were treated with 5% isopropanol for 30 minutes, rinsed thoroughly with Milli Q and autoclaved separately. The triplicate BESs were rinsed with Milli Q and assembled under anaerobic conditions. Modified minimal medium [119] was used for all BES experiments with 18 mM lactate as the carbon and electron source. In all BES experiments the electrode was used as the electron accepter, therefore fumarate was omitted from the medium. After autoclaving, medium was placed in an anaerobic chamber to cool before adding vitamins. The medium (250 ml) was added anaerobically to sterile reactors.

An inoculum of *S. oneidensis* (prepared as per section 4.1.1) was added to BESs that were connected to a potentiostat. The potentials +0.5 V, 0.0 V and -0.4 V vs. Ag/AgCl, were applied to the anode electrodes. Immediately after inoculation, the potential was set and the catalytic current production was monitored over time. Near maximum currents were produced after 21 hours (+0.5 and 0.0 V) or 29 hours (-0.4 V). Once the current for each potential approached maximum, the experiment was stopped. For the proteomic replicates, electrodes were removed from each BES, rinsed with fresh medium and stored at -80˚C. For the electrochemical replicates, turnover cyclic voltametric analysis was performed (see section 4.3.1).

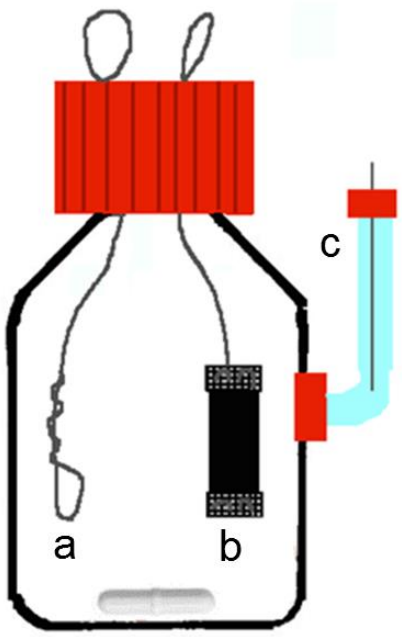

Figure 4.1: Representation of the single chambered BES used for both research question 1 and research question 2 showing the placement of the a) titanium wire used as counter electrode b) carbon cloth used as anode electrode c) Ag/AgCl reference electrode.

4.2.2 Multiple working electrodes BES reactor

4.2.2.1 Setup and operation

The experiments were performed in a BES with two working electrodes, a counter electrode and a reference electrode in the configuration shown in Figure 4.2. Graphite rods were used as the working electrodes, titanium wire was used for the counter electrode and a Ag/AgCl reference electrode (BASi, USA) was used in all BES experiments. The BESs (300 ml volume) and electrodes were rinsed thoroughly with Milli Q, autoclaved then placed in the anaerobic chamber overnight. Resazurin and cysteine were omitted from the medium for all BES experiments as they can act as electron shuttles and electron donors respectively [120]. In addition, fumarate was omitted from the medium to promote use of the anode as the electron acceptor. After autoclaving, medium was placed in an anaerobic chamber to cool before being added anaerobically to the sterile reactors. Once assembled, the reactors were removed from the anaerobic chamber and placed in an incubator (at 30 ºC) and connected to a potentiostat.

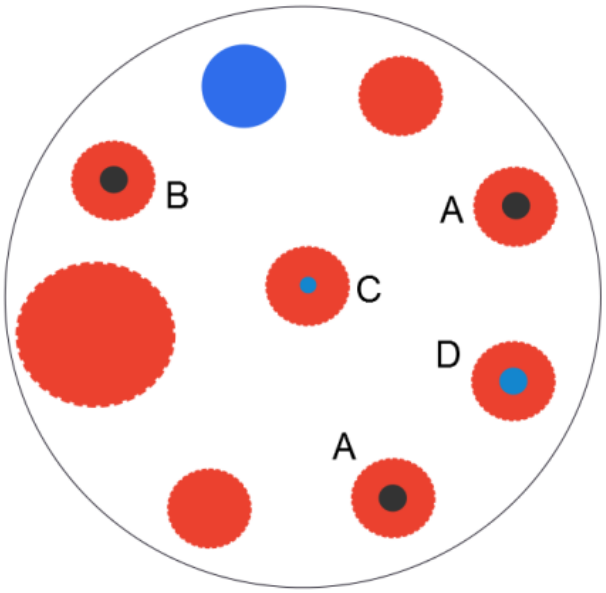

Figure 4.2: Top view diagram of electrode configuration of the BES. A, working electrodes; B, blank electrode; C, counter electrode; D, reference electrode.

All experiments were conducted under strictly sterile and anaerobic conditions under potentiostatic control. Following inoculation of replicate BES, *G. sulfurreducens* biofilms were grown at anode potentials of +0.1 V and +0.6 V at 30°C. Separate triplicate BES experiments were prepared for electrochemical measurements and to obtain biomass for protein extraction. The batch chronoamperometric experiments were monitored until near maximum current was reached (usually 6 days). Electrodes from one set of replicates were used for proteomic analysis, and electrodes from a second set of replicates was used for electrochemical analysis. When biofilm replicates were used for proteomic analysis, the experiments were stopped, reactors were placed into an anaerobic chamber and the working electrodes were removed and stored at -80°C. For replicates used for electrochemical analysis, both turnover and non-turnover cyclic voltametric analysis was performed (see section 4.3.2).

4.3 Cyclic voltammetry analysis

Cyclic Voltammetry (CV) is an electrochemical technique whereby the potential of an electrode of interest is varied (relative to a fixed reference electrode) over time between two potentials (*Ei* and *Ef*) at a fixed scan rate, and the corresponding current is measured. When plotting the current as function of potential a cyclic voltammogram is obtained. For more details on experimental variables see the article by Harnisch & Freguia [97]. Here CV was used to identify the electrochemical response as well as the potential of the redox active couple exchanging electrons with the electrode in electroactive microorganisms *S. oneidensis* and *G. sulfurreducens*. Under turnover conditions (i.e., in the presence of metabolic electron donors), the microorganisms are able to continuously supply electrons to the electrode when the potential of the electrode is sufficiently positive. Under these conditions, the voltammogram assumes the sigmoidal shape characteristic of a catalytic process. Analysis of the inflection point of the i-E curve by first derivative analysis allows the identification of the formal potential of the catalytic electron transfer site [97]. Conversely, voltammograms recorded under non-turnover conditions (*i.e.*, in the absence of metabolic electron donors), allow the identification of all possible electron transfer sites, including those that are not involved in the catalytic electron transfer. Here, substrate limited conditions allow no microbial re-oxidation and thus electrons are only passed between the microbes and the electrode. This enables the formation of a characteristic redox ‘peak’ that can be further analysed.

4.3.1 Turnover cyclic voltametric analysis of S. oneidensis anodic biofilms

Cyclic voltammograms were recorded under turnover conditions (in the presence of lactate as the electron donor lactate) with a scan rate of 2 mVs^{-1} between the potentials of -0.7 V and +0.5 V (Ag/AgCl). Current densities (j_{max}) were calculated by dividing the maximum current by the projected surface area of the anode electrode.

4.3.2 Turnover and non-turnover cyclic voltammetry analysis of G. sulfurreducens anodic biofilms

Once each of the BES replicates reached maximum current production, turnover CVs were recorded for *G. sulfurreducens* electrode biofilms in reactors containing NBAF anaerobic medium with acetate. A scan rate of 1 mVs^{-1} and a potential range of -0.7 V to +0.8 V (Ag/AgCl) was used.

To perform the non-turnover CVs, the medium was replaced anaerobically with fresh medium not containing electron donor (lactate). In order to deplete any residual electron donor remaining in the reactor or biofilm, the systems were operated for 24 hours with the working electrodes poised at the potentials of either 0.1 and 0.6 V. Nonturnover cyclic voltammetry was then performed under substrate limiting conditions with a scan rate of 1 mVs^{-1} and a potential range of -0.7 to +0.8 V (Ag/AgCl).

4.4 Proteomic analysis

4.4.1 Protein extraction and digestion

Protein extractions were performed on the whole electrodes containing biofilms. These were removed from -80 ˚C and submerged in 5 ml of extraction buffer (77 mg dithiothreitol & 1 tablet of complete Protease Inhibitor Cocktail (Roche) into 10 ml B-PER Bacterial Protein Extraction Reagent (Thermo Scientific)) and subjected to three freeze/thaw cycles by placing into -80 ˚C freezer and thawing at 4 ˚C. The buffer solution was sonicated to further lyse and remove attached cells from the electrode. The electrode was rinsed with an additional 5 ml of B-PER extraction buffer and then discarded. The B-PER solutions were combined and cell debris was removed by centrifugation at 15,000 g for 15 min. Proteins were precipitated by adding 10% total volume of 4 mg/ml sodium deoxycholate in 100% trichloroacetic acid and incubated overnight at 4 ˚C. Protein was recovered through centrifugation at 15,000 g for 10 min before washing in cold acetone, dried for 5 minutes and resuspended in buffer (2M thiourea, 7M Urea, 100mM ammonium bicarbonate). Total resuspended protein was quantified by 2D Quant (GE Healthcare).

The protein sample was then reduced and alkylate by treating with 5 mM dithiothreitol for 30 min at 56 ˚C, cooled to room temperature, treatment with iodoacetamide (25 mM final conc.) and incubated at room temperate in the dark (30 min). Protein samples were diluted with 50 mM ammonium bicarbonate buffer to reduce urea concentration to <2 M, and digested overnight with trypsin (Promega) at an enzyme to protein ratio of 1:25 at 37 ˚C. C18 Zip-tip (Millipore) clean-up was performed on the digested proteins [121]. Amount of sample was normalised to 1 µg for each and used for SWATH-MS. In addition, 2 µg aliquots of each sample were taken and pooled (18 µg total) for mass spectrometry analysis, which was performed in duplicate.

4.4.2 Mass spectrometry analysis

Peptides were directly analysed on a Triple-Tof 5600 instrument (ABSciex) equipped with a Nanospray III interface. Gas 1 was set to 10 psi, curtain gas to 30 psi, ion spray floating voltage 2700 V. Samples were scanned across m/z 350-1800 for 0.5 sec followed by the information dependant acquisition (IDA) on high sensitivity mode of 20 peptides with intensity greater than 100 counts across m/z 40-1800 for 0.05 sec. Collision energy was set to 40 +/- 15 V. SWATH analyses were scanned across m/z 350-1800 for 0.5 sec followed by high sensitivity DIA mode, using 26 Da (1 Da for window overlap) isolation windows for 0.1 sec, across m/z 400-1250. Collision energy for SWATH samples was automatically assigned based on m/z mass windows by Analyst software. Mass spectrometry (MS) data from information dependant acquisition were combined and searched using ProteinPilot software (ABSciex, Forster City CA). The search setting for enzyme digestion was set to Trypsin and cysteine alkylation was set to iodoacetamide. The searched databases were *S. oneidensis* MR1 (received from NCBI on the 28th of May 2012) or *G. sulfurreducens* DL-1 (received from Uniprot/Trembl on the 14th of October 2014) with the search effort set to thorough and cut off applied > 0.05 (10%). The false detection rate was determined using proteomics system performance evaluation pipeline software (PSPEP), an add-on to ProteinPilot, which uses a decoy database constructed by reversing all the protein sequences in the searched database.

4.4.3 SWATH-MS data analysis

The library acquired by information dependant acquisition (IDA library) and SWATH MS data were loaded into PeakView v 1.1 (for research outcomes described in section 5.1 and 5.2) or v1.2 (for the research outcome described in section 5.3) software for processing using the SWATH micro processing script (v1.1 or 1.2 respectively) using a confidence level of 99, the number of peptides set at 5 and the number of transitions used set at 3. A minimum of 2 peptide and 3 transitions was used for quantitative analysis. The R- based program MSstats [122] was used for statistical analysis of the spectral data. The “ion” data file exported from the Peakview software was loaded into MSstats as a .csv file using the following command:

Irene <- read.csv(" file pathway/ datafile.csv", sep=",")

The data file was then “pre-processed” were $\log_2$ transformation and normalisation are applied using the command:

QuantData <- dataProcess(Irene)

A comparison matrix was then created using the command:

(For *S. oneidensis* three potential comparison)
comparison1<-matrix(c(-1,1,0),nrow=1)
comparison2<-matrix(c(-1,0,1),nrow=1)
comparison3<-matrix(c(0,-1,1),nrow=1)
comparison<-rbind(comparison1,comparison2, comparison3)
row.names(comparison)<-c("0.0V--0.4V","+0.5V--0.4V","+0.5V-0.0V")
comparison

(For *G. sulfurreducens* two potential comparison)
comparison <- matrix(c(1,-1), nrow=1)
row.names(comparison) <- c("+0.1V-0.6V")

comparison

The comparison was then performed using the command:

potentialComparison <- groupComparison(contrast.matrix=comparison, data=QuantData, labeled=FALSE, interference=FALSE, featureVar=TRUE)

Where “data” is the name of the data set, “labelled=FALSE” represents a label free based study, “interference=FALSE” represents no additional model interaction was applied for interference transitions and “FetureVar=TRUE” indicating that the model should account for heterogeneous variation among intensities.

The final result was displayed using the command:

potentialComparison$ComparisonResult

Pathway Tools [123] was used for metabolic pathway reconstruction of the identified proteins. Text files of the log_2 fold change (log_2FC) data obtained from MSstats analysis was imported into the Pathway Tools software. Using the “Cellular Overview” tool the log_2FC information is directly displayed on a cellular metabolic pathway map of *S. oneidensis* MR-1 using a colour legend to represent the level of the log_2FC of each identified protein/enzyme on the map.

The mass spectrometry proteomics data have been deposited to the ProteomeXchange Consortium (http://proteomecentral.proteomexchange.org) via the PRIDE partner repository [124] with the dataset identifier PXD001472.

4.5 HPLC analysis

Organic acids were measured by HPLC with a Shimadzu system with an LC pump (LC-10ADVP) and an autoinjector (SIL-10ADVP). A HPX-87H 300 x 7.8 mm Bio-Rad Aminex ion exclusion HPLC column and/or a Phenomenex Rezex ROA –Organic Acid H+ 300mm x 7.8mm column was used as the stationary phase with 0.008N H_2SO_4 as the mobile phase with operation at 35-65 ˚C and a flow rate of 0.4 - 0.6 mL/min.

Riboflavin and Flavin mononucleotide were measured by UV-HPLC with a Shimadzu HPLC system with an LC pump (LC-10ADVP) and an autoinjector (SIL-10ADVP) coupled to a Shimadzu Fluorescence detector (RF-10AXL). The stationary phase was an Altima C8 250mmx4mm, 5um HPLC column with a 50: 50 methanol: water mobile phase operated at 35 ˚C. Samples were analysed under a flow rate of 0.7 mL/min with excitation at 450 nm and emission set at 530 nm.

5. Research outcomes

5.1 Use of SWATH-MS for quantitative proteomic analysis on biomass limited electrode biofilms of Shewanella oneidensis MR-1

5.1.1 Introduction

There have been several proteogenomic studies conducted on *Shewanella* [125-128]. However, these studies focus specifically on proteomics with the aim to improve annotation of the genome and are not comparative in that they do not study *Shewanella* under different conditions. Within the scope of BESs, many studies to date combine electrochemical aspects, e.g. growing active biofilm and optimizing current production, with microbial physiology [70, 98, 100-102, 129]. Consequently, there is great interest to study the proteomic basis of the adaptation of the model organism *Shewanella oneidensis* MR-1 to different electrode potentials.

Application of proteomics could be utilised to reveal metabolic and physiological details of the microorganisms performing EET. However, BESs are often operated at a small scale for convenience and to simplify operation. This becomes problematic for proteomic studies that require enough biomass for adequate protein extraction, especially for quantitative analyses. Recently, the first quantitative proteomic study was performed to determine details of EET [130]. In this study cell biomass levels were a problem, as replicate electrode samples were pooled for quantitative iTRAQ analysis, and relatively low numbers of unique proteins were detected, ranging from 115 to 233, from any particular sample. Consequently, these shortfalls limit the outcomes of proteomic investigations of electroactive biofilms in BESs.

SWATH-MS is a recently developed approach that provides extensive label-free quantitation of the measurable peptide ions in a sample [116]. The approach rapidly acquires high resolution Q-TOF mass spectrometer data through repeated analysis of sequential isolation windows (swaths) throughout the chromatographic elution range [117]. Of the few reports on the use of SWATH-MS for bacterial proteomics, to our knowledge this is the first to use the method on low biomass electrode biofilms. Here we compared the proteome of *S.*

oneidensis to detect functional differences while growing on an anodic electrode at different potentials. We show successful quantitative proteomic analysis of the anodic *Shewanella* biofilm samples using SWATH-MS without the need for fractionation, labelling or other procedures that can contribute to protein losses.

5.1.2 Results and Discussion

During operation of the BES, current production by *S. oneidensis* in the BES increased over time for all the anodic potentials of +0.5 V, +0.0 V and -0.4 V (Ag/AgCl) (Figure 5.1 A, Appendix F). Higher current densities were achieved at anodes poised at higher potentials. The amounts of protein extracted from the electrode biofilms were consistent between replicates, with higher amounts obtained from the electrodes at higher potentials (Figure 5.1 B).

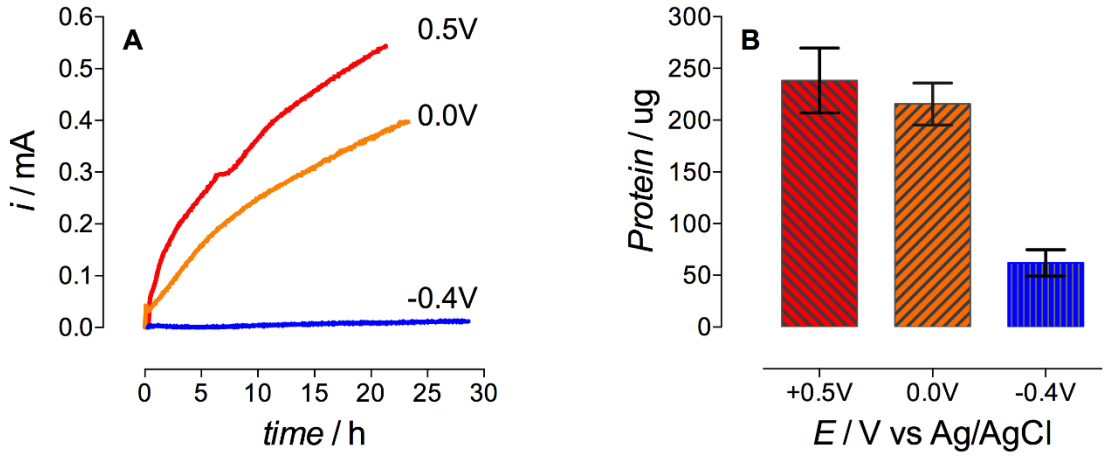

Figure 5.1: Profiles of current production from *Shewanella oneidensis* MR-1 at different anode potentials within the BES over time (A). Amounts of protein extracted from electrode biofilms of *S. oneidensis* after BES operation at different anode potentials (error bars indicate standard deviation) (B).

A total of 740 unique proteins were identified within the library acquired by information dependant acquisition (IDA) with a false detection rate of 0.01 calculated using a Paragon method within the ProteinPilot software (Appendix B). Of these unique proteins SWATH-MS analysis detected 704 proteins. The number of significantly different ($p<0.05$) abundant

proteins was determined between pairwise comparisons of the BES biofilms developed at the different potentials. There were 58, 115 and 41 differentially abundant proteins between the comparisons of +0.0 V to - 0.4 V, +0.5 V to -0.4 V and +0.5 V to +0.0 V respectively ($log_2FC>1$, $p<0.05$). The greatest number of significantly different abundant proteins was between electrode biofilms at the potentials of +0.5 and -0.4 V, hence this comparison became the focus of this study.

The TCA cycle is an essential metabolic pathway enabling energy generation and synthesis for many microorganisms. Consequently, to demonstrate detection of metabolic differences we focused on comparison of proteins involved in the bacterial TCA cycle at these electrode potentials (Figure 5.2). Although the TCA cycle typically operates under aerobic conditions, *S. oneidensis* has been shown to use this pathway partially during anaerobic respiration coupled to alternative electron acceptors such as fumarate and TMAO [131, 132].

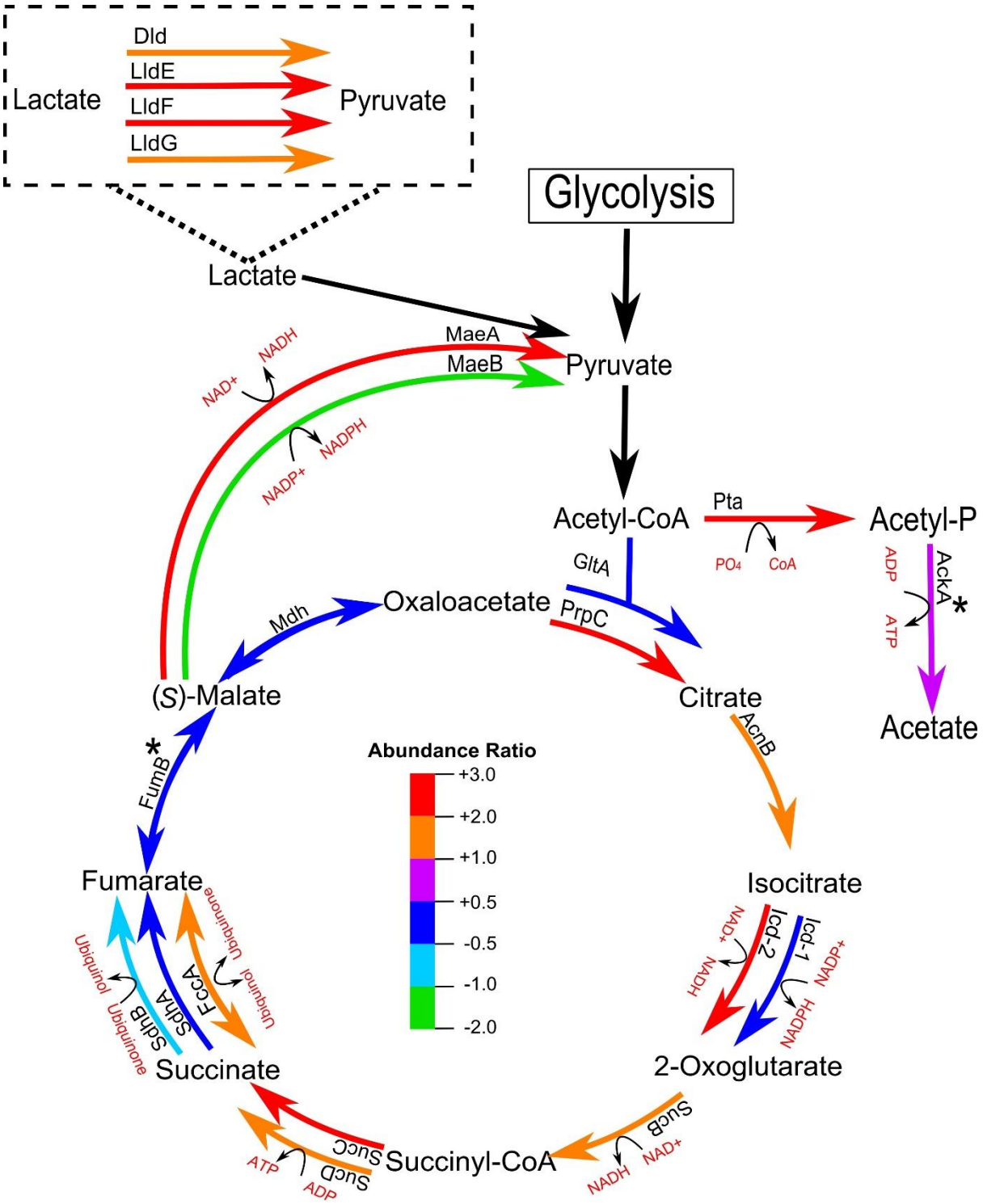

Figure 5.2: *Shewanella oneidensis* MR-1 TCA cycle as adapted using Pathway Tools software. The colour coded expression ratios indicate the Log_2 Fold Change occurring between protein abundances in +0.5 V relative to -0.4 V electrode biofilms. Inset box shows the abundance differences between the multiple enzymes that carry out the conversion of lactate to pyruvate. All Log_2 Fold Change values are significant ($p<0.05$) unless indicated with an asterisk (*).

The log_2FC for the majority of the TCA cycle proteins in the comparison of the +0.5 V to -0.4 V anode biofilms were positive (Figure 5.2 & Table 5.2). This indicated a higher abundance of these proteins at +0.5 V and a more active TCA cycle in comparison to -0.4 V. This correlates with the BES chronoamperometry results, with +0.5 V showing significantly higher current production and thus overall metabolic activity than that detected at -0.4 V (Figure 5.1A). This higher electron transfer rate was generated through increased carbon substrate (lactate) oxidation activity at the higher anode potential. The enzymes involved in the conversion of lactate to pyruvate (Dld, LldE,LldF & LldG) were higher in abundance at +0.5 V ($p<0.05$), suggesting a higher rate of carbon metabolism at the higher potential. This activity was confirmed as lactate utilisation was higher in the +0.5 V culture compared to the -0.4 V culture (Table 5.1).

Proteins of the TCA cycle with negative log_2FC were relatively higher in abundance at -0.4 V. The enzyme MaeB was significantly more abundant at -0.4 V and catalyses an NADP+ dependent conversion of malate to pyruvate (Figure 5.2). The protein MaeA, a NAD+ dependent malic enzyme was more abundant at +0.5 V. This protein carries out the same reaction, however this uses NAD+ rather than NADP+ for conversion of malate to pyruvate. In general bacterial metabolism, conversions utilising the NAD+/NADH couple are involved in oxidative catabolic reactions and respiratory electron transfer [133]. In contrast the NADP+/NADPH couple is utilised in anabolic reactions [133]. This appears to be a response of the cells corresponding to the different electrode potentials and is in agreement with the outcomes observed here in that more respiratory activity (NAD+ dependant reactions) was evident at +0.5 V compared to -0.4 V (Figure 5.1A). The higher potential of the anode would provide more opportunity for electron transfer through the respiratory pathway, given the higher energy gain associated with electron transfer between redox couples at greater potential difference.

Conversely, at low potential it is possible that the TCA cycle is functioning at a decreased level. Although under more reduced conditions, NADH levels will be high and this is known to inhibit key oxidative enzymes in the cycle [134]. Several studies report that under anaerobic conditions *S. oneidensis* possesses an incomplete TCA cycle [135], using either an oxidative or reductive branch for production of cell intermediates [131, 132]. However, activity of a complete TCA cycle has been detected under certain anaerobic conditions [132].

Although, in that instance the carbon flux through the TCA cycle was very low and acetate was a major product of lactate oxidation [132]. That was not the case in this study at the higher potential, as acetate production was less than 5% of the consumed lactate (Table 5.1), this result supporting the scheme of lactate utilisation proceeding through the TCA cycle. Conversely, acetate production at the low potential was significant (Table 5.1), and this activity has been observed previously in anaerobic conditions [131]. Consequently, the low potential acetate production was important for substrate level ATP production.

The reactions of the TCA pathway that are utilised would have great impact on the number of electrons consumed/produced [87], and the choice of those used is likely a dynamic process determined by environmental conditions [131]. When looking at protein abundances for each side of the TCA cycle, there is evidence to support this suggestion. At +0.5 V we see higher abundances for proteins involved in energy generating reactions, suggesting that the complete TCA cycle is being extensively utilised. Conversely at -0.4 V we observed equal abundances for proteins involved in the reductive branch of the cycle, suggesting that under these conditions there is less use of the oxidative branch of the TCA cycle. This is in agreement with previous observation where *S. oneidensis* uses a complete TCA cycle at higher redox potential and utilisation of the branched cycle was evident at lower redox potential [132]. With regard to the TCA cycle, the proteomic findings made here are in agreement with what is expected from the metabolic and energetic activities of *S. oneidensis.*

The number of protein identifications achieved in this study improves on quantitative proteomic investigations of an electrode biofilm. The SWATH-MS approach used here is advantageous for proteomic analysis on samples where biomass or protein quantities are limited. The sensitivity of SWATH-MS removes the need for fractionation and being label free, removes the need for several processing steps involved with labelling procedures which may contribute to loss of protein [136]. Furthermore, being label free, SWATH-MS is not subject to errors in quantification due to incomplete labelling [137]. The extraction method in combination with IDA analysis successfully obtained high levels of identifications from the electrode attached biofilm samples. In particular, this method could be used for detailed interrogation of the electron transfer proteins of BES biofilms.

Microbial electrochemical systems like microbial fuel cells have attracted attention as a promising alternative to unsustainable energy sources and technologies. Among the development of other components, the improved understanding and details of EET pathways of model organisms, such as *S. oneidensis* MR-1, provides opportunity to fine tune reactor conditions to the metabolic capabilities of the organism and achieve improved process performance. Establishing the SWATH-MS approach in this field opens the way for further investigations to improve the understanding of electroactive biofilms for advancing the BES technology.

5.1.3 Conclusions

SWATH-MS analysis is quantitative and enabled a relative comparison of protein abundance between biofilm samples. Using this technique we gained evidence that the TCA cycle of *S. oneidensis* electrode biofilm is more active when grown at a higher potential (+0.5 V). The results also suggest that at lower potential, utilisation of reactions dependent on NADPH rather than NADH was preferred, and this likely reflects decreased respiratory activity in this condition. Consequently, we suggest the use of the above mentioned extraction and SWATH-MS for quantitative proteomic analysis of electrode biofilm samples, and in general from samples where the quantity of protein is limited.

Table 5.1: Lactate and acetate levels detected in the medium before and following operation of the BES at the compared potentials including the total current produced. The symbol Δ represents the difference between values at the start and at the end of the BES experiment.

	Lactate Detected (mmol)	Δ lactate (mmol)	Δ acetate (mmol)	Δ lactate (coulombs equivalent)	Δ acetate (coulombs equivalent)	Current (coulombs)
Medium	3.5					
+0.5 V	2.4 ±0.2	1.2 ±0.2	0.06±0.02	1379.8 ±273.8	48.3 ±13.5	21.8 ±1.2
-0.4 V	3.5 ±0.2	0.1 ±0.1	0.08±0.01	185.2 ±110.8	64.7 ± 9.29	0.8 ±0.4

Table 5.2: Summary of statistics for TCA cycle proteins identified.

Protein ID	Enzyme Name	log_2FC	p-value	Sequence coverage %
AcnB	Aconitate hydratase	0.73	0.000000	47.4
Dld	FAD-dependent D-lactate dehydrogenase	0.68	0.000278	8.75
FccA	Fumarate reductase	0.58	0.000001	67.3
FumB	Anaerobic fumarate hydratase	-1.00	0.000000	30.8
GltA	Citrate synthase	-0.30	0.001513	69.2
Icd-1	Isocitrate dehydrogenase NADP-dependent	-0.56	0.000000	39.0
Icd-2	Isocitrate dehydrogenase NAD-dependent	1.70	0.000056	16.4
LldE	L-lactate dehydrogenase complex protein	1.26	0.000000	55.5
LldF	L-lactate dehydrogenase iron-sulfur cluster-binding protein	1.28	0.000000	20.7
LldG	L-lactate dehydrogenase complex protein	0.29	0.000000	56.6
MaeB	NADP-dependent malate dehydrogenase	-1.75	0.000000	30.2
Mdh	Malate dehydrogenase	-1.18	0.000000	78.8
PrpC	Citrate synthase	1.22	0.000000	14.4
SdhA	Succinate dehydrogenase flavoprotein subunit	-0.35	0.000000	50.8
SdhB	Succinate dehydrogenase iron-sulfur protein Subunit	-1.24	0.000000	4.7
MaeB	NAD-dependent malic enzyme	0.98	0.000048	19.4
SucB	2-oxoglutarate dehydrogenase complex	0.91	0.000345	14.9
SucC	Succinyl-CoA ligase subunit beta	1.19	0.000000	56.2
SucD	Succinyl-CoA ligase subunit alpha	0.61	0.000000	60.3
Pta	Phosphate acetyltransferase	2.1	0.000002	19.8
AckA	Acetate kinase	0.63	0.109583	21.6

5.2 Applied potential affects the abundance of Shewanella oneidensis MR-1 EET proteins

5.2.1 Introduction

Shewanella oneidensis MR-1 is versatile in that it has the ability to reduce a wide array of electron acceptors [87]. There have been numerous investigations focused to determine the proteins involved in DET pathways in *Shewanella* [11, 18, 19, 26, 31, 44, 90, 93, 94, 104]. However, the presence of 42 possible c-type cytochromes in the genome [24] has made such studies in *Shewanella* challenging. It is demonstrated that some electron transfer pathways may utilise alternative cytochromes, indicating modularity of the electron transfer pathway of *S. oneidensis* [20, 23]. The current model for extracellular electron transfer to external electron acceptors by *S. oneidensis* MR-1 is shown in Figure 2.2. This system consists of periplasmic cytochrome MtrA [90, 91], MtrC and OmcA [92], the trans membrane protein MtrB [93], and CymA [23, 94].

It is unclear under which conditions certain EET modes are exploited and whether multiple mechanisms are used simultaneously. As *Shewanella* has modularity in electron transfer proteins and the ability to utilise mediators and nanowires, there is the likelihood that electron transfer mechanisms could differ and be fine-tuned to different redox potentials. Hence, we hypothesise that different anode potentials will select for particular proteins within the electron transport pathway of *S. oneidensis.* This study uses both electrochemical and the recently developed proteomic method of SWATH-MS [116] to understand the details of EET by identifying the molecular mechanisms employed by biofilms of *Shewanella oneidensis* MR-1 at different applied potentials. The recently developed SWATH-MS proteomic method, has already been successfully used for quantitative proteomic analysis of anode grown *S. oneidensis* biofilms [27].

5.2.2 Results and Discussion

Electrochemical Performance

When *S. oneidensis* was exposed to graphite electrodes poised at +0.5 V, 0.0 V and -0.4 V, it produced maximum current densities (j_{max}) of 24.6 (± 1.9) µA cm-2 at t≈18.5 hrs, 16.9 (± 2.8) µA cm-2 at t≈23.5 hrs and 0.6 (± 0.2) µA cm-2 at t≈29 hrs, respectively (Figure 5.3 a, Appendix F).

These current density values are comparable with that previously reported for *Shewanellacea* at +0.5 V [138], 0.041 V [18, 139] and -0.195 V [98, 140]. Hence, it is evident that the generated electroactive biofilms are representative for *Shewanella oneidensis* MR-1 grown at the respective conditions. Previous research observing current density of *S. oneidensis* at different potentials, observed a decline at the potential +0.4 V (Ag/AgCl) [99]. However, no decline in current density at +0.5 V was observed in this study. This may be because experiments were performed in batch mode opposed to continuous mode used in the study mentioned. Using a batch system is expected to encourage growth of planktonic cells and the use of MET for respiration which does not require physical contact with the electrode [141]. This is opposed to continuous systems that encourage the use of DET, where proteins make direct contact with the electrode to respire [141]. It has been shown in continuous systems, that highly oxidising potentials may directly damage cellular proteins, including cytochromes in *S. oneidensis* [99]. Hence, the decline in current production may not be observed as direct contact between proteins and the electrode is required for protein damage to occur [99].

Once maximum current density (j_{max}) was achieved, cyclic voltammograms were recorded under turnover conditions (Appendix G), that is in the presence of metabolic electron donor (lactate) and were similar to those reported previously [139]. The formal potentials of the EET were determined from the first derivatives of the turnover CV (Figure 5.3 b and c) [97]. Formal potentials of the electron transfer sites of triplicate biofilms were determined (with standard deviations) to be -0.41 ±0.01 V for anodes grown at +0.5 V, -0.375 ±0.02 V grown at 0.0 V and -0.402 ±0.002 V grown at -0.4 V. These values are similar to previous reports of formal potentials detected for *Shewanella* spp. redox sites involved in MET, ranging between -0.41 V [18] to -0.33 V [24], indicating no apparent difference in the formal potential of MET among the systems run at different electrochemical potentials.

A second less distinctive peak was detected between the potentials -0.1 V and +0.4 V from the first derivative analysis of the CVs (Figure 5.3 c), suggesting this pathway plays a minor role in the overall EET (Figure 5.3 b). This secondary peak has been reported previously, and appeared to be unaffected by flavin concentrations [139]. This second mechanism that possesses a broader response to electrode potential may correspond to the DET mechanism, which likely involves interactions between c-type cytochromes and the electrode. The *S. oneidensis* genome codes for up to 42 such cytochromes [142], and the cytochromes well established in the EET process of *Shewanella oneidensis* MR-1 include MtrA, MtrC, OmcA, CymA and STC. The activity of these cytochromes are found to cover a broad range of potentials [143], and could explain the broad peak covering a large potential range rather than a distinctive peak at a specific potential (Figure 5.3 c). Additionally, other phenomena such as protein orientation as well as micro-environmental conditions are thought to cause variation in redox potential. For example, it has been shown that the electron transfer rate of a protein (or cytochrome) is improved if the active centre is orientated towards the electrode surface, [144, 145]. Such orientation would minimise the electron transfer 'barrier', thereby increasing the efficiency of the electron transfer process [144]. However, as proteins have large surface areas with low active site densities, there would be limited orientations of a cytochrome that would enable highly efficient electron transfer [144], capable of showing definitive peaks. The higher current generated in the turnover CVs at 0.0 V relative to +0.5 V was unexpected (Figure 5.3b). This could be related to a type of adaptation of the EET at the different potentials. As an electrode +0.5 V provides plentiful energy gain for biofilm growth, the biofilm may not need to perform with much effort to develop and generate current. On the other hand, an electrode poised at 0.0 V may not provide as much energy gain, therefore the biofilm needs to perform with a greater effort to develop and generate a current. One could speculate that the higher current generated at from the 0.0 V biofilm compared to the +0.5 V biofilm in the CV could be because the 0.0 V biofilm is more competent than the +0.5 V biofilm to transfer electrons, as the biofilm had to work harder during chronoamperometry at 0.0 V.

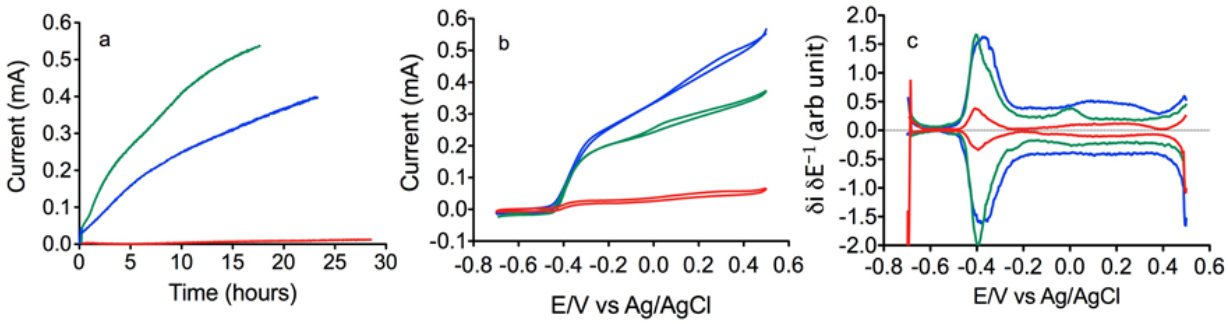

Figure 5.3: Representative chronoamperometry profiles from of *S. oneidensis* in the BES at +0.5 V (—), 0.0 V(—) and -0.4 (—) (a), along with respective turnover CV determined on the differently grown biofilms (b) and the corresponding first derivative analysis of the turnover CV (c).

Proteomic Analysis

Differential protein abundance from anodic *S. oneidensis* biofilms grown at different potentials was performed using the recently developed proteomic method SWATH-MS [116]. This approach is particularly useful for investigative analysis of low biomass samples, where quantitative proteomics is challenging. In section 5.1 SWATH-MS was successfully used for quantitative proteomic analysis of anode grown *S. oneidensis* biofilms [27].

The IDA spectral library revealed a total of 740 identified proteins (out of 4758 predicted proteins [146]) in the anode biofilm samples, with a false detection rate of 0.01 (Appendix B) SWATH-MS spectral analysis detected 697 of these proteins all biofilm samples. The number of significantly different ($p<0.05$) abundant proteins was determined by pairwise comparisons of the BES biofilms developed at the different potentials. There were 175, 219 and 54 differentially abundant proteins between the comparisons of 0.0 V to - 0.4 V, +0.5 V to -0.4 V and +0.5 V to 0.0 V respectively ($log_2FC>1$, $p<0.05$).

Increased metabolic activity at the higher electrode potential

A number of changes in relative protein abundance suggest that *S. oneidensis* had increased cell activities at the higher electrode potential, as can be expected as a higher microbial electrochemical activity was observed. In addition, higher amounts of total cellular protein was extracted from biofilms grown at higher potentials with 238 ± 30, 215 ± 20 and 62 ± 13 µg of protein extracted from electrodes poised at +0.5, 0.0 and -0.4 V respectively. At the higher potential the cellular electron transfer activity was significantly higher ($p <0.05$),

these being 5.4 $x10^{-9}$ ± 0.7 $x10^{-9}$, 4.97 $x10^{-9}$ ± 0.54 $x10^{-9}$, and 0.83 $x10^{-9}$ ± 0.71 $x10^{-9}$ mA per cell at 0.5, 0.0 and -0.4 V respectively, which was reflected in the proteomic analysis. From the 53 proteins that found more abundant at +0.5 V relative to -0.4 V, 24 were ribosomal proteins with log_2FC ranging from 1.5 to 3 (Table 5.3). Furthermore, elongation factor FusB (log_2FC 1.9) involved in protein synthesis and a ribosome maturation factor RimM (log_2FC 1.8) were also significantly more abundant at higher potential. As ribosomes are the key component of protein synthesis within the cell, this finding implicates a higher biosynthetic activity of cells grown at the higher potential. It has been found that protein turnover of *S. oneidensis* differs when respiring using different electron acceptors [101, 102], and that ribosomal protein expression is related to the redox potential of the metal electron acceptor [99]. However, recently it was discovered that ribosomal protein expression was not positively correlated to electrode potential, but rather to increased rates of EET [99]. This indicates that the increase in biosynthetic activity that we observe may be correlated to the higher rate of EET rather than the increasing electrode potential. However, it should be noted that EET increases because of larger thermodynamic gain resulting from a higher electrode potential, suggesting that potential does play a role until it becomes detrimental to the microorganism. Furthermore, the higher abundance of proteins involved in the energy generating reactions of the *S. oneidensis* TCA cycle (section 5.1.2) support higher metabolic activity at +0.5 V.

MET is the dominant form of EET for S. oneidensis

Peaks evident from turnover cyclic voltammetry analysis of the biofilms at the three electrode potentials within the batch BESs suggests the dominant EET mechanism is MET through the use of flavins. MET has been found to be the dominant form of EET for *Shewanella* in batch systems, were as continuous flow systems are found to wash out mediators, and therefore promote DET [141]. SWATH-MS revealed a higher abundance of riboflavin biosynthesis protein at +0.5 V (RibBA, log_2FC 0.96 compared to -0.4 V). However UV-HPLC results show a significant difference in riboflavin concentrations, $t(4) = 2.77$, $p < 0.05$, with the potential -0.4 V containing a higher concentration in the medium at the end of the experiment (151 ± 31 and 216 ± 20 nM detected for +0.5 V and -0.4 V respectively). Recently, it has been reported that *S. oneidensis* MR-1 can use flavins both as electron shuttles and as co-factors bound to the outer membrane cytochromes MtrC and OmcA [53, 147]. Riboflavin has a high affinity for OMCs with reduced hemes and are found to bind to cytochromes to enable a one electron reaction using a semiquionone [53]. The increased

concentration of flavin ‘bound’ to OmcA and MtrC, found in higher abundance at this potential could explain the relatively lower mediator concentration observed at the higher potential. Electrode biomass was found to be significantly higher at +0.5V compared to -0.4 V (section 5.1.2 Figure 5.4) with the amounts of protein extracted from electrodes at +0.5 V approximately 3.8 times more than -0.4 V. The higher relative abundance of OmcA and MtrC at +0.5 V along with the larger amount of biomass present would provide a greater availability of cytochromes for riboflavin to bind to, thereby reducing the amount of free flavin in the medium.

Abundance of specific cytochromes suggests outer membrane involvement in EET

Previous investigations implicate a particular set of proteins important for *Shewanella* EET [26, 31, 90, 93]. Mass spectrometry based quantitative proteomic analysis (SWATH-MS) revealed a higher abundance of these EET related proteins MtrABC and OmcA at +0.5 V and 0.0 V compared to -0.4 V (Figure 5.4), suggesting a relationship between the applied potential, current production, and the abundance of these EET related proteins. At the low potential used here (-0.4 V), very little current flows and thus the anode plays a minor role as a terminal electron acceptor. Consequently, the organism lowered its abundance of EET related proteins at the low potential in comparison to +0.5 V (Figure 5.4), as their activities were not required. Details of the regulation of the genes involved in EET (*mtrA*, *mtrB*, *mtrC*, *omcA & cymA*) are not well understood. Altered gene expression at the transcription level has been detected [101, 102, 142], however the regulator molecules responsible for the transcription of these genes are yet to be identified. It was anticipated that the relative abundance of EET proteins would decrease with decreasing anode potential and current production. However, it is found that the relative abundance of EET proteins was equal, if not higher in abundance in the 0.0 V biofilm compared to +0.5 V (Figure 5.4). Interestingly, this finding supports the earlier suggestion for the reasoning behind the higher current generated in the non-turnover CV’s at 0.0 V compared to +0.5 V (Figure 5.3b), where biofilms at 0.0 V require more effort to grow and generate current compared to biofilms at +0.5 V. This reasoning could also be used to explain the equal or higher EET protein abundance at this potential, as biofilm grown at 0.0 V may be more competent at electron transfer compared to biofilm grown at +0.5 V.

Differential gene expression has been studied when *S. oneidensis* was grown using either an electrode (+0.2 V vs Ag/AgCl), oxygen or soluble iron (III) as electron acceptors [102]. It was found that the genes *mtrABC* and *omcA* and that coding for riboflavin synthase were all up regulated during oxidation at the anode, in comparison to use of oxygen or iron as the electron acceptor. This coincides with the proteomic findings associating these proteins with EET when using an electrode as an electron acceptor.

Although present in the IDA library, SWATH-MS analysis was not able to successfully quantify CymA, an essential EET component within the biofilm samples. However, SWATH-MS does detect CymA in in very low amounts if the stringency of the analysis is decreased to one quantified peptide. In a recent investigation of *S. oneidensis* cell structure, during respiration using an insoluble electron acceptor, it is seen that the outer membranes extrude from the cell and these partake in EET [45]. They showed that cytochromes responsible for EET (MtrC and OmcA) were localised along the membrane extension or nanowire [45]. In this model the inner membrane is not included in the extension, and CymA is located on the inner membrane [23, 94]. The proteomic analysis revealed the relative abundance of MtrABC and OmcA is higher at +0.5 V compared to -0.4 V for biofilms grown at all applied electrode potentials (Figure 5.4). This data supports the model of the outer membrane extensions working as electron rich regions for transfer of electrons away from the bulk of the cell. Additionally, the protein abundance comparison may suggest that *Shewanella oneidensis* MR-1 use nanowires as a mechanism for EET at higher potentials where there is greater opportunity to perform EET. The low abundance of CymA in the analysis is an unexpected result, although the finding supports a recent model for *S. oneidensis* EET. Recent investigation of *S. oneidensis* cell structure, during respiration using an insoluble electron acceptor, demonstrates that the outer membrane extrudes from the cell and these extrusions partake in the EET [45]. The study showed that cytochromes responsible for EET (MtrC and OmcA) were localised along the membrane extension or nanowire [45]. In this model the inner membrane is not included in the extension, where CymA is located, and thus increased levels of CymA would not be required for this to occur [23, 94]. However, the limitations of the proteomic technique need to be considered. The inability to quantify a particular protein, in this case CymA could be a result of an inefficient extraction of this particular protein, as it has been shown that cytochromes can differ in their solubility, making some more difficult to isolate than others [148]. Furthermore, a negative result in proteomics is potentially meaningless [149], in that there are multiple reasons for obtaining false-

negative results in proteomics. For example, a peptide might have a modification that disrupts the search result, the dependency on the accuracy of the database being searched, and also the efficacy of the protein digestion [150].

In this thesis, the relative abundance of MtrABC and OmcA is higher at +0.5 V compared to -0.4 V for all of the applied electrode potentials (Figure 5.4). These findings reveal the increase in the relative abundance of EET proteins with increasing rate of EET and support the model of the outer membrane extensions working as electron rich regions for transfer of electrons away from the bulk of the cell. Additionally, the protein abundance comparison may suggest that *Shewanella* use nanowires as a mechanism for EET at higher potentials where there is greater opportunity to perform EET. Bacteria contain homologues of eukaryotic cytoskeletal proteins such as actin (microfilaments), tubulin (microtubules), other filamentous proteins in addition to MinD-ParA group of proteins exclusive to bacteria [151]. The bacterial cytoskeleton is known to play an important role in cell shape regulation and division as well as cell polarity [151]. Furthermore, microtubules and microfilaments have been suggested to be involved in the distortion of the cell membrane to alter the shape of a cell [152]. It could be speculated that the formation of these extensions are aided by the bacterial cytoskeleton. The bacterial homolog of the eukaryotic tubulin protein, is known as the cell division protein FtsZ [153]. FtsZ was quantified in the SWATH-MS analysis and showed no significant difference in abundance between the potentials +0.5 V and -0.4 V. However, a significant difference was found between +0.5 V and 0.0 V with abundance found to be higher at 0.0 V (log_2FC -0.82). The higher abundance of FtsZ at 0.0 V could be an indication of higher cell division at 0.0 V. However if involved in nanowire production as speculated, could suggest an increase in nanowire production at 0.0 V relative to +0.5 V. This is supported by evidence of slightly elevated levels of OmcA at 0.0 V compared to +0.5 V (log_2FC -0.19), however MtrABC showed no significant change between the potentials.

SWATH-MS analysis revealed several cytochromes higher in abundance at -0.4 V; cytochrome c oxidase, cbb3-type, subunit II (CcoO), c-type cytochrome (SO3420) and periplasmic cytochrome c (CytB), with log_2FC of -0.66, -0.43 and -0.96 respectively. CcoO has been found to be associated with the cell membrane [102, 154]. Both the genes for CcoO and SO3420 were found more highly expressed when *S. oneidensis* is grown on an electrode compared to growth using soluble Iron (III) citrate [102]. CytB complexes are transmembrane proteins that are known to interact with quinones and cytochromes [155].

The higher abundance of these cytochromes at -0.4 V suggests that these proteins are important for survival on an electrode at this potential. It is possible that these cytochromes play a role in EET at low potential as modularity of these mechanisms is proposed for *Shewanella* [26]. Furthermore, it is suggested that *c*-type cytochromes can play a role in temporary storage of charge thereby acting as capacitors [156], transferring the charge across the inner membrane when an acceptable electron acceptor is available. The anode potential of -0.4 V was not favourable for *S. oneidensis* EET. However, it may be that *S. oneidensis* increased its abundance of these cytochromes at the low potential, thereby increasing its ability to store electrons until a suitable electron acceptor is available. Such a role would enable *S. oneidensis* to have some respiratory activity in the absence of external electron acceptors.

Signs of higher motility at anode lower potential

A higher abundance of chemotaxis and motility related proteins were detected in biofilm cultures at -0.4V (Figure 5.5). Methyl-accepting chemotaxis proteins (MCPs), which are part of the cells motility mechanism for moving up gradients of attractants, were in higher abundance at -0.4 V compared to 0.0 V and +0.5 V (Figure 5.5). Additionally, flagellin related proteins were in higher abundance at -0.4V. This included FliD the flagellar filament capping protein (log_2FC -2.43), and FilC a flagellin filament (log_2FC -1.69). The higher abundance of both chemotaxis and flagellin related proteins at -0.4 V indicate a higher involvement of motility at this potential compared to +0.5 and 0.0 V. It is possible that biofilm cultures grown at lower potential are not as established compared to higher potential, therefore, cells may disassociate from the biofilm to seek more favourable conditions. In contrast, these findings conflict with an earlier study that looked at the motility behaviour of *S. oneidensis* cells in close proximity to an electrode [129]. It was found that when the electrode was poised at +0.6 V (vs. graphite reference electrode) the cells exhibited strong motility, while very limited motility was detected when the electrode was poised at zero or negative potentials. However, the cells that exhibited this behaviour were a small proportion of free swimming cells in the vicinity of the electrode. It was discovered that 11 flagellum related genes were upregulated in electrode biofilm samples compared to planktonic cells, which was said to support suggestions that *Shewanella* sp. Flagella play roles in both attachment of cells for biofilm formation and for electrokinetic purposes [102]. One explanation for the observed differences is that the proteomic analysis was performed on cells of an anodic biofilm.

Hence, free swimming cells may demonstrate different motility behaviours and may respond differently to electrode potentials compared to cells encased within a biofilm.

Other highly abundant proteins detected at higher potential

Numerous proteins were more abundant at the higher potential that were presumably involved in producing reducing power, passing electrons onto the ubiquinone pool and substrate level phosphorylation. As reported in section 5.1.2 a number of the TCA cycle enzymes, especially those involved in the production of reducing power, were more abundant at the higher potential. This included the proteins L-lactate dehydrogenase (LldE), NAD-dependant Isocitrate dehydrogenase, L-lactate dehydrogenase iron-sulfur cluster-binding protein (LldF), NAD-dependent malic enzyme (MaeA), Phosphate acetyltransferase (Pta) and Succinyl-CoA ligase [ADP-forming] subunit beta (SucC) with these having log_2FC of 2.8, 2.8, 2.6, 2.1, 2.1 and 2.0 respectively. Other associated proteins found in higher abundance were pyruvate formate lyase (PflB) and formate dehydrogenase (FdhA, FdhB-1and FdhB-2), the activity of which result in NADH production. Additionally, increased phosphate acetyl transferase and acetate kinase could cause substrate level phosphorylation, and increased levels of NADH-quinone reductase (subunit NqrF), could partake in the reduction of the ubiquinone pool [157]. The significant increase in abundance of these proteins at the higher potential indicate increased energy metabolism and this correlates with the higher current production generated by the cells at +0.5 V.

Other highly abundant proteins detected at lower potential

A putative periplasmic CbiK superfamily protein (SO1190) with a significantly high abundance at -0.4 V (log_2FC -2.9) was detected. Protein BLAST analysis found a 96% similarity to a nickel transporter of *Shewanella decolorationis* (Appendix D). Nickel is an essential cofactor for many enzymes and is transported into the cell by specific transport systems. Nickel is an important component of Ni-containing hydrogenases that play an important role in energy metabolism through the oxidation and production of hydrogen gas, which may be important at the low potential where *S. oneidensis* would have surplus reducing potential [158].

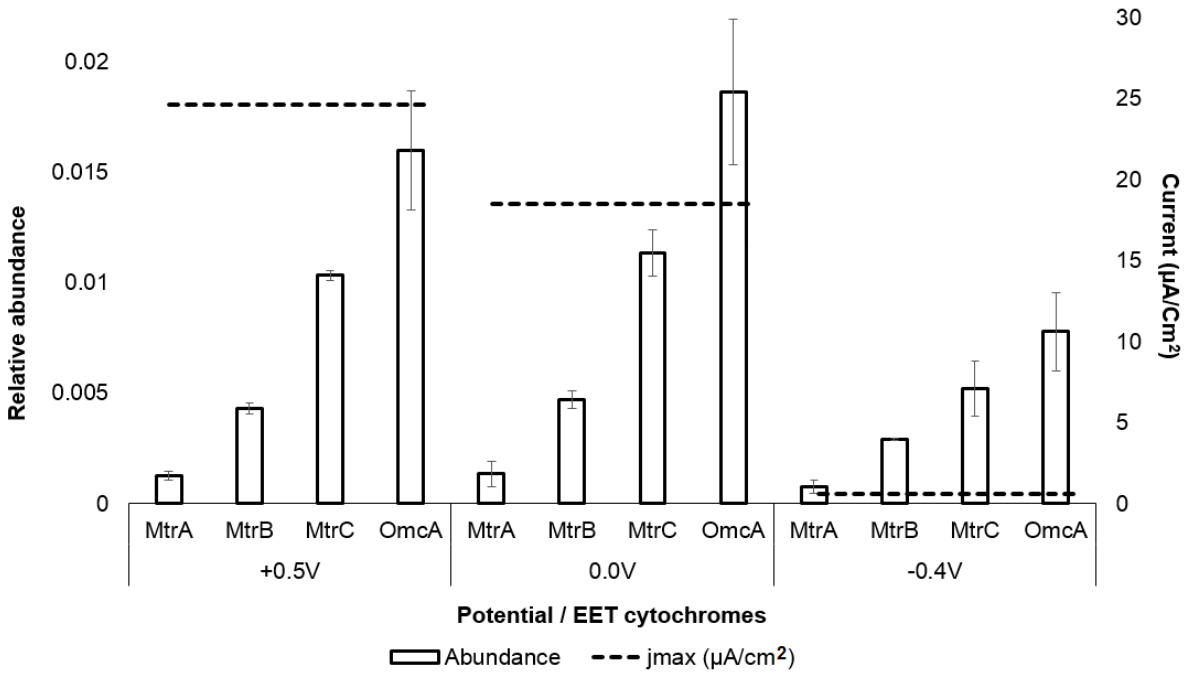

Figure 5.4: Relative abundance of individual EET proteins at the potentials +0.5 V, 0.0 V and -0.4 V (Ag/AgCl). Error bars indicate the standard deviation between triplicate experiments. The dashed line indicates the average current density at the different potentials.

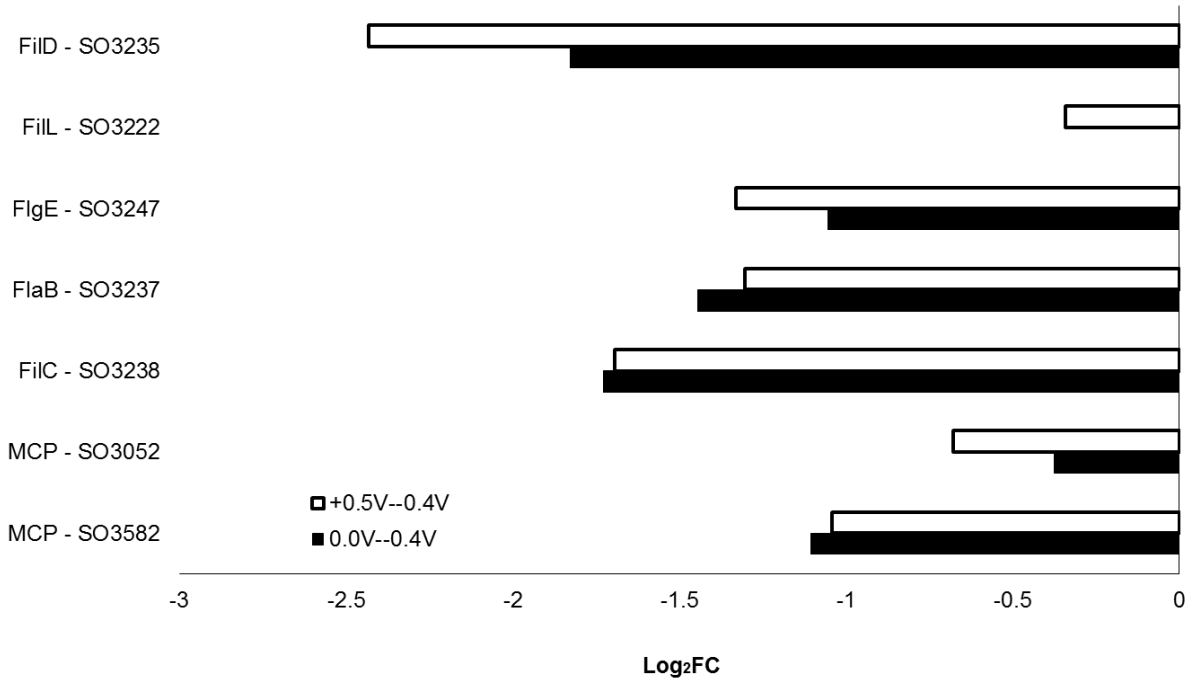

Figure 5.5: Abundance comparison of chemotaxis proteins between the potentials +0.5V vs -0.4V and 0.0V vs -0.4V ($p<0.05$).

5.2.3 Conclusions

Using both electrochemical and molecular techniques, this study has gained a deeper understanding of the proteomic response of *S. oneidensis* to changes in anodic potential. It is found that as demand for EET increases at higher potentials, so does the abundance of EET proteins and proteins for mediator synthesis.

Also confirmed through these investigations is that both MET and DET play a role in EET, with MET acting as the dominant mechanism of EET across all tested potentials for *S. oneidensis*. This agrees with the findings of other studies examining EET of *S. oneidensis* using batch BESs for electrochemical investigations [18, 19, 159]. DET was detected electrochemically through non-turnover CV as a broad peak covering a large potential range. Here we hypothesise that this is due to the range of *Shewanella* EET cytochromes possessing a wide range of potentials [143]. These findings support the existing model for the involvement of the *Shewanella* metal reducing mechanisms in extracellular electron transfer [25, 26].

Table 5.3: Summary of statistics for proteins with $log_2FC > 1.5$, $p < 0.05$. log_2FC represents the log_2 fold change in protein abundance between biofilms grown at +0.5 V relative to -0.4 V.

Protein ID	Enzyme name	log_2FC	p-value	Sequence coverage %
RpsH	Ribosomal protein S8	3.19	0.000	40
RplD	50S ribosomal protein L4	3.17	0.000	50.75
SO0581	Zn-binding protein	3.12	0.000	9.821
RpmB	Ribosomal protein L28	3.06	0.000	12.82
RplN	Ribosomal protein L14	2.94	0.000	36.89
LldE	L-lactate dehydrogenase	2.82	0.005	55.47
Icd	Isocitrate dehydrogenase NAD-dependent	2.82	0.000	7.164
RpsI	Ribosomal protein S9	2.81	0.000	34.62
RpsT	Ribosomal protein S20	2.79	0.000	17.05

LldF	L-lactate dehydrogenase iron-sulfur cluster-binding protein	2.61	0.000	55.47
RpsP	Ribosomal protein S16	2.57	0.000	43.9
ArgG	Argininosuccinate synthase	2.47	0.000	32.19
RpsP	50S ribosomal protein L6	2.33	0.000	67.23
SO2781	Hypothetical protein	2.28	0.000	5.172
RplB	50S ribosomal protein L2	2.20	0.000	37.23
NqrF	Na(+)-translocating NADH-quinone reductase subunit	2.20	0.000	2.851
FdhA	Fnr-inducilble formate dehydrogenase	2.16	0.000	39.26
RplV	Ribosomal protein L22	2.15	0.000	20.91
MaeA	NAD-dependent malic enzyme	2.15	0.000	19.4
Pta	Phosphate acetyltransferase	2.10	0.000	18.69
RplS	50S ribosomal protein L19	2.03	0.000	22.22
RplE	Ribosomal protein L5	2.03	0.000	46.93
SucC	Succinyl-CoA ligase [ADP-forming] subunit beta	2.02	0.000	48.45
FusB	Elongation factor G 2	1.94	0.000	29.99
RpsS	30S ribosomal protein S19	1.94	0.000	47.83
SO1887	DJ-1/PfpI family protein	1.93	0.000	12
PpiB	Peptidyl-prolyl cis-trans isomerase	1.91	0.000	13.96
RplO	50S ribosomal protein L15	1.89	0.000	38.19
RpsJ	30S ribosomal protein S10	1.88	0.000	43.69
SO4141	Oxidoreductase short-chain dehydrogenase/reductase family	1.87	0.000	5.761
rimM	Ribosome maturation factor	1.86	0.000	6.78
RpsD	30S ribosomal protein S4	1.84	0.000	31.07
RplT	50S ribosomal protein L20	1.82	0.000	16.1
Prc	Periplasmic C-terminal processing protease	1.82	0.000	1.466
PflB	Pyruvate formate-lyase	1.81	0.000	79.47
RpsQ	Ribosomal protein S17	1.81	0.000	46.34
RpmF	Ribosomal protein L32	1.80	0.000	57.14
RpmA	50S ribosomal protein L27	1.79	0.000	42.86

SO1627	Methionine aminopeptidase	1.76	0.000	13.21
SO1581	PhnA domain protein	1.71	0.000	4.813
YedY	Sulfoxide reductase catalytic subunit	1.71	0.000	13.66
FdhB	Formate dehydrogenase FeS subunit	1.71	0.000	23.28
AdhB	Alcohol dehydrogenase II	1.70	0.000	73.82
FdhA	Formate dehydrogenase molybdopterin-binding subunit	1.64	0.000	39.26
SO0768	NAD dependent epimerase family protein	1.59	0.000	6.19
RplA	50S ribosomal protein L1	1.57	0.000	51.07
RpsN	Ribosomal protein S14	1.57	0.000	30.69
Brf2	bacterioferritin subunit 2 Brf2	1.57	0.000	20.38
SO1068	4-hydroxybenzoyl-CoA thioesterase family protein	1.56	0.047	13.79
RpsA	30S ribosomal protein S1	1.54	0.000	30.99
FdhB	Fnr-inducible formate dehydrogenase FeS subunit	1.54	0.000	23.28
SO2469	TonB-dependent receptor	1.52	0.000	73.86
RplK	Ribosomal protein L11	1.50	0.000	43.66
SO2469	Putative periplasmic CbiK superfamily protein	-2.92	0.000	36.14
AhpC	Alkyl hydroperoxide reductase peroxiredoxin component	-2.72	0.000	75.66
SO3914	TonB-dependent siderophore receptor	-2.71	0.000	11.78
FliD	Flagellar filament capping protein	-2.43	0.000	37.72
YceI	UPF0312 family alkali-inducible periplasmic protein	-1.96	0.000	51.83
FlaG	Flagellin	-1.92	0.000	8.403
FliC	Flagellin	-1.69	0.000	59.71
SO3545	Outer membrane porin	-1.67	0.000	27.03
SO2938	Lambda phage encoded lipoprotein	-1.65	0.000	29.44
SO3907	Cytochrome oxidase copper metallochaperone	-1.64	0.000	31.25

FklB	Peptidyl-prolyl cis-trans isomerase	-1.56	0.000	43.14
Skp	Periplasmic chaperone for outer membrane proteins	-1.54	0.000	32.14

5.3.1 Introduction

The genome of *G. sulfurreducens* encodes for over 100 putative c-type cytochromes, substantially more than *S. oneidensis* [4]. Several of these cytochromes are known to be involved in *G. sulfurreducens* respiration with an electrode including periplasmic cytochrome c (PpcA), cytochrome c peroxidase (MacA), the outer membrane *c*-type cytochromes: B (OmcB), E (OmcE), F (OmcF), G (OmcG), H (OmcH), S (OmcS), T (OmcT), X (OmcX) and Z (OmcZ) [54], and more recently, outer membrane *c*-type cytochrome, OmcC, periplasmic *c*-type cytochromes OmaB and OmaC, and porin-like outer membrane proteins OmbB and OmbC [33]. A large number of cytochromes are expressed during respiration in the presence of Fe(III) oxides, consequently, there is still much speculation on the specific EET pathway of *G. sulfurreducens*, with several different models suggested [23, 160, 161].

Briefly, it is thought that electrons are transferred from the quinone/quinol pool located in the inner membrane, to the cytochrome MacA. Electrons are then transferred to PpcA, which facilitates electron transfer across the periplasm [161-164]. PpcA, and possibly other periplasmic cytochromes then transfer electrons to a Pcc complex (OmbB/OmbC, OmaB/OmaC and OmcB/OmcC porin-cytochrome protein complexes) that transfer the electrons through the outer membrane [33]. The electrons are then either accepted by terminal electron accepters OmcE and OmcS directly [165] or transferred to pilin or nanowires for long range electron transport [31]. OmcS is proposed to be physically attached to nanowires [14, 166-168] and is believed to be a terminal reductase [30]. In addition, the outer membrane cytochrome OmcZ plays an important role in *Geobacter* EET [35, 36, 169]. The OmcZ cytochrome is located at the biofilm-electrode interface of current producing cells [169] and is suggested to act as an electrochemical gate, allowing electron transfer from the biofilm to the electrode [169].

Geobacter frequently dominate BES anodes under anoxic conditions [112, 113]. Given the potential for practical application of BESs [170], there is much interest in studying this microorganism's EET abilities and pathways [13, 23, 28-31, 34-36, 52, 54, 163, 165, 169, 171-174]. It has been shown through the use of cyclic voltammetry that biofilms of *G. sulfurreducens* alter their EET response to changes in electrode potential [115]. A transcriptomic study looking at biofilms grown using an electrode or fumarate as an electron acceptor, found that biofilms producing current are adapted to transferring electrons to an

electrode. In addition, the importance of pilin and OmcZ to EET was indicated [35]. However, there are no studies that focus on the proteomic response of *G. sulfurreducens* to electrode potential. A study such as this, would allow both the changes in EET as well as the physiological response of the microorganism to electrode potential to be examined. As *Geobacter* possesses several OMCs, many of which are involved in EET we hypothesise that *G. sulfurreducens* may alter its EET response to suit the electrode potential. This study uses both electrochemical analyses and SWATH-MS proteomics as mentioned in previous sections (sections 5.1 and 5.2), with the aim to better understand the details of *Geobacter* EET and to observe its physiological response to different electrode potentials. The potentials of +0.1 V and +0.6 V were chosen based on previous research [115], to enable a direct comparison of electrochemical results. The previous study chose those potentials as the surface charge of a polarised electrode has been shown to be progressively more positive between the potentials of +0.1 V and +0.6 V [175]. Furthermore, negatively charged bacterial cells adhere favourably to surfaces possessing positive surface charge [176]. Therefore, these potentials were selected to promote biofilm attachment and growth on the electrodes.

5.3 Applied potential affects the abundance of Geobacter sulfurreducens EET proteins

5.3.2 Results and Discussion

During operation of the multi electrode BES (section 4.2.2), current production by *G. sulfurreducens* increased over time for both the anodic potentials +0.1 V and +0.6 V (all potentials reported vs Ag/AgCl, sat KCl being 0.197 V vs. SHE) (Figure 5.6, Appendix H). Higher maximum current densities (j_{max}) were observed for anodes operated +0.1 V in comparison to those at +0.6 V. This trend was observed for all six chronoamperometry experiments with j_{max} *being* 0.35 ± 0.07 mA/cm^2 and 0.19 ± 0.05 mA/cm^2 for +0.1 and +0.6 V respectively. The reason for the lower current density produced by G. sulfurreducens at higher potential could be suggested to be similar discovered for S. oneidensis, where lower current density was attributed to increased protein degradation caused by the high electrode potential [99]. Cyclic voltammograms were recorded under turnover conditions once the

current reached the j_{max} (Appendix J), and non-turnover conditions (Appendix K) after substrate depletion (Figure 5.7).

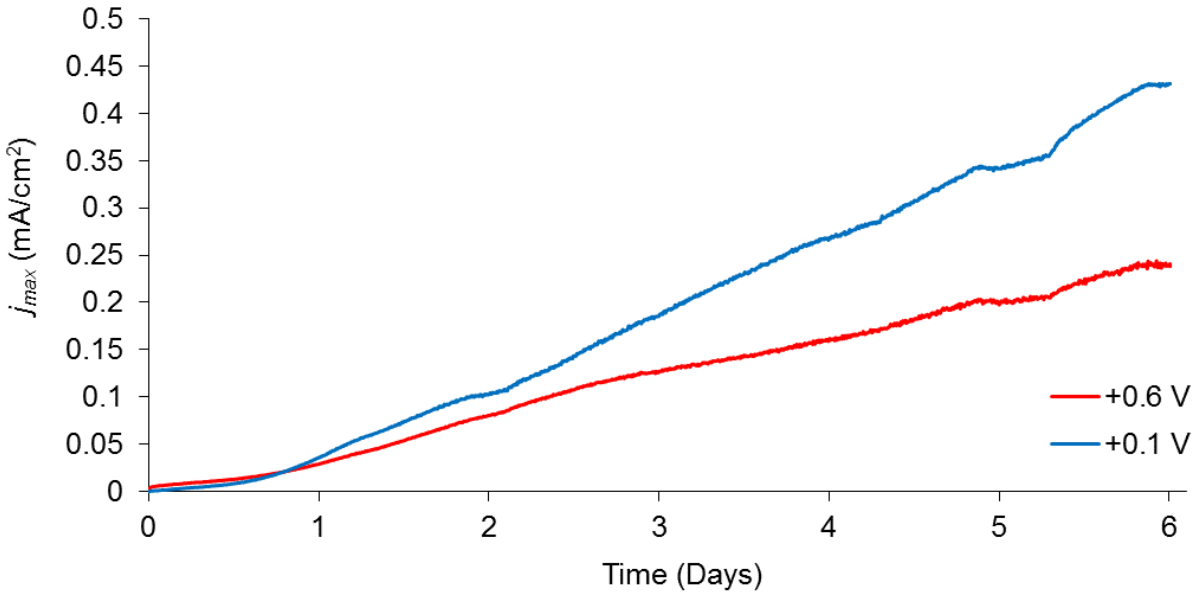

Figure 5.6: Representative chronoamperometry profiles of anodic biofilms of *G. sulfurreducens* grown at +0.6 V and at +0.1 V in batch BES (Ag/AgCl).

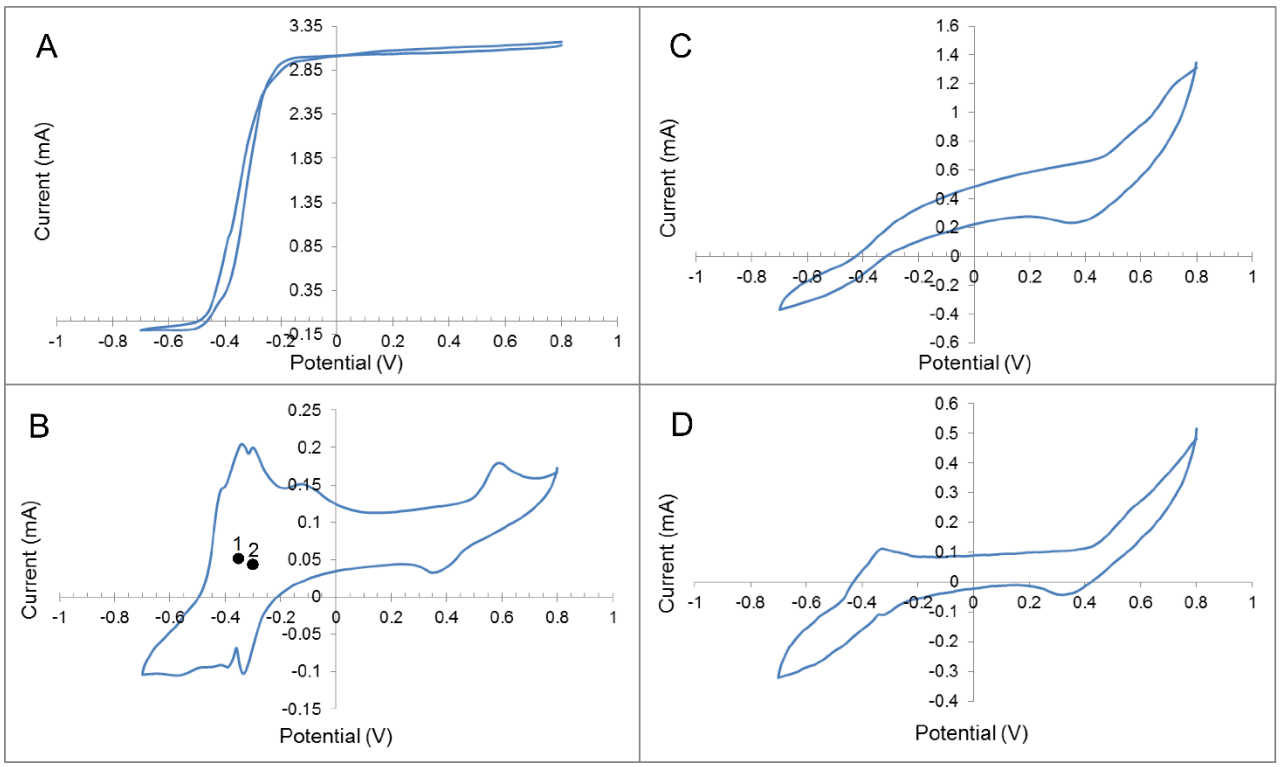

Figure 5.7: Cyclic voltammograms of anodic biofilm cultures of *G. sulfurreducens.* Turnover and non-turnover CVs of biofilms grown at +0.1 V (A and B respectively) and grown at +0.6 V (C and D respectively).

The turnover and non-turnover CVs obtained from the biofilms grown at +0.1 V (Figure 5.7 A and B respectively) are representative of those typically seen for *Geobacter* [177-179]. Using cyclic voltammetry, a previous study identified four redox systems at -0.515, -0.3.76, -0.29 and +0.59 V which they referred to as $E_{f,1}$ $E_{f,2}$ $E_{f,3}$ and $E_{f,4}$ respectively, with a major redox system consisting of $E_{f,2}$ and $E_{f,3}$ [178]. They found $E_{f,2}$ and $E_{f,3}$ contribute to anodic electron transfer, whereas $E_{f,1}$ and $E_{f,4}$ were found to be inactive. Plots representing $E_{f,2}$ and $E_{f,3}$ from our data are shown on Figure 5.7 B and labelled 1 and 2 with formal potentials calculated to be -0.355 and -0.3 V respectively, confirming the presence of redox active sites at these potentials in *G. sulfurreducens* electroactive biofilm.

The CVs recorded for the biofilms grown at +0.6 V are not typical, and show weak signals, possibly representative of a weak biofilm (Figure 5.7 C & D). First derivative analysis of the turnover CVs revealed two electron transfer peaks at negative potential for +0.1V (-0.34 ± 0.005 V and -0.41 ± 0.02 V, the average of which is -0.375 V ± 0.05 V), whereas only one peak was evident for +0.6V (-0.38 ± 0.02 V) (Figure 5.8 A and B). These potentials are

similar to that found for *G. sulfurreducens* previously [178], thereby confirming the reliability of the *G. sulfurreducens* biofilm.

Interestingly, first derivative analysis of turnover CVs for +0.6 V show peaks at a more positive potential (at approximately 0.52 ± 0.05 V) which were not found at +0.1 V (Figure 5.8 A and B). This second, more positive peak indicates a second EET site may be present at +0.6 V, and that *G. sulfurreducens* may have altered its EET mechanism in response to the high electrode potential. A previous study comparing non-turnover CVs of *G. sulfurreducens* grown at both +0.1 V and +0.6 V, found two very different redox waves between these potentials (Figure 2.7) [115]. This finding further suggests the existence of two potential EET domains responsible for electron transfer at different potentials.

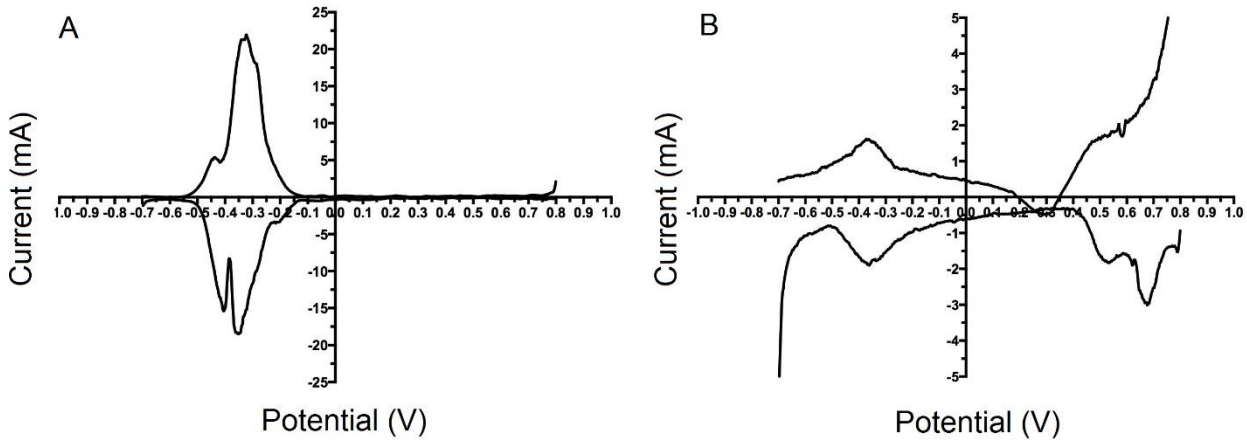

Figure 5.8: Representative first derivative analysis of turnover cyclic voltammograms recorded for anodic biofilms grown at +0.1 V (A) and +0.6 V (B) vs. Ag/AgCl.

The potential for oxygen evolution is theoretically 0.597 V vs Ag/AgCl. (Sat. KCl) at pH 7. For an anaerobic organism, growth on an electrode maintained at a potential close to that of oxygen could possibly be damaging to the cell. This suggests the weak biofilm could be a result of the damaging potential, which may be responsible for limiting the growth of *G. sulfurreducens* biofilm. It has been established that *G. sulfurreducens* can tolerate and respire with low concentrations of oxygen (5 to 10%) [180], however, this ability was inhibited by higher concentrations (15 to 20%). The ability of *G. sulfurreducens* to tolerate low levels of oxygen is apparent in its genome, with its capacity to encode for genes involved in

oxidative stress, such as a superoxide dismutase; SodA (which was identified within the biofilm samples to be only slightly elevated at +0.6 V with a log_2FC of -0.14), catalase (such as CccA showing no significant difference between potentials) as well as A-type flavodoxins [118].

Proteomic analysis

The SWATH-MS proteomic analysis of the biofilms revealed a total of 714 unique proteins (each with the number of peptides identified ≥ 1) that were identified within the IDA library with a false detection rate of 0.01. The number of proteins showing a significant difference in relative abundance ($p<0.05$) was determined by a pairwise comparison of all replicate BES biofilms developed at +0.1 V vs. +0.6 V. There were 65 differentially abundant proteins between the comparison +0.1 V vs. +0.6 V ($log_2FC>1$, $p<0.05$).

Abundance of EET related proteins

A speculative model of the *Geobacter* EET based on previous research and suggestions [23, 31, 33, 161, 162, 171, 181] is shown in Figure 5.9. This model suggests that electrons are transferred from the menoquinone pool within the inner membrane to MacA which then transfers electrons PpcA [163], which shuttles the electrons across the periplasm to a Pcc complex [33]. The Pcc complex passes electrons to the OMCs OmcE and OmcS, which may be responsible for the transfer of electrons to pili [161, 165] of which OmcS is attached [14, 166-168], however *G. sulfurreducens* can also transfer electrons directly using OMCs, without the involvement of pili [165].

Of the cytochromes presented in the model, the IDA spectral library (Appendix C), detected OmcT, OmcS, MacA, OmcZ and OmcX all of which are represented in the model (Figure 5.9). A BLAST search of the *G. sulfurreducens* PCA gene *omaC* (GSU 2732) revealed 100% sequence similarity to the *G. sulfurreducens* DL-1 gene KN400_2674 (Appendix E). The protein encoded by KN400_2647 was identified and allocated the name OmaC, which is also present in the model. Many other cytochromes not represented in the model were also identified within the IDA library, these were: KN400_2460, KN400_2674, KN400_2682, KN400_3189, KN400_2738, KN400_1258, KN400_3279, CbcY, PgcA, KN400_2738, CccA and CcpA. Of those identified, we were only able to quantify OmcS, OmcZ, MacA, OmaC and KN400_2682, as the remaining proteins did not meet the minimum requirement of possessing 2 quantified peptides. It should be noted, that the exact EET pathway for *G.*

sulfurreducens is still ambiguous. This is due to the 100 c-type cytochromes contained within *G. sulfurreducens* genome, and because of the number of cytochromes that are expressed under Fe(III) reducing conditions [118, 181].

Of the cytochromes not represented in the model, the genes for KN400_2682, KN400_2674, CbcY, PgcA and CcpA have been reported in previous studies. It was found that the gene GSU2732 homologue to KN400_2674 was significantly downregulated in an OmcF mutant compared to wild type, and it was implicated that OmcF is required for appropriate transcription of genes involved in electricity production [182]. Furthermore, in a study observing differences between current consuming versus current producing cells, the gene GSU2732 was found in higher abundance in current producing cells [183], a finding supported by a previous study showing the gene to be expressed in current producing cells [35]. In a study comparing the metabolic status of cells growing close to an anode electrode versus cells in the outer portion of the anode biofilm, the gene GSU2743 a homologue of KN400_2682 was found to be decreased in the outer biofilm and was said to not play a direct role in EET [184]. A study observing the proteins involved in electron transfer between Fe(III) and Mn(IV) oxides as well as a soluble electron accepter Fe(III) citrate found that the genes GSU2732 (KN400_2674) and PgcA had higher transcript levels higher on growth on Mn(IV) oxide vs soluble Fe(III) citrate however this was not the case with Fe(III) oxide [185]. The cbcY gene that encodes for the Cbc1 enzyme, a enaquinol; ferricytochrome c oxioreductase was found to be downregulated on growth with both Fe(III) and Mn(IV) oxides and the gene that encodes for the periplasmic dihaem cytochrome c peroxidase, ccpA was found to be upregulated on growth with both Fe(III) and Mn(IV) oxides [185].

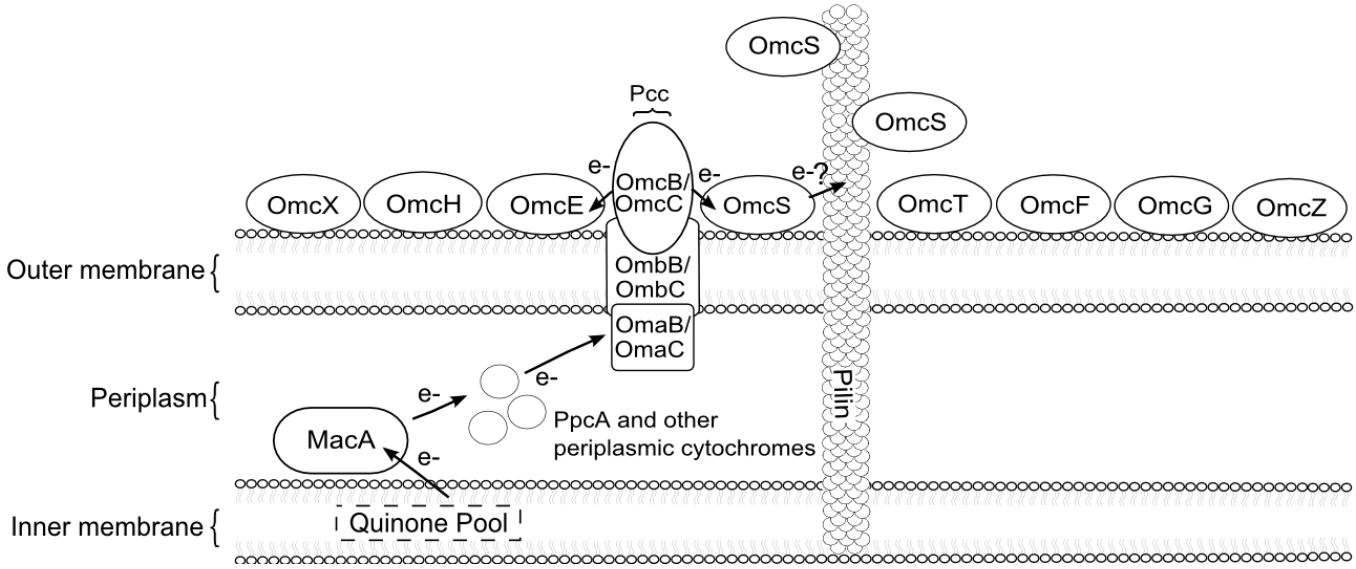

Figure 5.9: A speculative model of the *Geobacter* EET pathway and the location of cytochromes involved in EET. This model is based on suggestions from previous research [23, 31, 33, 161, 162, 171, 181].

The quantification of the cytochrome OmcS shows it to be significantly higher in relative abundance at +0.6 V compared to +0.1 V (log_2FC -2.4). Furthermore, the quantification of the cytochromes OmcZ, MacA and OmaC, show no significant difference in relative abundance between the two potentials (Table 5.4). An additional *c*-type cytochrome, not represented within the model was quantified (KN400_2682) having a log_2FC value of -0.24. In order to explain these findings, the following paragraphs will describe what is presented in the current literature.

Previous research suggests that the cytochrome OmcZ plays an important role in *Geobacter* EET [35, 36, 169]. When observing gene regulation of current producing cells, the *omcZ* gene was found to show the greatest up regulation when compared to biofilms using the soluble electron acceptor fumarate, suggesting OmcZ may have a key function in high current producing biofilms [35]. In addition, deletion of *omcZ* results in a decrease in current production in cells of *G. sulfurreducens* [35]. The OmcZ cytochrome is located at the biofilm-electrode interface of current producing cells [169]. The localisation of OmcZ and the finding that deletion of the *omcZ* gene results in an increase in the resistance of electron transfer between the biofilm and electrode [36], suggests that OmcZ may function as an electrochemical gate, allowing electron transfer from the biofilm to the electrode [169]. SWATH-MS revealed the relative abundance of OmcZ is similar between biofilm samples

grown at both potentials (+0.1 V and +0.6 V). This finding may support the current theory that OmcZ acts as an electrochemical gate, as current production, and EET occurs at both potentials however at different rates (Figure 5.6). This suggests that OmcZ abundance is not regulated by potential nor the rate of EET, and thus may provide a backbone, or a more essential component for EET as well as growth on an electrode in general.

OmcS is an OMC anchored by a transmembrane helix [28], which has been found to be associated with nanowires of *G. sulfurreducens* [173]. OmcS has been found to be important for growth on an electrode [165], with localisation of the protein on the outer membrane indicating the cytochrome behaves terminal electron protein, responsible for transferring electrons to solid external electron acceptors. SWATH-MS analysis revealed OmcS, to be higher in abundance at +0.6 V compared to +0.1 V, suggesting an increase in demand for this protein at higher potential. The presence of OmcS in both biofilm samples grown at +0.1 V and +0.6 V confirms its importance to *G. sulfurreducens* EET, with current production occurring at both these potentials. The higher abundance of the terminal electron protein OmcS at +0.6 V, despite the lower current production, could be a result of *G. sulfurreducens* changing its EET pathway in response to electrode potential. Transcriptomics has uncovered similar findings, with transcript levels of *omcS* found to be lower in current producing anodic biofilms relative to biofilms grown with fumarate as the electron acceptor [35]. Furthermore, this was confirmed with RT-PCR, with transcript levels of *omcS* declining with increasing current production, and deletion of the *omcS* gene showing no effect on current production [35]. The conclusions of the previous and current study suggest an inverse correlation between the relative abundance of OmcS and current production, which justifies the current observations of OmcS abundance between biofilms grown at +0.1 V and +0.6 V. Furthermore, it provides evidence to suggest that OmcS is not important for high current production. Conversely, it has been shown that transcript levels for the gene *omcS* increases as *G. sulfurreducens* colonises the electrode, before steadying and remaining high as current increases [165]. Furthermore, the *omcS* gene shows the highest increase in expression during growth on an electrode compared to growth using a soluble electron acceptor Fe(III) citrate [165]. Deletion of *omcS* has been shown to inhibit current production, which was restored with expression of the gene in *trans*, suggesting the importance of OmcS in electron transfer to an electrode [165]. However, these differences in results could be attributed to electrochemical restrictions limiting current production, as cells from anodic biofilms were harvested once current reached approximately 0.5 mA [165]. Both the study

presented in this PhD nor the previously mentioned study [35], placed any limits on the current generation of the anodic biofilms. The evidence suggests that abundance of OmcS is inversely correlated to the rate of EET. OmcS possesses a broad potential spectrum due to the presence of six heme groups contained within a single polypeptide chain [30]. This versatility allows it to interact with different electron acceptors and allows it to transfer more than one electron at once [30]. One possibility, is that in the absence of other suitable electron transfer proteins, OmcS may be used as the default electron transfer protein. It has been found through RT-PCR that expression of the gene *omcZ* downregulates *omcS* expression [37]. The proteomic results show both OmcS (log_2FC -2.44) and OmcZ (log_2FC -0.25) are higher, or only marginally higher at +0.6 V respectively. Although we provide insufficient evidence to support this finding, it would be of interest to study this detail further using proteomics focusing on the membrane fraction of anodic biofilms.

SWATH-MS detected the cytochromes MacA and OmaC at both potentials (+0.1 and +0.6 V), although differential abundance of these proteins in the biofilms was not evident. The periplasmic *c*-type cytochrome MacA has been found to be more highly expressed in cultures grown on the soluble Fe(III) citrate as an electron acceptor compared to fumarate [172]. The deletion of *macA* results in a significant reduction in the capacity for Fe(III) reduction, suggesting that MacA holds an important role in iron reduction [172]. MacA is a peroxidase which is suggested to transfer electrons to the cytochrome PpcA [163]. Both cytochromes are thought to play a role as periplasmic intermediate electron transfer constituents [163]. OmaC, a periplasmic *c*-type cytochrome, belongs to of one of two known Pcc protein complexes responsible for the transfer of electrons across the outer membrane [33]. It has been shown that deletion of the genes encoding the two Pcc (*ombB-omaB-omcB* and *ombC-omaC-omcC)* reduced *G. sulfurreducens* capacity to reduce Fe(III) citrate and ferrihydrite. However complementation with the functional gene cluster *ombB-omaB-omcB* restored 83% of its ability compared to wild type [33]. These findings confirm the importance of these genes, in the EET process of *G. sulfurreducens*.

The cytochrome KN400_2682 is not described in the literature. The successful identification and quantification of this cytochrome may suggest that it plays an important role in the EET of *G. sulfurreducens* DL-1.

The proteomic results surrounding *G. sulfurreducens* EET proteins support the model, with OmcS, OmcZ, MacA and OmaB all quantified. However, with increased current, we expect to find an increase in EET related proteins, in particular, cytochromes. It may be that unlike *S. oneidensis*, *G. sulfurreducens* may have little modulation and regulation of its EET mechanism at the different potentials investigated here. Also, other cytochromes, such as KN400_2682, may play a role in the EET. It is possible that other proteins are involved in EET that were not detected by this proteomic analysis. Further proteomic experiments comparing the protein expression of *G. sulfurreducens* grown on electrodes at other potentials or compared to a soluble electron acceptor may allow further identification of EET specific proteins.

Involvement of flavins in G. sulfurreducens EET

G. sulfurreducens genome encodes for a flavin biosynthesis pathway, and has recently been observed to secrete flavins during anaerobic growth [54]. SWATH-MS analysis detected RibBA, a riboflavin biosynthesis protein in higher abundance at +0.1 V (log_2FC 0.91) and a flavin sequestration protein (KN400_0171) was identified within the IDA and biofilm samples from both potentials, but was not quantified (Table 5.4 and Appendix C respectively). The higher abundance of RibBA at +0.1 V corresponds to the higher current production at this potential compared to +0.6 V (Figure 5.6). It is possible that *G. sulfurreducens* is preferentially uses flavin as a cofactor for DET, over the use of nanowires as it has been demonstrated that *G. sulfurreducens* uses self-secreted flavins to enhance EET when bound to OMCs [54].

Inability to quantify pilin related proteins

It has been shown that Fe(III) oxides associate with the conductive pili of *G. sulfurreducens,* which are also required for Fe(III) reduction [14]. Hence, one theory is that the pili function as “nanowires” enabling long range electron transfer to Fe(III) oxides. It is suggested that since OmcS is located on the outer membrane, it may not function as a terminal reductase, and rather, may participate in passing electrons to conductive pili or nanowires (Figure 3.1.1) [28]. The pilin related proteins PilA, PilP, PilQ, PilT, PilY1-2 and GspG were detected within the IDA spectral library, however these were not successfully identified or quantified by SWATH-MS analysis. This may be due to the concentration of the pilin peptides being below the limit of detection (LOD) and/or limit of quantitation (LOQ) within the SWATH-MS samples. The LOD and LOQ represent the lowest concentration of measurable peptides in

a sample that can be reliably measured [186]. In addition, the polar and insoluble nature of pilin subunits may hinder their extraction and isolation [187, 188].

The requirement of nanowires for EET appears to be dependent on both the current generated and the thickness of the biofilms. It has been shown that in thick biofilm, generating high current, pili are essential for electron transfer [13] and that pilin are essential for the formation of nanowires [14]. However, in low current biofilms, pilin based nanowires may not be as essential for EET to an electrode [165]. Transcript levels of *pilA* did not appear to be higher in *G. sulfurreducens* during EET with an electrode vs. Fe(III) citrate as the electron acceptor. Furthermore, deletion of *pilA* did not inhibit current production. These findings may be explained by a previous study on low current biofilm that suggests cells of *G. sulfurreducens* form a monolayer of cells on an electrode no more than a few cells thick [52]. These studies indicate that in low current biofilms, the tight connection between cells within this monolayer may eliminate the need for EET over long distances using nanowires. Another explanation may include the recent finding that *S. oneidensis* nanowires are not pilin based, but rather extensions of the outer membrane containing OMCs essential for EET [45]. The absence of pilin related proteins from the proteomic analysis could suggest that pilin are not be responsible for EET, and support other evidence towards a non-pilin based model of the nanowire. However, the absence of pilin protein from the proteomic analysis does not mean that pilin were not present in the sample and that the limitations of the proteomic method, and the insoluble nature of pilin proteins [187, 188] could be used to explain their absence from the analysis. The higher abundance of the OmcS protein at the higher potential (+0.6 V) despite the lower rate of EET is unclear. However, similar findings have been reported previously [35].

Tricarboxylic Acid Cycle

G. sulfurreducens has been shown to oxidize acetate using the TCA cycle [189, 190]. The $\log_2$FC for the proteins of the TCA cycle for the comparison between +0.1 V to +0.6 V anode biofilms were positive (Figure 5.10 and Table 5.4). This indicates a higher abundance of these proteins at +0.1 V and a more active TCA cycle in comparison to +0.6 V. This correlates with the chronoamperometric current density results, with +0.1 V showing significantly higher current production and thus overall metabolic activity than that detected at +0.6 V (Figure 5.6).

Interestingly, SucC was not detected within the biofilm cultures, however two Succinyl CoA:acetate CoA transferases; Ato-1 & Ato-2 were quantified, with log_2FC of 0.75 and 1.6 respectively. The succinyl-CoA:acetate CoA-transferase enzymes replace the succinyl-CoA synthetase enzyme in the TCA cycle by converting succinyl-CoA to succinate [189]. The enzyme Succinyl-CoA synthetase (SucC) has been shown to be absent in *G. sulfurreducens* cultures grown using acetate as the electron donor and fumarate or iron citrate as the electron acceptor [189, 191]. Furthermore, in *G. sulfurreducens* succinate can be produced from succinly CoA in a transferase reaction with acetate accepting the CoA (Succinyl CoA:acetate CoA transferase) [189, 191]. The genome of *G. sulfurreducens* does encode for two Succinyl-CoA synthetases (SucC and SucD) [192]. Reasons for why these enzymes are not detected in previous or in this study are currently unknown. This evidence suggests that the TCA pathway may function in a similar fashion during growth using an electrode compared to using a soluble molecule such as fumarate or iron citrate as the electron acceptor.

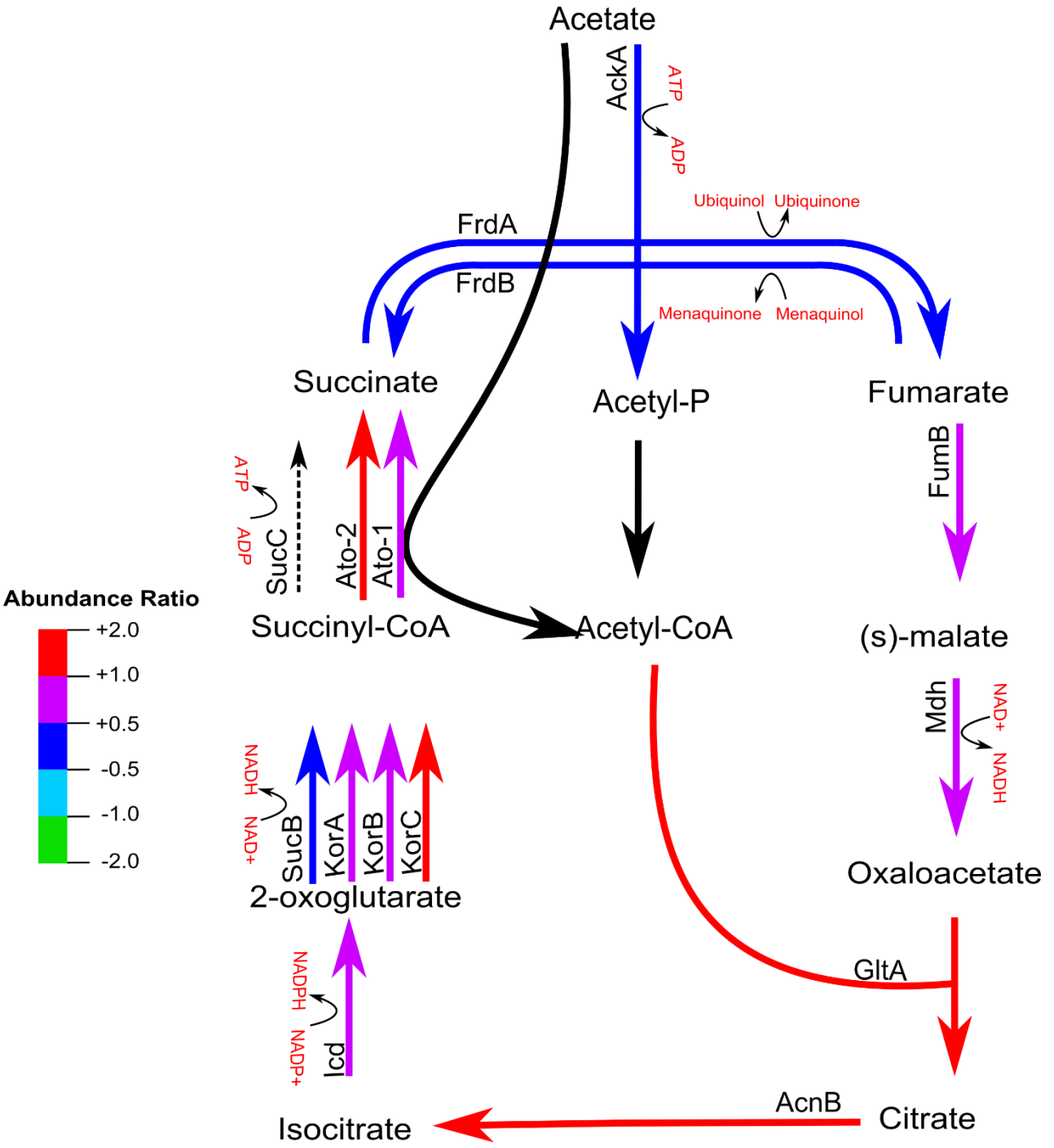

Figure 5.10: Comparative abundance of TCA cycle proteins detected in *Geobacter sulfurreducens* biofilms when grown at +0.1 V and +0.6 V in BESs. The colour coded expression ratios indicate the Log_2 Fold Change occurring between protein abundances in +0.1 V relative to +0.6 V electrode biofilms. Positive values indicate an increase in relative abundance of a protein at +0.1 V and negative values indicate higher abundance at +0.6 V. The dotted arrow indicates the absence of the SucC enzyme. All log_2FC values are significant ($p<0.05$).

Ribosomal proteins

The higher abundant proteins at +0.6 V (negative log_2FC values less than -1.0) were all ribosomal proteins with log_2FC values ranging from -2.65 to -1.63 (Table 5.4). This indicates increased biosynthetic activity of cells grown at +0.6 V, and that *G. sulfurreducens* may be in different states of growth between the two potentials. Similar results were observed with cultures of *S. oneidensis* grown at different potentials (sections 5.1.2 and 5.2.2) and have been reported previously [99]. However, previous studies attribute the increase in biosynthetic activity to higher rates of EET rather than increasing electrode potential for *S. oneidensis* (section 5.2) [99]. Here, a lower rate of EET is observed at +0.6 V, despite a higher abundance of ribosomal proteins. This finding supports the suggestion that the increase in biosynthetic activity may be correlated to the higher potential rather than the rate of EET, the opposite to what has been reported for *S. oneidensis* [99]. A previous study on *S. oneidensis* shows, despite lower growth, an increase in ribosomal gene expression was apparent during anaerobic respiration with an electrode compared to aerobic growth [102]. In addition, a correlation study of previous research on *S. oneidensis* [193] looked at the ribosomal protein expression levels of three different electron acceptors: iron, cobalt and manganese [99]. There was found to be a direct relationship between ribosomal gene expression and the redox potential of each of the solid electron acceptors. These finding provide evidence that the redox potential of the electron acceptor has an influence on the abundance of ribosomal proteins.

Another possible explication could be that ribosome abundance is related to poor growth rather than redox potential. During poor growth, cellular proteins may be degraded as they are not needed or are damaged [6]. It has been shown that *S. oneidensis* protein degradation rates increase at more oxidizing electrode potentials [99]. However, some bacteria have a ribosomal protection system, that modifies ribosomes to protect them from degradation [194]. Proteins involved in this protection system consist of a ribosome modulation factor (RMF), hibernation-promoting factor (HPF) and YfiA protein, a ribosomal subunit interface associated sigma-54 modulation protein (also known as RaiA) [194]. If this is occurring, ribosome abundance would be proportionally larger than that of other cellular proteins. SWATH-MS analysis quantified the abundance of RaiA, and revealed no significant difference in relative abundance between biofilms grown at +0.1 V or +0.6 V. RaiA interferes with protein synthesis by competing for the ribosomal binding sites of tRNAs [195, 196]. Hence, RaiA will only be active during times of stress or starvation when levels

of tRNA are low [85]. This could explain why RaiA is in similar abundance at both potentials, but we still find higher abundance of ribosomal proteins at the stressful, highly oxidising potential of +0.6 V.

A recent study used the marker genes *rplK* and *clpP* to monitor ribosomal production and protein degradation respectively, in biofilms of *S. oneidensis* grown at different electrode potentials [99]. They found that an increase *rplK* expression (or ribosome production) was not correlated to potential, but rather the rate of EET. Furthermore, *clpP* expression (protein degradation) was found correlate with increasing potential. Interestingly, we find ribosome protein abundance to increase with potential rather than EET. We detected the ATP-dependent protease ClpP, however identified no significant difference in abundance of the protein between the two potentials. In addition, a stress responsive alpha/beta domain protein (KN400_2931) and a universal stress protein (Usp-2) both identified showed no significant difference between the two potentials (Table 5.4). However, the periplasmic trypsin-like serine protease (DegP) was in higher abundance at +0.6 V (log_2FC -0.7). The multifunctional DegP protease is responsible for the degradation of denatured and aggregated proteins and also acts as a chaperone in *Escherichia coli* [197]. A higher abundance of DegP at +0.6 V may be indicative of elevated levels of denatured or damaged proteins. It is possible that as suggested previously [99], highly oxidising electrodes may directly damage proteins, including cytochromes involved in EET.

The higher abundance of ribosomal proteins found during lower rates of EET conflicts with the findings of previous studies (section 5.2) [22]. However, we do detect the presence of RaiA, a ribosomal modulation protein at both potentials, which may act to inhibit the degradation of ribosomal proteins. Due to its presence, and its mode of action, we hypothesis that *G. sulfurreducens* may employ this protein to protect ribosomal cells at the oxidative, stress inducing potential of +0.6 V. Furthermore, although we find that the protease ClpP, and the stress response proteins KN400_2931 and Usp-2 show no difference in relative abundance between potentials, we find the protease DegP in higher relative abundance at +0.6 V, suggesting an increased rate of protein degradation at this potential. This finding is further evidence to support the hypothesis that *G. sulfurreducens* experiences stress with protein destabilisation and protection of ribosomal degradation at the higher potential.

Limitations of the proteomic method

Of the studies that monitor the OMCs regulation of *G. sulfurreducens*, most employ transcriptomics as the method of choice [28, 35, 165, 172]. It has been said, that a negative result in proteomics is potentially meaningless [149], as there are a number of potential causes of a negative result. One reason why not all of the OMCs suggested in the model were identified, could be due to the occurrence of regulatory systems at both the transcriptomic and proteomic stages [198] preventing the translation from mRNA through to a mature protein. Furthermore, the inability to quantify a cytochrome could be a result of an inefficient extraction, as cytochromes can differ in their solubility, making some more difficult to isolate than others [148]. On the other hand, it could be due to the limitations of the proteomic method in that the OMCs could still be present, but in amounts lower than the LOD and/or LOQ for the MS technique. If the concentration of the peptides for certain OMCs are below these limits, they will be unable to be identified or quantified. Some other possible causes are; that a peptide of interest might have a modification that disrupts the search result; the dependency on the accuracy of the database being searched; and the efficacy of the digestion of the protein into peptides [150].

Despite the detection of a large number of proteins within the IDA library (Appendix C), only some of the cytochromes represented in *G. sulfurreducens* EET model were detected (Figure 5.9). We did however identify a large number of other cellular proteins. Since several outer membrane proteins were identified within the IDA library, it can be assumed that the problem does not lie with the extraction method employed in this study. However, there are several options available to overcome the limitations of the SWATH-MS technique, in particular, by concentrating on the proteins of interest. One way would be to use selected reaction monitoring technique, which can target specific peptides within a complex protein sample [199, 200]. Another possibility is to focus on the membrane fraction alone. Previous studies were able to detect outer membrane proteins within membrane [34] and extracellular [28] extracts using polyacrylamide gel techniques.

Table 5.4: Summary of statistics for a selection of some relevant proteins detected in this study. log_2FC represents the log_2 fold change in protein abundance between biofilms grown at +0.1 V relative to +0.6 V. Sequence coverage of the identified proteins was taken from the IDA.

Protein ID	Enzyme Name	log_2FC	p-value	Sequence coverage %
EET proteins				
OmcS	Cytochrome c	-2.44	0.000	29.17
OmcZ	Cytochrome c	-0.25	0.609	25.79
MacA	Cytochrome c peroxidase	-0.014	0.784	57.8
OmaC	Cytochrome c	-0.24	0.005	16.02
KN400_2682	Cytochrome c	-0.501	0.079	18.02
RibBA	Riboflavin biosynthesis protein	0.91	0.000	12.75
Tricarboxylic acid cycle				
GltA	Citrate synthase	1.15	0.000	76.42
AcnB	Aconitate hydratase	1.29	0.000	79.81
Icd	NADP-dependent Isocitrate dehydrogenase	0.78	0.000	69.32
SucB	Succinyl transferase component of 2-oxoglutarate dehydrogenase	-0.38	0.017	10.67
FrdA	Succinate dehydrogenase/fumarate reductase, flavoprotein subunit	0.28	0.000	65.31
FrdB	Succinate dehydrogenase/fumarate reductase, iron-sulfur protein	0.27	0.000	42.69
FumB	Fumarate hydratase	0.70	0.000	53.6
Mdh	Malate dehydrogenase	0.84	0.000	88.01
KorA	2-oxoglutarate:ferredoxin oxidoreductase, alpha subunit	0.98	0.000	88.59
KorB	2-oxoglutarate:ferredoxin oxidoreductase, beta subunit	0.97	0.000	77.29

KorC	2-oxoglutarate:ferredoxin oxidoreductase, gamma subunit	1.13	0.001	84.62
Ato-2	Succinyl:acetate coenzyme A transferase	1.58	0.000	27.69
Ato-1	Succinyl:acetate coenzyme A transferase	0.75	0.000	56.12
Ribosomal proteins				
RpsL	30S ribosomal protein S12	-2.65	0.000	28.46
RplE	50S ribosomal protein L5	-2.18	0.000	49.72
RplV	50S ribosomal protein L22	-1.87	0.000	31.53
RplM	50S ribosomal protein L13	-2.92	0.000	41.96
RpsD	30S ribosomal protein S4	-1.35	0.000	33.65
RplJ	50S ribosomal protein L10	-1.13	0.000	56.32
RplR	50S ribosomal protein L18	-1.18	0.000	41.8
RpsP	30S ribosomal protein S16	-1.34	0.000	35.23
RplW	50S ribosomal protein L23	-1.28	0.000	37.23
RplD	50S ribosomal protein L4	-1.85	0.000	55.07
RplN	50S ribosomal protein L14	-1.63	0.000	52.46
RaiA	ribosomal subunit interface associated sigma-54 modulation protein	0.08	0.525	64.09
Stress and degradation				
ClpP	ATP-dependent protease	-0.01	0.859	72.86
KN400_2913	Stress-responsive alpha/beta-barrel domain protein	0.03	0.746	68.75
Usp-2	Universal stress protein	-0.01	0.678	71.14
DegP	Periplasmic trypsin-like serine protease	-0.67	0.000	62.07
SodA	Superoxide dismutase	-0.14	0.000	82.81
CccA	Cytochrome c catalase	-0.36	0.248	29.98

5.3.3 Conclusions

Using a combined approach based on electrochemical and mass spectrometric analysis, we have gained deeper insight into the proteomic response of *G. sulfurreducens* to changes in anodic potential. A higher anodic potential of +0.6 V resulted in lower current production, and a lower rate of EET compared to an anodic potential of +0.1 V which showed a higher rate of EET. This finding suggests that *G. sulfurreducens* is better suited to performing EET at +0.1 V. This is further supported by SWATH-MS which found that proteins of the TCA cycle were in higher relative abundance at +0.1 V, consistent with the increased rate of EET at 0.1 V compared to +0.6 V. Furthermore, the relative abundance of OmcS, a key protein involved in *G. sulfurreducens* EET process was found to be inversely correlated to the rate of EET. This may be a result of *G. sulfurreducens* changing its EET pathway to suit the electrode potential.

Results obtained from proteomic analysis, suggest that riboflavin may play a role in *G. sulfurreducens* EET pathway. The presence of a riboflavin biosynthesis protein was evident at both potentials. In addition, we were unable to quantify pilin related proteins, which may imply that pilin proteins aren't as important to *Geobacter* EET as initially thought. This could be explained by the proposal that *Geobacter* nanowires are not composed of pilin, but, like *Shewanella*, are rather extensions of the outer membrane [45]. However, this suggestion is in contrast to many studies that show the involvement of pilin in *G. sulfurreducens* nanowires [13, 14, 40, 201, 202]. Furthermore, the evidence of flavin biosynthesis at +0.1 V along with a higher rate of EET may suggest the presence of the bound flavin model, were flavins interact with cytochromes to enhance EET [54]. Identifications of cytochromes known to be involved in *G. sulfurreducens* EET pathway, fit the expected model. However, *Geobacter* shows little modularity in its adaption to growth at different electrode potentials.

There is evidence that growth of biofilms at +0.6 V may be stressful to *G. sulfurreducens* cells. At +0.6 V weak signals from the CV analysis and a relative higher abundance of a trypsin like protease (DegP) were observed. Interestingly, a higher abundance of ribosomal

proteins at +0.6 V was detected. This finding along with the presence of a ribosomal modulation protein (RaiA), suggests that *G. sulfurreducens* employs a ribosomal protection mechanism against protein degradation induced by the stressful potential.

The current model of *Geobacter* EET needs to be better understood. Further omic' based studies are imperative to determining the roles and interactions of the proteins involved in EET. To date, there have been no proteomic or transcriptomic studies observing the effects of differing potentials on *Geobacter*, making this study the first of its kind.

5.4 Comparing the response to different electrode potentials between different species of electroactive microorganisms

The sections 5.1 – 5.3 describe the proteomic and electrochemical analysis of electroactive biofilms of two distinct species of DMRB, *S. oneidensis* MR-1 and *G. sulfurreducens* DL-1.

The number of proteins identified within the IDA library were consistent between the two species with 740 (out of a predicted 4,758 [146]) and 704 (out of a predicted 3466 [118]) identified for electroactive biofilms of *S. oneidensis* and *G. sulfurreducens* respectively (false detection rate = 0.01) (Appendix B and C). SWATH-MS analysis revealed 58, 115 and 41 significantly differentially abundant proteins between the comparisons of +0.0 V vs. -0.4 V, +0.5 V vs. -0.4 V and +0.5 V vs. +0.0 V for *S. oneidensis* and 65 significantly differentially abundant proteins between the comparison +0.1V vs. +0.6V for *G. sulfurreducens* ($log_2FC>1$, $p<0.05$).

As the genetic composition of these two microorganisms are unique, we expected to find different proteomic responses at different electrode potentials. For *S. oneidensis*, many of its fundamental EET related proteins were identified, and were found to increase in abundance with applied electrode potential (section 5.2.2 and Figure 5.4). In contrast, a limited number of EET proteins were quantified for G*. sulfurreducens*, one of which (OmcS) was found to increase in abundance at higher electrode potential. The remaining cytochromes detected in the analysis (OmcZ, MacA, OmaC and KN400_2682) showed no, or little change in abundance between different potentials (section 5.3.2 and Table 5.4). These findings show that these microorganisms respond differently to electrode potential at the proteomic level.

The rate of EET for *S. oneidensis* and *G. sulfurreducens* differed in response to electrode potential, with *S. oneidensis* showing higher rates of EET with higher potential (Figure 5.1 and 3.5) and *G. sulfurreducens* showing a decreased rate of EET with a higher potential (Figure 5.6). Since demand for EET proteins would increase with the rate of EET, it would be expected to observe a higher abundance of these proteins with higher rates of EET. This is what was found for *S. oneidensis* (section 5.2.2), however, OmcS, a key EET protein of *G. sulfurreducens* was found to increase in abundance with potential rather than the rate of EET (section 5.3.2). The favourable selection of OmcS may possibly be due to the

unsuitability of other, less versatile cytochromes at this potential, or could be a result of *G. sulfurreducens* changing its EET strategy to suit the electrode potential.

The modularity of *S. oneidensis* to EET at different potentials is evident in electrochemical and proteomic results (section 5.2.2). However, although differences were observed in the electrochemistry for biofilms of *G. sulfurreducens*, only one cytochrome showed evidence of modularity (section 5.3.2). This may suggest that modulation is not as important for *G. sulfurreducens,* and that *Shewanella* is possibly more versatile as it has a more flexible respiratory mechanisms [203] and is found in a larger range of environments [87, 204-210] compared to *Geobacter* [211-214]. However, *Geobacter* does demonstrate regulation of gene expression for EET related genes [35, 165], and changes in abundance of the terminal electron protein OmcS are observed. These unique findings are further evidence that *S. oneidensis* and *G. sulfurreducens* may differ in their electrochemical response to different electrode potentials.

It is established that *S. oneidensis* is capable of secreting flavins (for example, FMN and riboflavin), which it uses to facilitate MET [18, 19, 215]. Previously, self-secreted flavins were not found to be important for *G. sulfurreducens* EET [52]. However, recently it has been shown that *G. sulfurreducens* does secrete flavins to enhance EET [54]. Recent findings propose a bound flavin model for both *S. oneidensis* and *G. sulfurreducens*, where flavins are used as co-factors bound to outer membrane cytochromes [53, 54, 174]. Electrochemical results for *S. oneidensis* reveal that MET is the dominant mode of electron transfer across all potentials tested, with DET playing only a minor role (section 3.3.2.2). UV-HPLC analysis of the reactor medium at the conclusion of the experiment reveal that flavins are present in higher concentrations at -0.4 V in the liquid medium compared to +0.5 V. However, a greater abundance of EET cytochromes, riboflavin biosynthesis protein RibBA and a higher rate of EET was observed at +0.5 V. One possibility for this discrepancy may be explained by the bound flavin model of EET where ‘free’ flavin is captured and bound to OMCs and is therefore at comparatively lower levels in the medium. In addition, *G. sulfurreducens* genome encodes for a flavin biosynthesis pathway, and has recently been observed to excrete flavins during anaerobic growth [54]. A flavin sequestration protein (KN400_0171) was identified and RibBA was found to be relatively higher in abundance in *G. sulfurreducens* biofilms grown at +0.1 V compared to +0.6 V (sections 5.3.2). These findings may relate to the higher current production at this potential, as it has been

suggested that current production is enhanced in the presence of flavins in *S. oneidensis* [18, 53].

Nanowires are proposed to play a role in electron transport for both *S. oneidensis* and *G. sulfurreducens* [10, 14, 40], and were initially described to be 'pilus-like' [10] or composed of pilin proteins [14, 201]. The studies presented in this thesis, present little evidence for the utilisation of pili for *S. oneidensis* nor *G. sulfurreducens* (sections 3.3.2 and 3.3.3). Although pilin related proteins were identified within the IDA library, they were unable to be quantified by SWATH-MS analysis and suggest that pili are not required for *S. oneidensis*, which is supported by the revelation that *S. oneidensis* nanowires are extensions of the outer membrane [45]. Furthermore, the inability of SWATH-MS to quantify pili related proteins in *G. sulfurreducens* biofilms may suggest that pili are not important for *G. sulfurreducens* EET. However, it has previously been suggested that the *G. sulfurreducens* conductive pili and the nanowires of *S. oneidensis* are different in both composition and mechanism of electronic conduction [45, 167, 216].

The majority of proteins showing the greatest log_2FC difference in relative abundance between electrode potentials for *S. oneidensis* and *G. sulfurreducens* were the ribosomal proteins (sections 5.2.2 and 5.3.2). An increase in ribosomal proteins is indicative of an increase in cellular biosynthetic activity. Interestingly, the abundance of ribosomal proteins seems correlated to potential rather than current production or metabolism with both microorganisms showing a higher abundance of ribosomal protein with higher potentials. The observed increase in ribosomal abundance at higher potentials for both *S. oneidensis* and *G. sulfurreducens*, is supported by a study that suggests a direct relationship between ribosomal gene expression and the potential of electron acceptors [99], after reanalysing data from a previous study [193]. However, later it was suggested that *S. oneidensis* ribosomal expression may rather be related to EET and not electrode potential [99]. Current production and marker gene levels of ribosomal expression (*rplK*) over potentials ranging from 0.0 to 0.8 V vs SHE, show that at 0.6 V and 0.8 V vs SHE (0.4 V and 0.6 V vs Ag/AgCl) both current production and *rplK* expression levels decrease [99]. This finding is supported, as neither a decline in current production, nor ribosomal protein abundance at +0.5 V was observed between potentials showing a similar correlation between EET rate and ribosomal expression. These findings indicate that ribosomal levels, thus the biosynthetic activity of the cells increase with EET at electrode potential until the potential reaches a certain limit,

were it has a detrimental effect on the EET activity, and thus a decline in ribosomal levels and biosynthetic activity is observed.

No correlation was observed between ribosomal protein abundance and EET rate for biofilms of *G. sulfurreducens* grown at +0.1 V and +0.6 V. However, a correlation is observed between ribosomal protein abundance and electrode potential. Interestingly, the higher relative abundance of the ribosomal modulation protein RaiA at +0.6 V suggests that *G. sulfurreducens* may protect ribosomal proteins at this highly oxidising potential (section 5.3.2). This finding may explain the higher abundance of ribosomal proteins at +0.6 V despite the lower observed current production.

Metabolic response was similar between the two microorganisms, with both *S. oneidensis* and *G. sulfurreducens* showing an increase in abundance of TCA cycle related proteins with increased current production or EET rate. *S. oneidensis* and *G. sulfurreducens* show a higher rate of EET and a higher abundance of TCA cycle proteins at +0.5 V compared to -0.4 V (section 5.1.2, Figure 5.2) and at +0.1 V compared to +0.6 V (section 5.3.2, Figure 5.9) respectively. Similar metabolic profiles suggest the TCA cycle is important for carbon metabolism and electron flow for both *G. sulfurreducens* and *S. oneidensis* when grown on electrodes at different potentials. An increase in the metabolic turnover of electron source in response to the increased rate of EET caused by favourable electrode potentials is observed. It is possible that this finding may extend to other DMRB grown as anodic biofilms.

The number of proteins identified through SWATH-MS appeared to be consistent between both *S. oneidensis* and *G. sulfurreducens* biofilm samples. Both microorganisms appear to respond differently in their DET mechanisms, however there is evidence that both use flavins to preform EET. The abundance of *S. oneidensis* ribosomal proteins supports the finding that abundance increases with increasing rate of EET. However, ribosomal abundances of *G. sulfurreducens* suggest a correlation with electrode potential rather than the rate of EET. The metabolic responses of the microorganisms appears to be similar, with both showing an increase in abundance of carbon metabolism enzymes in response to higher rates of EET.

6. Conclusions and Recommendations

This thesis describes the effects of different electrode potential on both EET and the physiological response of *Shewanella oneidensis* MR-1 and *Geobacter sulfurreducens* DL-1 anodic biofilms using a combination of electrochemical and molecular techniques. In order to successfully observe the proteomic response of the microorganisms, an appropriate, quantitative proteomic method was required. SWATH-MS is demonstrated as a new cutting edge technique that can be used successfully on biomass limited electrode biofilms to quantitatively compare proteins between samples. Using this newly developed technique, the effects of electrode potential on EET and the physiology of these microorganisms are revealed. Not only is the EET adaptability of *Shewanella oneidensis* MR-1 and *Geobacter sulfurreducens* DL-1 described, but also the physiological response of these microorganisms.

Differences in the modularity of cytochromes involved in EET for S. oneidensis and G. sulfurreducens

Chronoamperometry was used to monitor the rate of EET at different electrode potentials for both *S. oneidensis* and *G. sulfurreducens. S. oneidensis* showed increasing rates of EET with increasing electrode potential, whereas *G. sulfurreducens* responded to an increased potential with a lower rate of EET. However, this might be limited to the potentials studied, as more intermittent potentials may not show the same effect. The importance and adaptability of *S. oneidensis* OMCs (MtrABC and OmcA) in EET to an electrode was confirmed, with an increase in abundance of these cytochromes apparent during higher rates of EET. A different story is observed for *G. sulfurreducens*, with only the cytochrome OmcS affected by the rate of EET caused by the change in potential, while the abundance of OmcZ, MacA, OmaC and the cytochrome KN400_2682 showed no significant difference between potentials in this study. Therefore, as expected, we find the two DMRB adapt differently in their EET response to electrodes of different potentials.

The change in abundance of OmcS is of interest, as it appears that OmcS may not be essential for electron transfer to an electrode [35, 36]. Repeating the study using same potentials used here with an OmcS mutant would help to confirm this suggestion, as well as to aid in deciphering the role of OmcS in *G. sulfurreducens* EET. SWATH-MS was unable to relatively quantify all the OMCs of interest, this included PpcA, OmcB, OmcE, OmcF, OmcG, OmcH, OmcT, OmcX, OmcC, OmaB, OmbB and OmbC. This could be a result of

certain limitations in the proteomic technique. One way to overcome this could be to observe the proteome of the membrane fraction alone, this would allow for greater concentration on membrane associated EET proteins. Another method to improve the resolution on specific outer membrane proteins would be to use a selected reaction monitoring (SRM) technique, which allows targeted proteomic analysis on specific peptides within a complex protein sample [199, 200]. Additionally, it could be beneficial to use a 2D LC-MS approach, where the peptide sample is fractionated by charge using an SCX column, before being analysed through LC-MS/MS. Simplification of the complex peptide mixture through fractionation would allow the detection and identification of the largest number of proteins possible [217, 218]. This method could be used in combination with observing the membrane fraction alone, to provide an even more detailed view. Improved coverage of bacterial proteomes have been previously achieved using SCX fractionation [219, 220].

S. oneidensis requires more changes to adapt to electrode potential compared to G. sulfurreducens

Cytochromes play important roles in both *S. oneidensis* and *G. sulfurreducens* dissimilatory metal reduction processes by facilitating electron transfer from the cytoplasm to the outside of the cell. *S. oneidensis* and *G. sulfurreducens* genomes encode for predicted 42 and 111 c-type cytochromes respectively. The extraordinary number of predicted cytochromes is a reflection of these microorganisms versatility in that they can reduce a wide range of metals, with *Shewanella* possessing the ability to respire using oxidised metals including Mn(III) [87, 221] and Mn(IV), Fe(III)[221], Cr(VI) [222], as well as soluble electron acceptors including fumarate, nitrate, trimethylamine N-oxide, dimethyl sulfoxide, sulphite, thiosulfate and elemental sulphur [2]. *Shewanella is* highly advanced in its ability to exploit its electron accepting capabilities, which is reflected in its distribution in nature. For example, strains of *Shewanella* have been isolated from a wide range of sources including Arctic marine sediment [204], freshwater lakes [87], Antarctic sea ice [205], freshwaters of the Amazon River [206] as well as human clinical samples [207, 208], sea animal intestines [209] and deep sea oil pipelines [210]. *Geobacter* on the other hand, while still versatile in its ability to reduce a wide range of electron acceptors, has been isolated from mainly freshwater sedimentary environments [211-214]. The diverse origins of isolation of *Shewanella* may aid in explaining why we find more response, or flexibility in its ability to adapt to alternative electrode potentials, opposed to *Geobacter* which is found mainly in one type of environment. In addition, it has been shown that *S. oneidensis* contains a modular EET

pathway, possessing many homologs of the major cytochromes known to participate in EET [26]. There are a limited number of studies that discuss the modularity of *Geobacter* EET proteins, however one recent study showed that *G. sulfurreducens* possesses two porin-cytochrome protein complexes, or Pcc, responsible for transferring electrons across the outer membrane [33]. Deletion of the genes encoding the two Pcc (*ombB-omaB-omcB* and *ombC-omaC-omcC)* reduced *G. sulfurreducens* ability to reduce Fe(III) citrate and ferrihydrite. However complementation with just one of the gene clusters (*ombB-omaB-omcB*) restored this ability to 83% of that by the wild type [33]. The study shows the modularity of this particular protein complex within *G. sulfurreducens* EET pathway. It could be speculated that despite the large number of cytochromes encoded in its genome, the *Geobacter* EET pathway may be optimised to very specific environments, and may show limited adaptability or modularity in its ability to adjust to different electrode potentials. However, regulation of EET related genes has been shown at the transcriptional level [35, 165] and Geobacteracea are often found to be the most dominant bacterial species in MFCs using a range of sediment mixed culture inoculums [105-107]. Another way to explain these findings could be that *Geobacter* is so efficient in its abilities to perform EET that it is not required to alter the proteins in the process in order to maintain its EET capability. Furthermore, this PhD thesis does show some evidence of *G. sulfurreducens* adaptability at the proteomic level, with the terminal electron protein OmcS found to change in abundance between potentials. Further evidence to support the greater versatility of *Shewanella* is its motility [119, 129], as opposed to *Geobacter* which is said to be non-motile [223]. This is reflected in the proteomic results presented in this thesis (sections 5.2.2 and 5.3.2) with the identification and quantification of flagellin related proteins present in *S. oneidensis* however absent in *G. sulfurreducens.*

Metabolic activity increases with the rate of EET for both S. oneidensis and G. sulfurreducens

There have been a number of studies that report details of the TCA cycle of *S. oneidensis* [131, 132, 224, 225] and *G sulfurreducens* [189, 226, 227]. However, there are no studies that employ quantitative proteomics to observe the TCA cycle under different environmental or metabolic conditions. This makes the studies presented in this thesis the first of their kind. The conclusion that that both *S. oneidensis* and *G. sulfurreducens* respond in a similar manner metabolically, increasing the use of their TCA cycle with increased EET rate is

presented in this thesis (sections 5.1.2 and 5.3.2). Furthermore, a branching of the *S. oneidensis* TCA cycle is observed, with the reductive branch favoured during higher rates of EET at higher potential. This result is supported by the current literature and therefore, confidence in the results generated through the SWATH-MS method can be established.

Limited proteomic evidence for pilin involvement in EET in anodic biofilms of S. oneidensis and G. sulfurreducens

The studies presented in this thesis offer little proteomic evidence to support the association of pilin protein with nanowires for *S. oneidensis* and *G. sulfurreducens* (sections 5.2.2 and 5.3.2). The inability of SWATH-MS to quantify pilin proteins could suggest that they do not play as pivotal role as what has been initially indicated. The role of pilin in *S. oneidensis* nanowires may not be as important as initially thought, with nanowires found to be extensions of the outer membrane [45]. However, the absence of pilin from the proteomic analysis could be due to one or more limitations of proteomic analysis, with the potential of a number of reasons for obtaining a false negative result [150]. Hence, alternative methods are required to study pilin involvement in EET, as there is much opposing evidence, supporting the role of pilin proteins in *G. sulfurreducens* current production [10, 13, 14], although one transcriptional study did not observe any alteration of *pilA* expression in *G. sulfurreducens* biofilm when grown on an anode compared to a soluble electron acceptor [165]. In addition, deletion of the *pilA* gene in *G. sulfurreducens* strain MA, has been shown to not inhibit the production of proteinaceous filaments [228]. However, Geobacter produces many filaments of which are not nanowires, therefore deletion of a number genes encoding homologs of type II pseudopilins was required to impair filament production [228].

It has been suggested that *G. sulfurreducens* conductive pili and the nanowires of *S. oneidensis* are different in both composition and their mechanism [216]. Hence, the involvement of pilin in *G. sulfurreducens* nanowires seems most likely. In contrast this was not supported by the findings of this study, possibly this may be due to imitations of the proteomic method. As we were able to detect pilin protein within the IDA of both *S. oneidensis* and *G. sulfurreducens* biofilm samples (Appendix B and C respectively), the issue is not with the extraction or protein identification method, but would have more to do with the sensitivity of SWATH-MS quantification or the complexity of the protein sample. If pilin is present within the biofilm at very low amounts, it is possible that the concentration of

pilin peptides are below the LOQ of the method used here. If this is the case, more selective techniques such as SRM, 2D LC-MS or real time RT-qPCR is required may aid in the quantitative identification of pilin in *G. sulfurreducens* nanowires. Further research into how pilin proteins may be involved in the EET process, in particular for *G. sulfurreducens* is required. There are methods available that would allow pilin to be extracted from electroactive biofilms to be studied separately [229]. Isolating and studying pilin proteins separately, would remove the interference that other cellular proteins may cause in different analytical methods, such as those mentioned above. Understanding the structure of nanowires is important for the development of new technologies or bioenergy applications.

Flavin plays an important role for EET in both S. oneidensis and G. sulfurreducens anodic biofilms

There is evidence to suggest that flavins play an important role in both *S. oneidensis* and *G. sulfurreducens* EET with both species showing an increase in relative abundance of the RibA riboflavin biosynthesis protein in biofilms with higher rates of EET. In addition, cyclic voltammograms of *S. oneidensis* attached to an anode reveal that the major mode electron transfer occurs at the potential specified for *S. oneidensis* MET, with only a minor role of DET. Furthermore, flavin was detected within the medium for *S. oneidensis* BES experiments (section 3.3.2.2). Many enzymes require co-factors in order to become active and catalyse a reaction. It has been discovered that two OMCs of *S. oneidensis*, OmcA and MtrC, require a cofactor in the form of a flavin in order to enhance the rate of electron transfer [53, 147] and it is speculated that *G. sulfurreducens* OMCs may operate in a similar fashion [54, 174]. With both *S. oneidensis* and *G. sulfurreducens* being DMRB, and both using cytochromes as their primary method of electron transfer, it may seem natural to assume that they operate in a similar way, both requiring flavins to enhance their EET process. However, further study is required to confirm the role that flavins play in *G.sulfurreducens* EET under the conditions studied in this thesis.

It would be interesting to investigate how the physiological responses of these microorganisms differ between batch versus continuous feed systems. The dominance of MET within an *S. oneidensis* biofilm *w*ithin a continuous fed BES, would be less compared to when grown in a batch system [141]. Furthermore, the majority of flavins present might be bound to EET cytochromes [174]. Without the dominance of MET, it would be interesting to observe how *S. oneidensis* adapts to changes in electrode potential. In addition, it would

be interesting to compare how protein abundance and EET changes in biofilms of *S. oneidensis* grown in batch versus continuous fed BES. The study of how these microorganisms respond to different modes of BES operation would provide information on how to optimise BES performance by enhancing or discouraging certain microbial processes.

Oxidising electrode potential impacts negatively on anodic biofilms of G. sulfurreducens

High oxidising electrode potentials appear to have a damaging effect on anodic biofilms of *G. sulfurreducens* (section 3.3.3.2). This was observed through the weakened signals detected by CV and through the decreased current production at +0.6 V (Figures 3.9 and 3.8 respectively). In addition this finding was supported by quantification of the multi-functional DegP protease, which was found to be higher in abundance at this more oxidizing potential. This suggests an increase in the requirement for protein degradation at +0.6 V which could possibly be a result of an increased presence of damaged or denatured proteins. In the event of “electrode stress”, these could mainly include proteins at the cells surface. It has been shown in the literature, that highly oxidising potentials may directly damage cellular proteins, including cytochromes in *S. oneidensis* [99] which is reflected in the decreased rate of EET at +0.6 V. The current finding provides insight into the tolerance of *G. sulfurreducens* to highly oxidative potential and shows the importance of electrode potential to the optimisation of current production within BESs. As *Geobacter* is a true anaerobe, it would be expected to be significantly affected by oxidative stress. Within highly oxidative environments, modifications to amino acid side chains can occur, which alter protein structure leading to a disturbance to protein function [230]. Furthermore, it has been shown *Escherichia coli* possess proteases that selectively degrade damaged proteins [231], and that damaged proteins are degraded preferentially over normal proteins [232]. One study observed the effects of oxidative damage by adding 2 mM hydrogen peroxide to anaerobic cultures of *E. coli* [233]. Along with a 30% decrease in cell viability, they found oxidative stress resulted oxidative damage to selective proteins such as those involved in glucose catabolism, chaperone function and protein synthesis [233]. Further investigation into examining cell damaging effects at high electrode potential could be facilitated by detecting cell viability through the use of live/dead staining and fluorescence microscopy.

The abundances of Ribosomal proteins is correlated to potential

Both *S. oneidensis* and *G. sulfurreducens* show a relative high abundance of ribosomal proteins at high potential (+0.5 V and +0.6 V) respectively, suggesting that ribosomal abundance is correlated to potential. A direct relationship between levels of ribosomal gene expression and the potential of the electron acceptor has been observed previously [99]. However observation of ribosomal marker gene levels (*rplK*) shows that ribosomal expression is related to the rate EET opposed to electrode potential [99]. The proteomic results from *S. oneidensis* support this finding as we observe an increase in relative abundance of ribosomal proteins with increasing rate of EET. However, proteomic results of *G. sulfurreducens* biofilm indicate the opposite, as we find an increase in the relative abundance of ribosomal proteins with potential rather than EET rate. However, the higher relative abundance of a ribosomal modulation protein at higher potential, may suggest that *G. sulfurreducens* induces a mechanism to protect its ribosomal proteins at highly oxidative potentials. The study in this thesis observes biofilms that are developing and increasing their current generation at the electrode were it appears that protein production is important. It would be interesting to study the protein production of established, stable biofilms to observe how these biofilms respire without protein production.

In order to gain better understanding of both the physiological response and ability of these microorganisms to adapt to changes in electrode potential, it would be beneficial to study a larger range of electrode potentials. Understanding how DMRB respond to changes to the potential of an electron acceptor will help to not only improve the performance of BESs by allowing the selection of electrode potentials suitable for particular microorganisms, but also provide improved fundamental understanding on microbial physiology and EET. There have been several transcriptomic studies performed on biofilms of *S. oneidensis*, some of which provide insight into how *S. oneidensis* adapts to different electron acceptors [102]. In addition, the stress response to changes in electrode potential has been examined through gene expression [99]. A microarray study observing the global gene expression of anodic biofilms of both *S. oneidensis* and *G. sulfurreducens* grown at different electrode potentials would provide information as to how these microorganisms adapt at the transcriptomic level. Although a powerful tool, the microarray technique possesses a number of limitations, including the effect of background hybridisation, the various hybridisation properties of probes and only possessing the ability to investigate transcript levels of specific probes on the array [234]. An alternative method would be to observe gene expression through RNA

sequencing or (RNA-Seq) which has the ability to overcome the limitations associated with microarrays and can identify most RNA molecules within a cell [234]. RNA-Seq analysis would provide a profile of the identity and quantity of RNA levels at any given moment in time. It would be interesting to compare transcriptomic data obtained through techniques, such as a microarray, RNA-Seq or RT- qPCR, to the proteomic data presented in this thesis in order to confirm the current findings. Furthermore, the use of enzyme assays would be useful to verify the proteomic results obtained for the TCA cycle. For example, if available, specific enzyme assays could be used to observe certain reaction steps of the pathway. This tool would be used to verify the higher or lower abundance of the specific enzyme being assayed.

The research presented in this thesis applies both electrochemical and molecular methods which, when performed in parallel, is a powerful tool that provides a deeper understanding of how electrode potential affects both the EET capabilities, and the physiologies of *S. oneidensis* and *G. sulfurreducens* biofilms. The greater understanding we have on the electron transfer capabilities of DMRB, the greater potential we have to be able to exploit this microbial process, thereby enabling us to capture energy generated by these microorganisms to use for the advantage of humankind.

The impact of electrode potential on biofilm development, and whether modes of EET change during biofilm development

Although not studied in this thesis, the structure of biofilms has been observed to change during microbial development on anodes of BESs [39, 81]. In a continuous time trial experiment of pure cultures over 72 hours, differences and similarities of anodic biofilm development between species was detected [81]. Over time it was found that biofilms of *S. oneidensis* and *G. sulfurreducens* became less dense, forming tower structures resulting in less coverage of the electrode, with the formation of channels and a reduction in biofilm mass [81]. The development of *G. sulfurreducens and S. oneidensis* biofilms differed in the formation of towers, which were observed more frequently throughout the biofilm of *G. sulfurreducens*. Another study observed similar findings with aerobic biofilms of *S. oneidensis* attaching and spreading laterally on a glass surface in a continuous flow chamber over 24 hrs before growing vertically and forming tower structures [39]. The biofilms observed in this thesis, were grown in batch BESs and observed during periods of maximum EET at different potentials. It would be interesting to observe whether the

mechanism of EET changes during the development of the biofilm, or how electrode potential effects biofilm development. SWATH-MS would be used to observe adaption of EET mechanisms over time and how electrode potential effects biofilm development. Such information could potentially allow for the optimisation of EET within BESs, through refining biofilm development or the potential at which biofilm is formed. A continuous flow, multi electrode BES could be used to monitor changes in mature biofilms over time. Electrodes could be removed from the BES at set intervals and the proteomics between samples compared.

The impact of electrode surface properties on the physiology and EET capabilities of DMRB

It has been shown that the surface properties of an electrode affect bacterial attachment, biofilm formation as well as EET [235]. Using quantitative proteomics to observe how electrode properties affect the physiology and EET capabilities of an electroactive biofilm, would provide greater insight into the positives and negatives of possible electrode surface properties. Furthermore, it could provide information to aid the optimisation of electrode selection for current production in BESs. Better understanding on how microorganisms adapt to different operational parameters may provide ideas into the optimisation of BES composition and performance.

7. References

[1] Rabaey, K., Rozendal, R. A., Microbial electrosynthesis - revisiting the electrical route for microbial production. *Nat Rev Microbiol* 2010, *8*, 706-716.
[2] Nealson, K. H., Belz, A., McKee, B., Breathing metals as a way of life: geobiology in action. *Antonie Van Leeuwenhoek International Journal of General and Molecular Microbiology* 2002, *81*, 215-222.
[3] Nealson, K., Scott, J., in: Dworkin, M., Falkow, S., Rosenberg, E., Schleifer, K.-H., Stackebrandt, E. (Eds.), *The Prokaryotes.*, Springer New York 2006, pp. 1133-1151.
[4] Mathews, C. K., van Holde, K. E., Ahern, K. G., *Biochemistry*, Benjamin Cummings, San Fransisco 2000.
[5] Madigan, T. M., Martinko, J. M., *Brock biology of microoorganisms*, Prentice Hall, Lebanon, 2005.
[6] Aguilar, C., Nealson, K. H., Biogeochemical cycling of manganese in Oneida Lake, New York: Whole lake studies of manganese. *Journal of Great Lakes Research* 1998, *24*, 93-104.
[7] Aller, R. C., Bioturbation and manganese cycling in hemipelagic sediments. *Philosophical Transactions of the Royal Society of London Series a-Mathematical Physical and Engineering Sciences* 1990, *331*, 51-68.
[8] Canfield, D. E., Thamdrup, B., Hansen, J. W., The anaerobic degredation of organic-matter in danish coastal sediments- iron reduction, manganses reduction, and sulfate reduction. *Geochimica Et Cosmochimica Acta* 1993, *57*, 3867-3883.
[9] Thamdrup, B., Glud, R. N., Hansen, J. W., Manganese oxidation and in-situ manganese fluxes from a coastal sediment. *Geochimica Et Cosmochimica Acta* 1994, *58*, 2563-2570.
[10] Gorby, Y. A., Yanina, S., McLean, J. S., Rosso, K. M., Moyles, D., Dohnalkova, A., Beveridge, T. J., Chang, I. S., Kim, B. H., Kim, K. S., Culley, D. E., Reed, S. B., Romine, M. F., Saffarini, D. A., Hill, E. A., Shi, L., Elias, D. A., Kennedy, D. W., Pinchuk, G., Watanabe, K., Ishii, S. i., Logan, B., Nealson, K. H., Fredrickson, J. K., Electrically conductive bacterial nanowires produced by Shewanella oneidensis strain MR-1 and other microorganisms. *Proceedings of the National Academy of Sciences of the United States of America* 2006, *103*, 11358-11363.
[11] Ringeisen, B. R., Bouhenni, R. A., Vora, G. J., Biffinger, J. C., Shirodkar, S., Brockman, K., Ray, R., Wu, P., Johnson, B. J., Biddle, E. M., Marshall, M. J., Fitzgerald, L. A., Little, B. J., Fredrickson, J. K., Beliaev, A. S., Saffarini, D. A., The role of Shewanella oneidensis MR-1 outer surface structures in extracellular electron transfer. *Electroanal* 2010, *22*, 856-864.
[12] Leung, K. M., Wanger, G., Guo, Q., Gorby, Y., Southam, G., Lau, W. M., Yang, J., Bacterial nanowires: conductive as silicon, soft as polymer. *Soft Matter* 2011, *7*, 6617-6621.
[13] Reguera, G., Nevin, K. P., Nicoll, J. S., Covalla, S. F., Woodard, T. L., Lovley, D. R., Biofilm and nanowire production leads to increased current in Geobacter sulfurreducens fuel cells. *Appl Environ Microb* 2006, *72*, 7345-7348.
[14] Reguera, G., McCarthy, K. D., Mehta, T., Nicoll, J. S., Tuominen, M. T., Lovley, D. R., Extracellular electron transfer via microbial nanowires. *Nature* 2005, *435*, 1098-1101.
[15] Cutruzzola, F., Arese, M., Ranghino, G., van Pouderoyen, G., Canters, G., Brunori, M., Pseudomonas aeruginosa cytochrome C551: probing the role of the hydrophobic patch in electron transfer. *Journal of inorganic biochemistry* 2002, *88*, 353-361.
[16] Liu, J., Qiao, Y., Lu, Z. S., Song, H., Li, C. M., Enhance electron transfer and performance of microbial fuel cells by perforating the cell membrane. *Electrochemistry Communications* 2012, *15*, 50-53.
[17] Pham, T., Boon, N., De Maeyer, K., Höfte, M., Rabaey, K., Verstraete, W., Use of Pseudomonas species producing phenazine-based metabolites in the anodes of microbial fuel cells to improve electricity generation. *Applied Microbiology and Biotechnology* 2008, *80*, 985-993.
[18] Marsili, E., Baron, D. B., Shikhare, I. D., Coursolle, D., Gralnick, J. A., Bond, D. R., Shewanella Secretes flavins that mediate extracellular electron transfer. *Proceedings of the National Academy of Sciences of the United States of America* 2008, *105*, 3968-3973.
[19] von Canstein, H., Ogawa, J., Shimizu, S., Lloyd, J. R., Secretion of flavins by Shewanella species and their role in extracellular electron transfer. *Appl Environ Microb* 2008, *74*, 615-623.

[20] Biffinger, J. C., Pietron, J., Bretschger, O., Nadeau, L. J., Johnson, G. R., Williams, C. C., Nealson, K. H., Ringeisen, B. R., The influence of acidity on microbial fuel cells containing Shewanella oneidensis. *Biosensors & Bioelectronics* 2008, *24*, 900-905.
[21] Venkataraman, A., Rosenbaum, M. A., Perkins, S. D., Werner, J. J., Angenent, L. T., Metabolite-based mutualism between Pseudomonas aeruginosa PA14 and Enterobacter aerogenes enhances current generation in bioelectrochemical systems. *Energy & Environmental Science* 2011.
[22] K. Rabaey, L. T. A., U. Schroder, J. Keller, *Bioelectrochemical Systems: from extracellular electron transfer to biotechnological application.*, IWA Publishing, London 2009.
[23] Shi, L., Squier, T. C., Zachara, J. M., Fredrickson, J. K., Respiration of metal (hydr)oxides by Shewanella and Geobacter: a key role for multihaem c-type cytochromes. *Molecular Microbiology* 2007, *65*, 12-20.
[24] Carmona-Martinez, A. A., Harnisch, F., Fitzgerald, L. A., Biffinger, J. C., Ringeisen, B. R., Schroder, U., Cyclic voltammetric analysis of the electron transfer of Shewanella oneidensis MR-1 and nanofilament and cytochrome knock-out mutants. *Bioelectrochemistry* 2011, *81*, 74-80.
[25] Fredrickson, J. K., Romine, M. F., Beliaev, A. S., Auchtung, J. M., Driscoll, M. E., Gardner, T. S., Nealson, K. H., Osterman, A. L., Pinchuk, G., Reed, J. L., Rodionov, D. A., Rodrigues, J. L., Saffarini, D. A., Serres, M. H., Spormann, A. M., Zhulin, I. B., Tiedje, J. M., Towards environmental systems biology of Shewanella. *Nat Rev Microbiol* 2008, *6*, 592-603.
[26] Gralnick, J. A., Coursolle, D., Modularity of the Mtr respiratory pathway of Shewanella oneidensis strain MR-1. *Molecular Microbiology* 2010, *77*, 995-1008.
[27] Grobbler, C., Virdis, B., Nouwens, A., Harnisch, F., Rabaey, K., Bond, P. L., Use of SWATH mass spectrometry for quantitative proteomic investigation of Shewanella oneidensis MR-1 biofilms grown on graphite cloth electrodes. *Systematic and Applied Microbiology* 2014.
[28] Mehta, T., Coppi, M. V., Childers, S. E., Lovley, D. R., Outer membrane c-type cytochromes required for Fe(III) and Mn(IV) oxide reduction in Geobacter sulfurreducens. *Appl Environ Microbiol* 2005, *71*, 8634-8641.
[29] Nevin, K. P., Lovley, D. R., Lack of production of electron-shuttling compounds or solubilization of Fe(III) during reduction of insoluble Fe(III) oxide by Geobacter metallireducens. *Appl Environ Microb* 2000, *66*, 2248-2251.
[30] Qian, X., Mester, T. n., Morgado, L., Arakawa, T., Sharma, M. L., Inoue, K., Joseph, C., Salgueiro, C. A., Maroney, M. J., Lovley, D. R., Biochemical characterization of purified OmcS, a c-type cytochrome required for insoluble Fe(III) reduction in Geobacter sulfurreducens. *Biochimica et Biophysica Acta (BBA) - Bioenergetics* 2011, *1807*, 404-412.
[31] Shi, L. A., Richardson, D. J., Wang, Z. M., Kerisit, S. N., Rosso, K. M., Zachara, J. M., Fredrickson, J. K., The roles of outer membrane cytochromes of Shewanella and Geobacter in extracellular electron transfer. *Environ. Microbiol. Rep.* 2009, *1*, 220-227.
[32] Mehta, T., Coppi, M. V., Childers, S. E., Lovley, D. R., Outer membrane c-type cytochromes required for Fe(III) and Mn(IV) oxide reduction in Geobacter sulfurreducens. *Appl Environ Microb* 2005, *71*, 8634-8641.
[33] Liu, Y., Wang, Z., Liu, J., Levar, C., Edwards, M. J., Babauta, J. T., Kennedy, D. W., Shi, Z., Beyenal, H., Bond, D. R., Clarke, T. A., Butt, J. N., Richardson, D. J., Rosso, K. M., Zachara, J. M., Fredrickson, J. K., Shi, L., A trans-outer membrane porin-cytochrome protein complex for extracellular electron transfer by Geobacter sulfurreducens PCA. *Environ. Microbiol. Rep.* 2014, *6*, 776-785.
[34] Leang, C., Coppi, M. V., Lovley, D. R., OmcB, a c-type polyheme cytochrome, involved in Fe(III) reduction in Geobacter sulfurreducens. *Journal of Bacteriology* 2003, *185*, 2096-2103.
[35] Nevin, K. P., Kim, B.-C., Glaven, R. H., Johnson, J. P., Woodard, T. L., Methe, B. A., DiDonato, R. J., Jr., Covalla, S. F., Franks, A. E., Liu, A., Lovley, D. R., Anode biofilm transcriptomics reveals outer surface components essential for high density current production in Geobacter sulfurreducens fuel cells. *PLoS One* 2009, *4*.
[36] Richter, H., Nevin, K. P., Jia, H., Lowy, D. A., Lovley, D. R., Tender, L. M., Cyclic voltammetry of biofilms of wild type and mutant Geobacter sulfurreducens on fuel cell anodes indicates possible roles of OmcB, OmcZ, type IV pili, and protons in extracellular electron transfer. *Energy & Environmental Science* 2009, *2*, 506-516.

[37] Park, I., Kim, B. C., Homologous overexpression of omcZ, a gene for an outer surface c-type cytochrome of Geobacter sulfurreducens by single-step gene replacement. *Biotechnol Lett* 2011, *33*, 2043-2048.
[38] Lovley, D. R., Phillips, E. J. P., Lonergan, D. J., Widman, P. K., Fe(III) and S-O reduction by pelobacter carbinolicus. *Appl Environ Microb* 1995, *61*, 2132-2138.
[39] Thormann, K. M., Saville, R. M., Shukla, S., Pelletier, D. A., Spormann, A. M., Initial Phases of biofilm formation in Shewanella oneidensis MR-1. *Journal of Bacteriology* 2004, *186*, 8096-8104.
[40] El-Naggar, M. Y., Wanger, G., Leung, K. M., Yuzvinsky, T. D., Southam, G., Yang, J., Lau, W. M., Nealson, K. H., Gorby, Y. A., Electrical transport along bacterial nanowires from Shewanella oneidensis MR-1. *Proceedings of the National Academy of Sciences of the United States of America* 2010, *107*, 18127-18131.
[41] Vargas, M., Malvankar, N. S., Tremblay, P.-L., Leang, C., Smith, J. A., Patel, P., Synoeyenbos-West, O., Nevin, K. P., Lovley, D. R., Aromatic Amino Acids Required for Pili Conductivity and Long-Range Extracellular Electron Transport in Geobacter sulfurreducens. *mBio* 2013, *4*.
[42] Malvankar, N. S., Vargas, M., Nevin, K., Tremblay, P.-L., Evans-Lutterodt, K., Nykypanchuk, D., Martz, E., Tuominen, M. T., Lovley, D. R., Structural Basis for Metallic-Like Conductivity in Microbial Nanowires. *mBio* 2015, *6*.
[43] Polizzi, N. F., Skourtis, S. S., Beratan, D. N., Physical constraints on charge transport through bacterial nanowires. *Faraday Discussions* 2012, *155*.
[44] Wigginton, N. S., Rosso, K. M., Hochella, M. F., Mechanisms of electron transfer in two decaheme cytochromes from a metal reducing bacterium. *The Journal of Physical Chemistry B* 2007, *111*, 12857-12864.
[45] Pirbadian, S., Barchinger, S. E., Leung, K. M., Byun, H. S., Jangir, Y., Bouhenni, R. A., Reed, S. B., Romine, M. F., Saffarini, D. A., Shi, L., Gorby, Y. A., Golbeck, J. H., El-Naggar, M. Y., Shewanella oneidensis MR-1 nanowires are outer membrane and periplasmic extensions of the extracellular electron transport components. *Proceedings of the National Academy of Sciences* 2014, *111*, 12883-12888.
[46] Rabaey, K., Angenent, L., Schroder, U., Keller, J., *Bioelectrochemical systems : from extracellular electron transfer to biotechnological application*, IWA Publishing, London; New York 2010.
[47] Rabaey, K., Boon, N., Hofte, M., Verstraete, W., Microbial phenazine production enhances electron transfer in biofuel cells. *Environmental Science & Technology* 2005, *39*, 3401-3408.
[48] Rabaey, K., Boon, N., Siciliano, S. D., Verhaege, M., Verstraete, W., Biofuel cells select for microbial consortia that self-mediate electron transfer. *Appl Environ Microb* 2004, *70*, 5373-5382.
[49] Venkataraman, A., Rosenbaum, M., Arends, J. B. A., Halitschke, R., Angenent, L. T., Quorum sensing regulates electric current generation of Pseudomonas aeruginosa PA14 in bioelectrochemical systems. *Electrochemistry Communications* 2010, *12*, 459-462.
[50] Gooderham, W. J., Hancock, R. E., Regulation of virulence and antibiotic resistance by two-component regulatory systems in Pseudomonas aeruginosa. *FEMS Microbiol Rev* 2009, *33*, 279-294.
[51] Venkataraman, A., Rosenbaum, M. A., Werner, J. J., Winans, S. C., Angenent, L. T., Metabolite transfer with the fermentation product 2,3-butanediol enhances virulence by Pseudomonas aeruginosa. *The ISME journal* 2014, *8*, 1210-1220.
[52] Bond, D. R., Lovley, D. R., Electricity production by Geobacter sulfurreducens attached to electrodes. *Appl Environ Microbiol* 2003, *69*, 1548-1555.
[53] Okamoto, A., Hashimoto, K., Nealson, K. H., Nakamura, R., Rate enhancement of bacterial extracellular electron transport involves bound flavin semiquinones. *Proc Natl Acad Sci U S A* 2013, *110*, 7856-7861.
[54] Okamoto, A., Saito, K., Inoue, K., Nealson, K. H., Hashimoto, K., Nakamura, R., Uptake of self-secreted flavins as bound cofactors for extracellular electron transfer in Geobacter species. *Energy & Environmental Science* 2014, *7*, 1357-1361.
[55] Jacobson, K. S., Drew, D. M., He, Z., Use of a liter scale microbial desalination cell as a platform to study bioelectrochemical desalination with salt solution or artificial seawater. *Environmental Science & Technology* 2011, *45*, 4652-4657.

[56] Luo, H., Jenkins, P. E., Ren, Z., Concurrent desalination and hydrogen generation using microbial electrolysis and desalination cells. *Environmental Science & Technology* 2011, *45*, 340-344.
[57] Liu, X. W., Li, W. W., Yu, H. Q., Cathodic catalysts in bioelectrochemical systems for energy recovery from wastewater. *Chemical Society reviews* 2014, *43*, 7718-7745.
[58] Liu, H., Ramnarayanan, R., Logan, B. E., Production of electricity during wastewater treatment using a single chamber microbial fuel cell. *Environ Sci Technol* 2004, *38*, 2281-2285.
[59] Cao, X., Huang, X., Liang, P., Boon, N., Fan, M., Zhang, L., Zhang, X., A completely anoxic microbial fuel cell using a photo-biocathode for cathodic carbon dioxide reduction. *Energy & Environmental Science* 2009, *2*, 498-501.
[60] Fornero, J. J., Rosenbaum, M., Cotta, M. A., Angenent, L. T., Carbon dioxide addition to microbial fuel cellcathodes maintains sustainable catholyte pH and improves anolyte pH, alkalinity, and conductivity. *Environmental Science & Technology* 2010, *44*, 2728-2734.
[61] Tront, J. M., Fortner, J. D., Plotze, M., Hughes, J. B., Puzrin, A. M., Microbial fuel cell technology for measurement of microbial respiration of lactate as an example of bioremediation amendment. *Biotechnol. Lett.* 2008, *30*, 1385-1390.
[62] Morris, J. M., Jin, S., Crimi, B., Pruden, A., Microbial fuel cell in enhancing anaerobic biodegradation of diesel. *Chemical Engineering Journal* 2009, *146*, 161-167.
[63] Morris, J. M., Jin, S., Feasibility of using microbial fuel cell technology for bioremediation of hydrocarbons in groundwater. *Journal of Environmental Science and Health Part a-Toxic/Hazardous Substances & Environmental Engineering* 2008, *43*, 18-23.
[64] Zhang, Y., Angelidaki, I., Submersible microbial fuel cell sensor for monitoring microbial activity and BOD in groundwater: focusing on impact of anodic biofilm on sensor applicability. *Biotechnology and Bioengineering* 2011, *108*, 2339-2347.
[65] Dewan, A., Donovan, C., Heo, D., Beyenal, H., Evaluating the performance of microbial fuel cells powering electronic devices. *Journal of Power Sources* 2010, *195*, 90-96.
[66] Logan, B. E., Hamelers, B., Rozendal, R., Schroder, U., Keller, J., Freguia, S., Aelterman, P., Verstraete, W., Rabaey, K., Microbial Fuel Cells: Methodology and Technology. *Environmental Science & Technology* 2006, *40*, 5181-5192.
[67] Wagner, R. C., Call, D. F., Logan, B. E., Optimal set anode potentials vary in bioelectrochemical systems. *Environmental Science & Technology* 2010, *44*, 6036-6041.
[68] Watson, V. J., Logan, B. E., Power production in MFCs inoculated with Shewanella oneidensis MR-1 or mixed cultures. *Biotechnol Bioeng* 2010, *105*, 489-498.
[69] Ringeisen, B. R., Henderson, E., Wu, P. K., Pietron, J., Ray, R., Little, B., Biffinger, J. C., Jones-Meehan, J. M., High power density from a miniature microbial fuel cell using Shewanella oneidensis DSP10. *Environmental Science & Technology* 2006, *40*, 2629-2634.
[70] Lanthier, M., Gregory, K. B., Lovley, D. R., Growth with high planktonic biomass in Shewanella oneidensis fuel cells. *FEMS microbiology letters* 2008, *278*, 29-35.
[71] Kipf, E., Koch, J., Geiger, B., Erben, J., Richter, K., Gescher, J., Zengerle, R., Kerzenmacher, S., Systematic screening of carbon-based anode materials for microbial fuel cells with Shewanella oneidensis MR-1. *Bioresource technology* 2013, *146*, 386-392.
[72] Popov, A., Kim, J., Dinsdale, R., Esteves, S., Guwy, A., Premier, G., The effect of physico-chemically immobilized methylene blue and neutral red on the anode of microbial fuel cell. *Biotechnol Bioproc E* 2012, *17*, 361-370.
[73] Lowy, D. A., Tender, L. M., Zeikus, J. G., Park, D. H., Lovley, D. R., Harvesting energy from the marine sediment-water interface II. Kinetic activity of anode materials. *Biosens Bioelectron* 2006, *21*, 2058-2063.
[74] Park, D., Kim, S., Shin, I., Jeong, Y., Electricity production in biofuel cell using modified graphite electrode with Neutral Red. *Biotechnol. Lett.* 2000, *22*, 1301-1304.
[75] Guo, K., Chen, X., Freguia, S., Donose, B. C., Spontaneous modification of carbon surface with neutral red from its diazonium salts for bioelectrochemical systems. *Biosensors and Bioelectronics* 2013, *47*, 184-189.
[76] Higgins, S. R., Foerster, D., Cheung, A., Lau, C., Bretschger, O., Minteer, S. D., Nealson, K., Atanassov, P., Cooney, M. J., Fabrication of macroporous chitosan scaffolds doped with carbon nanotubes and their characterization in microbial fuel cell operation. *Enzyme and microbial technology* 2011, *48*, 458-465.

[77] Jourdin, L., Freguia, S., Donose, B. C., Chen, J., Wallace, G. G., Keller, J., Flexer, V., A novel carbon nanotube modified scaffold as an efficient biocathode material for improved microbial electrosynthesis. *Journal of Materials Chemistry A* 2014, *2*, 13093-13102.
[78] Guo, K., Soeriyadi, A. H., Patil, S. A., Prevoteau, A., Freguia, S., Gooding, J. J., Rabaey, K., Surfactant treatment of carbon felt enhances anodic microbial electrocatalysis in bioelectrochemical systems. *Electrochemistry Communications* 2014, *39*, 1-4.
[79] Flexer, V., Marque, M., Donose, B. C., Virdis, B., Keller, J., Plasma treatment of electrodes significantly enhances the development of anodic electrochemically active biofilms. *Electrochimica Acta* 2013, *108*, 566-574.
[80] Toutain CM, C. N., O'Toole GA, *Molecular Basis of Biofilm Development by Pseudomonads.*, ASM Press, Washington 2004.
[81] Read, S. T., Dutta, P., Bond, P. L., Keller, J., Rabaey, K., Initial development and structure of biofilms on microbial fuel cell anodes. *BMC Microbiology* 2010, *10*, 98.
[82] Stewart, P. S., Franklin, M. J., Physiological heterogeneity in biofilms. *Nat Rev Microbiol* 2008, *6*, 199-210.
[83] McLean, J. S., Wanger, G., Gorby, Y. A., Wainstein, M., McQuaid, J., Ishii, S. I., Bretschger, O., Beyenal, H., Nealson, K. H., Quantification of electron transfer rates to a solid phase electron acceptor through the stages of biofilm formation from single cells to multicellular communities. *Environmental Science & Technology* 2010, *44*, 2721-2727.
[84] Torres, C. I., Krajmalnik-Brown, R., Parameswaran, P., Marcus, A. K., Wanger, G., Gorby, Y. A., Rittmann, B. E., Selecting anode respiring bacteria based on anode potential: phylogenetic, electrochemical, and microscopic characterization. *Environmental Science & Technology* 2009, *43*, 9519-9524.
[85] Torres, C. I., Marcus, A. K., Parameswaran, P., Rittmann, B. E., Kinetic experiments for evaluating the Nernst-Monod model for anode-respiring bacteria (ARB) in a biofilm anode. *Environmental Science & Technology* 2008, *42*, 6593-6597.
[86] Angenent, L. T., Rosenbaum, M. A., Bar, H. Y., Beg, Q. K., Segre, D., Booth, J., Cotta, M. A., Shewanella oneidensis in a lactate-fed pure-culture and a glucose-fed co-culture with Lactococcus lactis with an electrode as electron acceptor. *Bioresource technology* 2011, *102*, 2623-2628.
[87] Myers, C. R., Nealson, K. H., Bacterial manganese reduction and growth with manganese oxide as teh sole electron-acceptor. *Science* 1988, *240*, 1319-1321.
[88] Venkateswaran, K., Moser, D. P., Dollhopf, M. E., Lies, D. P., Saffarini, D. A., MacGregor, B. J., Ringelberg, D. B., White, D. C., Nishijima, M., Sano, H., Burghardt, J., Stackebrandt, E., Nealson, K. H., Polyphasic taxonomy of the genus Shewanella and description of Shewanella oneidensis sp. nov. *International Journal of Systematic Bacteriology* 1999, *49*, 705-724.
[89] Bretschger, O., Obraztsova, A., Sturm, C. A., Chang, I. S., Gorby, Y. A., Reed, S. B., Culley, D. E., Reardon, C. L., Barua, S., Romine, M. F., Zhou, J., Beliaev, A. S., Bouhenni, R., Saffarini, D., Mansfeld, F., Kim, B.-H., Fredrickson, J. K., Nealson, K. H., Current production and metal oxide reduction by Shewanella oneidensis MR-1 wild type and mutants. *Appl Environ Microb* 2007, *73*, 7003-7012.
[90] Beliaev, A. S., Saffarini, D. A., McLaughlin, J. L., Hunnicutt, D., MtrC, an outer membrane decahaem c cytochrome required for metal reduction in Shewanella putrefaciens MR-1. *Molecular Microbiology* 2001, *39*, 722-730.
[91] Pitts, K. E., Dobbin, P. S., Reyes-Ramirez, F., Thomson, A. J., Richardson, D. J., Seward, H. E., Characterization of the Shewanella oneidensis MR-1 decaheme cytochrome MtrA: expression in Escherichia coli confers the ability to reduce soluble Fe(III) chelates. *J Biol Chem* 2003, *278*, 27758-27765.
[92] Hartshorne, R. S., Reardon, C. L., Ross, D., Nuester, J., Clarke, T. A., Gates, A. J., Mills, P. C., Fredrickson, J. K., Zachara, J. M., Shi, L., Beliaev, A. S., Marshall, M. J., Tien, M., Brantley, S., Butt, J. N., Richardson, D. J., Characterization of an electron conduit between bacteria and the extracellular environment. *Proceedings of the National Academy of Sciences of the United States of America* 2009, *106*, 22169-22174.
[93] Myers, C. R., Myers, J. M., MtrB is required for proper incorporation of the cytochromes OmcA and OmcB into the outer membrane of Shewanella putrefaciens MR-1. *Appl Environ Microb* 2002, *68*, 5585-5594.

[94] Schwalb, C., Chapman, S. K., Reid, G. A., The tetraheme cytochrome CymA is required for anaerobic respiration with dimethyl sulfoxide and nitrite in Shewanella oneidensis. *Biochemistry* 2003, *42*, 9491-9497.
[95] Gordon, E. H., Pike, A. D., Hill, A. E., Cuthbertson, P. M., Chapman, S. K., Reid, G. A., Identification and characterization of a novel cytochrome c(3) from Shewanella frigidimarina that is involved in Fe(III) respiration. *Biochem J* 2000, *349*, 153-158.
[96] Leys, D., Meyer, T. E., Tsapin, A. S., Nealson, K. H., Cusanovich, M. A., Van Beeumen, J. J., Crystal structures at atomic resolution reveal the novel concept of electron-harvesting as a role for the small tetraheme cytochrome c. *Journal of Biological Chemistry* 2002, *277*, 35703-35711.
[97] Harnisch, F., Freguia, S., A basic tutorial on cyclic voltammetry for the investigation of electroactive microbial biofilms. *Chemistry, an Asian journal* 2012, *7*, 466-475.
[98] Peng, L., You, S.-J., Wang, J.-Y., Electrode potential regulates cytochrome accumulation on Shewanella oneidensis cell surface and the consequence to bioelectrocatalytic current generation. *Biosensors and Bioelectronics* 2010, *25*, 2530-2533.
[99] TerAvest , M. A., Angenent, L. T., Oxidizing electrode potentials decrease current production and coulombic efficiency through cytochrome c inactivation in Shewanella oneidensis MR-1. *ChemElectroChem* 2014, *1*, 2000-2006.
[100] Carmona-Martinez, A. A., Harnisch, F., Kuhlicke, U., Neu, T. R., Schroeder, U., Electron transfer and biofilm formation of Shewanella putrefaciens as function of anode potential. *Bioelectrochemistry* 2013, *93*, 23-29.
[101] Beliaev, A. S., Thompson, D. K., Khare, T., Lim, H., Brandt, C. C., Li, G., Murray, A. E., Heidelberg, J. F., Giometti, C. S., Yates, J., 3rd, Nealson, K. H., Tiedje, J. M., Zhoui, J., Gene and protein expression profiles of Shewanella oneidensis during anaerobic growth with different electron acceptors. *Omics : a journal of integrative biology* 2002, *6*, 39-60.
[102] Rosenbaum, M. A., Bar, H. Y., Beg, Q. K., Segre, D., Booth, J., Cotta, M. A., Angenent, L. T., Transcriptional analysis of Shewanella oneidensis MR-1 with an electrode compared to Fe(III)citrate or oxygen as terminal electron acceptor. *PLoS One* 2012, *7*, e30827.
[103] Nissen, S., Liu, X., Chourey, K., Hettich, R. L., Wagner, D. D., Pfiffner, S. M., Loffler, F. E., Comparative c-type cytochrome expression analysis in Shewanella oneidensis strain MR-1 and Anaeromyxobacter dehalogenans strain 2CP-C grown with soluble and insoluble oxidized metal electron acceptors. *Biochemical Society transactions* 2012, *40*, 1204-1210.
[104] Ross, D. E., Flynn, J. M., Baron, D. B., Gralnick, J. A., Bond, D. R., Towards electrosynthesis in Shewanella: energetics of reversing the Mtr pathway for reductive metabolism. *PLoS One* 2011, *6*.
[105] Tender, L. M., Reimers, C. E., Stecher, H. A., 3rd, Holmes, D. E., Bond, D. R., Lowy, D. A., Pilobello, K., Fertig, S. J., Lovley, D. R., Harnessing microbially generated power on the seafloor. *Nature biotechnology* 2002, *20*, 821-825.
[106] Holmes, D. E., Bond, D. R., O'Neil, R. A., Reimers, C. E., Tender, L. R., Lovley, D. R., Microbial communities associated with electrodes harvesting electricity from a variety of aquatic sediments. *Microbial ecology* 2004, *48*, 178-190.
[107] Jung, S., Regan, J., Comparison of anode bacterial communities and performance in microbial fuel cells with different electron donors. *Applied Microbiology and Biotechnology* 2007, *77*, 393-402.
[108] Krushkal, J., Yan, B., Lovley, D. R., Genome-wide similarity search for transcription factors and their binding sites in a metal-reducing prokaryote Geobacter sulfurreducens. *Biosystems* 2007, *90*, 421-441.
[109] Lovley, D. R., Bond, D. R., Holmes, D. E., Tender, L. M., Electrode-reducing microorganisms that harvest energy from marine sediments. *Science* 2002, *295*, 483-485.
[110] Tender, L. M., Reimers, C. E., Stecher, H. A., Holmes, D. E., Bond, D. R., Lowy, D. A., Pilobello, K., Fertig, S. J., Lovley, D. R., Harnessing microbially generated power on the seafloor. *Nat Biotechnol* 2002, *20*, 821-825.
[111] Lovley, D. R., Holmes, D. E., Bond, D. R., O'Neill, R. A., Reimers, C. E., Tender, L. R., Microbial communities associated with electrodes harvesting electricity from a variety of aquatic sediments. *Microbial ecology* 2004, *48*, 178-190.
[112] Regan, J. M., Jung, S., Comparison of anode bacterial communities and performance in microbial fuel cells with different electron donors. *Applied Microbiology and Biotechnology* 2007, *77*, 393-402.

[113] Schroder, U., Liu, Y., Harnisch, F., Fricke, K., Sietmann, R., Improvement of the anodic bioelectrocatalytic activity of mixed culture biofilms by a simple consecutive electrochemical selection procedure. *Biosensors & Bioelectronics* 2008, *24*, 1006-1011.
[114] Millo, D., Harnisch, F., Patil, S. A., Ly, H. K., Schroder, U., Hildebrandt, P., In situ spectroelectrochemical investigation of electrocatalytic microbial biofilms by surface-enhanced resonance Raman spectroscopy. *Angew Chem Int Ed Engl* 2011, *50*, 2625-2627.
[115] Busalmen, J. P., Esteve-Nunez, A., Feliu, J. M., Whole cell electrochemistry of electricity producing microorganisms evidence an adaptation for optimal exocellular electron transport. *Environmental Science & Technology* 2008, *42*, 2445-2450.
[116] Vowinckel, J., Capuano, F., Campbell, K., Deery, M. J., Lilley, K. S., Ralser, M., The beauty of being (label)-free: sample preparation methods for SWATH-MS and next-generation targeted proteomics *F1000Research* 2014, *2*, 272.
[117] Gillet, L. C., Navarro, P., Tate, S., Rost, H., Selevsek, N., Reiter, L., Bonner, R., Aebersold, R., Targeted Data Extraction of the MS/MS Spectra Generated by Data-independent Acquisition: A New Concept for Consistent and Accurate Proteome Analysis. *Mol Cell Proteomics* 2012, *11*.
[118] Methé, B. A., Nelson, K. E., Eisen, J. A., Paulsen, I. T., Nelson, W., Heidelberg, J. F., Wu, D., Wu, M., Ward, N., Beanan, M. J., Dodson, R. J., Madupu, R., Brinkac, L. M., Daugherty, S. C., DeBoy, R. T., Durkin, A. S., Gwinn, M., Kolonay, J. F., Sullivan, S. A., Haft, D. H., Selengut, J., Davidsen, T. M., Zafar, N., White, O., Tran, B., Romero, C., Forberger, H. A., Weidman, J., Khouri, H., Feldblyum, T. V., Utterback, T. R., Van Aken, S. E., Lovley, D. R., Fraser, C. M., Genome of Geobacter sulfurreducens: metal reduction in subsurface environments. *Science* 2003, *302*, 1967-1969.
[119] Harris, H. W., El-Naggar, M. Y., Nealson, K. H., Shewanella oneidensis MR-1 chemotaxis proteins and electron-transport chain components essential for congregation near insoluble electron acceptors. *Biochemical Society transactions* 2012, *40*, 1167-1177.
[120] Ishii, S. i., Shimoyama, T., Hotta, Y., Watanabe, K., Characterization of a filamentous biofilm community established in a cellulose-fed microbial fuel cell. *BMC Microbiology* 2008, *8*, 6-6.
[121] Kappler, U., Nouwens, A. S., The molybdoproteome of Starkeya novella - insights into the diversity and functions of molybdenum containing proteins in response to changing growth conditions. *Metallomics* 2013, *5*, 325-334.
[122] Choi, M., Chang, C. Y., Clough, T., Broudy, D., Killeen, T., Maclean, B., Vitek, O., MSstats: an R package for statistical analysis of quantitative mass spectrometry-based proteomic experiments. *Bioinformatics* 2014.
[123] Karp, P. D., Paley, S. M., Krummenacker, M., Latendresse, M., Dale, J. M., Lee, T. J., Kaipa, P., Gilham, F., Spaulding, A., Popescu, L., Altman, T., Paulsen, I., Keseler, I. M., Caspi, R., Pathway Tools version 13.0: integrated software for pathway/genome informatics and systems biology. *Brief Bioinform* 2010, *11*, 40-79.
[124] Vizcaino, J. A., Cote, R. G., Csordas, A., Dianes, J. A., Fabregat, A., Foster, J. M., Griss, J., Alpi, E., Birim, M., Contell, J., O'Kelly, G., Schoenegger, A., Ovelleiro, D., Perez-Riverol, Y., Reisinger, F., Rios, D., Wang, R., Hermjakob, H., The Proteomics Identifications (PRIDE) database and associated tools: status in 2013. *Nucleic Acids Res* 2013, *41*, D1063-D1069.
[125] Gupta, N., Benhamida, J., Bhargava, V., Goodman, D., Kain, E., Kerman, I., Nguyen, N., Ollikainen, N., Rodriguez, J., Wang, J., Lipton, M. S., Romine, M., Bafna, V., Smith, R. D., Pevzner, P. A., Comparative proteogenomics: combining mass spectrometry and comparative genomics to analyze multiple genomes. *Genome Res* 2008, *18*, 1133-1142.
[126] Gupta, N., Tanner, S., Jaitly, N., Adkins, J. N., Lipton, M., Edwards, R., Romine, M., Osterman, A., Bafna, V., Smith, R. D., Pevzner, P. A., Whole proteome analysis of post-translational modifications: Applications of mass-spectrometry for proteogenomic annotation. *Genome Res* 2007, *17*, 1362-1377.
[127] Kolker, E., Picone, A. F., Galperin, M. Y., Romine, M. F., Higdon, R., Makarova, K. S., Kolker, N., Anderson, G. A., Qiu, X. Y., Auberry, K. J., Babnigg, G., Beliaev, A. S., Edlefsen, P., Elias, D. A., Gorby, Y. A., Holzman, T., Klappenbach, J. A., Konstantinidis, K. T., Land, M. L., Lipton, M. S., McCue, L. A., Monroe, M., Pasa-Tolic, L., Pinchuk, G., Purvine, S., Serres, M. H., Tsapin, S., Zakrajsek, B. A., Zhou, J. H., Larimer, F. W., Lawrence, C. E., Riley, M., Collart, F. R., Yates, J. R., Smith, R. D., Giometti, C. S., Nealson, K. H., Fredrickson, J. K., Tiedje, J. M., Global profiling of Shewanella oneidensis MR-1: Expression of hypothetical genes and improved functional

annotations. *Proceedings of the National Academy of Sciences of the United States of America* 2005, *102*, 2099-2104.
[128] Romine, M. F., Elias, D. A., Monroe, M. E., Auberry, K., Fang, R. H., Fredrickson, J. K., Anderson, G. A., Smith, R. D., Lipton, M. S., Validation of Shewanella oneidensis MR-1 small proteins by AMT tag-based proteome analysis. *Omics-a Journal of Integrative Biology* 2004, *8*, 239-254.
[129] Harris, H. W., El-Naggar, M. Y., Bretschger, O., Ward, M. J., Romine, M. F., Obraztsova, A. Y., Nealson, K. H., Electrokinesis is a microbial behavior that requires extracellular electron transport. *Proceedings of the National Academy of Sciences of the United States of America* 2010, *107*, 326-331.
[130] Pereira-Medrano, A. G., Knighton, M., Fowler, G. J. S., Ler, Z. Y., Pham, T. K., Ow, S. Y., Free, A., Ward, B., Wright, P. C., Quantitative proteomic analysis of the exoelectxogenic bacterium Arcobacter butzleri ED-1 reveals increased abundance of a flagellin protein under anaerobic growth on an insoluble electrode. *J Proteomics* 2013, *78*, 197-210.
[131] Brutinel, E. D., Gralnick, J. A., Anomalies of the anaerobic tricarboxylic acid cycle in Shewanella oneidensis revealed by Tn-seq. *Molecular Microbiology* 2012, *86*, 273-283.
[132] Tang, Y. J., Meadows, A. L., Kirby, J., Keasling, J. D., Anaerobic central metabolic pathways in Shewanella oneidensis MR-1 reinterpreted in the light of isotopic metabolite Labeling. *Journal of Bacteriology* 2007, *189*, 894-901.
[133] Csonka, L. N., Fraenkel, D. G., Pathways of NADPH formation in Escherichia coli. *Journal of Biological Chemistry* 1977, *252*, 3382-3391.
[134] Voet, D., Voet, J. G., *Biochemsitry*, John Wiley & Sons. Inc, New York 2004.
[135] Scott, J. H., Nealson, K. H., A biochemical-study of the intermediary carbon metabolism of Shewanella putrefaciens. *Journal of Bacteriology* 1994, *176*, 3408-3411.
[136] Tuli, L., Ressom, H. W., LC-MS based detection of differential protein expression. *Journal of proteomics & bioinformatics* 2009, *2*, 416-438.
[137] Cappadona, S., Baker, P. R., Cutillas, P. R., Heck, A. J. R., van Breukelen, B., Current challenges in software solutions for mass spectrometry-based quantitative proteomics. *Amino Acids* 2012, *43*, 1087-1108.
[138] Cho, E. J., Ellington, A. D., Optimization of the biological component of a bioelectrochemical cell. *Bioelectrochemistry* 2007, *70*, 165-172.
[139] Baron, D., LaBelle, E., Coursolle, D., Gralnick, J. A., Bond, D. R., Electrochemical measurement of electron transfer kinetics by Shewanella oneidensis MR-1. *J Biol Chem* 2009, *284*, 28865-28873.
[140] Peng, L., You, S. J., Wang, J. Y., Carbon nanotubes as electrode modifier promoting direct electron transfer from Shewanella oneidensis. *Biosensors & Bioelectronics* 2010, *25*, 1248-1251.
[141] TerAvest, M. A., Rosenbaum, M. A., Kotloski, N. J., Gralnick, J. A., Angenent, L. T., Oxygen allows Shewanella oneidensis MR-1 to overcome mediator washout in a continuously fed bioelectrochemical system. *Biotechnology and Bioengineering* 2014, *111*, 692-699.
[142] Meyer, T. E., Tsapin, A. I., Vandenberghe, I., De Smet, L., Frishman, D., Nealson, K. H., Cusanovich, M. A., Van Beeumen, J. J., Identification of 42 possible cytochrome c genes in the Shewanella oneidensis genome and characterization of six soluble cytochromes. *Omics-a Journal of Integrative Biology* 2004, *8*, 57-77.
[143] Firer-Sherwood, M., Pulcu, G. S., Elliott, S. J., Electrochemical interrogations of the Mtr cytochromes from Shewanella: opening a potential window. *Journal of Biological Inorganic Chemistry* 2008, *13*, 849-854.
[144] Armstrong, F. A., Hirst, J., Reversibility and efficiency in electrocatalytic energy conversion and lessons from enzymes. *Proc Natl Acad Sci U S A* 2011, *108*, 14049-14054.
[145] Uosaki, K. H., H.A.O, Adsorption behaviour of 4,40-bipyridyl at a gold/water interface and its role in the electron transfer reaction between cytochrome c and a gold electrode. *Journal of Electroanalytical Chemistry* 1981, *122*, 321-327.
[146] Heidelberg, J. F., Paulsen, I. T., Nelson, K. E., Gaidos, E. J., Nelson, W. C., Read, T. D., Eisen, J. A., Seshadri, R., Ward, N., Methe, B., Clayton, R. A., Meyer, T., Tsapin, A., Scott, J., Beanan, M., Brinkac, L., Daugherty, S., DeBoy, R. T., Dodson, R. J., Durkin, A. S., Haft, D. H., Kolonay, J. F., Madupu, R., Peterson, J. D., Umayam, L. A., White, O., Wolf, A. M., Vamathevan, J., Weidman, J., Impraim, M., Lee, K., Berry, K., Lee, C., Mueller, J., Khouri, H., Gill, J., Utterback, T. R., McDonald,

L. A., Feldblyum, T. V., Smith, H. O., Venter, J. C., Nealson, K. H., Fraser, C. M., Genome sequence of the dissimilatory metal ion-reducing bacterium Shewanella oneidensis. *Nature biotechnology* 2002, *20*, 1118-1123.
[147] Okamoto, A., Kalathil, S., Deng, X., Hashimoto, K., Nakamura, R., Nealson, K. H., Cell-secreted flavins bound to membrane cytochromes dictate electron transfer reactions to surfaces with diverse charge and pH. *Scientific Reports* 2014, *4*, 5628.
[148] Giometti, C. S., Tale of two metal reducers: comparative proteome analysis of Geobacter sulferreducens PCA and Shewanella oneidensis MR-1. *Methods Biochem Anal* 2006, *49*, 97-111.
[149] Baker, M., Mass spectrometry for biologists. *Nat Meth* 2010, *7*, 157-161.
[150] Matthiesen, R., *Mass Spectrometry Data Analysis in Proteomics*, Humana Press 2007.
[151] Shih, Y.-L., Rothfield, L., The Bacterial Cytoskeleton. *Microbiology and Molecular Biology Reviews* 2006, *70*, 729-754.
[152] Hill, T. L., Microfilament or microtubule assembly or disassembly against a force. *Proceedings of the National Academy of Sciences of the United States of America-Biological Sciences* 1981, *78*, 5613-5617.
[153] Erickson, H. P., Atomic structures of tubulin and FtsZ. *Trends in cell biology* 1998, *8*, 133-137.
[154] Tang, X., Yi, W., Munske, G. R., Adhikari, D. P., Zakharova, N. L., Bruce, J. E., Profiling the membrane proteome of Shewanella oneidensis MR-1 with new affinity labeling probes. *Journal of proteome research* 2007, *6*, 724-734.
[155] ten Brink, F., Schoepp-Cothenet, B., van Lis, R., Nitschke, W., Baymann, F., Multiple Rieske/cytb complexes in a single organism. *Biochimica et Biophysica Acta (BBA) - Bioenergetics* 2013, *1827*, 1392-1406.
[156] Esteve-Nunez, A., Sosnik, J., Visconti, P., Lovley, D. R., Fluorescent properties of c-type cytochromes reveal their potential role as an extracytoplasmic electron sink in Geobacter sulfurreducens. *Environ Microbiol* 2008, *10*, 497-505.
[157] Kato, S., Yumoto, I., Detection of the Na+-translocating NADH-quinone reductase in marine bacteria using a PCR technique. *Canadian Journal of Microbiology* 2000, *46*, 325-332.
[158] Mulrooney, S. B., Hausinger, R. P., Nickel uptake and utilization by microorganisms. *Fems Microbiology Reviews* 2003, *27*, 239-261.
[159] Kotloski, N. J., Gralnick, J. A., Flavin electron shuttles dominate extracellular electron transfer by Shewanella oneidensis. *mBio* 2013, *4*.
[160] Weber, K. A., Achenbach, L. A., Coates, J. D., Microorganisms pumping iron: anaerobic microbial iron oxidation and reduction. *Nat Rev Micro* 2006, *4*, 752-764.
[161] Lovley, D. R., Bug juice: harvesting electricity with microorganisms. *Nat Rev Micro* 2006, *4*, 497-508.
[162] Lovley, D. R., Holmes, D. E., Nevin, K. P., Dissimilatory Fe(III) and Mn(IV) Reduction. *Advances in Microbial Physiology* 2004, *Volume 49*, 219-286.
[163] Seidel, J., Hoffmann, M., Ellis, K. E., Seidel, A., Spatzal, T., Gerhardt, S., Elliott, S. J., Einsle, O., MacA is a second cytochrome c peroxidase of Geobacter sulfurreducens. *Biochemistry* 2012, *51*, 2747-2756.
[164] Lloyd, J. R., Leang, C., Hodges Myerson, A. L., Coppi, M. V., Cuifo, S., Methe, B., Sandler, S. J., Lovley, D. R., Biochemical and genetic characterization of PpcA, a periplasmic c-type cytochrome in Geobacter sulfurreducens. *Biochemical Journal* 2003, *369*, 153-161.
[165] Holmes, D. E., Chaudhuri, S. K., Nevin, K. P., Mehta, T., Methe, B. A., Liu, A., Ward, J. E., Woodard, T. L., Webster, J., Lovley, D. R., Microarray and genetic analysis of electron transfer to electrodes in Geobacter sulfurreducens. *Environmental Microbiology* 2006, *8*, 1805-1815.
[166] Leang, C., Qian, X. L., Mester, T., Lovley, D. R., Alignment of the c-type cytochrome OmcS along pili of Geobacter sulfurreducens. *Appl Environ Microb* 2010, *76*, 4080-4084.
[167] Malvankar, N. S., Vargas, M., Nevin, K. P., Franks, A. E., Leang, C., Kim, B. C., Inoue, K., Mester, T., Covalla, S. F., Johnson, J. P., Rotello, V. M., Tuominen, M. T., Lovley, D. R., Tunable metallic-like conductivity in microbial nanowire networks. *Nature Nanotechnology* 2011, *6*, 573-579.
[168] Reardon, P. N., Mueller, K. T., Structure of the type IVa major pilin from the electrically conductive bacterial nanowires of Geobacter sulfurreducens. *Journal of Biological Chemistry* 2013, *288*, 29260-29266.

[169] Inoue, K., Leang, C., Franks, A. E., Woodard, T. L., Nevin, K. P., Lovley, D. R., Specific localization of the c-type cytochrome OmcZ at the anode surface in current-producing biofilms of Geobacter sulfurreducens. *Environ. Microbiol. Rep.* 2011, *3*, 211-217.
[170] Logan, B. E., Rabaey, K., Conversion of wastes into bioelectricity and chemicals by using microbial electrochemical technologies. *Science* 2012, *337*, 686-690.
[171] Butler, J., Young, N., Lovley, D., Evolution of electron transfer out of the cell: comparative genomics of six Geobacter genomes. *BMC Genomics* 2010, *11*, 40.
[172] Butler, J. E., Kaufmann, F., Coppi, M. V., Núñez, C., Lovley, D. R., MacA, a diheme c-type cytochrome involved in Fe(III) reduction by Geobacter sulfurreducens. *Journal of Bacteriology* 2004, *186*, 4042-4045.
[173] Leang, C., Qian, X., Mester, T., Lovley, D. R., Alignment of the c-type cytochrome OmcS along pili of Geobacter sulfurreducens. *Appl Environ Microb* 2010, *76*, 4080-4084.
[174] Okamoto, A., Nakamura, R., Nealson, K. H., Hashimoto, K., Bound flavin model suggests similar electron transfer mechanisms in Shewanella and Geobacter. *Chemelectrochem* 2014, *1*, 1808-1812.
[175] Barisci, J. N., Wallace, G. G., Chattopadhyay, D., Papadimitrakopoulos, F., Baughman, R. H., Electrochemical properties of single-wall carbon nanotube electrodes. *Journal of the Electrochemical Society* 2003, *150*, E409-E415.
[176] Busalmen, J. P., de Sanchez, S. R., Electrochemical polarization-induced changes in the growth of individual cells and biofilms of Pseudomonas fluorescens (ATCC 17552). *Appl Environ Microb* 2005, *71*, 6235-6240.
[177] Liu, Y., Harnisch, F., Fricke, K., Sietmann, R., Schroder, U., Improvement of the anodic bioelectrocatalytic activity of mixed culture biofilms by a simple consecutive electrochemical selection procedure. *Biosensors & Bioelectronics* 2008, *24*, 1006-1011.
[178] Fricke, K., Harnisch, F., Schroder, U., On the use of cyclic voltammetry for the study of anodic electron transfer in microbial fuel cells. *Energy & Environmental Science* 2008, *1*, 144-147.
[179] Katuri, K. P., Kavanagh, P., Rengaraj, S., Leech, D., Geobacter sulfurreducens biofilms developed under different growth conditions on glassy carbon electrodes: insights using cyclic voltammetry. *Chemical Communications* 2010, *46*, 4758-4760.
[180] Lin, W. C., Coppi, M. V., Lovley, D. R., Geobacter sulfurreducens can grow with oxygen as a terminal electron acceptor. *Appl Environ Microbiol* 2004, *70*, 2525-2528.
[181] Bird, L. J., Bonnefoy, V., Newman, D. K., Bioenergetic challenges of microbial iron metabolisms. *Trends in Microbiology*, *19*, 330-340.
[182] Kim, B.-C., Postier, B. L., DiDonato, R. J., Chaudhuri, S. K., Nevin, K. P., Lovley, D. R., Insights into genes involved in electricity generation in Geobacter sulfurreducens via whole genome microarray analysis of the OmcF-deficient mutant. *Bioelectrochemistry* 2008, *73*, 70-75.
[183] Strycharz, S. M., Glaven, R. H., Coppi, M. V., Gannon, S. M., Perpetua, L. A., Liu, A., Nevin, K. P., Lovley, D. R., Gene expression and deletion analysis of mechanisms for electron transfer from electrodes to Geobacter sulfurreducens. *Bioelectrochemistry* 2011, *80*, 142-150.
[184] Franks, A. E., Nevin, K. P., Glaven, R. H., Lovley, D. R., Microtoming coupled to microarray analysis to evaluate the spatial metabolic status of Geobacter sulfurreducens biofilms. *The ISME journal* 2010, *4*, 509-519.
[185] Aklujkar, M., Coppi, M. V., Leang, C., Kim, B. C., Chavan, M. A., Perpetua, L. A., Giloteaux, L., Liu, A., Holmes, D. E., Proteins involved in electron transfer to Fe(III) and Mn(IV) oxides by Geobacter sulfurreducens and Geobacter uraniireducens. *Microbiology (Reading, England)* 2013, *159*, 515-535.
[186] Armbruster, D. A., Pry, T., Limit of blank, limit of detection and limit of quantitation. *The Clinical Biochemist Reviews* 2008, *29*, S49-S52.
[187] Giltner, C. L., Nguyen, Y., Burrows, L. L., Type IV pilin proteins: versatile molecular modules. *Microbiology and molecular biology reviews : MMBR* 2012, *76*, 740-772.
[188] Craig, L., Pique, M. E., Tainer, J. A., Type IV pilus structure and bacterial pathogenicity. *Nat Rev Microbiol* 2004, *2*, 363-378.
[189] Galushko, A. S., Schink, B., Oxidation of acetate through reactions of the citric acid cycle by Geobacter sulfurreducens in pure culture and in syntrophic coculture. *Archives of Microbiology* 2000, *174*, 314-321.

[190] Mikoulinskaia, O., Akimenko, V., Galouchko, A., Thauer, R. K., Hedderich, R., Cytochrome c-dependent methacrylate reductase from Geobacter sulfurreducens AM-1. *European Journal of Biochemistry* 1999, *263*, 346-352.
[191] Mahadevan, R., Bond, D. R., Butler, J. E., Esteve-Nunez, A., Coppi, M. V., Palsson, B. O., Schilling, C. H., Lovley, D. R., Characterization of metabolism in the Fe(III)-reducing organism Geobacter sulfurreducens by constraint-based modeling. *Appl Environ Microb* 2006, *72*, 1558-1568.
[192] Nagarajan, H., Butler, J. E., Klimes, A., Qiu, Y., Zengler, K., Ward, J., Young, N. D., Methé, B. A., Palsson, B. Ø., Lovley, D. R., Barrett, C. L., De novo assembly of the complete genome of an enhanced electricity producing variant of Geobacter sulfurreducens using only short reads. *PLoS One* 2010, *5*, e10922.
[193] Beliaev, A. S., Klingeman, D. M., Klappenbach, J. A., Wu, L., Romine, M. F., Tiedje, J. M., Nealson, K. H., Fredrickson, J. K., Zhou, J., Global transcriptome analysis of Shewanella oneidensis MR-1 exposed to different terminal electron acceptors. *J Bacteriol* 2005, *187*, 7138-7145.
[194] Polikanov, Y. S., Blaha, G. M., Steitz, T. A., How hibernation factors RMF, HPF, and YfiA turn off protein synthesis. *Science (New York, N.Y.)* 2012, *336*, 915-918.
[195] Vila-Sanjurjo, A., Schuwirth, B. S., Hau, C. W., Cate, J. H., Structural basis for the control of translation initiation during stress. *Nature structural & molecular biology* 2004, *11*, 1054-1059.
[196] Sharma, M. R., Donhofer, A., Barat, C., Marquez, V., Datta, P. P., Fucini, P., Wilson, D. N., Agrawal, R. K., PSRP1 is not a ribosomal protein, but a ribosome-binding factor that is recycled by the ribosome-recycling factor (RRF) and elongation factor G (EF-G). *J Biol Chem* 2010, *285*, 4006-4014.
[197] Jones, C. H., Dexter, P., Evans, A. K., Liu, C., Hultgren, S. J., Hruby, D. E., Escherichia coli DegP protease cleaves between paired hydrophobic residues in a natural substrate: the PapA pilin. *Journal of Bacteriology* 2002, *184*, 5762-5771.
[198] Rogers, S., Girolami, M., Kolch, W., Waters, K. M., Liu, T., Thrall, B., Wiley, H. S., Investigating the correspondence between transcriptomic and proteomic expression profiles using coupled cluster models. *Bioinformatics* 2008, *24*, 2894-2900.
[199] Chang, E. J., Archambault, V., McLachlin, D. T., Krutchinsky, A. N., Chait, B. T., Analysis of protein phosphorylation by hypothesis-driven multiple-stage mass spectrometry. *Analytical chemistry* 2004, *76*, 4472-4483.
[200] Prakash, A., Tomazela, D. M., Frewen, B., Maclean, B., Merrihew, G., Peterman, S., Maccoss, M. J., Expediting the development of targeted SRM assays: using data from shotgun proteomics to automate method development. *Journal of proteome research* 2009, *8*, 2733-2739.
[201] Fitzgerald, L. A., Petersen, E. R., Ray, R. I., Little, B. J., Cooper, C. J., Howard, E. C., Ringeisen, B. R., Biffinger, J. C., Shewanella oneidensis MR-1 Msh pilin proteins are involved in extracellular electron transfer in microbial fuel cells. *Process Biochemistry* 2012, *47*, 170-174.
[202] Lovley, D. R., Long-range electron transport to Fe(III) oxide via pili with metallic-like conductivity. *Biochemical Society transactions* 2012, *40*, 1186-1190.
[203] Jain, A., Connolly, J. O., Woolley, R., Krishnamurthy, S., Marsili, E., Extracellular electron transfer mechanism in Shewanella loihica PV-4 biofilms formed at indium tin oxide and graphite electrodes. *International Journal of Electrochemical Science* 2013, *8*, 1778-1793.
[204] Jensen, M. J., Tebo, B. M., Baumann, P., Mandel, M., Nealson, K. H., Characterization of alteromonas-hanedai (Sp-Nov), a nonfermentative luminous species of marine origin. *Current Microbiology* 1980, *3*, 311-315.
[205] Bowman, J. P., McCammon, S. A., Nichols, D. S., Skerratt, J. H., Rea, S. M., Nichols, P. D., McMeekin, T. A., Shewanella gelidimarina sp. nov. and Shewanella frigidimarina sp. nov., novel Antarctic species with the ability to produce eicosapentaenoic acid (20:5 omega 3) and grow anaerobically by dissimilatory Fe(III) reduction. *International Journal of Systematic Bacteriology* 1997, *47*, 1040-1047.
[206] Venkateswaran, K., Dollhopf, M. E., Aller, R., Stackebrandt, E., Nealson, K. H., Shewanella amazonensis sp. nov., a novel metal-reducing facultative anaerobe from Amazonian shelf muds. *International Journal of Systematic Bacteriology* 1998, *48*, 965-972.
[207] Chen, Y. S., Lin, Y. C., Yen, M. Y., Wang, J. H., Wang, J. H., Wann, S. R., Cheng, D. L., Skin and soft-tissue manifestations of Shewanella putrefaciens infection. *Clinical Infectious Diseases* 1997, *25*, 225-229.

[208] To, K. K. W., Wong, S. S. Y., Cheng, V. C. C., Tang, B. S. F., Li, I. W. S., Chan, J. F. W., Seto, W. K., Tse, H., Yuen, K. Y., Epidemiology and clinical features of Shewanella infection over an eight-year period. *Scandinavian Journal of Infectious Diseases* 2010, *42*, 757-762.
[209] Satomi, M., Oikawa, H., Yano, Y., Shewanella marinintestina sp nov., Shewanella schlegeliana sp nov and Shewanella sairae sp nov., novel eicosapentaenoic-acid-producing marine bacteria isolated from sea-animal intestines. *International Journal of Systematic and Evolutionary Microbiology* 2003, *53*, 491-499.
[210] Pickard, C., Foght, J. M., Pickard, M. A., Westlake, D. W. S., Oil-field and fresh-water isolates of Shewanella putrefaciens have lipopolysaccharide polyacrylamide gel profiles characteristic of marine bacteria. *Canadian Journal of Microbiology* 1993, *39*, 715-717.
[211] Coates, J. D., Phillips, E. J. P., Lonergan, D. J., Jenter, H., Lovley, D. R., Isolation of Geobacter species from diverse sedimentary environments. *Appl Environ Microb* 1996, *62*, 1531-1536.
[212] Shelobolina, E. S., Vrionis, H. A., Findlay, R. H., Lovley, D. R., Geobacter uraniireducens sp nov., isolated from subsurface sediment undergoing uranium bioremediation. *International Journal of Systematic and Evolutionary Microbiology* 2008, *58*, 1075-1078.
[213] Lovley, D. R., Stolz, J. F., Nord, G. L., Phillips, E. J. P., Anaerobic production of magnetite by a dissimilatory iron-reducing microorganism. *Nature* 1987, *330*, 252-254.
[214] Straub, K., in: Reitner, J., Thiel, V. (Eds.), *Encyclopedia of Geobiology*, Springer Netherlands 2011, pp. 412-413.
[215] Coursolle, D., Baron, D. B., Bond, D. R., Gralnick, J. A., The Mtr respiratory pathway is essential for reducing flavins and electrodes in Shewanella oneidensis. *Journal of Bacteriology* 2010, *192*, 467-474.
[216] Lovley, D. R., Malvankar, N. S., Seeing is believing: novel imaging techniques help clarify microbial nanowire structure and function. *Environ Microbiol* 2014.
[217] Chan, K., Issaq, H., in: Zhou, M., Veenstra, T. (Eds.), *Proteomics for Biomarker Discovery*, Humana Press 2013, pp. 311-315.
[218] Walther, T. C., Mann, M., Mass spectrometry–based proteomics in cell biology. *The Journal of Cell Biology* 2010, *190*, 491-500.
[219] Manes, N. P., Gustin, J. K., Rue, J., Mottaz, H. M., Purvine, S. O., Norbeck, A. D., Monroe, M. E., Zimmer, J. S., Metz, T. O., Adkins, J. N., Smith, R. D., Heffron, F., Targeted protein degradation by Salmonella under phagosome-mimicking culture conditions investigated using comparative peptidomics. *Mol Cell Proteomics* 2007, *6*, 717-727.
[220] Mostovenko, E., Hassan, C., Rattke, J., Deelder, A. M., van Veelen, P. A., Palmblad, M., Comparison of peptide and protein fractionation methods in proteomics. *EuPA Open Proteomics* 2013, *1*, 30-37.
[221] Nealson, K. H., Saffarini, D., Iron and manganese in anaerobic respiration- environmental significance, physisology, and regulation. *Annual Review of Microbiology* 1994, *48*, 311-343.
[222] Myers, C. R., Carstens, B. P., Antholine, W. E., Myers, J. M., Chromium(VI) reductase activity is associated with the cytoplasmic membrane of anaerobically grown Shewanella putrefaciens MR-1. *Journal of Applied Microbiology* 2000, *88*, 98-106.
[223] Caccavo, F., Lonergan, D. J., Lovley, D. R., Davis, M., Stolz, J. F., McInerney, M. J., Geobacter sulfurreducens sp-nov, a hydrogen-oxidizing and acetate-oxidising dissimilatory metal-reducing microorganism. *Appl Environ Microb* 1994, *60*, 3752-3759.
[224] Tang, Y. J., Hwang, J. S., Wemmer, D. E., Keasling, J. D., Shewanella oneidensis MR-1 fluxome under various oxygen conditions. *Appl Environ Microb* 2007, *73*, 718-729.
[225] Pinchuk, G. E., Hill, E. A., Geydebrekht, O. V., De Ingeniis, J., Zhang, X., Osterman, A., Scott, J. H., Reed, S. B., Romine, M. F., Konopka, A. E., Beliaev, A. S., Fredrickson, J. K., Reed, J. L., Constraint-based model of Shewanella oneidensis MR-1 metabolism: A tool for data analysis and hypothesis generation. *Plos Computational Biology* 2010, *6*.
[226] Segura, D., Mahadevan, R., Juárez, K., Lovley, D. R., Computational and experimental analysis of redundancy in the central metabolism of Geobacter sulfurreducens. *PLoS Computational Biology* 2008, *4*, e36.
[227] King, E. L., Tuncay, K., Ortoleva, P., Meile, C., In silico Geobacter sulfurreducens metabolism and Its representation in reactive transport models. *Appl Environ Microb* 2009, *75*, 83-92.

[228] Klimes, A., Franks, A. E., Glaven, R. H., Tran, H., Barrett, C. L., Qiu, Y., Zengler, K., Lovley, D. R., Production of pilus-like filaments in Geobacter sulfurreducens in the absence of the type IV pilin protein PilA. *FEMS microbiology letters* 2010, *310*, 62-68.
[229] Collinson, S. K., Emödy, L., Müller, K. H., Trust, T. J., Kay, W. W., Purification and characterization of thin, aggregative fimbriae from Salmonella enteritidis. *Journal of Bacteriology* 1991, *173*, 4773-4781.
[230] Cabiscol, E., Tamarit, J., Ros, J., Oxidative stress in bacteria and protein damage by reactive oxygen species. *International microbiology : the official journal of the Spanish Society for Microbiology* 2000, *3*, 3-8.
[231] Davies, K. J. A., Lin, S. W., Degredation of oxidativly denatured proteins in Escherichia coli. *Free Radical Biology and Medicine* 1988, *5*, 215-223.
[232] Stadtman, E. R., Covalent modification reactions are marking steps in protein turnover. *Biochemistry* 1990, *29*, 6323-6331.
[233] Tamarit, J., Cabiscol, E., Ros, J., Identification of the major oxidatively damaged proteins in Escherichia coli cells exposed to oxidative stress. *Journal of Biological Chemistry* 1998, *273*, 3027-3032.
[234] Marioni, J. C., Mason, C. E., Mane, S. M., Stephens, M., Gilad, Y., RNA-seq: An assessment of technical reproducibility and comparison with gene expression arrays. *Genome Res* 2008, *18*, 1509-1517.
[235] Guo, K., Freguia, S., Dennis, P. G., Chen, X., Donose, B. C., Keller, J., Gooding, J. J., Rabaey, K., Effects of surface charge and hydrophobicity on anodic biofilm formation, community composition, and current generation in bioelectrochemical systems. *Environmental Science & Technology* 2013, *47*, 7563-7570.

Appendix A- Publication

G Model
SYAPM-25668; No. of Pages 5
ARTICLE IN PRESS

Systematic and Applied Microbiology xxx (2014) xxx–xxx

Contents lists available at ScienceDirect

Systematic and Applied Microbiology

journal homepage: www.elsevier.de/syapm

Short Communication

Use of SWATH mass spectrometry for quantitative proteomic investigation of *Shewanella oneidensis* MR-1 biofilms grown on graphite cloth electrodes

Christy Grobbler[a], Bernardino Virdis[b], Amanda Nouwens[c], Falk Harnisch[d], Korneel Rabaey[e], Philip L. Bond[a,c,*]

[a] The University of Queensland, Advanced Water Management Centre, St. Lucia, QLD 4072, Australia
[b] The University of Queensland, Centre for Microbial Electrosynthesis, St. Lucia, QLD 4072, Australia
[c] The University of Queensland, School of Chemical and Molecular Biosciences, St. Lucia, QLD 4072, Australia
[d] Department of Environmental Microbiology, UFZ – Helmholtz Centre for Environmental Research, Leipzig, Germany
[e] Laboratory of Microbial Ecology and Technology, Faculty of Bioscience Engineering, Coupure Links 653, B-9000 Ghent, Belgium

ARTICLE INFO

Article history:
Received 4 September 2014
Received in revised form
17 November 2014
Accepted 19 November 2014

Keywords:
Bioelectrochemical system
Electroactive biofilms
Proteomics
Shewanella oneidensis MR1
SWATH-MS

ABSTRACT

Quantitative proteomics from low biomass, biofilm samples is not well documented. In this study we show successful use of SWATH-MS for quantitative proteomic analysis of a microbial electrochemically active biofilm. *Shewanella oneidensis* MR-1 was grown on carbon cloth electrodes under continuous anodic electrochemical polarizations in a bioelectrochemical system (BES). Using lactate as the electron donor, anodes serving as terminal microbial electron acceptors were operated at three different electrode potentials (+0.71 V, +0.21 V & −0.19 V vs. SHE) and the development of catalytic activity was monitored by measuring the current traces over time. Once maximum current was reached (usually within 21–29 h) the electrochemical systems were shut off and biofilm proteins were extracted from the electrodes for proteomic assessment. SWATH-MS analysis identified 704 proteins, and quantitative comparison was made of those associated with tricarboxcylic acid (TCA) cycle. Metabolic differences detected between the biofilms suggested a branching of the *S. oneidensis* TCA cycle when grown at the different electrode potentials. In addition, the higher abundance of enzymes involved in the TCA cycle at higher potential indicates an increase in metabolic activity, which is expected given the assumed higher energy gains. This study demonstrates high numbers of identifications on BES biofilm samples can be achieved in comparison to what is currently reported. This is most likely due to the minimal preparation steps required for SWATH-MS.

Introduction

Bioelectrochemical systems (BESs) exploit microbial oxidation and reduction reactions to catalyse extracellular electron transfer (EET) and cause electron flow between an anode and a cathode [22]. Currently, there is great interest around EET research, as BESs have many potential applications, including bioremediation and production of valuable chemicals and fuels [22]. The more common microorganisms found to proliferate in BES anodic compartments are dissimilatory metal reducing bacteria [11]. For an oxidation process at an anode, dissimilatory metal reducing bacteria harness the energy generated through the oxidation of simple substrates (e.g. fatty acids) and the transfer of electrons to the anode electrode [19]. Here they form biofilms on anodes that perform EET and provide the current to the BES [23].

Shewanella and *Geobacter* species are the most intensively studied bacteria for extracellular respiration in BES. Both are known to respire using solid electron acceptors by passing electrons through redox-proteins dominated by c-type cytochromes for EET [27]. *Shewanella oneidensis MR-1* is extremely versatile in that it has the ability to reduce a wide array of electron acceptors [18,30]. It has 42

Abbreviations: BES, bioelectrochemical systems; EET, extracellular electron transfer; TCA, tricarboxylic acid; IDA, information dependent acquisition; NADP, nicotinamide adenine dinucleotide phosphate; NAD, nicotinamide adenine dinucleotide; SHE, standard hydrogen electrode; KCl, potassium chloride; NCBI, National Center for Biotechnology Information.

* Corresponding author at: Advanced Water Management Centre, The University of Queensland, Office 410, Level 4 Gerhmann Building (60), Brisbane, QLD 4072, Australia. Tel.: +61 07 33463226; fax: +61 0733654726.
E-mail addresses: c.grobbler@uq.edu.au (C. Grobbler), phil.bond@awmc.uq.edu.au (P.L. Bond).

http://dx.doi.org/10.1016/j.syapm.2014.11.007
0723-2020/

Please cite this article in press as: C. Grobbler, et al., Use of SWATH mass spectrometry for quantitative proteomic investigation of *Shewanella oneidensis* MR-1 biofilms grown on graphite cloth electrodes, Syst. Appl. Microbiol. (2014), http://dx.doi.org/10.1016/j.syapm.2014.11.007

possible c-type cytochromes [16] and it is apparent that alternative cytochromes are used within its respiration pathways, indicating modularity of the electron transfer mechanisms of *S. oneidensis* [7]. There is much interest in the electron transfer mechanisms of *S. oneidensis* with a recent study proposing that nanowires are extensions of the outer membrane and periplasim and containing key cytochromes involved for EET [21]. There have been several proteogenomic studies conducted on *Shewanella* [8,9,14,24]. However, these studies focus specifically on proteomics with the aim to improve annotation of the genome and are not comparative in that they do not study *Shewanella* under different conditions.

Within the scope of BES, many studies to date combine electrochemical aspects, e.g. growing active biofilm and optimising current production, with microbial physiology. A recent study demonstrated biofilms of *Shewanella putrefaciens* produced more current and more biofilm with increasing anode potential [2]. Other studies also reveal a strong effect of the anode potential on EET [10,15]. Consequently, there is great interest to study the proteomic basis of the adaptation of the model organism *Shewanella oneidensis* MR-1 to different electrode potentials.

Recent molecular investigations of BES biofilms have aimed to determine the mechanistic details of the EET process [4,13,17,25]. For example, examination of *S. oneidensis* gene expression discovered that up-regulation of genes coding for certain respiratory proteins (*mtrABC*, *omA* and *cctA*) occurred when using an electrode as opposed to oxygen or iron citrate as the terminal electron acceptor [25]. Recently, the first quantitative proteomic study was performed to determine details of EET [20]. Protein abundances of *Arcobacter butzleri ED-1* using either oxygen or a BES electrode as the terminal electron acceptor were compared [20]. Notable findings were that two novel cytochromes, potentially involved in EET, and flagellin were upregulated during growth on the electrode. These initial yet pioneering studies applying 'omic (including genomic, proteomic, transcriptomic or metabolomic) approaches are providing unique insight into the mechanisms of EET.

Further application of proteomics could be utilised to reveal metabolic and physiological details of the microorganisms performing EET. However, BESs are often operated at a small scale for convenience and to simplify operation. This becomes problematic for proteomic studies that require enough biomass for adequate protein extraction, especially for quantitative analyses. Indeed it was apparent that cell biomass levels were a problem in the *Arcobacter* study mentioned above [20], as replicate electrode samples were pooled for quantitative iTRAQ analysis, and relatively low numbers of unique proteins were detected, ranging from 115 to 233, from any particular sample. Consequently, these shortfalls limit the outcomes of proteomic investigations of electroactive biofilms in BES.

SWATH-MS is a recently developed approach that provides extensive label-free quantitation of the measurable peptide ions in a sample [33]. The approach rapidly acquires high resolution Q-TOF mass spectrometer data through repeated analysis of sequential isolation windows (swaths) throughout the chromatographic elution range [6]. Of the few reports on the use of SWATH-MS for bacterial proteomics, to our knowledge this is the first to use the method on low biomass electrode biofilms.

Here we compared the proteome of *S. oneidensis* to detect functional differences while growing on an anodic electrode at different potentials. We show successful quantitative proteomic analysis of the anodic *Shewanella* biofilm samples using SWATH-MS without the need for fractionation, labelling or other procedures that can contribute to protein losses. Furthermore, as a result of the high numbers of identifications and quantitative data obtained from this study, we propose this procedure is very well suited for proteomic studies of low biomass biofilms.

Materials and methods

Three sterile BESs were assembled under anaerobic conditions and filled with a defined minimal medium for all experiments using 18 mM of lactate as the electron donor, carbon cloth as the electron acceptor and titanium wire as the counter electrode (refer to Supplementary Information for details of BESs operation). Each BES was inoculated with *S. oneidensis* at a constant OD_{600}. All experiments were conducted in triplicate anaerobically under potentiostatic control using the Ag/AgCl reference electrode (3M KCl, BASi (USA)) at 30 °C. *S. oneidensis* biofilms were grown at the anodes of bioelectrochemical reactors polarised at +0.71, +0.21 and −0.19 V vs SHE. These batch chronoaperometric experiments continued until near maximum currents were produced (Fig. 1A). Anodic electrodes were then removed from replicate BES reactors under anaerobic conditions and stored at −80 °C. Used medium was filtered and analysed for lactate and acetate concentration using HPLC (see the Supplementary Information for details).

Protein extractions were performed to maximise protein yield from the whole electrodes containing biofilms. Precise details are described in the Supplementary Information. In brief, electrodes were submerged in extraction buffer and subjected to three freeze/thaw cycles and sonicated to further lyse cells. The electrode was rinsed with additional extraction buffer which was combined with the cell lysate. The extraction solutions were centrifuged to remove cell debris and proteins were then precipitated. Protein was recovered through centrifugation, washed in cold acetone and resuspended in buffer. Total resuspended protein was quantified then reduced, alkylated and digested.

Following purification, 1 μg from each digested protein sample was used for SWATH-MS analyses. Additional 2 μg aliquots of each sample were pooled in duplicate to create a spectral library using IDA mode mass spectrometry. Samples were analysed using a Triple-Tof5 600 instrument (ABSciex). Mass spectrometry (MS) data from IDA analyses were combined and searched using ProteinPilot software v4.5 (ABSciex, Forster City CA) a database of *Shewanella oneidensis* MR-1 specific proteins acquired from NCBI on the 28th May 2012 containing 4052 entries. A decoy database containing reversed protein sequences was used to determine the false discovery rate of identifications. The IDA spectral library, protein sequences and SWATH MS data were loaded into PeakView software v1.2 for processing. The MSstats program [3] was used for statistical analysis of the acquired spectra and Pathway Tools [12] was used to visualise the statistical data on metabolic pathways of *S. oneidensis*.

Results and discussion

During operation of the BES, current production by *S. oneidensis* in the BES increased over time for all the anodic potentials of +0.71 V, +0.21 V and −0.19 V (SHE) (Fig. 1A). Higher current densities were achieved at anodes poised at higher potentials. The amounts of protein extracted from the electrode biofilms were consistent between replicates, with higher amounts obtained from the electrodes at higher potentials (Fig. 1B).

A total of 740 unique proteins were identified within the library acquired by information dependant acquisition (IDA) with a false detection rate of 0.01 calculated using a Paragon method within the ProteinPilot software. Of these unique proteins SWATH-MS analysis detected 704 in each biofilm sample. The number of significantly different ($p < 0.05$) abundant proteins was determined between pairwise comparisons of the BES biofilms developed at the different potentials. There were 58, 115 and 41 differentially abundant proteins between the comparisons of +0.21 V to −0.19 V, +0.71 V to −0.19 V and +0.71 V to +0.21 V respectively ($\log_2 FC > 1$, $p < 0.05$).

Please cite this article in press as: C. Grobbler, et al., Use of SWATH mass spectrometry for quantitative proteomic investigation of *Shewanella oneidensis* MR-1 biofilms grown on graphite cloth electrodes, Syst. Appl. Microbiol. (2014), http://dx.doi.org/10.1016/j.syapm.2014.11.007

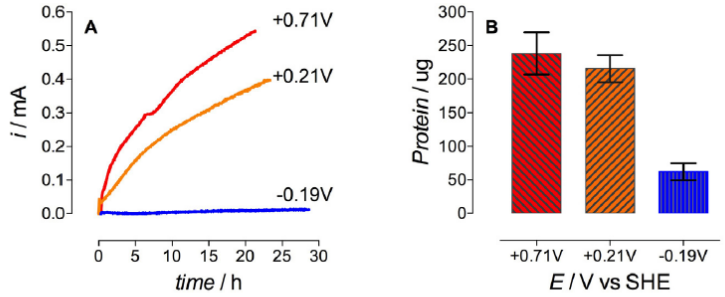

Fig. 1. Profiles of current production from *Shewanella oneidensis MR-1* at different anode potentials within the BES over time (A). Amounts of protein extracted from electrode biofilms of *S. oneidensis* after BES operation at different anode potentials (error bars indicate standard deviation) (B).

The greatest number of significantly different abundant proteins was between electrode biofilms at the potentials of +0.71 and −0.19 V. The TCA cycle is an essential metabolic pathway enabling energy generation and synthesis for many microorganisms. Consequently, to demonstrate detection of metabolic differences we focused on comparison of proteins involved in the bacterial TCA cycle at these electrode potentials (Fig. 2). Although the TCA cycle typically operates under aerobic conditions, *S. oneidensis* has been shown to use this pathway partially during anaerobic respiration coupled to alternative electron acceptors such as fumarate and TMAO [1,28].

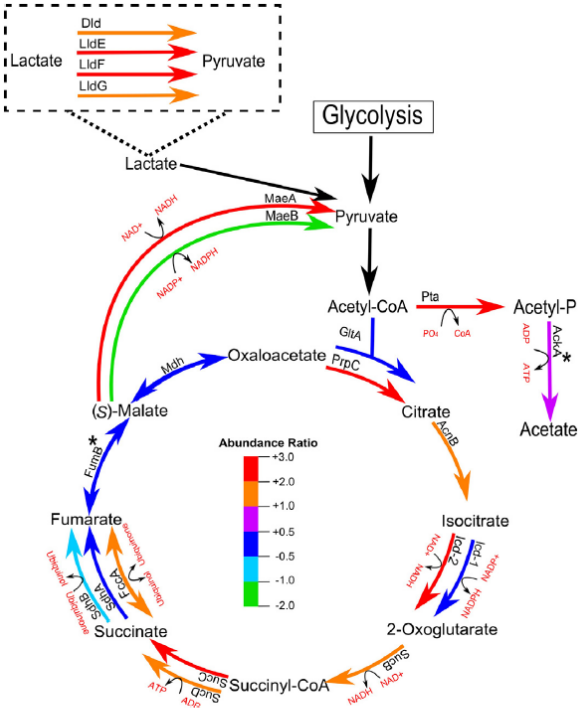

Fig. 2. *Shewanella oneidensis* MR-1 prokaryotic TCA cycle as adapted using Pathway Tools software. The colour coded expression ratios indicate the Log2 Fold Change occurring between protein abundances in +0.71 V relative to −0.19 V electrode biofilms. Full names of the abbreviated proteins are located in Table S2. Inset box shows the abundance differences between the multiple enzymes that carry out the conversion of lactate to pyruvate. All Log2 Fold Change values are significant ($p < 0.05$) unless indicated with an asterisk (*).

The $\log_2$ fold change ($\log_2$FC) for the majority of the TCA cycle proteins in the comparison of the +0.71 V to −0.19 V anode biofilms were positive (Fig. 2). This indicated a higher abundance of these proteins at +0.71 V and a more active TCA cycle in comparison to −0.19 V. This correlates with the BES chronoamperometry results, with +0.71 V showing significantly higher current production and thus overall metabolic activity than that detected at −0.19 V (Fig. 1A). This higher electron transfer rate was generated through increased carbon substrate (lactate) oxidation activity at the higher anode potential. The enzymes involved in the conversion of lactate to pyruvate (Dld, LldE, LldF & LldG) were higher in abundance at +0.71 V ($p < 0.05$), suggesting a higher rate of carbon metabolism at the higher potential. This activity was confirmed as lactate utilisation was higher in the +0.71 V culture in comparison to the −0.19 V culture (SI Table 1).

Proteins of the TCA cycle with negative $\log_2$FC were relatively in higher abundance at −0.19 V. The protein MaeB was statistically more abundant at −0.19 V and this enzyme catalyses an NADP-dependent conversion of malate to pyruvate (Fig. 2). The protein MaeA, a NAD-dependent malic enzyme was more abundant at +0.71 V. This protein carries out the same reaction, however this uses NAD^+ rather than $NADP^+$ for conversion of malate to pyruvate. In general bacterial metabolism, conversions utilising the NAD^+/NADH couple are involved in oxidative catabolic reactions and respiratory electron transfer [5]. In contrast the NADP+/NADPH couple is utilised in anabolic reactions [5]. This appears to be a response of the cells corresponding to the different electrode potentials and is in agreement with the outcomes observed here in that more respiratory activity (NAD+ reactions) was evident at +0.71 V compared to −0.19 V (Fig. 1A). The higher potential of the anode would provide more opportunity for electron transfer through the respiratory pathway, given the higher energy gain associated with electron transfer between redox couples at greater potential difference.

Conversely, at low potential it is possible that the TCA cycle is functioning at a decreased level. Although under more reduced conditions, NADH levels will be high and this is known to inhibit key oxidative enzymes in the cycle [32]. Several studies report that under anaerobic conditions *S. oneidensis* possesses an incomplete TCA cycle [26], using either an oxidative or reductive branch for production of cell intermediates [1,28]. However, activity of a complete TCA cycle has been detected under certain anaerobic conditions [28]. Although, in that instance the carbon flux through the TCA cycle was very low and acetate was a major product of lactate oxidation [28]. That was not the case in this study at the higher potential, as acetate production was less than 5% of the consumed lactate (Table S1), this result supporting the scheme of lactate utilisation proceeding through the TCA cycle. Conversely, acetate production at the low potential was significant (Table S1), and this activity

Please cite this article in press as: C. Grobbler, et al., Use of SWATH mass spectrometry for quantitative proteomic investigation of *Shewanella oneidensis* MR-1 biofilms grown on graphite cloth electrodes, Syst. Appl. Microbiol. (2014), http://dx.doi.org/10.1016/j.syapm.2014.11.007

has been observed previously in anaerobic conditions [1]. Consequently, at the low potential the acetate production was important for substrate level ATP production.

The reactions of the TCA pathway that are utilised would have great impact on the number of electrons consumed/produced [18], and the choice of those used is likely a dynamic process determined by environmental conditions [1]. When looking at protein abundances for each side of the TCA cycle, there is evidence to support this suggestion. At +0.71 V we see higher abundances for proteins involved in energy generating reactions, suggesting that the complete TCA cycle is being extensively utilised. Conversely at −0.19 V we observed equal abundances for proteins involved in the reductive branch of the cycle, suggesting in these conditions there is less use of the oxidative branch of the TCA cycle. This is in agreement with previous observation where *S. oneidensis* uses a complete TCA cycle at higher redox potential and utilisation of the branched cycle was evident at lower redox potential [28]. With regard to the TCA cycle, the proteomic findings made here are in agreement with what is expected from the metabolic and energetic activities of *S. oneidensis*.

The number of protein identifications achieved in this study improves on quantitative proteomic investigations of an electrode biofilm. The SWATH-MS approach used here is advantageous for proteomic analysis on samples where biomass or protein quantities are very low. The sensitivity of SWATH-MS removes the need for fractionation and being label free, removes the need for several processing steps involved with labelling procedures which may contribute to loss of protein [29]. The extraction method in combination with IDA analysis successfully obtained high levels of identifications from the electrode attached biofilm samples. In particular, this method could be used for detailed interrogation of the electron transfer proteins of BES biofilms.

Microbial electrochemical systems like microbial fuel cells have attracted attention as a promising alternative to unsustainable energy sources and technologies. Among the development of other components, the improved understanding and details of EET pathways of model organisms, such as *S. oneidensis MR-1*, provides opportunity to fine tune reactor conditions to the metabolic capabilities of the organism and achieve improved process performance. Establishing the SWATH-MS approach in this field opens the way for further investigations to improve our understanding of electroactive biofilms for advancing the BES technology.

The SWATH-MS analysis is quantitative and enabled a relative comparison of protein abundance between our biofilm samples. Using this technique we gained evidence that the TCA cycle of *S. oneidensis* electrode biofilm is more active when grown at a higher potential (+0.71 V). The results also suggest that at lower potential, utilisation of reactions dependent on NADPH rather than NADH was preferred, and this likely reflects decreased respiratory activity in this condition. Consequently, we suggest the use of the above mentioned extraction and SWATH-MS for quantitative proteomic analysis of electrode biofilm samples, and in general from samples where the quantity of protein is limited.

The mass spectrometry proteomics data have been deposited to the ProteomeXchange Consortium (http://proteomecentral.proteomexchange.org) via the PRIDE partner repository [31] with the dataset identifier PXD001472.

Conflict of interest

The authors have declared no conflict of interest.

Acknowledgements

The authors would like to thank the Australian Research Council for their financial support (project DP0879245). B.V. acknowledges the financial support for CEMES through The University of Queensland. We acknowledge the PRIDE team for the deposition of our data to the ProteomeXchange Consortium (http://proteomecentral.proteomexchange.org).

Appendix A. Supplementary data

Supplementary data associated with this article can be found, in the online version, at http://dx.doi.org/10.1016/j.syapm.2014.11.007.

References

[1] Brutinel, E.D., Gralnick, J.A. (2012) Anomalies of the anaerobic tricarboxylic acid cycle in *Shewanella oneidensis* revealed by Tn-seq. Mol. Microbiol. 86, 273–283.
[2] Carmona-Martínez, A.A., Harnisch, F., Kuhlicke, U., Neu, T.R., Schröder, U. (2012) Electron transfer and biofilm formation of *Shewanella putrefaciens* as function of anode potential. Bioelectrochemistry 93, 23–29.
[3] Choi, M., Chang, C.Y., Clough, T., Broudy, D., et al. (2014) MSstats: an R package for statistical analysis of quantitative mass spectrometry-based proteomic experiments. Bioinformatics 30, 2524–2526.
[4] Cristiani, P., Franzetti, A., Gandolfi, I., Guerrini, E., Bestetti, G. (2013) Bacterial DGGE fingerprints of biofilms on electrodes of membraneless microbial fuel cells. Int. Biodeter. Biodegr. 84, 211–219.
[5] Csonka, L.N., Fraenkel, D.G. (1977) Pathways of NADPH formation in *Escherichia coli*. J. Biol. Chem. 252, 3382–3391.
[6] Gillet, L.C., Navarro, P., Tate, S., Rost, H., et al. (2012) Targeted data extraction of the MS/MS spectra generated by data-independent acquisition: a new concept for consistent and accurate proteome analysis. Mol. Cell. Proteomics, 11.
[7] Gralnick, J.A., Coursolle, D. (2010) Modularity of the Mtr respiratory pathway of *Shewanella oneidensis* strain MR-1. Mol. Microbiol. 77, 995–1008.
[8] Gupta, N., Benhamida, J., Bhargava, V., Goodman, D., et al. (2008) Comparative proteogenomics: combining mass spectrometry and comparative genomics to analyze multiple genomes. Genome Res. 18, 1133–1142.
[9] Gupta, N., Tanner, S., Jaitly, N., Adkins, J.N., et al. (2007) Whole proteome analysis of post-translational modifications: applications of mass-spectrometry for proteogenomic annotation. Genome Res. 17, 1362–1377.
[10] Harris, H.W., El-Naggar, M.Y., Bretschger, O., Ward, M.J., et al. (2010) Electrokinesis is a microbial behavior that requires extracellular electron transport. Proc. Natl. Acad. Sci. U. S. A. 107, 326–331.
[11] Rabaey, K., A., L.T., Schroder, U., Keller, J. 2009 Bioelectrochemical Systems: From Extracellular Electron Transfer to Biotechnological Application, IWA Publishing, London.
[12] Karp, P.D., Paley, S.M., Krummenacker, M., Latendresse, M., et al. (2010) Pathway Tools version 13.0: integrated software for pathway/genome informatics and systems biology. Brief. Bioinform. 11, 40–79.
[13] Kiely, P.D., Call, D.F., Yates, M.D., Regan, J.M., Logan, B.E. (2010) Anodic biofilms in microbial fuel cells harbor low numbers of higher-power-producing bacteria than abundant genera. Appl. Microbiol. Biotechnol. 88, 371–380.
[14] Kolker, E., Picone, A.F., Galperin, M.Y., Romine, M.F., et al. (2005) Global profiling of *Shewanella oneidensis* MR-1: expression of hypothetical genes and improved functional annotations. Proc. Natl. Acad. Sci. U. S. A. 102, 2099–2104.
[15] Liu, H.A., Matsuda, S., Kato, S., Hashimoto, K., Nakanishi, S. (2010) Redox-responsive switching in bacterial respiratory pathways involving extracellular electron transfer. ChemSusChem 3, 1253–1256.
[16] Meyer, T.E., Tsapin, A.I., Vandenberghe, I., De Smet, L., et al. (2004) Identification of 42 possible cytochrome c genes in the *Shewanella oneidensis* genome and characterization of six soluble cytochromes. OMICS 8, 57–77.
[17] Michaelidou, U., ter Heijne, A., Euverink, G.J.W., Hamelers, H.V.M., et al. (2011) Microbial communities and electrochemical performance of titanium-based anodic electrodes in a microbial fuel cell. Appl. Environ. Microbiol. 77, 1069–1075.
[18] Myers, C.R., Nealson, K.H. (1988) Bacterial manganese reduction and growth with manganese oxide as the sole electron-acceptor. Science 240, 1319–1321.
[19] Nealson, K., Scott, J. (2006) In: Dworkin, M., Falkow, S., Rosenberg, E., Schleifer, K.-H., Stackebrandt, E. (Eds.), The Prokaryotes, Springer, New York, pp. 1133–1151.
[20] Pereira-Medrano, A.G., Knighton, M., Fowler, G.J.S., Ler, Z.Y., et al. (2013) Quantitative proteomic analysis of the exoelectxogenic bacterium *Arcobacter butzleri* ED-1 reveals increased abundance of a flagellin protein under anaerobic growth on an insoluble electrode. J. Proteomics 78, 197–210.
[21] Pirbadian, S., Barchinger, S.E., Leung, K.M., Byun, H.S., et al. (2014) *Shewanella oneidensis* MR-1 nanowires are outer membrane and periplasmic extensions of the extracellular electron transport components. Proc. Natl. Acad. Sci. U. S. A. 111, 12883–12888.
[22] Rabaey, K., Rozendal, R.A. (2010) Microbial electrosynthesis – revisiting the electrical route for microbial production. Nat. Rev. Microbiol. 8, 706–716.
[23] Read, S.T., Dutta, P., Bond, P.L., Keller, J., Rabaey, K. (2010) Initial development and structure of biofilms on microbial fuel cell anodes. BMC Microbiol. 10, 98.
[24] Romine, M.F., Elias, D.A., Monroe, M.E., Auberry, K., et al. (2004) Validation of *Shewanella oneidensis* MR-1 small proteins by AMT tag-based proteome analysis. OMICS 8, 239–254.

Please cite this article in press as: C. Grobbler, et al., Use of SWATH mass spectrometry for quantitative proteomic investigation of *Shewanella oneidensis* MR-1 biofilms grown on graphite cloth electrodes, Syst. Appl. Microbiol. (2014), http://dx.doi.org/10.1016/j.syapm.2014.11.007

[25] Rosenbaum, M.A., Bar, H.Y., Beg, Q.K., Segre, D., et al. (2012) Transcriptional analysis of *Shewanella oneidensis* MR-1 with an electrode compared to Fe(III)citrate or oxygen as terminal electron acceptor. PLOS ONE, 7.
[26] Scott, J.H., Nealson, K.H. (1994) A biochemical-study of the intermediary carbon metabolism of *Shewanella putrefaciens*. J. Bacteriol. 176, 3408–3411.
[27] Shi, L.A., Richardson, D.J., Wang, Z.M., Kerisit, S.N., et al. (2009) The roles of outer membrane cytochromes of *Shewanella* and *Geobacter* in extracellular electron transfer. Env. Microbiol. Rep. 1, 220–227.
[28] Tang, Y.J., Meadows, A.L., Kirby, J., Keasling, J.D. (2007) Anaerobic central metabolic pathways in *Shewanella oneidensis* MR-1 reinterpreted in the light of isotopic metabolite labeling. J. Bacteriol. 189, 894–901.
[29] Tuli, L., Ressom, H.W. (2009) LC-MS based detection of differential protein expression. J. Proteomics Bioinform. 2, 416–438.
[30] Venkateswaran, K., Moser, D.P., Dollhopf, M.E., Lies, D.P., et al. (1999) Polyphasic taxonomy of the genus *Shewanella* and description of *Shewanella oneidensis* sp. nov. Int. J. Syst. Bacteriol. 49, 705–724.
[31] Vizcaino, J.A., Cote, R.G., Csordas, A., Dianes, J.A., et al. (2013) The Proteomics Identifications (PRIDE) database and associated tools: status in 2013. Nucleic Acids Res. 41, D1063–D1069.
[32] Voet, D., Voet, J.G. 2004 Biochemsitry, John Wiley & Sons, Inc., New York.
[33] Vowinckel, J., Capuano, F., Campbell, K., Deery, M.J., et al. (2014) The beauty of being (label)-free: sample preparation methods for SWATH-MS and next-generation targeted proteomics. F1000Res. 2, 272.

Please cite this article in press as: C. Grobbler, et al., Use of SWATH mass spectrometry for quantitative proteomic investigation of *Shewanella oneidensis* MR-1 biofilms grown on graphite cloth electrodes, Syst. Appl. Microbiol. (2014), http://dx.doi.org/10.1016/j.syapm.2014.11.007

Appendix B – IDA Library for *Shewanella oneidensis* MR-1 anodic biofilms

N	Unused	Total	%Cov	%Cov (50)	%Cov (95)	Accession	SO identifier	Protein	Peptides (95%)
1	104.20	104.20	74.68	74.68	73.86	637344259	SO2427	TonB-dependent receptor, putative	97
2	93.38	93.38	81.05	80.53	79.47	637344725	SO2912	formate acetyltransferase	67
3	85.43	85.43	68.81	67.12	65.02	637346229	SO4509	formate dehydrogenase, alpha subunit	53
4	75.57	75.57	67.28	66.28	64.43	637342935	SO0970	fumarate reductase flavoprotein subunit precursor	64
5	74.22	74.22	70.74	67.45	67.45	637343075	SO1126	chaperone protein DnaK	51
6	73.58	75.12	65.16	63.80	61.43	637344722	SO2907	TonB-dependent receptor domain protein	51
7	73.47	73.47	68.74	68.51	68.51	637343711	SO1825	MotA/TolQ/ExbB proton channel family protein	49
8	64.05	64.05	87.54	87.54	85.46	637346360	SO4652	sulfate ABC transporter, periplasmic sulfate-binding protein	43
9	61.86	61.86	82.20	81.47	79.82	637342689	SO0704	chaperonin GroEL	57
10	57.55	57.55	89.77	84.86	82.52	637346132	SO4410	glutamine synthetase	39
11	55.80	55.80	82.23	80.46	80.46	637342236	SO0229	translation elongation factor Tu	54
12	54.26	54.26	48.57	47.62	47.62	637343665	SO1779	decaheme cytochrome c	36
13	53.34	58.07	48.42	42.53	39.26	637346233	SO4513	formate dehydrogenase, alpha subunit	30
14	52.45	52.45	59.90	59.90	57.65	637343686	SO1798	peptidyl-prolyl cis-trans isomerase D	26
15	50.36	50.36	55.39	52.09	52.09	637344469	SO2644	phosphoenolpyruvate synthase	32
16	47.82	47.82	88.89	86.72	84.82	637345657	SO3896	outer membrane porin, putative	67
17	47.58	47.58	54.13	48.58	47.58	637343163	SO1209	polyribonucleotide nucleotidyltransferase	28
18	46.75	46.75	72.76	72.76	66.26	637346076	SO4349	ketol-acid reductoisomerase	32
19	45.42	45.42	53.89	50.58	46.69	637345609	SO3844	peptidase, M13 family	25
20	45.29	45.29	14.56	14.56	14.56	637346043	SO4317	RTX toxin, putative	23
21	44.51	44.51	77.57	75.37	73.16	637345052	SO3237	flagellin	60
22	44.12	44.12	38.04	38.04	37.08	637343369	SO1429	anaerobic dimethyl sulfoxide reductase, A subunit	24
23	42.92	42.92	47.40	43.82	38.03	637342434	SO0432	aconitate hydratase	22
24	0.00	42.80	28.58	27.66	25.53	637346560	SOA0112	lipoprotein, putative	23
24	42.80	42.80	28.58	27.66	25.53	637346562	SOA0115	lipoprotein, putative	23
25	42.64	42.64	83.80	75.81	74.51	637346451	SO4747	ATP synthase subunit B	29
26	42.04	42.04	43.04	42.62	42.62	637343030	SO1075	hypothetical protein	22
27	41.65	41.65	50.65	43.04	43.04	637343662	SO1776	outer membrane protein precursor MtrB	29
28	40.65	48.36	38.38	37.15	36.14	637344299	SO2469	hypothetical TonB-dependent receptor	26
29	39.51	39.51	55.59	54.41	44.71	637342431	SO0429	peptidase, M13 family	21
30	38.97	38.97	67.25	56.34	54.97	637346453	SO4749	ATP synthase subunit A	24
31	38.60	38.60	65.05	63.58	61.47	637342428	SO0426	dihydrolipoamide dehydrogenase	21
32	38.00	38.00	66.67	66.67	66.67	637345665	SO3904	outer membrane channel precursor protein	20
33	38.00	38.00	82.61	82.61	82.61	637344719	SO2903	cysteine synthase A	33

34	37.55	37.55	29.51	25.52	25.52	637342406	SO0404	hypothetical protein	21
35	37.51	37.51	77.91	77.91	75.82	637345396	SO3599	sulfate ABC transporter, periplasmic sulfate-binding protein	30
36	37.13	37.13	33.87	33.23	29.71	637343815	SO1930	2-oxoglutarate dehydrogenase, E1 component	20
37	36.41	36.41	42.62	42.32	42.32	637343664	SO1778	decaheme cytochrome c	21
38	36.00	36.00	51.21	48.96	47.75	637345510	SO3733	hypothetical protein	20
39	35.88	35.88	52.65	52.65	52.65	637346551	SOA0100	hypothetical protein	20
40	35.83	35.83	45.37	45.37	45.37	637343891	SO2016	heat shock protein 90	21
41	34.74	34.74	65.11	65.11	62.89	637345701	SO3942	serine protease, HtrA/DegQ/DegS family	18
42	34.41	34.41	50.96	50.96	49.26	637346046	SO4320	agglutination protein	23
43	34.00	34.00	82.81	82.81	82.81	637343710	SO1824	hypothetical protein	32
44	33.85	33.85	35.69	32.21	27.20	637344245	SO2411	DNA gyrase, A subunit	19
45	32.53	32.53	78.78	78.78	69.45	637342748	SO0770	malate dehydrogenase	18
46	32.03	32.03	50.85	43.03	42.18	637343813	SO1928	succinate dehydrogenase catalytic subunit	19
47	32.00	32.00	89.01	73.82	73.82	637343422	SO1490	alcohol dehydrogenase II	19
48	31.68	31.68	45.39	45.39	45.39	637343681	SO1793	trigger factor	18
49	31.53	31.53	39.00	34.82	32.52	637344456	SO2629	isocitrate dehydrogenase, NADP-dependent	17
50	31.35	31.35	69.16	64.49	55.37	637343810	SO1926	citrate synthase	19
51	30.68	30.68	32.14	32.14	29.99	637342812	SO0842	elongation factor EF-2	15
52	30.11	30.11	78.72	71.43	69.30	637342263	SO0256	DNA-directed RNA polymerase alpha subunit	20
53	30.00	30.00	67.16	67.16	67.16	637344874	SO3070	aspartate semialdehyde dehydrogenese	17
54	30.00	30.00	64.65	64.65	64.65	637343046	SO1095	O-acetylhomoserine (thiol)-lyase, putative	17
55	29.55	29.55	74.68	74.68	72.38	637342899	SO0932	phosphoglycerate kinase	16
56	29.32	29.32	41.40	34.53	34.53	637342235	SO0228	elongation factor EF-2	16
57	28.89	28.89	44.37	44.37	38.99	637346550	SOA0099	hypothetical protein	16
58	28.02	28.02	54.27	54.27	52.01	637345249	SO3440	enolase	17
59	27.84	27.84	41.54	37.52	34.51	637343009	SO1051	periplasmic glucan biosynthesis protein, putative	15
60	27.83	27.83	62.59	53.48	51.56	637345277	SO3471	serine hydroxymethyltransferase	15
61	27.37	27.37	42.04	37.71	29.75	637344958	SO3142	peptidyl-dipeptidase Dcp	13
62	26.68	26.68	28.06	27.14	22.79	637344321	SO2492	oxidoreductase, acyl-CoA dehydrogenase family	14
63	26.38	26.38	60.58	58.39	55.47	637346423	SO4719	hypothetical protein	14
64	26.02	26.02	59.01	59.01	59.01	637342608	SO0617	bifunctional N-succinyldiaminopimelate-aminotransferase/acetylornithine transaminase protein	13
65	26.00	26.00	90.08	90.08	90.08	637345862	SO4133	uridine phosphorylase	16
66	25.26	25.26	36.58	30.99	30.99	637344237	SO2402	30S ribosomal protein S1	14
67	25.19	25.19	22.30	19.37	19.37	637342426	SO0424	pyruvate dehydrogenase complex, E1 component, pyruvate dehydrogenase	14
68	25.03	25.03	55.58	44.19	44.19	637342846	SO0876	aminopeptidase B	13
69	24.59	24.59	59.76	57.06	56.76	637344037	SO2178	cytochrome c551 peroxidase	12
70	24.40	24.40	55.38	49.49	45.64	637343111	SO1164	D-alanyl-D-alanine carboxypeptidase	12

71	24.29	24.29	57.57	47.39	44.91	637344876	SO3072	3-oxoacyl-(acyl-carrier-protein) synthase I	12
72	24.23	24.23	50.20	50.20	43.14	637343021	SO1065	FKBP-type peptidyl-prolyl cis-trans isomerase FkpA	13
73	24.17	24.17	62.67	56.95	56.95	637343215	SO1270	polyamine ABC transporter, periplasmic polyamine-binding protein	13
74	24.16	24.16	33.66	33.66	32.28	637345516	SO3740	NAD(P) transhydrogenase subunit alpha	12
75	24.00	24.00	77.34	77.34	77.34	637344833	SO3024	tryptophan synthase, alpha subunit	16
76	23.91	23.91	56.19	50.77	48.45	637343817	SO1932	succinyl-CoA synthetase subunit beta	14
77	23.71	23.71	46.15	39.12	34.29	637342288	SO0279	argininosuccinate lyase	11
78	23.71	23.71	37.80	37.80	35.84	637342897	SO0930	transketolase	13
79	23.31	23.31	80.08	80.08	80.08	637343172	SO1221	purine nucleoside phosphorylase	16
80	23.22	23.22	62.14	45.95	45.95	637342896	SO0929	S-adenosylmethionine synthetase	12
81	23.00	23.00	40.79	37.72	37.72	637345050	SO3235	flagellar hook-associated protein FliD	14
82	22.86	22.86	55.00	46.36	41.36	637344904	SO3099	long-chain fatty acid transport protein, putative	11
83	22.14	22.14	45.08	42.83	40.16	637345104	SO3293	inositol-5-monophosphate dehydrogenase	12
84	22.00	22.00	91.14	91.14	91.14	637345272	SO3466	riboflavin synthase, beta subunit	13
85	22.00	22.00	95.36	95.36	95.36	637344698	SO2881	superoxide dismutase, Fe	15
86	22.00	22.00	75.66	75.66	75.66	637342924	SO0958	alkyl hydroperoxide reductase, C subunit	11
87	22.00	22.00	17.26	17.26	17.26	637342759	SO0781	glycine dehydrogenase	11
88	21.44	21.44	50.12	50.12	50.12	637343221	SO1276	4-aminobutyrate aminotransferase	12
89	21.35	21.35	32.38	32.38	29.19	637344598	SO2768	acyl-CoA dehydrogenase family protein	11
90	20.62	20.62	42.75	33.91	32.19	637342287	SO0278	argininosuccinate synthase	12
91	20.01	20.01	27.59	19.44	18.51	637343121	SO1174	leucyl-tRNA synthetase	10
92	20.00	20.00	49.07	46.89	46.89	637344199	SO2361	cytochrome c oxidase, cbb3-type, subunit III	10
93	20.00	20.00	16.17	15.04	15.04	637343832	SO1949	invasin domain protein	13
94	20.00	20.00	60.34	60.34	60.34	637343818	SO1933	succinyl-CoA synthase, alpha subunit	10
95	19.92	19.92	62.69	62.69	62.69	637342285	SO0276	acetylglutamate kinase	13
96	19.51	19.51	51.07	51.07	51.07	637342228	SO0221	50S ribosomal protein L1	12
97	19.48	19.48	42.14	32.39	32.39	637345608	SO3842	hypothetical protein	13
98	19.26	19.26	45.81	45.81	45.81	637346039	SO4313	porphobilinogen deaminase	11
99	19.21	19.21	42.05	42.05	42.05	637343572	SO1665	UTP-glucose-1-phosphate uridylyltransferase	12
100	18.99	18.99	25.04	23.75	23.75	637346073	SO4345	dihydroxy-acid dehydratase	10
101	18.89	18.89	26.15	18.28	16.59	637342818	SO0848	periplasmic nitrate reductase	10
102	18.73	18.73	42.03	42.03	36.20	637344305	SO2476	polysaccharide biosynthesis protein	10
103	18.69	18.69	55.12	48.06	45.58	637343538	SO1630	elongation factor Ts	9
104	18.04	18.04	28.92	27.03	27.03	637345344	SO3545	OmpA family protein	11
105	18.00	18.00	30.19	26.34	26.34	637345732	SO3980	cytochrome c552 nitrite reductase	10
106	18.00	18.00	28.74	28.74	28.74	637346041	SO4315	hemX protein	9
107	17.87	17.87	53.27	41.67	37.50	637344181	SO2345	glyceraldehyde 3-phosphate dehydrogenase	10
108	17.77	17.77	20.18	19.29	19.29	637345514	SO3737	sulfite reductase (NADPH) hemoprotein beta-component (cysI)	10
109	17.70	17.70	16.10	11.86	11.86	637343545	SO1637	bacterial surface antigen	9

110	17.69	17.69	43.46	43.46	39.69	637346407	SO4702	glutathione reductase	11
111	17.64	17.64	92.31	92.31	92.31	637345466	SO3681	universal stress protein family	13
112	17.53	17.53	25.18	25.18	22.09	637346404	SO4699	oligopeptidase A	12
113	17.32	17.32	33.53	33.53	33.53	637343972	SO2107	periplasmic glucans biosynthesis protein MdoG	9
114	17.27	17.27	30.81	28.10	28.10	637344077	SO2222	fumarate hydratase, class I, anaerobic, putative	10
115	17.08	17.08	27.10	27.10	27.10	637344585	SO2753	prolyl endopeptidase	11
116	16.73	16.73	44.82	40.72	33.01	637342273	SO0265	hypothetical protein	8
117	16.38	16.38	23.73	23.73	22.16	637343643	SO1755	phosphoglucomutase/phosphomannomutase family protein	8
118	16.36	16.36	18.68	16.29	15.09	637345009	SO3193	polysaccharide biosynthesis protein	9
119	16.24	16.24	46.23	46.23	41.82	637345345	SO3546	transaldolase	9
120	16.21	16.21	36.89	28.60	24.03	637344264	SO2433	aspartyl-tRNA synthetase	9
121	16.13	16.13	42.21	37.02	30.70	637346253	SO4537	2 hypothetical Zn-dependent peptidase	8
122	16.11	16.13	43.69	35.98	34.58	637344153	SO2310	seryl-tRNA synthetase	8
123	16.10	16.10	27.14	27.14	25.99	637344316	SO2487	phosphogluconate dehydratase	8
124	16.03	16.03	85.19	85.19	85.19	637342408	SO0406	thioredoxin 1	10
125	16.02	16.02	58.45	56.08	56.08	637344617	SO2791	cytidine deaminase	8
126	16.01	16.01	40.48	28.06	28.06	637343158	SO1203	transcription elongation factor NusA	8
127	16.01	16.01	22.63	20.73	19.17	637344857	SO3052	methyl-accepting chemotaxis protein	8
128	16.00	16.00	44.16	37.23	37.23	637342241	SO0234	50S ribosomal protein L2	9
129	16.00	16.00	50.47	50.47	50.47	637343893	SO2018	adenylate kinase	9
130	16.00	16.00	32.51	32.51	32.51	637343168	SO1215	outer membrane protein OmpK, putative	9
131	16.00	16.00	42.65	42.65	42.65	637343143	SO1190	hypothetical protein	8
132	16.00	16.00	57.40	57.40	57.40	637343052	SO1101	S-ribosylhomocysteinase	9
133	16.00	16.00	45.91	45.91	45.91	637342455	SO0456	immunogenic-related protein	8
134	15.81	15.81	48.72	48.72	48.08	637342234	SO0227	30S ribosomal protein S7	9
135	15.78	15.78	25.23	23.54	23.54	637344566	SO2743	acetyl-coenzyme A synthetase	9
136	15.52	15.52	41.01	41.01	41.01	637342411	SO0409	hypothetical protein	8
137	15.39	15.39	22.00	22.00	20.53	637343717	SO1831	hypothetical protein	8
138	15.21	15.21	38.96	34.33	34.33	637345273	SO3467	3,4-dihydroxy-2-butanone 4-phosphate synthase/GTP cyclohydrolase II, putative	8
139	15.19	15.19	61.99	61.99	61.99	637345838	SO4105	MSHA pilin protein MshA	12
140	15.15	15.15	54.19	46.93	46.93	637342250	SO0243	ribosomal protein L5	8
141	15.09	15.09	55.47	55.47	55.47	637343449	SO1520	hypothetical protein	11
142	14.99	14.99	33.78	28.21	22.30	637344400	SO2570	lipoprotein, putative	8
143	14.97	14.97	62.50	34.52	34.52	637345930	SO4208	delta-aminolevulinic acid dehydratase	9
144	14.95	14.95	55.02	49.76	49.76	637342602	SO0611	stringent starvation protein A	8
145	14.75	14.75	50.99	50.99	47.03	637342337	SO0333	thiol:disulfide interchange protein DsbA	9
146	14.66	14.66	37.92	37.92	35.39	637344306	SO2477	alcohol dehydrogenase, iron-containing	9
147	14.55	14.55	75.61	75.61	70.73	637345018	SO3202	purine-binding chemotaxis protein CheW	8
148	14.49	14.49	59.33	59.33	54.00	637345687	SO3927	ribosomal protein L9	9
149	14.44	14.44	25.50	25.50	23.27	637344111	SO2264	cysteine desulfurase	7

150	14.29	14.29	25.00	18.99	15.36	637345363	SO3564	peptidyl-dipeptidase Dcp	7
151	14.16	14.16	40.18	39.88	35.28	637342284	SO0275	N-acetyl-gamma-glutamyl-phosphate reductase	7
152	14.05	14.05	44.19	31.74	31.74	637343220	SO1275	succinate-semialdehyde dehydrogenase	8
153	14.03	14.03	46.86	41.36	34.03	637346399	SO4693	multidrug resistance protein, AcrA/AcrE family	7
154	14.00	14.00	71.51	66.13	66.13	637345148	SO3343	hypothetical protein	8
155	14.00	14.00	51.83	51.83	51.83	637345173	SO3370	hypothetical protein	7
156	14.00	14.00	77.27	77.27	77.27	637343548	SO1640	(3R)-hydroxymyristoyl-(acyl-carrier-protein) dehydratase	7
157	14.00	14.00	41.96	41.96	41.96	637343370	SO1430	anaerobic dimethyl sulfoxide reductase, B subunit	8
158	14.00	14.00	67.23	67.23	67.23	637342253	SO0246	50S ribosomal protein L6	8
159	13.99	13.99	37.79	26.51	22.96	637344320	SO2491	pyruvate kinase II	7
160	13.89	13.89	19.07	17.90	17.90	637342063	SO0049	phosphoglyceromutase	7
161	13.86	13.86	19.80	19.80	18.69	637344729	SO2916	phosphate acetyltransferase	7
162	13.82	13.82	56.61	56.61	56.61	637343447	SO1518	hypothetical protein	12
163	13.68	13.68	73.66	73.66	73.66	637345839	SO4106	MSHA pilin protein MshB	8
164	13.63	13.63	39.81	31.07	31.07	637342262	SO0255	30S ribosomal protein S4	7
165	13.58	13.58	51.27	51.27	45.69	637345146	SO3341	antioxidant, AhpC/TSA family	7
166	13.55	13.55	98.55	98.55	98.55	637344613	SO2787	cold shock domain family protein	8
167	13.51	13.51	15.62	15.62	11.78	637345675	SO3914	TonB-dependent receptor, putative	8
168	13.50	13.50	30.23	26.36	24.09	637343417	SO1484	isocitrate lyase	7
169	13.41	13.41	47.76	43.28	43.28	637343615	SO1717	hypothetical protein	7
170	13.37	13.37	23.73	22.50	19.51	637343877	SO2001	5'-nucleotidase	7
171	13.36	13.36	83.33	83.33	83.33	637342688	SO0703	co-chaperonin GroES	10
172	13.23	13.23	32.38	29.52	21.81	637344424	SO2596	hypothetical protein	7
173	13.23	13.23	21.40	19.51	19.51	637344553	SO2731	periplasmic glucans biosynthesis protein MdoG	7
174	13.10	13.10	37.17	37.17	37.17	637343703	SO1816	hypothetical protein	8
175	12.95	12.95	11.89	10.39	5.91	637342232	SO0225	DNA-directed RNA polymerase beta' subunit	6
176	12.94	12.95	70.47	70.47	58.39	637345221	SO3420	cytochrome c'	9
177	12.91	12.91	71.54	70.77	65.38	637344963	SO3146	DNA-binding protein, H-NS family	9
178	12.89	12.89	20.69	17.03	17.03	637343448	SO1519	iron-sulfur cluster-binding protein	7
179	12.73	12.73	37.71	37.71	34.34	637346091	SO4365	hypothetical protein	8
180	12.72	12.72	36.45	29.08	26.10	637343312	SO1368	leucyl aminopeptidase	7
181	12.69	12.69	51.70	48.30	48.30	637343769	SO1879	dihydrodipicolinate synthase	7
182	12.65	12.65	21.11	19.21	14.70	637344078	SO2223	peptidase, putative	7
183	12.49	12.49	16.23	16.23	14.11	637343964	SO2098	quinone-reactive Ni/Fe hydrogenase, large subunit	6
184	12.24	12.24	68.71	51.94	43.23	637344193	SO2355	universal stress protein family	6
185	12.23	12.23	20.62	17.00	15.63	637342569	SO0578	hypothetical protein	6
186	12.19	12.19	35.52	31.49	27.96	637344188	SO2350	aspartate aminotransferase	6
187	12.06	12.06	36.36	36.36	36.36	637342601	SO0610	ubiquinol-cytochrome c reductase, cytochrome c1	6
188	12.04	12.04	51.11	43.33	43.33	637343685	SO1797	DNA-binding protein, HU family	8
189	12.01	12.01	24.95	16.51	16.51	637345346	SO3547	glucose-6-phosphate isomerase	6

190	12.00	12.00	25.30	16.21	16.21	637346196	SO4480	aldehyde dehydrogenase	6
191	12.00	12.00	19.29	14.57	14.57	637344840	SO3033	ferric alcaligin siderophore receptor	6
192	12.00	12.00	65.36	53.07	53.07	637343489	SO1568	hypothetical protein	7
193	12.00	12.00	53.23	50.75	50.75	637342239	SO0232	50S ribosomal protein L4	6
194	12.00	12.00	29.76	29.76	29.76	637342405	SO0403	hypothetical protein	6
195	12.00	12.00	46.70	46.70	46.70	637342307	SO0298	phosphoheptose isomerase	8
196	11.66	11.66	47.60	47.60	47.60	637344590	SO2759	uracil phosphoribosyltransferase	6
197	11.55	11.55	36.81	31.59	22.25	637345962	SO4235	3-isopropylmalate dehydrogenase	7
198	11.55	11.55	40.35	36.26	29.53	637346561	SOA0114	outer membrane protein A	7
199	11.46	11.46	53.28	53.28	53.28	637342230	SO0223	ribosomal protein L7/L12	9
200	11.44	11.46	63.20	63.20	63.20	637343581	SO1675	hypothetical protein	6
201	11.39	11.39	54.81	54.81	54.81	637342249	SO0242	ribosomal protein L24	6
202	11.37	11.37	46.58	46.58	42.24	637345582	SO3815	hypothetical protein	6
203	11.20	11.20	18.41	12.03	12.03	637346448	SO4743	TonB-dependent receptor, putative	6
204	11.11	11.11	36.45	33.73	33.73	637342627	SO0640	alcohol dehydrogenase, zinc-containing	7
205	11.05	11.05	61.02	60.17	60.17	637342260	SO0253	30S ribosomal protein S13	6
206	11.02	11.02	35.40	19.54	15.09	637343068	SO1117	cytosol aminopeptidase, putative	6
207	10.94	10.94	29.22	29.22	29.22	637346142	SO4423	1 hypothetical ferric aerobactin receptor	6
208	10.72	10.72	56.00	56.00	52.00	637342301	SO0292	ribulose-phosphate 3-epimerase	5
209	10.56	10.56	34.22	34.22	31.11	637342727	SO0748	hypothetical protein	6
210	10.43	10.43	23.49	11.95	9.84	637342486	SO0491	peptidase, M13 family	5
211	10.42	10.42	27.87	27.87	23.47	637342832	SO0862	D-3-phosphoglycerate dehydrogenase	7
212	10.40	10.40	26.13	26.13	15.04	637345450	SO3664	long-chain-fatty-acid--CoA ligase	6
213	10.33	10.33	50.26	50.26	46.07	637344709	SO2893	hypothetical protein	6
214	10.20	10.20	14.03	14.03	14.03	637344397	SO2566	asmA protein	6
215	10.07	10.07	58.96	54.48	54.48	637343713	SO1827	TonB system transport protein ExbD2	5
216	10.02	10.02	38.89	30.81	30.81	637346119	SO4396	acyl carrier protein phosphodiesterase	5
217	10.00	29.94	70.70	64.47	59.71	637345053	SO3238	flagellin	38
218	10.00	10.00	30.13	23.80	23.80	637345942	SO4215	cell division protein FtsZ	5
219	10.00	10.00	33.05	28.49	28.49	637345792	SO4047	cytochrome c family protein	5
220	10.00	10.00	28.92	26.27	26.27	637345062	SO3247	flagellar hook protein	5
221	10.00	10.00	36.81	33.88	33.88	637342332	SO0326	hypothetical protein	5
222	10.00	10.00	28.28	28.28	28.28	637346230	SO4510	formate dehydrogenase, iron-sulfur subunit	7
223	10.00	10.00	64.55	64.55	64.55	637345651	SO3888	hypothetical protein	8
224	10.00	10.00	19.40	19.40	19.40	637345619	SO3855	malate oxidoreductase	5
225	10.00	10.00	69.77	69.77	69.77	637344568	SO2745	glutaredoxin	5
226	10.00	10.00	67.13	67.13	67.13	637344120	SO2274	nucleoside diphosphate kinase	5
227	10.00	10.00	29.13	29.13	29.13	637343453	SO1524	heat shock protein GrpE	5
228	10.00	10.00	29.51	29.51	29.51	637343002	SO1044	amino acid ABC transporter, periplasmic amino acid-binding protein	5
229	9.96	10.00	29.65	29.65	29.65	637344464	SO2638	leucine dehydrogenase	5
230	9.87	9.87	45.29	35.37	27.99	637345800	SO4056	cystathionine gamma-synthase	5

231	9.80	11.89	19.86	19.86	19.86	637342950	SO0987	methyl-accepting chemotaxis protein	6
232	9.77	9.77	40.51	21.90	19.34	637343534	SO1625	2,3,4,5-tetrahydropyridine-2-carboxylate N-succinyltransferase	5
233	9.57	9.57	38.03	38.03	38.03	637345699	SO3940	50S ribosomal protein L13	5
234	9.54	9.54	56.29	47.90	42.51	637342255	SO0248	ribosomal protein S5	6
235	9.51	9.51	31.73	31.73	31.73	637345793	SO4048	cytochrome c family protein	5
236	9.48	9.48	29.74	25.82	22.88	637345913	SO4190	putative manganese-dependent inorganic pyrophosphatase	5
237	9.44	9.44	43.69	43.69	43.69	637342237	SO0230	30S ribosomal protein S10	5
238	9.42	9.42	33.41	25.35	20.05	637345428	SO3637	survival protein surA	5
239	9.32	9.32	35.56	35.56	35.56	637344411	SO2583	hypothetical protein	5
240	9.29	9.29	35.67	35.67	35.67	637343743	SO1856	3-hydroxydecanoyl-ACP dehydratase	5
241	9.21	9.21	37.07	22.13	19.47	637344257	SO2424	zinc carboxypeptidase domain protein	5
242	9.09	9.09	15.25	15.25	15.25	637346307	SO4597	heavy metal efflux system protein, putative	5
243	9.08	9.08	45.07	43.66	43.66	637342227	SO0220	ribosomal protein L11	5
244	9.01	9.01	64.44	62.22	62.22	637343819	SO1935	regulator of nucleoside diphosphate kinase	5
245	8.58	8.58	50.41	50.41	27.27	637343537	SO1629	30S ribosomal protein S2	6
246	8.52	8.52	19.85	15.12	15.12	637346171	SO4453	electron transfer flavoprotein-ubiquinone oxidoreductase, putative	5
247	8.43	8.43	56.47	56.47	40.00	637346208	SO4492	hypothetical protein	5
248	8.35	8.35	37.26	32.08	29.25	637342238	SO0231	ribosomal protein L3	7
249	8.29	8.29	64.89	59.54	43.51	637345690	SO3930	30S ribosomal protein S6	6
250	8.27	8.27	43.01	39.78	34.41	637344166	SO2328	elongation factor P	5
251	8.27	8.27	41.06	41.06	33.33	637343714	SO1828	TonB2 protein	4
252	8.27	8.27	52.53	52.53	43.04	637346347	SO4640	antioxidant, AhpC/Tsa family	4
253	8.23	8.23	44.07	44.07	30.93	637344552	SO2730	peptidase E	4
254	8.20	42.80	26.99	26.99	24.86	637346559	SOA0110	lipoprotein, putative	23
255	8.20	8.20	32.62	32.62	29.08	637345594	SO3827	2-dehydro-3-deoxyphosphooctonate aldolase	4
256	8.13	8.13	47.67	38.00	30.33	637343588	SO1682	3-hydroxyisobutyrate dehydrogenase	5
257	8.13	8.13	32.43	32.43	26.35	637343977	SO2112	ribosomal protein L25	4
258	8.08	8.08	41.94	41.94	37.79	637345708	SO3951	hypothetical protein	6
259	8.08	8.08	30.79	30.79	20.00	637342803	SO0831	glutathione synthetase	4
260	8.05	8.05	17.88	17.88	15.37	637346381	SO4674	2-amino-3-ketobutyrate coenzyme A ligase	4
261	8.04	8.04	35.98	14.64	14.64	637345054	SO3239	flagellar hook-associated protein FlgL	4
262	8.04	8.04	18.82	18.82	18.82	637343071	SO1122	gamma-glutamyl phosphate reductase	5
263	8.03	8.03	52.45	36.36	36.36	637344144	SO2300	translation initiation factor IF-3	5
264	8.03	8.03	21.69	17.81	17.81	637343940	SO2073	histidinol dehydrogenase	4
265	8.03	8.03	60.25	59.63	59.63	637345919	SO4197	ribonuclease activity regulator protein RraA	4
266	8.02	8.02	23.72	12.03	12.03	637345515	SO3738	sulfite reductase (NADPH) flavoprotein alpha-component	4
267	8.02	8.02	35.58	28.85	28.85	637344201	SO2363	cytochrome c oxidase, cbb3-type, subunit II	5
268	8.02	8.02	10.75	8.88	8.88	637344143	SO2299	threonyl-tRNA synthetase	4

269	8.02	8.02	41.55	32.42	32.42	637343096	SO1150	ribose-5-phosphate isomerase A	5
270	8.02	8.02	47.76	44.03	44.03	637342677	SO0691	hypothetical protein	4
271	8.01	8.01	24.91	13.42	13.42	637344746	SO2934	hypothetical protein	4
272	8.01	8.01	58.16	47.96	47.96	637343953	SO2087	integration host factor, alpha subunit	5
273	8.01	8.01	13.90	10.42	10.42	637343368	SO1428	outer membrane protein	4
274	8.01	8.01	40.13	40.13	35.67	637342066	SO0052	export protein SecB	6
275	8.00	10.00	17.71	9.92	9.92	637343223	SO1278	methyl-accepting chemotaxis protein	5
276	8.00	8.00	30.59	23.14	23.14	637346600	SOA0161	zinc-binding dehydrogenase	4
277	8.00	8.00	11.45	8.10	8.10	637342030	SO0021	fatty oxidation complex, alpha subunit	4
278	8.00	8.00	33.33	33.33	33.33	637346328	SO4619	yhgI protein	5
279	8.00	8.00	55.19	55.19	55.19	637345676	SO3915	hypothetical protein	5
280	8.00	8.00	31.07	31.07	31.07	637345118	SO3310	hypothetical protein	4
281	8.00	8.00	19.44	19.44	19.44	637343589	SO1683	3-ketoacyl-(acyl-carrier-protein) reductase	4
282	8.00	8.00	38.05	38.05	38.05	637343086	SO1139	peptidyl-prolyl cis-trans isomerase FklB	4
283	8.00	8.00	24.35	24.35	24.35	637342328	SO0322	hypothetical protein	4
284	8.00	8.00	38.19	38.19	38.19	637342257	SO0250	50S ribosomal protein L15	6
285	8.00	8.00	40.00	40.00	40.00	637342252	SO0245	ribosomal protein S8	4
286	8.00	8.00	32.53	32.53	32.53	637342229	SO0222	ribosomal protein L10	4
287	8.00	8.00	29.95	29.95	29.95	637342125	SO0112	hypothetical protein	4
288	7.93	7.93	14.85	7.81	7.81	637342977	SO1016	NADH dehydrogenase gamma subunit	4
289	7.82	7.82	43.33	42.22	42.22	637342595	SO0603	host factor-I protein	5
290	7.59	7.59	20.70	20.70	20.70	637344740	SO2928	acyl-CoA thioesterase I, putative	4
291	7.54	7.54	23.11	23.11	23.11	637344906	SO3101	hypothetical protein	4
292	7.48	7.48	12.44	12.44	12.44	637346252	SO4537	peptidase, putative	5
293	7.46	7.46	15.88	15.88	15.88	637342123	SO0110	hypothetical protease	4
294	7.37	7.37	32.02	32.02	32.02	637345394	SO3597	hypothetical protein	4
295	7.32	7.32	24.75	24.75	16.41	637344240	SO2406	aspartate aminotransferase	4
296	7.21	7.21	23.10	23.10	17.33	637342557	SO0564	hypothetical protein	4
297	7.21	7.21	14.79	14.79	14.79	637345006	SO3190	polysaccharide biosynthesis protein	4
298	7.20	7.21	35.48	27.02	27.02	637344605	SO2776	3-oxoacyl-(acyl-carrier-protein) reductase	4
299	7.14	7.14	36.90	32.14	32.14	637343546	SO1638	outer membrane protein OmpH	4
300	7.14	7.14	43.85	43.85	43.85	637345577	SO3810	OmpA-like transmembrane domain protein	4
301	7.14	7.14	45.27	45.27	45.27	637343122	SO1175	hypothetical protein	4
302	7.07	7.07	31.10	31.10	31.10	637344398	SO2567	ribonuclease activity regulator protein RraA	5
303	7.03	7.03	46.94	46.94	46.94	637342844	SO0874	DnaK suppressor protein	4
304	6.98	6.98	50.85	50.85	50.85	637345223	SO3422	ribosomal subunit interface protein	4
305	6.96	6.96	38.06	23.89	23.89	637346110	SO4384	hypothetical protein	5
306	6.86	6.86	37.84	37.84	37.84	637343540	SO1632	ribosome recycling factor	4
307	6.84	6.84	20.00	20.00	20.00	637344177	SO2340	alpha keto acid dehydrogenase complex, E1 component, beta subunit	4
308	6.83	6.83	54.80	54.80	49.72	637342078	SO0065	molybdenum cofactor biosynthesis protein	4

309	6.80	6.80	21.55	17.04	17.04	637344728	SO2915	acetate/propionate kinase	5
310	6.79	6.79	19.07	13.95	13.95	637343246	SO1300	glutamate-1-semialdehyde-2,1-aminomutase	4
311	6.76	6.76	14.44	14.44	14.44	637342858	SO0888	amidase	4
312	6.72	6.72	56.52	56.52	47.83	637342242	SO0235	30S ribosomal protein S19	6
313	6.67	6.67	46.34	46.34	46.34	637342247	SO0240	ribosomal protein S17	4
314	6.57	6.57	9.71	9.71	9.71	637342153	SO0144	protease II	4
315	6.56	6.56	28.37	28.37	13.50	637342344	SO0340	branched-chain amino acid aminotransferase	4
316	6.54	6.54	19.07	19.07	19.07	637344244	SO2410	phosphoserine aminotransferase	4
317	6.53	6.53	36.89	36.89	36.89	637342248	SO0241	ribosomal protein L14	4
318	6.48	6.48	15.90	15.90	15.90	637342869	SO0900	oxidoreductase, aldo/keto reductase family	4
319	6.47	6.47	44.60	44.60	25.82	637344315	SO2486	keto-hydroxyglutarate-aldolase/keto-deoxy-phosphogluconate aldolase	3
320	6.41	6.41	36.36	36.36	21.97	637345467	SO3682	hypothetical protein	3
321	6.37	6.37	33.69	33.69	24.82	637344599	SO2769	hypothetical protein	4
322	6.29	6.29	30.99	19.72	14.08	637342900	SO0933	fructose-bisphosphate aldolase	3
323	6.29	6.29	27.64	18.55	18.55	637345145	SO3340	hypothetical Small-conductance mechanosensitive channel	4
324	6.28	6.29	19.48	19.48	16.85	637343507	SO1589	hypothetical protein	3
325	6.28	6.28	19.60	18.09	16.33	637343708	SO1821	outer membrane porin, putative	4
326	6.26	6.26	48.02	48.02	35.15	637343682	SO1794	ATP-dependent Clp protease proteolytic subunit	3
327	6.19	6.19	20.05	20.05	17.86	637342757	SO0779	aminomethyltransferase	3
328	6.19	6.19	27.69	27.69	22.31	637342261	SO0254	30S ribosomal protein S11	3
329	6.18	6.18	11.71	11.71	9.91	637343663	SO1777	decaheme cytochrome c MtrA	5
330	6.13	6.13	14.13	7.61	6.64	637342089	SO0076	hypothetical protein	3
331	6.09	6.09	31.71	31.71	24.39	637343675	SO1790	peptidyl-prolyl cis-trans isomerase B	4
332	6.06	6.06	16.63	16.63	13.58	637345214	SO3413	threonine synthase	3
333	6.01	6.01	13.13	6.76	6.76	637345099	SO3286	cytochrome d ubiquinol oxidase, subunit I	3
334	6.01	6.01	42.31	34.62	34.62	637345698	SO3939	ribosomal protein S9	3
335	6.00	8.00	23.66	21.26	13.31	637345382	SO3582	methyl-accepting chemotaxis protein	4
336	6.00	8.00	15.70	13.57	13.57	637346593	SOA0154	heavy metal efflux protein, putative	4
337	6.00	8.00	11.78	11.78	11.78	637346045	SO4319	HlyD family secretion protein	4
338	6.00	6.00	9.50	7.17	7.17	637346226	SO4506	iron-sulfur cluster-binding protein	3
339	6.00	6.00	22.46	16.31	16.31	637345742	SO3991	fructose-1,6-bisphosphatase	3
340	6.00	6.00	65.00	41.00	41.00	637345133	SO3325	nrfJ-related protein	5
341	6.00	6.00	46.67	29.44	29.44	637344749	SO2938	hypothetical protein	3
342	6.00	6.00	10.57	6.83	6.83	637342802	SO0830	alkaline phosphatase	3
343	6.00	6.00	53.33	40.00	40.00	637342541	SO0548	DNA-binding protein, HU family	3
344	6.00	6.00	28.99	18.36	18.36	637342365	SO0361	guanylate kinase	3
345	6.00	6.00	37.50	33.09	33.09	637342245	SO0238	50S ribosomal protein L16	5
346	6.00	6.00	28.50	28.50	28.50	637346374	SO4666	cytochrome c	4
347	6.00	6.00	44.00	44.00	44.00	637346273	SO4561	hypothetical protein	3

348	6.00	6.00	16.46	16.46	16.46	637345810	SO4070	hypothetical protein	3
349	6.00	6.00	17.65	17.65	17.65	637345740	SO3988	aerobic respiration control protein ArcA	3
350	6.00	6.00	31.25	31.25	31.25	637345668	SO3907	hypothetical protein	3
351	6.00	6.00	15.38	15.38	15.38	637345579	SO3812	peptidyl-prolyl cis-trans isomerase A	4
352	6.00	6.00	17.20	17.20	17.20	637345499	SO3718	thiol:disulfide interchange protein, DsbA family	3
353	6.00	6.00	42.86	42.86	42.86	637345440	SO3651	50S ribosomal protein L27	3
354	6.00	6.00	27.27	27.27	27.27	637344917	SO3112	preprotein translocase subunit YajC	3
355	6.00	6.00	7.62	7.62	7.62	637344853	SO3048	isoquinoline 1-oxidoreductase, beta subunit, putative	3
356	6.00	6.00	6.06	6.06	6.06	637344678	SO2857	sodium/solute symporter family protein	3
357	6.00	6.00	19.67	19.67	19.67	637344155	SO2312	ecotin precursor	3
358	6.00	6.00	21.45	21.45	21.45	637344147	SO2303	thioredoxin reductase	5
359	6.00	6.00	39.64	39.64	39.64	637344087	SO2236	glucose-specific PTS system enzyme IIA component	3
360	6.00	6.00	26.32	26.32	26.32	637344057	SO2201	hypothetical protein	3
361	6.00	6.00	17.89	17.89	17.89	637343780	SO1891	3-oxoadipate CoA-succinyl transferase, beta subunit	3
362	6.00	6.00	20.51	20.51	20.51	637343332	SO1390	peptidyl-prolyl cis-trans isomerase, FKBP-type	3
363	6.00	6.00	36.02	36.02	36.02	637343322	SO1378	ThiJ/PfpI family protein	3
364	6.00	6.00	43.90	43.90	43.90	637343301	SO1357	ribosomal protein S16	4
365	6.00	6.00	10.68	10.68	10.68	637342610	SO0619	succinylglutamic semialdehyde dehydrogenase	3
366	5.89	5.89	12.13	6.72	6.72	637343741	SO1854	hypothetical protein	3
367	5.77	5.77	14.94	11.65	11.65	637343816	SO1931	2-oxoglutarate dehydrogenase, E2 component, dihydrolipoamide succinyltransferase	3
368	5.77	5.77	12.02	12.02	12.02	637343547	SO1639	UDP-3-O-(3-hydroxymyristoyl) glucosamine n-acyltransferase	4
369	5.77	5.77	13.18	13.18	10.29	637342719	SO0740	melanin biosynthesis protein TyrA, putative	3
370	5.72	5.72	11.75	11.75	10.25	637343687	SO1800	hypothetical protein	4
371	5.72	5.72	33.62	33.62	33.62	637342254	SO0247	50S ribosomal protein L18	3
372	5.68	5.68	19.37	12.84	7.94	637345375	SO3577	clpB protein	3
373	5.62	5.62	14.11	7.90	7.90	637343059	SO1108	Na(+)-translocating NADH-quinone reductase subunit F	3
374	5.60	5.60	10.47	7.64	7.64	637344890	SO3088	fatty oxidation complex, alpha subunit	5
375	5.54	5.54	20.87	17.39	17.39	637342244	SO0237	ribosomal protein S3	3
376	5.49	5.49	8.75	5.58	5.58	637345359	SO3560	peptidase, M16 family	3
377	5.40	5.40	46.33	46.33	26.55	637344579	SO2747	peptidoglycan-associated lipoprotein	3
378	5.39	5.40	22.14	14.50	14.50	637342264	SO0257	50S ribosomal protein L17	4
379	5.38	5.40	18.32	18.32	18.32	637343191	SO1242	hypothetical protein	3
380	5.32	5.32	25.31	25.31	25.31	637344307	SO2478	3-deoxy-manno-octulosonate cytidylyltransferase	3
381	5.25	5.25	19.69	19.69	10.50	637342597	SO0605	hflK protein	3
382	5.24	5.24	26.44	21.26	21.26	637345037	SO3222	flagellar basal body-associated protein	3
383	5.23	5.23	18.81	18.81	18.81	637342496	SO0501	hypothetical protein	4

384	5.21	5.21	33.07	33.07	33.07	637342362	SO0358	endoribonuclease L-PSP, putative	3
385	5.10	5.10	21.77	21.77	21.77	637342233	SO0226	30S ribosomal protein S12	3
386	5.00	5.00	21.60	21.60	17.20	637344578	SO2746	hypothetical protein	3
387	4.96	4.96	8.96	4.11	3.56	637345212	SO3411	protease, putative	3
388	4.81	4.81	33.33	19.48	19.48	637345666	SO3905	hypothetical protein	3
389	4.78	4.78	15.63	15.63	15.63	637343549	SO1641	UDP-N-acetylglucosamine acyltransferase	3
390	4.76	4.76	6.19	6.19	6.19	637345109	SO3299	Pal/histidase family protein	3
391	4.71	4.71	30.41	23.50	23.50	637342152	SO0142	3,4-dihydroxy-2-butanone 4-phosphate synthase	3
392	4.66	4.66	17.46	17.46	11.24	637343204	SO1258	adenylosuccinate synthetase, putative	3
393	4.66	4.66	12.86	12.86	12.86	637344603	SO2774	3-oxoacyl-(acyl-carrier-protein) synthase II	4
394	4.63	4.63	20.08	20.08	20.08	637343849	SO1966	conserved hypothetical protein TIGR00266	3
395	4.62	4.62	8.03	3.57	3.57	637342231	SO0224	DNA-directed RNA polymerase, beta subunit	3
396	4.60	4.60	8.29	4.75	4.75	637343089	SO1142	carbamoyl-phosphate synthase large subunit	3
397	4.60	4.60	9.52	6.60	6.60	637345341	SO3542	putative phosphoketolase	3
398	4.51	4.51	25.07	16.22	8.56	637343247	SO1301	aspartate carbamoyltransferase	2
399	4.50	4.50	5.95	3.44	3.44	637345225	SO3424	valyl-tRNA synthetase	3
400	4.41	4.41	16.67	16.67	16.67	637343583	SO1677	acetyl-CoA acetyltransferase	3
401	4.39	4.39	12.10	4.80	4.80	637343492	SO1571	hypothetical protein	3
402	4.38	4.38	17.03	17.03	13.97	637345539	SO3765	hypothetical protein	2
403	4.35	4.35	11.04	6.13	5.03	637343415	SO1482	TonB-dependent receptor, putative	2
404	4.33	4.33	17.43	14.83	8.42	637343584	SO1678	methylmalonate-semialdehyde dehydrogenase	2
405	4.29	4.29	32.03	21.71	21.71	637343087	SO1140	dihydrodipicolinate reductase	3
406	4.21	4.21	27.60	11.20	11.20	637342018	SO0009	DNA polymerase III, beta subunit	3
407	4.19	4.19	37.58	28.48	22.42	637344046	SO2190	creA protein	2
408	4.15	4.15	9.29	4.37	2.73	637345679	SO3918	hypothetical protein	2
409	4.14	4.14	11.66	11.66	8.46	637342678	SO0693	aldose 1-epimerase	2
410	4.11	4.11	21.41	12.07	8.20	637342031	SO0022	prolidase	3
411	4.10	4.10	28.16	28.16	21.36	637345441	SO3652	ribosomal protein L21	2
412	4.08	4.08	24.60	24.60	24.60	637344621	SO2795	glyoxalase family protein	3
413	4.07	4.07	8.69	8.69	5.85	637345358	SO3559	glutamate--cysteine ligase	2
414	4.06	4.06	27.43	18.57	13.50	637345981	SO4256	ribonuclease PH	2
415	4.06	4.06	15.25	15.25	14.69	637346185	SO4470	hypothetical protein	2
416	4.06	4.06	24.08	24.08	20.41	637345669	SO3908	enoyl-CoA hydratase/isomerase family protein	2
417	4.06	4.06	31.88	31.88	26.09	637342419	SO0417	pilin, putative	3
418	4.04	6.06	10.44	10.44	8.97	637346555	SOA0106	methyl-accepting chemotaxis protein	3
419	4.04	4.04	14.35	14.35	11.11	637342441	SO0441	phosphoribosylamine--glycine ligase	2
420	4.02	4.02	37.89	37.89	37.89	637344236	SO2401	integration host factor, beta subunit	3
421	4.02	4.02	30.19	7.97	7.97	637345851	SO4118	malate oxidoreductase, putative	2
422	4.00	6.00	9.21	6.29	6.29	637342294	SO0285	type IV pilus biogenesis protein PilQ	3
423	4.00	4.00	30.19	14.29	14.29	637344961	SO3144	electron transfer flavoprotein, alpha subunit	2

424	4.00	4.00	30.23	13.66	13.66	637343913	SO2042	hypothetical protein	2
425	4.00	4.00	8.75	7.33	5.69	637343450	SO1521	iron-sulfur cluster-binding protein	2
426	4.00	4.00	14.81	6.58	6.58	637343066	SO1115	aminoacyl-histidine dipeptidase	2
427	4.00	4.00	31.98	13.37	13.37	637342780	SO0805	CBS domain protein	2
428	4.00	4.00	43.81	27.62	27.62	637346500	SOA0041	transcriptional regulator, PemK family	2
429	4.00	4.00	19.05	7.94	7.94	637345604	SO3837	ribose-phosphate pyrophosphokinase	2
430	4.00	4.00	42.94	21.47	21.47	637345353	SO3554	phosphoribosylaminoimidazole carboxylase, catalytic subunit	2
431	4.00	4.00	4.58	3.20	3.20	637345237	SO3428	alanyl-tRNA synthetase	2
432	4.00	4.00	27.93	13.96	13.96	637345217	SO3417	peptidyl-prolyl cis-trans isomerase SlyD	3
433	4.00	4.00	19.83	10.74	10.74	637344092	SO2241	hypothetical protein	2
434	4.00	4.00	13.49	6.88	6.88	637343965	SO2099	quinone-reactive Ni/Fe hydrogenase, small subunit precursor	2
435	4.00	4.00	26.87	18.50	18.50	637343694	SO1807	phage shock protein A	2
436	4.00	4.00	16.67	13.73	13.73	637343564	SO1656	ROK family protein	2
437	4.00	4.00	13.21	13.21	13.21	637343536	SO1627	methionine aminopeptidase	3
438	4.00	4.00	33.33	22.22	22.22	637343304	SO1360	50S ribosomal protein L19	2
439	4.00	4.00	16.72	8.52	8.52	637343291	SO1347	signal peptidase I	2
440	4.00	4.00	5.52	4.38	4.38	637343229	SO1284	RNA polymerase sigma-70 factor	2
441	4.00	4.00	23.81	17.01	17.01	637343160	SO1205	ribosome-binding factor A	2
442	4.00	4.00	21.52	15.82	15.82	637343144	SO1191	transcription elongation factor GreA	2
443	4.00	4.00	15.15	8.82	8.82	637343132	SO1185	conserved hypothetical protein TIGR00092	2
444	4.00	4.00	28.06	15.47	15.47	637343003	SO1045	hypothetical protein	2
445	4.00	4.00	19.66	11.53	11.53	637342848	SO0878	phosphoribulokinase	2
446	4.00	4.00	20.21	14.36	14.36	637342782	SO0807	hypoxanthine-guanine phosphoribosyltransferase	2
447	4.00	4.00	11.60	7.00	7.00	637342442	SO0442	bifunctional phosphoribosylaminoimidazolecarboxamide formyltransferase/IMP cyclohydrolase	2
448	4.00	4.00	14.40	6.40	6.40	637342348	SO0344	citrate synthase	2
449	4.00	4.00	34.55	20.91	20.91	637342243	SO0236	ribosomal protein L22	3
450	4.00	4.00	16.39	16.39	16.39	637346510	SOA0051	hypothetical protein	2
451	4.00	4.00	7.51	7.51	7.51	637346427	SO4723	molybdopterin biosynthesis MoeA protein, putative	2
452	4.00	4.00	20.64	20.64	20.64	637346377	SO4670	enhancing lycopene biosynthesis protein	2
453	4.00	4.00	51.72	51.72	51.72	637346359	SO4651	hypothetical protein	2
454	4.00	4.00	13.30	13.30	13.30	637346188	SO4473	outer membrane protein, putative	2
455	4.00	4.00	6.28	6.28	6.28	637346035	SO4309	diaminopimelate decarboxylase	2
456	4.00	4.00	10.08	10.08	10.08	637345775	SO4028	single-strand binding protein	2
457	4.00	4.00	13.41	13.41	13.41	637345693	SO3934	RNA methyltransferase, TrmH family, group 3	2
458	4.00	4.00	7.55	7.55	7.55	637345662	SO3901	lacZ expression regulator	2
459	4.00	4.00	15.43	15.43	15.43	637345578	SO3811	lipoprotein, putative	2
460	4.00	4.00	17.03	17.03	17.03	637345546	SO3772	hypothetical protein	2
461	4.00	4.00	16.06	16.06	16.06	637345538	SO3764	hypothetical protein	2

462	4.00	4.00	20.27	20.27	20.27	637345482	SO3698	hypothetical protein	2
463	4.00	4.00	3.44	3.44	3.44	637345454	SO3669	heme transport protein	2
464	4.00	4.00	11.01	11.01	11.01	637345330	SO3529	penicillin tolerance protein LytB	2
465	4.00	4.00	32.61	32.61	32.61	637345172	SO3369	hypothetical protein	2
466	4.00	4.00	2.55	2.55	2.55	637345100	SO3287	phosphoribosylformylglycinamidine synthase	2
467	4.00	4.00	21.77	21.77	21.77	637345035	SO3220	flagellar motor switch protein	2
468	4.00	4.00	14.46	14.46	14.46	637344962	SO3145	electron transfer flavoprotein, beta subunit	2
469	4.00	4.00	5.92	5.92	5.92	637344828	SO3019	anthranilate synthase component I	2
470	4.00	4.00	10.00	10.00	10.00	637344695	SO2878	hypothetical protein	2
471	4.00	4.00	9.45	9.45	9.45	637344637	SO2813	short chain dehydrogenase	2
472	4.00	4.00	31.36	31.36	31.36	637344546	SO2723	HIT family protein	2
473	4.00	4.00	12.29	12.29	12.29	637344246	SO2413	3-demethylubiquinone-9 3-methyltransferase	2
474	4.00	4.00	10.06	10.06	10.06	637344183	SO2347	glyceraldehyde-3-phosphate dehydrogenase	2
475	4.00	4.00	13.66	13.66	13.66	637344172	SO2335	seqA protein	2
476	4.00	4.00	28.57	28.57	28.57	637344168	SO2330	flavodoxin	2
477	4.00	4.00	23.81	23.81	23.81	637344123	SO2277	16 kDa heat shock protein A	2
478	4.00	4.00	11.75	11.75	11.75	637344101	SO2254	hypothetical protein	2
479	4.00	4.00	23.53	23.53	23.53	637343915	SO2044	lactoylglutathione lyase	2
480	4.00	4.00	27.27	27.27	27.27	637343800	SO1913	hypothetical protein	2
481	4.00	4.00	11.97	11.97	11.97	637343677	SO1792	methylenetetrahydrofolate dehydrogenase/methylene tetrahydrofolate cyclohydrolase	2
482	4.00	4.00	15.89	15.89	15.89	637343579	SO1673	outer membrane protein OmpW, putative	3
483	4.00	4.00	8.33	8.33	8.33	637343560	SO1652	hypothetical protein	2
484	4.00	4.00	10.20	10.20	10.20	637343295	SO1351	pyridoxal phosphate biosynthetic protein	2
485	4.00	4.00	31.40	31.40	31.40	637343271	SO1327	sensor histidine kinase-related protein	2
486	4.00	4.00	20.38	20.38	20.38	637343062	SO1111	bacterioferritin subunit 2	2
487	4.00	4.00	5.86	5.86	5.86	637343054	SO1103	Na(+)-translocating NADH-quinone reductase subunit A	2
488	4.00	4.00	22.84	22.84	22.84	637343016	SO1060	hypothetical protein	3
489	4.00	4.00	12.65	12.65	12.65	637342901	SO0934	hypothetical protein	3
490	4.00	4.00	20.29	20.29	20.29	637342890	SO0923	hypothetical protein	2
491	4.00	4.00	9.74	9.74	9.74	637342857	SO0887	hypothetical protein	2
492	4.00	4.00	17.80	17.80	17.80	637342840	SO0870	3-methyl-2-oxobutanoate hydroxymethyltransferase	3
493	4.00	4.00	25.93	25.93	25.93	637342767	SO0788	hypothetical protein	2
494	4.00	4.00	17.61	17.61	17.61	637342322	SO0316	hypothetical phosphatidylethanolamine-binding protein	2
495	4.00	4.00	13.11	13.11	13.11	637342226	SO0219	transcription antitermination protein NusG	2
496	3.73	3.73	15.50	12.40	10.08	637342029	SO0020	acetyl-CoA acetyltransferase	2
497	3.70	3.70	13.44	13.44	13.44	637345091	SO3275	hypothetical protein	2
498	3.67	3.67	21.19	16.10	16.10	637344146	SO2302	50S ribosomal protein L20	2
499	3.66	3.66	10.70	10.70	10.70	637343951	SO2085	phenylalanyl-tRNA synthetase alpha subunit	3

500	3.64	3.66	14.23	14.23	14.23	637343212	SO1267	hypothetical Glutamine amidotransferase	2
501	3.57	3.57	9.71	4.95	4.95	637345103	SO3292	bifunctional GMP synthase/glutamine amidotransferase protein	2
502	3.57	3.57	22.71	22.71	22.71	637344191	SO2353	hypothetical protein	2
503	3.53	3.53	54.74	54.74	48.42	637345718	SO3962	ribosomal subunit interface protein	2
504	3.37	3.37	57.14	57.14	57.14	637344609	SO2780	ribosomal protein L32	2
505	3.33	3.33	32.05	32.05	32.05	637342747	SO0769	arginine repressor	2
506	3.20	3.20	4.35	4.35	4.35	637343567	SO1659	decaheme cytochrome c	3
507	3.20	3.20	14.47	14.47	14.47	637343478	SO1556	hypothetical protein	3
508	3.19	3.19	38.33	38.33	38.33	637342256	SO0249	ribosomal protein L30	2
509	3.08	3.08	9.73	6.13	6.13	637344897	SO3095	hypothetical protein	2
510	3.07	3.08	11.45	11.45	11.45	637342302	SO0293	phosphoglycolate phosphatase	2
511	3.06	3.06	16.96	16.96	16.96	637345320	SO3519	nitrogen regulatory protein P-II 1	2
512	3.05	3.05	7.60	7.60	7.60	637342111	SO0098	histidine ammonia-lyase	2
513	3.02	3.02	20.37	20.37	20.37	637343250	SO1304	HesB/YadR/YfhF family protein	2
514	2.99	2.99	33.75	33.75	33.75	637345866	SO4138	hypothetical protein	2
515	2.95	2.95	3.25	3.25	3.25	637342427	SO0425	pyruvate dehydrogenase complex, E2 component, dihydrolipoamide acetyltransferase	2
516	2.90	2.90	27.81	13.91	13.91	637343157	SO1202	hypothetical protein	2
517	2.87	2.87	14.97	6.54	6.54	637345078	SO3262	acetolactate synthase isozyme I, large subunit	2
518	2.72	2.72	19.92	19.92	16.02	637343169	SO1217	deoxyribose-phosphate aldolase	2
519	2.66	2.66	7.42	2.97	2.36	637343269	SO1325	glutamate synthase, large subunit	2
520	2.63	2.63	27.53	6.62	6.62	637344551	SO2728	heat shock protein HtpX	2
521	2.57	2.57	21.35	21.35	21.35	637342611	SO0620	hypothetical protein	2
522	2.52	2.52	25.51	25.51	21.43	637342599	SO0608	ubiquinol-cytochrome c reductase, iron-sulfur subunit	2
523	2.51	2.51	8.79	3.84	3.84	637345694	SO3935	ribonuclease R	2
524	2.37	2.37	14.29	14.29	14.29	637342208	SO0208	RNA-binding protein	2
525	2.35	2.35	9.61	9.61	9.61	637344415	SO2587	delta-aminolevulinic acid dehydratase	3
526	2.30	2.30	25.41	18.23	18.23	637343887	SO2012	adenine phosphoribosyltransferase	2
527	2.27	2.27	15.79	13.53	13.53	637344365	SO2533	hypothetical protein	3
528	2.26	2.27	5.76	4.28	4.28	637342702	SO0719	TonB-dependent receptor, putative	2
529	2.26	2.26	8.72	8.72	8.72	637344175	SO2338	succinylglutamate desuccinylase	2
530	2.25	2.26	7.63	7.63	1.47	637344429	SO2601	carboxyl-terminal protease	1
531	2.23	2.23	15.23	15.23	5.76	637345869	SO4141	oxidoreductase, short-chain dehydrogenase/reductase family	2
532	2.20	2.20	27.59	27.59	13.79	637343024	SO1068	hypothetical protein	1
533	2.19	2.19	22.53	22.53	5.49	637344533	SO2708	nitroreductase family protein	1
534	2.15	2.15	27.10	27.10	11.21	637342515	SO0521	hypothetical protein	1
535	2.06	2.06	45.52	32.41	11.03	637345210	SO3409	OsmC/Ohr family protein	1
536	2.06	2.06	14.95	7.94	4.67	637344859	SO3054	metallo-beta-lactamase family protein	1
537	2.05	2.05	4.10	3.08	1.54	637344230	SO2395	acyl-CoA dehydrogenase family protein	1

538	2.05	2.05	8.97	4.48	3.26	637342430	SO0428	hypothetical protein	1
539	2.04	2.04	16.42	13.13	7.16	637343465	SO1538	isocitrate dehydrogenase	1
540	2.04	2.04	16.39	16.39	16.39	637345713	SO3957	3-deoxy-D-manno-octulosonate 8-phosphate phosphatase	2
541	2.04	2.04	19.58	19.58	19.58	637343821	SO1937	ferric uptake regulator	2
542	2.03	2.03	18.18	18.18	11.36	637344591	SO2760	phosphoribosylaminoimidazole synthetase	1
543	2.03	2.03	19.80	19.80	9.90	637342240	SO0233	50S ribosomal protein L23	1
544	2.02	2.02	29.66	29.66	14.48	637344656	SO2839	hypothetical protein	1
545	2.01	2.01	26.39	6.67	6.67	637345702	SO3943	protease DegS	1
546	2.01	2.01	45.76	38.98	23.73	637342341	SO0337	hypothetical translation initiation inhibitor, yjgF family	2
547	2.01	2.01	24.36	12.82	12.82	637345973	SO4247	ribosomal protein L28	1
548	2.01	2.01	8.10	8.10	8.10	637345117	SO3309	PQQ enzyme repeat domain protein	2
549	2.01	2.01	8.42	2.63	2.63	637344462	SO2636	hypothetical protein	1
550	2.01	2.01	23.26	8.53	8.53	637343644	SO1756	glyoxalase family protein	1
551	2.01	2.01	4.77	1.99	1.99	637343437	SO1507	hypothetical protein	1
552	2.01	2.01	9.61	6.78	6.78	637343302	SO1358	16S rRNA-processing protein	1
553	2.01	2.01	36.17	13.48	13.48	637342941	SO0976	organic hydroperoxide resistance protein	1
554	2.01	2.01	20.98	8.29	8.29	637342768	SO0789	short chain dehydrogenase	1
555	2.01	2.01	30.69	30.69	30.69	637342251	SO0244	ribosomal protein S14	2
556	2.01	2.01	3.70	2.14	2.14	637342165	SO0162	phosphoenolpyruvate carboxykinase	1
557	2.00	55.80	82.23	80.46	80.46	637342224	SO0217	translation elongation factor Tu	51
558	2.00	8.00	23.28	23.28	23.28	637346234	SO4514	formate dehydrogenase, iron-sulfur subunit	5
559	2.00	4.00	10.79	6.03	6.03	637343014	SO1056	methyl-accepting chemotaxis protein	2
560	2.00	2.00	11.40	3.29	3.29	637344461	SO2635	adenylosuccinate lyase	1
561	2.00	2.00	6.17	3.22	3.22	637343365	SO1424	hypothetical protein	1
562	2.00	2.00	7.16	1.40	1.40	637346507	SOA0048	prolyl oligopeptidase family protein	1
563	2.00	2.00	27.14	14.29	14.29	637345863	SO4134	hypothetical protein	1
564	2.00	2.00	12.53	6.26	6.26	637345816	SO4078	pmba protein	1
565	2.00	2.00	23.57	12.10	12.10	637345709	SO3952	mce-related protein	1
566	2.00	2.00	18.88	16.81	5.31	637344949	SO3134	C4-dicarboxylate-binding periplasmic protein	1
567	2.00	2.00	9.33	4.66	4.66	637343835	SO1952	gamma-glutamyltranspeptidase	1
568	2.00	2.00	16.16	4.66	4.66	637343770	SO1880	lipoprotein-34 NlpB	1
569	2.00	2.00	8.31	2.87	2.87	637342761	SO0783	hypothetical protein	1
570	2.00	2.00	15.49	7.75	7.75	637342641	SO0655	hypothetical protein	1
571	2.00	2.00	1.59	0.59	0.59	637342191	SO0189	fibronectin type III domain protein	1
572	2.00	2.00	11.30	7.34	7.34	637346454	SO4750	ATP synthase F1, delta subunit	1
573	2.00	2.00	6.17	2.56	2.56	637346241	SO4523	iron-regulated outer membrane virulence protein	1
574	2.00	2.00	4.77	0.99	0.99	637345569	SO3800	serine protease, subtilase family	1
575	2.00	2.00	8.40	3.15	3.15	637345275	SO3469	riboflavin biosynthesis protein RibD	1
576	2.00	2.00	9.33	6.74	6.74	637345056	SO3239	3 hypothetical flagellar hook-associated protein	1
577	2.00	2.00	38.58	17.32	17.32	637345025	SO3209	chemotaxis protein CheY	1

578	2.00	2.00	14.80	8.38	8.38	637345002	SO3185	polysaccharide biosynthesis protein	1
579	2.00	2.00	9.26	4.81	4.81	637344844	SO3037	exodeoxyribonuclease III	1
580	2.00	2.00	4.79	3.10	3.10	637344741	SO2929	hypothetical protein	1
581	2.00	2.00	27.97	12.71	12.71	637344650	SO2832	hypothetical protein	1
582	2.00	2.00	12.64	5.17	5.17	637344610	SO2781	hypothetical protein	1
583	2.00	2.00	47.22	16.67	16.67	637344452	SO2625	translation initiation factor IF-1	1
584	2.00	2.00	12.68	7.98	7.98	637344430	SO2602	putative solute/DNA competence effector	1
585	2.00	2.00	8.90	5.51	5.51	637343622	SO1726	phosphate transport system regulatory protein PhoU	1
586	2.00	2.00	5.49	3.35	3.35	637343576	SO1670	fumarylacetoacetate hydrolase family protein	1
587	2.00	2.00	8.29	2.59	2.59	637343088	SO1141	carbamoyl-phosphate synthase small subunit	1
588	2.00	2.00	11.11	5.97	5.97	637343026	SO1070	catalase	1
589	2.00	2.00	7.78	3.04	3.04	637342923	SO0956	alkyl hydroperoxide reductase, F subunit	1
590	2.00	2.00	2.83	2.83	2.83	637342831	SO0861	hypothetical protein	1
591	2.00	2.00	8.24	3.13	3.13	637342734	SO0756	3-deoxy-7-phosphoheptulonate synthase	1
592	2.00	2.00	27.45	13.73	13.73	637342549	SO0556	hypothetical protein	1
593	2.00	2.00	12.76	5.65	5.65	637342533	SO0541	metallo-beta-lactamase family protein	2
594	2.00	2.00	15.53	7.28	7.28	637342292	SO0283	type IV pilus biogenesis protein PilO	1
595	2.00	2.00	16.85	10.33	10.33	637342275	SO0267	thiol:disulfide interchange protein DsbE	1
596	2.00	2.00	46.03	22.22	22.22	637342246	SO0239	ribosomal protein L29	1
597	2.00	2.00	4.94	2.07	2.07	637342160	SO0152	hypothetical carboxypeptidase	1
598	2.00	2.00	33.33	16.67	16.67	637342041	SO0032	polypeptide deformylase	1
599	2.00	2.00	9.16	9.16	9.16	637346450	SO4746	ATP synthase F1, epsilon subunit	1
600	2.00	2.00	6.56	6.56	6.56	637346432	SO4728	hypothetical protein	1
601	2.00	2.00	3.45	3.45	3.45	637346325	SO4616	polysaccharide deacetylase family protein	1
602	2.00	2.00	5.33	5.33	5.33	637346227	SO4507	TorA specific chaperone, putative	1
603	2.00	2.00	13.25	13.25	13.25	637346168	SO4450	molybdenum cofactor biosynthesis protein D	1
604	2.00	2.00	9.03	9.03	9.03	637346167	SO4449	molybdenum cofactor biosynthesis protein E	1
605	2.00	2.00	2.30	2.30	2.30	637346100	SO4374	histidine ammonia-lyase, putative	1
606	2.00	2.00	14.02	14.02	14.02	637346037	SO4311	cyay protein	2
607	2.00	2.00	9.87	9.87	9.87	637345976	SO4250	deoxyuridine 5'-triphosphate nucleotidohydrolase	1
608	2.00	2.00	10.34	10.34	10.34	637345888	SO4162	ATP-dependent protease peptidase subunit	1
609	2.00	2.00	16.00	16.00	16.00	637345688	SO3928	ribosomal protein S18	1
610	2.00	2.00	5.45	5.45	5.45	637345525	SO3749	hypothetical protein	1
611	2.00	2.00	3.41	3.41	3.41	637345517	SO3741	pyridine nucleotide transhydrogenase	1
612	2.00	2.00	17.05	17.05	17.05	637345336	SO3537	ribosomal protein S20	1
613	2.00	2.00	14.41	14.41	14.41	637345205	SO3403	ribosomal subunit interface protein	1
614	2.00	2.00	15.09	15.09	15.09	637345069	SO3254	negative regulator of flagellin synthesis FlgM	1
615	2.00	2.00	8.40	8.40	8.40	637345051	SO3236	flagellin FlaG	1

616	2.00	2.00	8.25	8.25	8.25	637344913	SO3108	siroheme synthase, N-terminal component, putative	1
617	2.00	2.00	16.16	16.16	16.16	637344843	SO3036	hypothetical protein	1
618	2.00	2.00	6.40	6.40	6.40	637344713	SO2897	cell division protein ZipA	1
619	2.00	2.00	7.77	7.77	7.77	637344688	SO2869	hypothetical protein	1
620	2.00	2.00	12.30	12.30	12.30	637344672	SO2851	hypothetical protein	1
621	2.00	2.00	16.88	16.88	16.88	637344604	SO2775	acyl carrier protein	1
622	2.00	2.00	9.35	9.35	9.35	637344592	SO2761	phosphoribosylglycinamide formyltransferase	1
623	2.00	2.00	6.90	6.90	6.90	637344550	SO2727	cytochrome c3	1
624	2.00	2.00	1.37	1.37	1.37	637344530	SO2705	DNA topoisomerase I	1
625	2.00	2.00	10.14	10.14	10.14	637344496	SO2670	hypothetical protein	2
626	2.00	2.00	6.20	6.20	6.20	637344445	SO2618	ATP-binding protein, Mrp/Nbp35 family	1
627	2.00	2.00	9.21	9.21	9.21	637344431	SO2603	hypothetical protein	1
628	2.00	2.00	16.84	16.84	16.84	637344328	SO2499	hypothetical protein	1
629	2.00	2.00	6.93	6.93	6.93	637344233	SO2398	orotidine 5`-phosphate decarboxylase	1
630	2.00	2.00	3.99	3.99	3.99	637344223	SO2388	beta-lactamase	1
631	2.00	2.00	18.12	18.12	18.12	637344082	SO2228	CBS domain protein	1
632	2.00	2.00	5.26	5.26	5.26	637344047	SO2191	cystathionine beta-lyase	1
633	2.00	2.00	6.65	6.65	6.65	637343939	SO2072	histidinol-phosphate aminotransferase	1
634	2.00	2.00	14.66	14.66	14.66	637343930	SO2062	hypothetical protein	1
635	2.00	2.00	11.93	11.93	11.93	637343889	SO2014	conserved hypothetical protein TIGR00103	1
636	2.00	2.00	8.64	8.64	8.64	637343873	SO1995	peptidyl-prolyl cis-trans isomerase, FkbP family	1
637	2.00	2.00	4.68	4.68	4.68	637343814	SO1929	succinate dehydrogenase catalytic subunit	1
638	2.00	2.00	8.97	8.97	8.97	637343781	SO1892	acetate CoA-transferase, subunit A	1
639	2.00	2.00	9.60	9.60	9.60	637343600	SO1698	hypothetical protein	1
640	2.00	2.00	9.61	9.61	9.61	637343595	SO1691	lipoprotein Blc	2
641	2.00	2.00	4.81	4.81	4.81	637343500	SO1581	phnA protein	1
642	2.00	2.00	8.67	8.67	8.67	637343482	SO1560	phosphate-binding protein	1
643	2.00	2.00	7.14	7.14	7.14	637343443	SO1513	hypothetical protein	1
644	2.00	2.00	29.69	29.69	29.69	637343281	SO1337	hypothetical protein	1
645	2.00	2.00	7.96	7.96	7.96	637343252	SO1306	hypothetical protein	1
646	2.00	2.00	5.61	5.61	5.61	637343207	SO1261	mercaptopyruvate sulfurtransferase	1
647	2.00	2.00	5.09	5.09	5.09	637343167	SO1214	NupC family protein	1
648	2.00	2.00	21.10	21.10	21.10	637343117	SO1170	iojap domain protein	1
649	2.00	2.00	2.00	2.00	2.00	637342981	SO1019	NADH dehydrogenase I, C/D subunits	1
650	2.00	2.00	4.69	4.69	4.69	637342966	SO1006	dienelactone hydrolase family protein	1
651	2.00	2.00	2.85	2.85	2.85	637342870	SO0902	Na(+)-translocating NADH-quinone reductase subunit A	2
652	2.00	2.00	4.53	4.53	4.53	637342808	SO0837	beta-lactamase, putative	1
653	2.00	2.00	7.59	7.59	7.59	637342784	SO0809	azurin precursor	1
654	2.00	2.00	10.44	10.44	10.44	637342726	SO0747	ferredoxin--NADP reductase	1
655	2.00	2.00	5.69	5.69	5.69	637342615	SO0624	catabolite gene activator	1
656	2.00	2.00	5.46	5.46	5.46	637342587	SO0595	hypothetical protein	1

657	2.00	2.00	12.71	12.71	12.71	637342582	SO0592	oligoribonuclease	1
658	2.00	2.00	7.08	7.08	7.08	637342577	SO0587	glycerophosphoryl diester phosphodiesterase, putative	1
659	2.00	2.00	9.82	9.82	9.82	637342571	SO0581	hypothetical protein	1
660	2.00	2.00	6.32	6.32	6.32	637342547	SO0554	hypothetical protein	1
661	2.00	2.00	9.59	9.59	9.59	637342507	SO0512	3-dehydroquinate dehydratase	1
662	2.00	2.00	11.70	11.70	11.70	637342468	SO0471	hypothetical dioxygenase	1
663	2.00	2.00	3.30	3.30	3.30	637342281	SO0272	competence/damage-inducible protein CinA	1
664	2.00	2.00	7.10	7.10	7.10	637342198	SO0196	selenide, water dikinase	1
665	2.00	2.00	5.17	5.17	5.17	637342130	SO0118	hypothetical protein	1
666	2.00	2.00	8.45	8.45	8.45	637342093	SO0080	hypothetical 4-hydroxybenzoyl-CoA thioesterase	1
667	2.00	2.00	8.90	8.90	8.90	637342010	SO0001	flavodoxin	1
668	1.92	2.00	23.91	23.91	23.91	637342364	SO0360	DNA-directed RNA polymerase omega subunit	1
669	1.74	2.00	5.59	5.59	5.59	637342435	SO0433	regulator of sigma D	1
670	1.67	1.67	7.90	7.90	7.90	637346392	SO4685	hypothetical protein	2
671	1.62	1.62	5.56	5.56	5.56	637342975	SO1014	NADH dehydrogenase subunit I	1
672	1.62	1.62	6.88	6.88	6.88	637342776	SO0799	hypothetical protein	1
673	1.62	1.62	6.19	6.19	6.19	637342746	SO0768	Putative NADH-flavin reductase	1
674	1.62	1.62	9.55	9.55	9.55	637342520	SO0526	acetyltransferase, GNAT family	1
675	1.52	1.52	21.36	15.53	15.53	637344150	SO2307	outer membrane lipoprotein carrier protein LolA	1
676	1.45	1.45	31.82	10.00	10.00	637343851	SO1968	hypothetical protein	1
677	1.44	1.44	7.55	3.14	3.14	637345765	SO4017	transglycosylase, Slt family	1
678	1.44	1.44	4.61	2.70	2.70	637346462	SO4758	glucose-inhibited division protein A	1
679	1.44	1.44	13.26	4.17	4.17	637345251	SO3442	MazG family protein	1
680	1.38	1.38	2.08	2.08	2.08	637343466	SO1539	hypothetical protein	1
681	1.32	1.32	3.66	1.77	1.77	637344976	SO3159	hypothetical protein	1
682	1.31	1.31	31.85	31.85	23.29	637342349	SO0345	methylisocitrate lyase	3
683	1.26	1.26	5.60	5.60	5.60	637344420	SO2592	dihydroorotate dehydrogenase	1
684	1.26	1.26	12.00	12.00	12.00	637343776	SO1887	hypothetical protein	1
685	1.21	1.21	1.96	1.96	1.96	637344367	SO2536	acyl-CoA dehydrogenase	1
686	1.21	1.21	8.81	8.81	8.81	637344198	SO2360	hypothetical protein	1
687	1.21	1.21	4.26	4.26	4.26	637343934	SO2067	phosphoribosyl-ATP pyrophosphatase/phosphoribosyl-AMP cyclohydrolase	1
688	1.08	1.08	8.45	6.28	6.28	637345338	SO3539	peptidase, M28D family	1
689	1.04	1.04	12.67	8.60	8.60	637343876	SO1999	phospholipase/carboxylesterase family protein	1
690	0.98	0.98	26.79	26.79	26.79	637342738	SO0761	nitrogen regulatory protein P-II 1	2
691	0.97	0.97	19.79	19.79	8.02	637346302	SO4591	tetraheme cytochrome c	1
692	0.95	0.95	8.05	4.98	4.98	637345963	SO4236	2-isopropylmalate synthase	1
693	0.82	0.82	5.45	1.96	1.96	637344924	SO3120	oxidoreductase, Gfo/Idh/MocA family	1
694	0.82	0.82	7.63	7.63	7.63	637344974	SO3157	lipoprotein, putative	1
695	0.73	0.73	13.46	13.46	8.33	637346455	SO4751	ATP synthase subunit B	1

696	0.71	0.71	12.50	7.41	7.41	637345979	SO4254	GTP cyclohydrolase I	1
697	0.70	0.71	3.85	3.85	3.85	637343049	SO1098	hypothetical Alkylated DNA repair protein	1
698	0.69	0.70	7.90	3.95	3.95	637342875	SO0907	Na(+)-translocating NADH-quinone reductase subunit F	1
699	0.69	0.69	10.15	7.15	3.66	637343330	SO1388	aminopeptidase P, putative	1
700	0.63	0.63	3.12	3.12	3.12	637343585	SO1679	acyl-CoA dehydrogenase family protein	1
701	0.63	0.63	2.49	2.49	2.49	637343159	SO1204	translation initiation factor IF-2	1
702	0.62	0.62	2.86	2.86	2.86	637344747	SO2935	short chain dehydrogenase	1
703	0.49	0.49	2.51	2.51	2.51	637343761	SO1870	arginine decarboxylase	1
704	0.47	0.47	12.50	12.50	12.50	637344145	SO2301	ribosomal protein L35	1
705	0.37	0.37	24.41	24.41	9.45	637344112	SO2265	NifU family protein	1
706	0.36	0.36	3.70	3.70	3.70	RRRRR 637342598	REVERS	D SO0242 ribosomal protein L24	1
707	0.35	0.35	27.69	27.69	18.46	637345235	SO3426	carbon storage regulator	1
708	0.34	0.35	3.72	3.72	3.72	637343352	SO1410	hypothetical protein	1
709	0.31	0.31	19.09	19.09	19.09	637344697	SO2880	glutaredoxin domain protein	2
710	0.29	0.29	4.80	4.80	4.80	637344448	SO2621	conserved hypothetical protein TIGR00486	1
711	0.28	0.28	17.26	17.26	17.26	637342097	SO0084	HAD-superfamily hydrolase, subfamily IA, variant 1 family protein	2
712	0.26	0.26	0.70	0.70	0.70	RRRRR 637343430	REVERS	D SO1500 sensory box protein	1
713	0.25	0.25	22.00	8.00	8.00	637344980	SO3163	lipoprotein	1
714	0.24	0.24	6.32	6.32	1.98	637344054	SO2198	hypothetical aminopeptidase	1
715	0.23	0.23	2.87	1.58	1.58	RRRRR 637343662	REVERS	D SO1776 outer membrane protein precursor MtrB	1
716	0.23	0.23	4.17	4.17	4.17	RRRRR 637343849	REVERS	D SO1966 conserved hypothetical protein TIGR00266	1
717	0.20	0.20	3.81	3.81	3.81	637343266	SO1322	5-methylthioadenosine nucleosidase/S-adenosylhomocysteine nucleosidase	1
718	0.18	0.18	5.25	2.33	2.33	RRRRR 637345036	REVERS	D SO3221 flagellar motor switch protein	1
719	0.15	0.15	3.80	1.01	1.01	RRRRR 637344469	REVERS	D SO2644 phosphoenolpyruvate synthase	1
720	0.15	0.15	9.82	9.82	9.82	637345585	SO3819	nitrogen regulatory protein P-II	1
721	0.15	0.15	8.20	8.20	8.20	637345458	SO3673	hemin ABC transporter, periplasmic hemin-binding protein	1
722	0.14	0.14	5.84	5.84	5.84	637344606	SO2777	acyl carrier protein S-malonyltransferase	1
723	0.13	0.13	5.43	1.81	1.81	RRRRR 637342029	REVERS	D SO0020 acetyl-CoA acetyltransferase	1
724	0.13	0.13	6.38	6.38	2.84	637343164	SO1210	TPR domain protein	1
725	0.12	0.12	0.80	0.80	0.00	RRRRR 637342990	REVERS	D SO1030 5-methyltetrahydrofolate--homocysteine methyltransferase	0
726	0.12	0.12	9.62	9.62	9.62	RRRRR 637342249	REVERS	D SO0242 ribosomal protein L24	1
727	0.11	0.11	13.13	13.13	0.00	637343519	SO1608	hypothetical protein	0
728	0.11	0.11	2.25	2.25	2.25	637345105	SO3294	exodeoxyribonuclease VII large subunit	1
729	0.11	0.11	3.45	3.45	3.45	637344882	SO3078	2 chorismate synthase	1
730	0.10	0.10	4.47	0.84	0.84	RRRRR 637343641	REVERS	D SO1751 hypothetical protein	1

731	0.10	0.10	9.11	6.29	2.17	637342978	SO1017	NADH dehydrogenase I, F subunit	1
732	0.10	0.10	11.11	3.92	3.92	637345067	SO3252	chemotaxis protein CheV	1
733	0.10	0.10	20.78	10.24	10.24	637342303	SO0294	tryptophanyl-tRNA synthetase	1
734	0.10	0.10	6.12	6.12	6.12	637344176	SO2339	alpha keto acid dehydrogenase complex, E1 component, alpha subunit	1
735	0.09	0.09	6.01	6.01	6.01	637344892	SO3090	MoxR domain protein	1
736	0.08	0.08	2.77	2.77	2.77	637342964	SO1003	hypothetical protein	1
737	0.08	0.08	14.18	14.18	14.18	637342561	SO0568	hypothetical protein	1

Note: N is the rank of the protein relative to the other identified proteins in the list. Unused, is a measure of confidence reflecting the total amount of peptides identified unique to the given protein. Total, represents a measure of confidence reflecting the total amount of peptide identified (including those not unique) to the given protein. %cov, is the sequence coverage given as the percentage of amino acid sequences in each protein sequence identified with a 50% confidence level (%cov(50)) and with a 95% confidence level (%cov(95)). Accession represents the accession number for the protein, the SO identifier represents the species specific gene ID for the protein and peptides 95% represents the number of peptide sequences identified for the protein with a 95% confidence.

Appendix C- IDA library for *Geobacter sulfurreducens* DL-1 anodic biofilms

N	Unused	Total	%Cov	%Cov (50)	%Cov (95)	Gene ID	Gene name	Description	Peptides (95%)
1	102.78	102.78	91.25	85.12	83.59	D7AFN3_GEOSK	ompJ	Outer membran channel OmpJ	136
2	93.18	93.18	82.72	81.43	81.25	D7AG51_GEOSK	groL	60 kDa chaperonin	100
3	91.44	91.44	82.05	80.76	79.81	D7AJ92_GEOSK	acnB	Aconitate hydratase 2	59
4	84.46	84.46	80.81	70.54	69.32	D7AIQ0_GEOSK	icd	Isocitrate dehydrogenase, NADP-dependent	62
5	78.72	78.72	63.07	57.92	53.96	D7AGP2_GEOSK	fdnG	Periplasmically oriented, membrane-bound formate dehydrogenase, major subunit, selenocysteine-containing	45
6	70.81	70.81	55.82	46.61	45.86	D7AM08_GEOSK	por	Pyruvate-flavodoxin oxidoreductase	37
7	70.01	70.01	89.15	89.15	89.15	D7AM23_GEOSK	atpD	ATP synthase subunit beta	55
8	66.5	66.5	81.21	73.41	72.4	D7AMU3_GEOSK	fusA-3	Elongation factor G	48
9	63.61	63.61	70.02	67.66	65.31	D7AHW0_GEOSK	frdA	Succinate dehydrogenase/fumarate reductase, flavoprotein subunit	53
10	63.46	63.46	72.91	72.91	72.91	D7AFZ8_GEOSK	hcp	Hydroxylamine reductase	36
11	61.97	61.97	65.41	65.41	61.95	D7ALW9_GEOSK	dnaK	Chaperone protein DnaK	43
12	59.69	59.69	59.55	58.25	49.42	D7AII0_GEOSK	ompB	Laccase family multicopper oxidase	35
13	57.48	57.48	86.38	81.91	81.91	D7AJR5_GEOSK	glnA	Glutamine synthetase	37
14	56.03	56.03	61.49	57.43	56.31	D7AFQ7_GEOSK	ppdK	Pyruvate phosphate dikinase	36
15	54.81	54.81	62.16	59.19	56.89	D7AJ23_GEOSK	pnp	Polyribonucleotide nucleotidyltransferase	34
16	53.27	53.27	82.58	81.06	81.06	D7AMU2_GEOSK	tuf-1	Elongation factor Tu	52
17	53.19	53.19	83.96	83.46	81.2	D7AI23_GEOSK	KN400_1216	Amino acid aminotransferase, putative	33
18	53.06	53.06	66.6	60.44	58.85	D7AM21_GEOSK	atpA	ATP synthase subunit alpha	29
19	52.97	52.97	62.88	62.88	62.88	D7AJM4_GEOSK	tig	Trigger factor	29
20	52.74	52.74	79.72	77.16	75.06	D7AEA7_GEOSK	KN400_0328	Peptidoglycan-binding outer membrane protein, OmpB and OmpA domain-containing	33
21	50.54	50.54	73.13	72.9	72.9	D7AHW7_GEOSK	metY-1	acetyl-L-homoserine sulfhydrylase	38
22	50.11	50.11	75.18	73.93	73.93	D7AGQ0_GEOSK	hybL	Periplasmically oriented, membrane-bound [NiFe]-hydrogenase, large subunit	33
23	48.37	48.37	40.36	31.31	31.31	D7AMU7_GEOSK	rpoB	DNA-directed RNA polymerase subunit beta	27
24	48.07	48.07	90.54	88.96	88.01	D7AIQ1_GEOSK	mdh	Malate dehydrogenase	53
25	48.04	48.04	88.59	88.59	88.59	D7AIQ3_GEOSK	korA	2-oxoglutarate:ferredoxin oxidoreductase, alpha subunit	47
26	48	48	59.15	53.6	53.6	D7AHD1_GEOSK	fumB	Fumarate hydratase, class I	25
27	47.37	47.37	64.78	56.12	56.12	D7AF42_GEOSK	ato-1	Succinyl:acetate coenzyme A transferase	34
28	46.71	46.71	44.63	40.35	32.85	D7AFM8_GEOSK	KN400_3241	Biotin-dependent acyl-CoA carboxylase, biotin carboxylase subunit	23
29	45.49	45.49	52.14	42.77	39.19	D7AFY3_GEOSK	clpB	ATP-dependent chaperone ClpB	25

30	45.18	45.18	68.77	62.29	59.04	D7AKX7_GEOSK	rpsA	30S ribosomal protein S1	29
31	45.12	45.12	72.89	70.67	66.89	D7AI85_GEOSK	gdhA	Glutamate dehydrogenase	26
32	44.04	44.04	80.27	76.42	76.42	D7AHN9_GEOSK	gltA	Citrate synthase	50
33	43.26	43.26	54.37	52.75	51.46	D7AG96_GEOSK	pckG	Phosphoenolpyruvate carboxykinase [GTP]	23
34	41.87	41.87	57.43	48.91	48.91	D7AFN5_GEOSK	KN400_3248	Uncharacterized protein	21
35	41.82	41.86	67.65	64.71	64.71	D7AMR3_GEOSK	rpoA	DNA-directed RNA polymerase subunit alpha	27
36	41.78	41.78	63.11	60.98	60.98	D7ALU8_GEOSK	hemY	Protoporphyrinogen oxidase	23
37	41.43	41.43	62.2	62.02	61.5	D7AFM7_GEOSK	KN400_3240	Biotin-dependent acyl-CoA carboxylase, carboxyltransferase subunit	32
38	39.62	39.62	51.58	49.87	45.51	D7AGH6_GEOSK	KN400_0691	Uncharacterized protein	21
39	39.21	39.21	65.52	62.07	62.07	D7AE78_GEOSK	deg	Periplasmic trypsin-like serine protease DegP	24
40	38.33	38.33	71.3	69.23	69.23	D7AKA6_GEOSK	ilvC	Ketol-acid reductoisomerase	26
41	38.28	38.28	73.51	72.28	70.05	D7AFM2_GEOSK	roo	Rubredoxin:oxygen/nitric oxide oxidoreductase	21
42	37.08	37.08	42.28	34.23	33.45	D7AKM1_GEOSK	pilQ	Type IV pilus secretin lipoprotein PilQ	19
43	37.07	37.07	75.07	71.99	70.03	D7AFY1_GEOSK	ilvE	Branched-chain amino acid aminotransferase	22
44	37.01	37.01	77.59	69.88	67.95	D7AJ37_GEOSK	glyA	Serine hydroxymethyltransferase	26
45	36.94	36.94	69.05	65.82	63.05	D7AFN7_GEOSK	purA	Adenylosuccinate synthetase	23
46	35.82	35.82	72.43	68.93	67.29	D7AMA9_GEOSK	eno	Enolase	24
47	34.63	34.63	39.56	39.56	37.88	D7AIP8_GEOSK	aspS	Aspartate--tRNA(Asp/Asn) ligase	21
48	34.03	34.03	80.59	80.59	77.29	D7AIQ4_GEOSK	korB	2-oxoglutarate:ferredoxin oxidoreductase, thiamin diphosphate-binding subunit	26
49	34.02	34.02	57.46	49.5	49.5	D7AHY1_GEOSK	KN400_1174	RNA-binding S1 domain protein	21
50	34.01	34.01	73.41	73.41	73.41	D7AJ35_GEOSK	fabF-2	3-oxoacyl-[acyl-carrier-protein] synthase 2	22
51	33.96	33.96	61.38	57.94	57.94	D7AJG8_GEOSK	livK-2	Branched-chain amino acid ABC transporter, periplasmic amino acid-binding protein, putative	20
52	33.85	33.85	69.96	59.66	59.66	D7AGS5_GEOSK	KN400_0790	Peptidoglycan-binding outer membrane protein, OmpB, OmpA and OmpA domain containing	19
53	32.38	32.38	55.51	55.51	52.47	D7AGR5_GEOSK	KN400_0780	Amino acid ABC transporter, periplasmic amino acid-binding protein	23
54	32.15	32.15	42.02	39.89	39.89	D7AJD2_GEOSK	maeB	Malate oxidoreductase, NADP-dependent, phosphate acetyltransferase-like domain-containing	19
55	32	32	68.17	68.17	68.17	D7AJ60_GEOSK	gapA	Glyceraldehyde-3-phosphate dehydrogenase	19
56	31.96	31.96	47.38	44.48	44.48	D7AKA9_GEOSK	ilvD	Dihydroxy-acid dehydratase	16
57	31.85	31.85	58.78	58.78	58.78	D7AK23_GEOSK	metY-2	acetyl-L-homoserine sulfhydrylase	20
58	31.8	31.8	39.74	34.72	34.72	D7AKD0_GEOSK	fusA-1	Translation elongation factor G	16
59	31.64	31.64	53.49	47.31	47.31	D7ALT7_GEOSK	dnaN	DNA polymerase III subunit beta	16
60	30.97	30.97	79.17	69.91	66.2	D7AKB7_GEOSK	tsf	Elongation factor Ts	21
61	30.58	30.58	33.04	29.14	25.35	D7AES6_GEOSK	ileS	Isoleucine--tRNA ligase	16

62	30.5	30.5	41.45	32.84	29.9	D7AJ18_GEOSK	infB	Translation initiation factor IF-2	16
63	30.24	30.24	67.06	67.06	67.06	D7AGU9_GEOSK	hemE	Uroporphyrinogen decarboxylase	20
64	30.04	30.04	61.87	55.64	55.64	D7ADC7_GEOSK	lysA	Diaminopimelate decarboxylase	16
65	29.91	29.91	48.5	37.91	30.33	D7AM89_GEOSK	yaeT	Outer membrane protein assembly factor BamA	15
66	29.87	29.87	44.15	36.92	36.92	D7AJY2_GEOSK	htpG	Chaperone protein HtpG	15
67	29.79	29.79	75.75	75.75	73.57	D7AMW2_GEOSK	asd	Aspartate-semialdehyde dehydrogenase	17
68	29.71	29.71	69.72	69.72	69.72	D7AJ58_GEOSK	tpi	Triosephosphate isomerase	17
69	29.67	29.67	58.33	46.2	44.38	D7AFN1_GEOSK	KN400_3244	(R)-methylmalonyl-CoA mutase, isobutyryl-CoA mutase-like catalytic subunit	16
70	29.49	29.49	62.39	60	60	D7AKT3_GEOSK	KN400_2497	LysM domain protein	15
71	29.34	29.34	80.84	65.42	64.02	D7AHX4_GEOSK	KN400_1167	Ketose-1,6-bisphosphate aldolase, class II, putative	16
72	29.22	29.22	92.91	92.91	92.91	D7AMU8_GEOSK	rplL	50S ribosomal protein L7/L12	40
73	28.91	28.91	69.36	62.14	57.8	D7AF17_GEOSK	macA	Cytochrome c peroxidase, 2 heme-binding sites	14
74	28.71	28.71	62.31	58.72	55.13	D7AE88_GEOSK	nuoD	NADH-quinone oxidoreductase subunit D	15
75	28.12	28.12	87.62	79.8	79.8	D7AF89_GEOSK	cysK	Cysteine synthase A	20
76	28.01	28.01	75.76	73.28	73.28	D7AM83_GEOSK	gnnB	UDP-2-acetamido-2-deoxy-alpha-D-ribo-hexopyranos-3-ulose 3-aminotransferase	16
77	27.97	28.01	62.12	60.91	60.91	D7ADH8_GEOSK	KN400_0185	ABC transporter, periplasmic substrate-binding protein	17
78	27.68	27.68	58.12	58.12	58.12	D7AI53_GEOSK	pyrC	Dihydroorotase	15
79	27.54	27.54	50.65	50.65	38.7	D7AJ16_GEOSK	nusA	Transcription elongation factor NusA	15
80	27.03	27.03	55.43	48.73	48.73	D7AKQ8_GEOSK	KN400_2472	Nitrite/sulfite reductase domain protein	14
81	26.78	26.78	62.1	48.99	48.99	D7AE79_GEOSK	pepA	Probable cytosol aminopeptidase	14
82	26.06	26.06	71.79	57.26	57.26	D7AMV0_GEOSK	rplA	50S ribosomal protein L1	17
83	26	28	60.53	58.16	58.16	D7AJG7_GEOSK	livK-1	Branched-chain amino acid ABC transporter, periplasmic amino acid-binding protein, putative	16
84	25.48	25.48	55.56	46.15	44.44	D7AK28_GEOSK	KN400_2378	Peptidylprolyl cis-trans isomerase, PpiC-type	14
85	25.47	25.48	82.81	82.81	82.81	D7AHU2_GEOSK	sodA	Superoxide dismutase, iron/manganese-containing	16
86	25.36	25.36	65.05	46.32	39.79	D7AJV9_GEOSK	ahcY	Adenosylhomocysteinase	13
87	24.49	24.49	29.44	28.09	26.06	D7AE90_GEOSK	nuoF-1	NADH dehydrogenase I, F subunit	12
88	24.01	24.01	79.44	79.44	79.44	D7ADY5_GEOSK	tal	Probable transaldolase	15
89	24	24	60.38	54.4	54.4	D7AFL2_GEOSK	hemC	Porphobilinogen deaminase	15
90	23.78	23.78	49.74	46.91	41.62	D7AII3_GEOSK	KN400_1425	ABC transporter, periplasmic substrate-binding protein, 1 heme-binding site	15
91	23.46	23.46	26.89	20.8	20.8	D7AFK5_GEOSK	KN400_3218	Pentapeptide repeat protein	13
92	23.44	23.44	84.62	84.62	84.62	D7AIQ5_GEOSK	korC	2-oxoglutarate:ferredoxin oxidoreductase, gamma subunit	16
93	22.8	22.8	21.65	16.2	16.2	D7AMU6_GEOSK	rpoC	DNA-directed RNA polymerase subunit beta'	15
94	22.64	22.64	45.49	43.76	40.88	D7AFT7_GEOSK	purH	Bifunctional purine biosynthesis protein PurH	14

95	22.41	22.41	48.03	48.03	48.03	D7AJ63_GEOSK	purB	Adenylosuccinate lyase	13
96	22.41	22.41	30.77	28.52	26.83	D7AEA4_GEOSK	KN400_0325	Cytochrome c nitrite reductase, 8 heme-binding sites	13
97	22.22	22.22	64.64	64.64	64.09	D7AJX0_GEOSK	raiA	Ribosomal subunit interface-associated sigma-54 modulation protein RaiA	12
98	22	22	26.62	26.62	26.62	D7AFL8_GEOSK	hppA	K(+)-insensitive pyrophosphate-energized proton pump	11
99	21.64	21.64	22.03	20.6	20.6	D7ADZ0_GEOSK	KN400_2924	Ligand-gated TonB-dependent outer membrane channel	11
100	21.63	21.63	33.97	27.89	27.89	D7AL70_GEOSK	KN400_2112	Peptidylprolyl cis-trans isomerase, putative	12
101	20.48	20.48	28.03	28.03	26.15	D7AJH2_GEOSK	iorA-1	Indolepyruvate oxidoreductase subunit IorA	10
102	20.44	20.44	68.97	66.21	66.21	D7ADC8_GEOSK	dapA	4-hydroxy-tetrahydrodipicolinate synthase	11
103	20.42	20.42	49.48	33.39	25.87	D7AK91_GEOSK	KN400_2441	Uncharacterized protein	12
104	20.32	20.32	23.37	18.89	16.83	D7AE91_GEOSK	nuoG-1	NADH dehydrogenase I, G subunit	11
105	20.31	21.42	43.13	43.13	39.94	D7ALV2_GEOSK	KN400_0017	Peptidylprolyl cis-trans isomerase lipoprotein, PpiC-type	13
106	20.27	20.27	80.56	77.08	68.75	D7AIN6_GEOSK	KN400_1478	Glyoxalate/3-oxopropanoate/4-oxobutanoate reductase-related protein	14
107	20.07	20.07	59.49	45.02	45.02	D7AI52_GEOSK	pyrB	Aspartate carbamoyltransferase	12
108	20.03	20.03	30.35	26.67	26.67	D7AIP5_GEOSK	proS	Proline--tRNA ligase	10
109	20.01	20.01	62.04	52.19	45.99	D7AMT7_GEOSK	rplB	50S ribosomal protein L2	13
110	20.01	20.01	42.69	36.54	33.08	D7AL99_GEOSK	guaA	GMP synthase [glutamine-hydrolyzing]	10
111	20.01	20.01	48.48	41.22	41.22	D7AE84_GEOSK	hemL	Glutamate-1-semialdehyde 2,1-aminomutase	10
112	20.01	20.01	35.32	35.32	35.32	D7AKJ8_GEOSK	KN400_2027	Branched-chain amino acid ABC transporter, periplasmic amino acid-binding protein, putative	10
113	20	20	56.72	54.43	54.43	D7AGP8_GEOSK	hybA	Periplasmically oriented, membrane-bound [NiFe]-hydrogenase, iron-sulfur cluster-binding subunit	11
114	20	20	61.9	56.67	56.67	D7AMU0_GEOSK	rplC	50S ribosomal protein L3	12
115	20	20	43.18	42.43	42.43	D7AHS1_GEOSK	tyrS	Tyrosine--tRNA ligase	11
116	20	20	72.26	72.26	72.26	D7AH13_GEOSK	KN400_0854	Lipoprotein, putative	16
117	20	20	80.7	80.7	80.7	D7AE99_GEOSK	prx-3	Probable thiol peroxidase	13
118	19.96	19.96	77.05	77.05	77.05	D7AMC7_GEOSK	purE-2	N5-carboxyaminoimidazole ribonucleotide mutase	13
119	19.75	19.75	28.72	27.29	27.29	D7AM92_GEOSK	lysS	Lysine--tRNA ligase	10
120	19.66	19.66	21.32	17.78	16.44	D7AK32_GEOSK	KN400_2382	ATP-dependent protease, putative	10
121	19.65	19.65	30.22	21.94	20.65	D7ALU0_GEOSK	gyrA	DNA gyrase subunit A	11
122	19.54	19.54	13.68	12.98	12.11	D7AK26_GEOSK	pyc	Pyruvate carboxylase	10
123	19.35	19.35	66.18	59.9	55.07	D7AMT9_GEOSK	rplD	50S ribosomal protein L4	12
124	19.18	19.18	66.15	58.46	56	D7AM46_GEOSK	hemB	Delta-aminolevulinic acid dehydratase	9

125	18.91	18.91	43.93	34.94	32.22	D7AH73_GEOSK	KN400_0914	Zinc-dependent peptidase, M16 family	11
126	18.88	18.88	51.68	43.12	38.53	D7AJR3_GEOSK	trpS	Tryptophanyl-tRNA synthetase	12
127	18.63	18.63	33.87	30.38	23.84	D7ALI8_GEOSK	KN400_2615	C1 family peptidase domain protein	12
128	18.63	18.63	37.47	25.05	25.05	D7AG29_GEOSK	KN400_3262	Uncharacterized protein	9
129	18.48	18.48	80.57	73.71	68	D7AMV2_GEOSK	nusG	Transcription termination/antitermination protein NusG	10
130	18.43	18.43	77.46	77.46	77.46	D7AE89_GEOSK	nuoE-1	NADH dehydrogenase I, E subunit	11
131	18.19	18.19	62.89	62.89	62.37	D7ALW0_GEOSK	KN400_0025	Peptidoglycan-binding outer membrane lipoprotein Pal, OmpA family	11
132	18.03	18.03	42.93	37.79	35.48	D7AJW4_GEOSK	metK	S-adenosylmethionine synthase	9
133	18.01	18.01	42.03	38.84	38.84	D7AMP2_GEOSK	ccpA	Cytochrome c peroxidase, 2 heme-binding sites	9
134	18	18	68.94	61.36	61.36	D7AMS6_GEOSK	rpsH	30S ribosomal protein S8	11
135	18	18	32.22	27.36	27.36	D7AJS4_GEOSK	KN400_1866	IPT/TIG domain protein	9
136	18	18	32.51	32.51	32.51	D7AM64_GEOSK	argG	Argininosuccinate synthase	9
137	18	18	77.83	77.83	77.83	D7AGR9_GEOSK	wrbA	NAD(P)H dehydrogenase (quinone)	10
138	17.95	17.95	58.96	54.98	54.98	D7AKB8_GEOSK	rpsB	30S ribosomal protein S2	10
139	17.87	17.87	71.14	71.14	71.14	D7AHQ1_GEOSK	usp-2	Universal stress protein	9
140	17.7	17.7	32.83	32.83	32.83	D7AM62_GEOSK	argD	Acetylornithine aminotransferase	10
141	17.52	17.52	32.83	25.32	25.32	D7AI00_GEOSK	gltX	Glutamate--tRNA ligase	9
142	17.45	17.45	46.89	36.47	33.87	D7AJ39_GEOSK	KN400_1631	Efflux pump, RND family, outer membrane protein	12
143	17.43	17.43	39.01	39.01	39.01	D7AJN0_GEOSK	KN400_1822	Aspartokinase	10
144	17.35	17.35	43.09	40.33	37.29	D7AMW3_GEOSK	leuB	3-isopropylmalate dehydrogenase	11
145	17.32	17.32	70.3	64.24	58.18	D7AFL6_GEOSK	KN400_3229	Ferritin-like domain protein	10
146	16.97	16.97	34.24	30.02	28.04	D7ALP8_GEOSK	KN400_2675	Uncharacterized protein	9
147	16.85	16.85	71.66	51.79	51.79	D7AJ32_GEOSK	fabD-2	Malonyl CoA-acyl carrier protein transacylase	10
148	16.84	16.85	42.3	42.3	42.3	D7AHD7_GEOSK	KN400_0980	Uncharacterized protein	11
149	16.74	16.74	83.49	83.49	81.65	D7AFK8_GEOSK	trxA	Thioredoxin	11
150	16.57	16.57	63.13	58.1	49.72	D7AMS8_GEOSK	rplE	50S ribosomal protein L5	10
151	16.52	16.52	47.83	45.45	42.69	D7AHW1_GEOSK	frdB	Succinate dehydrogenase/fumarate reductase, iron-sulfur protein	15
152	16.35	16.35	46.88	44.51	41.54	D7AIC6_GEOSK	cys	Sulfate ABC transporter, periplasmic sulfate-binding protein	9
153	16.19	16.19	85.05	80.93	58.76	D7AFY7_GEOSK	rplY	50S ribosomal protein L25	12
154	16.1	16.1	35.14	30.74	28.04	D7AL71_GEOSK	purC	Phosphoribosylaminoimidazole-succinocarboxamide synthase	8
155	16.09	16.09	68.92	56.76	56.76	D7AFZ3_GEOSK	rplI	50S ribosomal protein L9	11
156	16.04	16.04	48.85	37.66	37.66	D7AL29_GEOSK	argJ	Arginine biosynthesis bifunctional protein ArgJ	9
157	16.04	16.04	40.75	38.01	38.01	D7AFQ5_GEOSK	glyQ	Glycine--tRNA ligase alpha subunit	10
158	16.02	16.02	45.82	45.82	45.82	D7AJ66_GEOSK	purQ	Phosphoribosylformylglycinamidine synthase, PurQ domain	10

159	16.01	16.01	70.15	66.17	66.17	D7AFG4_GEOSK	prx-2	Peroxiredoxin, typical 2-Cys subfamily	9
160	16.01	16.01	48.05	29.76	29.76	D7ADD0_GEOSK	dapL	LL-diaminopimelate aminotransferase	8
161	15.88	15.88	54.52	39.45	32.16	D7AHJ6_GEOSK	KN400_1039	Amino acid aminotransferase, putative	8
162	15.85	15.85	22.58	22.58	19.7	D7AHB3_GEOSK	KN400_0956	Phage tail sheath protein, putative	11
163	15.83	15.83	53.14	48.95	48.95	D7AIP6_GEOSK	pyrF	Orotidine 5'-phosphate decarboxylase	9
164	15.72	15.72	45.16	45.16	45.16	D7AMT6_GEOSK	rpsS	30S ribosomal protein S19	9
165	15.66	15.66	27.17	24.64	24.64	D7AHN6_GEOSK	KN400_1079	Acyl-CoA synthetase, AMP-forming	9
166	15.61	15.61	63.07	43.72	35.43	D7AKS1_GEOSK	KN400_2485	Carboxynorspermidine/carboxyspermidine dehydrogenase	9
167	15.59	15.59	47.01	42.89	27.63	D7AG92_GEOSK	gatA	Glutamyl-tRNA(Gln) amidotransferase subunit A	8
168	15.56	15.56	78.1	78.1	47.45	D7AHP3_GEOSK	ndk	Nucleoside diphosphate kinase	10
169	15.49	15.49	29.17	29.17	29.17	D7AKN5_GEOSK	omcS	Cytochrome c, 6 heme-binding sites	14
170	15.46	15.46	70.21	70.21	70.21	D7AMV1_GEOSK	rplK	50S ribosomal protein L11	10
171	15.3	15.3	47.07	43.79	36.53	D7AKA0_GEOSK	leuC	3-isopropylmalate dehydratase large subunit	9
172	15.23	15.23	47.86	41.81	30.98	D7AHN8_GEOSK	KN400_1081	Prolidase family protein	9
173	15.2	15.2	69.67	63.51	56.87	D7AFM9_GEOSK	tmk-2	Thymidylate kinase	8
174	14.99	14.99	30.67	28.9	26.42	D7AKA8_GEOSK	ilvB	Acetolactate synthase	8
175	14.89	14.89	34.36	31.99	31.99	D7ALX3_GEOSK	serS	Serine--tRNA ligase	8
176	14.87	14.87	46.85	44.06	40.91	D7AHP5_GEOSK	mta	S-methyl-5'-thioadenosine phosphorylase	7
177	14.87	14.87	78.49	73.66	73.66	D7AML6_GEOSK	KN400_2725	OsmC family protein	9
178	14.78	14.78	70.33	67.58	56.04	D7AJ68_GEOSK	pyrE	Orotate phosphoribosyltransferase	7
179	14.76	14.76	47.6	40.38	33.65	D7AMR4_GEOSK	rpsD	30S ribosomal protein S4	8
180	14.62	14.62	87.17	83.96	80.21	D7AMC6_GEOSK	KN400_2251	Peptidoglycan-binding outer membrane lipoprotein Pal, OmpA family	10
181	14.26	14.26	35.97	30.19	29.98	D7AMP0_GEOSK	cccA	Cytochrome c catalase, 2 heme-binding sites	9
182	14.23	14.23	47.8	42.23	39.3	D7AJI0_GEOSK	KN400_1772	Uncharacterized protein	8
183	14.16	14.16	73.68	69.01	64.91	D7AH35_GEOSK	KN400_0876	Peptidyl-prolyl cis-trans isomerase	11
184	14.16	14.16	49.71	49.71	45.71	D7AK99_GEOSK	leuD	Isopropylmalate/citramalate isomerase, small subunit	9
185	14.06	14.06	39.64	33.33	30.33	D7ALM5_GEOSK	pta	Phosphate acetyltransferase	8
186	14.04	14.04	37.82	37.82	35.9	D7AMU4_GEOSK	rpsG	30S ribosomal protein S7	9
187	14.03	14.03	53.7	53.7	53.7	D7AMS3_GEOSK	rpsE	30S ribosomal protein S5	8
188	14.02	14.02	38.7	27.97	27.97	D7ALA1_GEOSK	KN400_2143	Aminopeptidase, M42 family	7
189	14.02	14.02	34.3	34.3	30.81	D7AL34_GEOSK	KN400_2076	TRAP proton/solute symporter, periplasmic substrate-binding protein	7
190	14.01	14.01	52.43	47.03	47.03	D7AKB5_GEOSK	frr	Ribosome-recycling factor	7
191	14.01	14.01	39.96	39.96	37.18	D7ADV0_GEOSK	KN400_2884	Rhodanese homology domain pair protein	8
192	14.01	14.01	58.66	58.66	58.66	D7AMS5_GEOSK	rplF	50S ribosomal protein L6	9
193	14	14	36.59	34.76	34.76	D7AL12_GEOSK	KN400_2576	NADPH:quinone oxidoreductase family protein PIG3	7

194	14	14	54.59	53.57	53.57	D7AKZ0_GEOSK	KN400_2554	TPR domain protein	7
195	14	14	84.81	84.81	84.81	D7AKL3_GEOSK	accB	Acetyl-CoA carboxylase, biotin carboxyl carrier protein	8
196	14	14	61.62	43.43	43.43	D7AG30_GEOSK	ppiA	Peptidyl-prolyl cis-trans isomerase	8
197	14	14	57.89	57.89	57.89	D7AMP3_GEOSK	KN400_2752	Rubrerythrin	9
198	14	14	8.632	8.632	8.632	D7AKE2_GEOSK	KN400_1971	Repeat-containing protein	7
199	14	14	32.75	32.75	32.75	D7AK24_GEOSK	KN400_2374	McbC-like oxidoreductase for polypeptide thioester cyclization	7
200	14	14	46.91	46.91	46.91	D7AE87_GEOSK	nuoC	NADH-quinone oxidoreductase subunit C	7
201	14	14	48.56	48.56	48.56	D7AE64_GEOSK	KN400_0285	Uncharacterized protein	7
202	13.84	13.84	60.28	51.22	39.37	D7AM22_GEOSK	atpG	ATP synthase gamma chain	8
203	13.48	13.48	38.5	28.98	26.99	D7AGS9_GEOSK	KN400_0794	Efflux pump, RND family, outer membrane protein	8
204	13.28	13.28	51.68	46.65	37.71	D7AFH7_GEOSK	KN400_3190	Aspartate/glutamate/phosphoserine/alanine/cysteate aminotransferase, putative	7
205	13.23	13.23	45.13	45.13	44.62	D7AM10_GEOSK	mglA	Cell polarity determinant GTPase MglA	8
206	13.05	13.05	41.71	27.89	27.89	D7AJ59_GEOSK	pgk	Phosphoglycerate kinase	8
207	12.9	12.9	69.03	66.45	66.45	D7AJC1_GEOSK	ribH	6,7-dimethyl-8-ribityllumazine synthase	7
208	12.84	12.84	21.92	13.96	11.01	D7AJS2_GEOSK	KN400_1864	Periplasmic polysaccharide biosynthesis/export protein	7
209	12.76	12.76	57.85	57.85	54.71	D7AH34_GEOSK	prx-1	Peroxiredoxin, typical 2-Cys subfamily	8
210	12.69	12.69	49.03	41.94	41.94	D7AM84_GEOSK	gnnA	UDP-N-acetylglucosamine 3-dehydrogenase, NAD-dependent	7
211	12.55	12.55	14.57	12.4	11.16	D7AIU7_GEOSK	thrS	Threonine--tRNA ligase	6
212	12.52	12.52	57.38	57.38	52.46	D7AMT0_GEOSK	rplN	50S ribosomal protein L14	6
213	12.41	12.41	34.74	34.74	28.51	D7AH72_GEOSK	KN400_0913	Zinc-dependent peptidase, M16 family	8
214	12.35	12.35	42.71	30.43	28.64	D7AKK4_GEOSK	nifS-1	Nitrogen fixation iron-sulfur cluster assembly cysteine desulfurase NifS	7
215	12.2	12.2	56.32	56.32	56.32	D7AMU9_GEOSK	rplJ	50S ribosomal protein L10	7
216	12.12	12.12	19.79	13.89	12.06	D7AIS0_GEOSK	rnr	Ribonuclease R	6
217	12.08	12.08	48.39	48.39	42.86	D7AMR9_GEOSK	adk	Adenylate kinase	6
218	12.02	12.02	25.89	15.24	15.24	D7AG91_GEOSK	gatB	Aspartyl/glutamyl-tRNA(Asn/Gln) amidotransferase subunit B	6
219	12.01	12.01	63.64	45.45	45.45	D7AJI4_GEOSK	efp-2	Elongation factor P	7
220	12.01	12.01	43.5	35.77	35.77	D7AGV7_GEOSK	KN400_3406	Lipoprotein, putative	6
221	12.01	12.01	48.66	45.09	45.09	D7AEY9_GEOSK	KN400_0424	Winged-helix transcriptional response regulator	9
222	12	12	46.38	46.38	40	D7AJE3_GEOSK	apr	Adenosine-5'-phosphosulfate reductase, glutathione-dependent	7
223	12	12	35.07	28.73	28.73	D7AGY8_GEOSK	KN400_0829	Protein disulfide bond isomerase, DsbC/DsbG-like	8
224	12	12	28.29	26.3	26.3	D7AM93_GEOSK	KN400_2218	ATS1 domain repeat lipoprotein	6
225	12	12	33.12	31.55	31.55	D7AM41_GEOSK	fmt	Methionyl-tRNA formyltransferase	8

226	12	12	77.67	67.96	67.96	D7AK58_GEOSK	KN400_2408	Uncharacterized protein	6
227	12	12	76.88	72.86	72.86	D7AJM3_GEOSK	clp	ATP-dependent Clp protease proteolytic subunit	6
228	12	12	52.2	52.2	52.2	D7AL08_GEOSK	KN400_2572	Lipoprotein, putative	7
229	12	12	39.63	39.63	39.63	D7AKS3_GEOSK	proC	Pyrroline-5-carboxylate reductase	6
230	12	12	46.94	46.94	46.94	D7AF92_GEOSK	hspA-1	ATP-independent chaperone, alpha-crystallin/Hsp20 family	7
231	12	12	31.9	31.9	31.9	D7ADQ3_GEOSK	fabH-1	3-oxoacyl-[acyl-carrier-protein] synthase 3	6
232	11.92	11.92	27.7	25.79	25.79	D7AL56_GEOSK	omcZ	Cytochrome c, 8 heme-binding sites	7
233	11.92	11.92	53.66	53.66	53.66	D7AJ73_GEOSK	KN400_1665	Ferritin-like domain protein	6
234	11.84	11.84	49.14	36.57	36.57	D7AMR2_GEOSK	rplQ	50S ribosomal protein L17	11
235	11.83	11.83	41.25	38.28	34.98	D7AM63_GEOSK	argF	Ornithine carbamoyltransferase, catabolic	7
236	11.37	11.37	44.68	44.68	43.62	D7ADI5_GEOSK	KN400_0192	Nitroreductase-like family 3 protein	7
237	11.28	11.28	50.7	50.7	50.7	D7AGJ6_GEOSK	rnk-1	RNA polymerase-binding protein Rnk	6
238	11.21	11.21	30.22	26.17	26.17	E1PTD8_GEOSK	KN400_3437	Transport protein, Tim44-like domain, putative	6
239	11.15	11.15	31.83	20.99	19.41	D7AJK3_GEOSK	ctpA-2	Periplasmic carboxy-terminal processing protease	8
240	11.07	11.07	45.74	45.74	45.74	D7AES2_GEOSK	hup	Histone-like protein	9
241	11.03	11.03	29.21	18.23	16.35	D7AIV2_GEOSK	pheT	Phenylalanine--tRNA ligase beta subunit	7
242	10.93	10.93	35.39	17.34	17.34	D7ALM6_GEOSK	ackA	Acetate kinase	6
243	10.81	10.81	22.73	21.93	20.05	D7AG42_GEOSK	KN400_3275	NADH-dependent flavin oxidoreductase,	6
244	10.73	10.73	35.53	28.37	28.37	D7AFV3_GEOSK	gmd	GDP-mannose 4,6-dehydratase	6
245	10.63	10.63	90.38	90.38	80.77	D7AIA8_GEOSK	KN400_1301	UPF0345 protein KN400_1301	5
246	10.5	10.5	44.41	36.51	25.89	D7AGP7_GEOSK	hybS	Periplasmically oriented, membrane-bound [NiFe]-hydrogenase, small subunit	5
247	10.46	10.46	37.18	37.18	29.24	D7AGP3_GEOSK	fdnH	Periplasmically oriented, membrane-bound formate dehydrogenase, iron-sulfur cluster-binding subunit	5
248	10.42	10.42	43.85	36.54	32.31	D7AFR5_GEOSK	thiG	Thiazole synthase	6
249	10.35	10.35	31.04	31.04	27.2	D7AFY9_GEOSK	ychF	Ribosome-binding ATPase YchF	7
250	10.35	10.35	31.23	28.25	24.54	D7ALG3_GEOSK	KN400_2590	Amino acid ABC transporter, periplasmic amino acid-binding protein	5
251	10.34	10.34	28.99	28.99	28.99	D7AG23_GEOSK	KN400_3256	Lipoprotein, putative	5
252	10.27	10.27	30.57	30.57	19.71	D7AKG4_GEOSK	neuB	N-acetylneuraminate synthase	7
253	10.26	10.26	65.59	47.31	47.31	D7AFN4_GEOSK	KN400_3247	Uncharacterized protein	6
254	10.23	10.23	55.56	55.56	49.57	D7AFZ0_GEOSK	rpsF	30S ribosomal protein S6	5
255	10.2	10.2	18.37	13	11.61	D7AEN1_GEOSK	rpoD	RNA polymerase sigma factor RpoD	6
256	10.17	10.17	27.3	26.24	22.7	D7AF85_GEOSK	dapF	Diaminopimelate epimerase	5
257	10.13	10.13	39.16	39.16	35.66	D7AIE5_GEOSK	ghr	Glyoxalate/3-oxopropanoate/4-oxobutanoate reductase	5
258	10.12	10.12	45.76	38.38	38.38	D7ADX4_GEOSK	modE	Molybdate transport regulatory protein ModE	6

259	10.1	12.18	35.75	18.86	16.23	D7AGB5_GEOSK	KN400_3348	Outer membrane channel, OmpJ related protein	9
260	10.09	10.1	49.44	32.71	32.71	D7ALL9_GEOSK	tupA	Tungstate ABC transporter, periplasmic tungstate-binding protein	8
261	10.09	10.09	24.22	24.22	21.11	D7AHF2_GEOSK	KN400_0995	Peptidoglycan-binding lipoprotein,	5
262	10.07	10.07	35.55	29.57	29.57	D7AK88_GEOSK	KN400_2438	NHL repeat domain protein	6
263	10.03	10.03	67.28	48.77	48.77	D7AL62_GEOSK	KN400_2104	Nucleoside diphosphate-sugar dehydratase, putative	5
264	10.01	10.01	29.85	14	14	D7AKT1_GEOSK	topA	DNA topoisomerase 1	6
265	10.01	10.01	35.93	35.93	35.93	D7AJU7_GEOSK	KN400_1889	Transcriptional regulator, Ros/MucR family	6
266	10	10	32.58	15.24	15.24	D7AL11_GEOSK	KN400_2575	Alpha-amylase family protein	5
267	10	10	67.78	52.78	52.78	D7AM20_GEOSK	atpH	ATP synthase subunit delta	8
268	10	10	12.45	7.932	7.932	D7AJ65_GEOSK	purSL	Phosphoribosylformylglycinamidine synthase subunit PurL	5
269	10	10	72.12	72.12	72.12	D7AM06_GEOSK	KN400_0071	Nucleoid-associated protein KN400_0071	5
270	10	10	48.39	35.48	35.48	D7ALY4_GEOSK	elbB	Isoprenoid biosynthesis amidotransferase-like protein ElbB	5
271	10	10	50.6	35.71	35.71	D7AKY7_GEOSK	KN400_2551	Rubrerythrin	7
272	10	10	60.12	60.12	49.13	D7AI87_GEOSK	ftn	Ferritin	6
273	10	10	44.32	39.46	39.46	D7AGV3_GEOSK	KN400_3402	Amino acid-binding ACT domain regulatory protein	5
274	10	10	56.86	56.86	56.86	D7AMU1_GEOSK	rpsJ	30S ribosomal protein S10	7
275	10	10	21.48	21.48	21.48	D7AKR7_GEOSK	KN400_2481	Dienelactone hydrolase family protein	5
276	10	10	17.75	17.75	17.75	D7AJJ2_GEOSK	pgcA	Lipoprotein cytochrome c, 3 heme-binding sites	5
277	10	10	50.55	50.55	50.55	D7AIV3_GEOSK	ihfA-1	Integration host factor, alpha subunit	5
278	10	10	4.275	4.275	4.275	D7AI32_GEOSK	KN400_1225	ATS1 domain repeat protein	5
279	10	10	30.82	30.82	30.82	D7AEQ9_GEOSK	ssb-2	Single-stranded DNA-binding protein	5
280	9.92	9.92	40.58	37.92	21.29	D7AMJ6_GEOSK	trpB2	Tryptophan synthase beta chain	6
281	9.89	9.89	69.47	56.84	56.84	D7AG50_GEOSK	groS	10 kDa chaperonin	6
282	9.83	9.83	71.88	71.88	71.88	D7AK25_GEOSK	KN400_2375	Uncharacterized protein	6
283	9.77	9.77	78.72	58.87	58.87	D7AGE6_GEOSK	KN400_3379	Ankyrin repeat protein	7
284	9.68	9.68	23.27	19.82	19.82	D7AM27_GEOSK	KN400_0092	Amino acid aminotransferase, putative	5
285	9.42	9.42	68.75	68.75	68.75	D7ADX9_GEOSK	KN400_2913	Stress-responsive alpha/beta-barrel domain protein, Dabb family	5
286	9.41	9.41	36.92	36.92	33.85	D7AF68_GEOSK	KN400_0503	Helix-turn-helix transcriptional regulator, IclR family	6
287	9.41	9.41	39.65	39.65	39.65	D7AKK5_GEOSK	nifU	Nitrogen fixation protein NifU	6
288	9.39	9.39	40.99	40.99	40.99	D7AFC8_GEOSK	yajQ	UPF0234 protein KN400_3141	5
289	9.29	9.29	37.61	30.45	24.18	D7ALU2_GEOSK	gpsA	Glycerol-3-phosphate dehydrogenase [NAD(P)+]	7
290	9.19	9.19	32.91	32.91	32.91	D7AF40_GEOSK	trxB	Thioredoxin reductase	5
291	9.08	9.08	31.98	31.98	31.98	D7AJV6_GEOSK	KN400_1898	Uncharacterized protein	5
292	8.75	8.75	33.14	26.16	26.16	D7AM88_GEOSK	KN400_2213	OmpH-like outer membrane protein, putative	5
293	8.66	8.66	16.9	11.78	11.78	D7AK43_GEOSK	KN400_2393	Aconitate hydratase, putative	5

294	8.66	8.66	35.22	26.85	23.15	D7ADU9_GEOSK	KN400_2883	Outer membrane channel, putative	6
295	8.64	8.64	35.38	28.88	25.63	D7AGH8_GEOSK	KN400_0693	Peptidase, C14 family	5
296	8.62	8.62	70.68	51.5	43.98	D7AHV0_GEOSK	KN400_1143	TPR domain protein	6
297	8.55	8.55	24.35	18.2	18.2	D7AFT8_GEOSK	purD	Phosphoribosylamine--glycine ligase	5
298	8.41	8.41	26.96	23.2	20.69	D7AII9_GEOSK	accA	Acetyl-coenzyme A carboxylase carboxyl transferase subunit alpha	4
299	8.36	8.36	34.01	24.49	21.77	D7AHG4_GEOSK	aguB	N-carbamylputrescine amidohydrolase	5
300	8.27	8.27	33.58	26.57	23.25	D7AJI8_GEOSK	pyrK	Dihydroorotate dehydrogenase B (NAD(+)), electron transfer subunit	4
301	8.22	8.22	58.93	54.46	54.46	D7AJR6_GEOSK	glnB	Nitrogen regulatory protein P-II	5
302	8.21	8.21	25.1	17.45	17.45	D7ALD6_GEOSK	metG	Methionine--tRNA ligase	5
303	8.1	8.1	51.06	41.49	37.23	D7AMT8_GEOSK	rplW	50S ribosomal protein L23	4
304	8.07	8.07	52.94	52.94	47.06	D7AFF6_GEOSK	rplU	50S ribosomal protein L21	4
305	8.05	8.05	19.67	12.46	10.16	D7AJP0_GEOSK	ftsH-2	ATP-dependent zinc metalloprotease FtsH	4
306	8.02	8.02	41.84	32.22	32.22	D7AJN5_GEOSK	pdxJ	Pyridoxine 5'-phosphate synthase	4
307	8.02	8.02	45.27	39.86	39.86	D7AMS1_GEOSK	rplO	50S ribosomal protein L15	6
308	8.01	8.01	8.994	6.633	5.677	D7AL53_GEOSK	KN400_2095	Dystroglycan-type cadherin-like domain repeat protein	4
309	8.01	8.01	34.24	21.74	21.74	D7AHM3_GEOSK	KN400_1066	Iron-sulfur cluster-binding oxidoreductase	4
310	8.01	8.01	25.27	18.68	18.68	D7AKC2_GEOSK	KN400_1951	Cytidylate kinase-like domain phospholipid-binding protein, putative	4
311	8	16.03	35	30.96	27.69	D7ADE1_GEOSK	ato-2	Succinyl:acetate coenzyme A transferase	15
312	8	8	35.77	26.76	21.97	D7AMB4_GEOSK	aroF	Phospho-2-dehydro-3-deoxyheptonate aldolase	4
313	8	8	16.01	9.416	9.416	D7AJQ7_GEOSK	nadB	L-aspartate oxidase	4
314	8	8	25.29	23.2	19.95	D7ALP2_GEOSK	KN400_2669	Uncharacterized protein	4
315	8	8	46.23	33.77	33.77	D7AJI7_GEOSK	pyrD	Dihydroorotate dehydrogenase	4
316	8	8	47.69	47.69	47.69	D7AMV9_GEOSK	rpsI	30S ribosomal protein S9	9
317	8	8	18.12	15.44	15.44	D7AMM4_GEOSK	etfA	Electron transfer flavoprotein, alpha subunit	4
318	8	8	43.5	33	33	D7ALY3_GEOSK	KN400_0048	Outer membrane protein, putative	6
319	8	8	21.83	13.2	13.2	D7AKC9_GEOSK	KN400_1958	SPOR domain protein	4
320	8	8	31.56	16.52	16.52	D7AIV1_GEOSK	pheS	Phenylalanine--tRNA ligase alpha subunit	4
321	8	8	31.44	25.77	25.77	D7AIR2_GEOSK	KN400_1504	LemA family lipoprotein	4
322	8	8	33.54	27.85	27.85	D7AI58_GEOSK	greA	Transcription elongation factor GreA	4
323	8	8	43.86	37.89	37.89	D7AH02_GEOSK	folD-2	Bifunctional protein FolD	4
324	8	8	47.74	40	40	D7AGU3_GEOSK	prx-4	Peroxiredoxin, 1-Cys subfamily	5
325	8	8	42.5	30.5	30.5	D7AGS8_GEOSK	KN400_0793	Organic solvent tolerance ABC transporter, periplasmic substrate-binding protein	4
326	8	8	22.9	18.18	18.18	D7AEA8_GEOSK	KN400_0329	Peptidylprolyl cis-trans isomerase, PpiC-type	4
327	8	8	26.75	22.93	22.93	D7ADS7_GEOSK	tklB	Transketolase, B protein	4
328	8	8	25.5	25.5	25.5	D7ALW8_GEOSK	grpE	Protein GrpE	4

329	8	8	30.06	30.06	30.06	D7AKA7_GEOSK	ilvN	Acetolactate synthase, small subunit	4
330	8	8	77.78	77.78	77.78	D7AJI3_GEOSK	infA	Translation initiation factor IF-1	5
331	8	8	73.88	73.88	73.88	D7AJ08_GEOSK	KN400_1600	(R)-methylmalonyl-CoA mutase, adenosylcobamide-binding subunit	4
332	8	8	59.78	59.78	59.78	D7AGT9_GEOSK	KN400_0804	Peptidylprolyl cis-trans isomerase, PpiC-type	4
333	8	8	39.83	39.83	39.83	D7AFX3_GEOSK	rplS	50S ribosomal protein L19	6
334	8	8	34.12	34.12	34.12	D7AE86_GEOSK	nuoB	NADH-quinone oxidoreductase subunit B	4
335	7.81	7.81	15.98	15.98	14.29	D7AM97_GEOSK	KN400_2222	Uncharacterized protein	4
336	7.6	7.6	50	22.95	22.95	D7AJE7_GEOSK	queD	6-carboxy-5,6,7,8-tetrahydropterin synthase	4
337	7.41	7.41	16.97	16.97	16.97	D7AJC3_GEOSK	hom	Homoserine dehydrogenase	5
338	7.39	7.39	76.47	67.23	67.23	D7AH59_GEOSK	KN400_0900	Uncharacterized protein	4
339	7.36	7.36	26.42	22.72	17.78	D7AE05_GEOSK	cbiET	Cobalt-precorrin-6B C5,C15-methyltransferase and C12-decarboxylase	5
340	7.28	7.28	12.98	12.98	12.98	D7AFC9_GEOSK	rimO	Ribosomal protein S12 methylthiotransferase Rim	4
341	7.24	7.24	36.79	20.98	20.98	D7AM57_GEOSK	pilT-1	Twitching motility pilus retraction protein	5
342	7.23	7.23	48.95	41.96	41.96	D7AMW0_GEOSK	rplM	50S ribosomal protein L13	4
343	7.21	7.21	33.13	23.93	23.93	D7AJ31_GEOSK	fabH-2	3-oxoacyl-[acyl-carrier-protein] synthase 3	4
344	7.19	7.19	27.29	21.04	18.75	D7AG43_GEOSK	pyk	Pyruvate kinase	4
345	7.13	7.13	40.79	33.55	33.55	D7AF30_GEOSK	KN400_0465	Ferritin-like domain protein	4
346	7.05	7.05	55.26	52.63	52.63	D7AFW9_GEOSK	KN400_0620	UPF0109 protein KN400_0620	4
347	6.92	6.92	35.25	33.61	33.61	D7AMR6_GEOSK	rpsM	30S ribosomal protein S13	4
348	6.75	6.75	47.24	34.36	34.36	D7AM09_GEOSK	mglB	Cell polarity determinant GTPase-activating protein MglB	4
349	6.72	6.72	56.76	56.76	56.76	D7AKJ2_GEOSK	hfq	RNA-binding protein Hfq	4
350	6.68	6.68	16.06	10.83	8.484	D7AG77_GEOSK	glnS	Glutamine--tRNA ligase	4
351	6.59	6.59	55.45	55.45	31.75	D7AMC8_GEOSK	can-2	Carbonic anhydrase	4
352	6.55	6.55	31.49	27.23	27.23	D7AFK4_GEOSK	KN400_3217	LysM domain protein	4
353	6.27	6.27	42.71	38.54	30.21	D7AKX6_GEOSK	ihfB-2	Integration host factor, beta subunit	3
354	6.26	6.27	20.11	20.11	20.11	D7AIP4_GEOSK	ispG	4-hydroxy-3-methylbut-2-en-1-yl diphosphate synthase	4
355	6.25	6.25	23.06	17.39	9.83	D7AI91_GEOSK	pgi	Glucose-6-phosphate isomerase	3
356	6.2	6.2	32.28	22.49	14.02	D7AH90_GEOSK	metC-2	Cystathionine gamma-synthase/beta-lyase	3
357	6.18	6.18	24.01	20.28	13.52	D7AKY0_GEOSK	aroA	3-phosphoshikimate 1-carboxyvinyltransferase	3
358	6.07	6.07	34.47	26.21	17.96	D7AM19_GEOSK	atpF	ATP synthase subunit b	3
359	6.04	6.04	20.68	20.68	17.67	D7ALZ3_GEOSK	KN400_0058	Laccase family multicopper oxidase	3
360	6.03	6.03	22.5	12.75	12.75	D7AJC0_GEOSK	ribA	Riboflavin biosynthesis protein RibBA	4
361	6.03	6.03	74.24	74.24	74.24	D7ADH6_GEOSK	KN400_0183	Cold shock DNA/RNA-binding protein	7
362	6.02	6.02	11.39	9.158	9.158	D7AL26_GEOSK	KN400_2068	Response regulator	3
363	6.01	6.01	52.31	33.85	33.85	D7AKQ2_GEOSK	yedF	Selenium metabolism protein YedF, putative	3
364	6.01	6.01	15.42	8.333	8.333	D7ADT0_GEOSK	metH	5-methyltetrahydrofolate--homocysteine S-	3

								methyltransferase, cobalamin-dependent	
365	6.01	6.01	48.36	48.36	41.8	D7AMS4_GEOSK	rplR	50S ribosomal protein L18	3
366	6	6	41.44	31.53	31.53	D7AMT5_GEOSK	rplV	50S ribosomal protein L22	3
367	6	6	26	20.67	20.67	D7AM86_GEOSK	fabZ	3-hydroxyacyl-[acyl-carrier-protein] dehydratase FabZ	3
368	6	6	40.85	34.51	34.51	D7ALQ4_GEOSK	KN400_2681	Uncharacterized protein	3
369	6	6	9.375	7.617	7.617	D7AKA3_GEOSK	leuA	2-isopropylmalate synthase	3
370	6	6	39.47	22.37	22.37	D7AJW0_GEOSK	KN400_1902	Uncharacterized protein	3
371	6	6	42.05	38.64	38.64	D7AJ22_GEOSK	rpsO	30S ribosomal protein S15	4
372	6	6	13.65	9.41	9.41	D7AHX9_GEOSK	serA	D-3-phosphoglycerate dehydrogenase	3
373	6	6	13.48	12.64	12.64	D7AGV0_GEOSK	KN400_3399	Radical SAM domain iron-sulfur cluster-binding oxidoreductase	3
374	6	6	33.17	28.29	28.29	D7AED5_GEOSK	KN400_0356	Uncharacterized protein	3
375	6	6	27.44	20.58	20.58	D7ADS8_GEOSK	tklA	Transketolase, A protein	4
376	6	6	56.03	56.03	56.03	D7AM29_GEOSK	KN400_0094	Glyoxalase/bleomycin resistance protein/dioxygenase superfamily protein	4
377	6	6	36.65	36.65	36.65	D7AL98_GEOSK	KN400_2140	Ferritin-like domain protein	3
378	6	6	39.6	39.6	39.6	D7AJN2_GEOSK	KN400_1824	CBS domain pair-containing protein	4
379	6	6	28.13	28.13	28.13	D7AJH1_GEOSK	iorB-1	Indolepyruvate:ferredoxin oxidoreductase, beta subunit	3
380	6	6	33.57	33.57	33.57	D7AJG9_GEOSK	KN400_1761	ACT domain protein	3
381	6	6	35.07	35.07	35.07	D7AHQ3_GEOSK	KN400_1096	Response receiver	3
382	6	6	29.81	29.81	29.81	D7AHI3_GEOSK	KN400_1026	UPF0225 protein KN400_1026	3
383	6	6	32.84	32.84	32.84	D7AFN2_GEOSK	mceE	Methylmalonyl-CoA epimerase	3
384	6	6	24.03	24.03	24.03	D7AF88_GEOSK	iscR-1	Helix-turn-helix iron-sulfur cluster-binding transcriptional regulator IscR	3
385	6	6	80.3	80.3	80.3	D7AF33_GEOSK	KN400_0468	Uncharacterized protein	5
386	6	6	59.46	59.46	59.46	D7AF32_GEOSK	KN400_0467	Thioredoxin/NifU-like domain protein	3
387	6	6	16.75	16.75	16.75	D7AEN9_GEOSK	hisH	Imidazole glycerol phosphate synthase subunit HisH	3
388	6	6	29.58	29.58	29.58	D7AED0_GEOSK	KN400_0351	Peptidyl-prolyl cis-trans isomerase	3
389	6	6	14.66	14.66	14.66	D7ADC9_GEOSK	dapB	4-hydroxy-tetrahydrodipicolinate reductase	3
390	5.89	5.89	31.36	14.5	14.5	D7AFD7_GEOSK	obg	GTPase obg	3
391	5.89	5.89	10.88	7.88	7.88	D7AKZ2_GEOSK	secD	Protein translocase subunit SecD	3
392	5.85	5.89	26.26	19.53	19.53	D7AJJ6_GEOSK	KN400_1788	Trans-isoprenyl diphosphate synthase	3
393	5.85	5.89	23.95	14.71	14.71	D7AGR7_GEOSK	KN400_0782	Oxidoreductase, short-chain dehydrogenase/reductase family	3
394	5.82	5.82	14.84	7.908	7.908	D7AJK9_GEOSK	pulQ	Type II secretion system secretin lipoprotein PulQ	4
395	5.73	5.73	24.24	24.24	16.02	D7ALP7_GEOSK	KN400_2674	Cytochrome c, 8 heme-binding sites	3
396	5.6	5.6	19.09	16.49	16.49	D7AJC5_GEOSK	thrC	Threonine synthase	6

397	5.59	5.59	37.72	17.97	17.97	D7AGB3_GEOSK	KN400_3346	Branched-chain amino acid ABC transporter, periplasmic amino acid-binding lipoprotein, putative	5
398	5.55	5.55	26.18	5.956	5.956	D7AFB5_GEOSK	KN400_3128	TPR domain protein	4
399	5.53	5.53	23.42	17.52	14.66	D7ALA0_GEOSK	guaB	Inosine-5'-monophosphate dehydrogenase	4
400	5.51	5.51	66.67	66.67	66.67	D7AHW5_GEOSK	KN400_1158	Uncharacterized protein	3
401	5.48	5.48	19.84	19.84	15.79	D7AKP7_GEOSK	KN400_2461	Rhodanese homology domain pair protein	3
402	5.46	5.46	25.88	25.88	25.88	D7AMT1_GEOSK	rpsQ	30S ribosomal protein S17	3
403	5.43	5.43	23.01	14.16	14.16	D7AEL3_GEOSK	murD	UDP-N-acetylmuramoylalanine--D-glutamate ligase	3
404	5.26	5.26	15.24	15.24	15.24	D7AGH7_GEOSK	KN400_0692	Uncharacterized protein	3
405	5.2	5.2	26.18	21.89	21.89	D7AIM7_GEOSK	KN400_1469	Carbonic anhydrase	3
406	5.18	5.18	23.84	23.84	20.55	D7AIE4_GEOSK	namA	NADPH-dependent enal/enone/nitroreductase,	3
407	5.1	5.1	77.27	77.27	77.27	D7AKA2_GEOSK	KN400_1931	Cold shock DNA/RNA-binding protein	6
408	5.06	5.06	45.09	38.15	38.15	D7AF80_GEOSK	ymdB	acetyl-ADP-ribose deacetylase	3
409	5	5	20.47	16.67	16.67	D7AES4_GEOSK	KN400_3071	Uncharacterized protein	3
410	4.98	4.98	25.13	25.13	25.13	D7AF04_GEOSK	efp-1	Elongation factor P	3
411	4.96	4.96	16.93	16.93	16.93	D7ADG6_GEOSK	KN400_0173	Oxidoreductase, short-chain dehydrogenase/reductase family	4
412	4.88	4.88	17.53	17.53	8.454	D7ALM8_GEOSK	KN400_2655	Uncharacterized protein	3
413	4.86	4.86	36.84	36.84	36.84	D7AJR9_GEOSK	KN400_1861	Phosphatase/phosphohexomutase-related hydrolase	3
414	4.82	4.82	25.56	10.67	10.67	D7AK46_GEOSK	sucB	Dihydrolipoyllysine-residue succinyltransferase component of 2-oxoglutarate dehydrogenase complex	3
415	4.7	4.7	33.61	27.46	27.46	D7AEN8_GEOSK	hisA	1-(5-phosphoribosyl)-5-[(5-phosphoribosylamino)methylideneamino] imidazole-4-carboxamide isomerase	3
416	4.45	4.45	38.75	23.13	12.5	D7AGI3_GEOSK	KN400_0698	Desulfoferrodoxin, putative	2
417	4.4	4.4	28.37	20.76	20.76	D7AGZ9_GEOSK	galU	Glucose-1-phosphate uridylyltransferase	4
418	4.38	4.38	20.48	20.48	20.48	D7AGY7_GEOSK	scdA	Iron-sulfur cluster repair protein ScdA	3
419	4.29	4.29	10.53	9.273	9.273	D7AJP9_GEOSK	apgM	Probable 2,3-bisphosphoglycerate-independent phosphoglycerate mutase	3
420	4.29	4.29	31.4	31.4	31.4	D7AFC2_GEOSK	cheY4 4H	Response receiver CheY associated with MCPs of class 44H	3
421	4.21	4.21	28.18	21.36	21.36	D7AES0_GEOSK	KN400_3067	Lipoprotein, putative	3
422	4.17	4.17	20.8	14	11.2	D7AFF8_GEOSK	cafA	Ribonuclease G	3
423	4.16	4.16	17.22	17.22	9.272	D7AGW5_GEOSK	KN400_0806	Pirin family protein	2
424	4.08	4.08	42.72	31.07	23.3	D7AFZ1_GEOSK	rpsR	30S ribosomal protein S18	2
425	4.08	4.08	33.33	23.93	17.95	D7AIV0_GEOSK	rplT	50S ribosomal protein L20	2
426	4.07	4.07	25.12	17.67	12.56	D7AJK2_GEOSK	KN400_1794	DNA/RNA-binding protein, putative	2
427	4.06	4.06	31.14	31.14	13.77	D7AM40_GEOSK	def-1	Peptide deformylase	2

428	4.04	4.04	20.7	10.75	8.333	D7AEM7_GEOSK	yqfO	Putative GTP cyclohydrolase 1 type 2	2
429	4.03	4.03	14.97	11.31	6.847	D7AHC7_GEOSK	KN400_0970	Uncharacterized protein	2
430	4.02	4.02	19.11	19.11	12.89	D7AKV4_GEOSK	cysE-1	Serine acetyltransferase	2
431	4.02	4.02	8.434	8.434	6.024	D7AEQ0_GEOSK	rho	Transcription termination factor Rho	2
432	4.02	4.02	21.56	21.56	21.56	D7ADJ6_GEOSK	KN400_0203	Peptidyl-prolyl cis-trans isomerase	3
433	4.01	4.01	21.9	20.8	20.8	D7AIY9_GEOSK	KN400_1581	Mechanosensitive ion channel family protein	3
434	4.01	4.01	27.46	16.42	16.42	D7AGN6_GEOSK	acuI	NADP-dependent menaquinol:acrylyl-CoA oxidoreductase	3
435	4.01	4.01	26.79	26.79	22.02	D7AIA2_GEOSK	resA	Apocytochrome c disulfide reductase lipoprotein ResA	2
436	4	4	13.72	6.029	6.029	D7AEC5_GEOSK	gcv	Glycine cleavage system P protein, subunit 2	2
437	4	4	30.82	16.13	16.13	D7AIB6_GEOSK	KN400_1309	Lipoprotein, putative	2
438	4	4	41.98	24.43	24.43	D7AFD3_GEOSK	rsfS	Ribosomal silencing factor RsfS	2
439	4	4	37.4	28.46	28.46	D7AMU5_GEOSK	rpsL	30S ribosomal protein S12	3
440	4	4	73.77	21.31	21.31	D7AMS7_GEOSK	rpsZ	30S ribosomal protein S14 type Z	2
441	4	4	38.46	38.46	23.08	D7AMM2_GEOSK	mscL	Large-conductance mechanosensitive channel	2
442	4	4	19.64	13.93	13.93	D7AMI7_GEOSK	accD	Acetyl-coenzyme A carboxylase carboxyl transferase subunit beta	2
443	4	4	11.24	11.24	8.357	D7AM87_GEOSK	lpxD	UDP-3-acylglucosamine N-acyltransferase	2
444	4	4	23.05	10.55	10.55	D7AM85_GEOSK	lpxA-1	Acyl-(Acyl carrier protein)--UDP-N-acetylglucosamine/UDP-2-N-acetylglucose-2, 3-diamine 3-N-acyltransferase	2
445	4	4	23.74	19.42	19.42	D7ALW3_GEOSK	KN400_0028	Biopolymer transport membrane protein, TolR-related	2
446	4	4	27.63	11.51	11.51	D7ALV7_GEOSK	nadA	Quinolinate synthase A	2
447	4	4	12.58	7.669	7.669	D7ALE4_GEOSK	galE	UDP-glucose/UDP-N-acetylglucosamine 4-epimerase	2
448	4	4	8.144	8.144	5.871	D7AJM9_GEOSK	cimA	Citramalate synthase	2
449	4	4	32.7	20.13	20.13	D7AJ15_GEOSK	rim	Ribosome maturation factor RimP	2
450	4	4	13.4	8.247	8.247	D7AIW3_GEOSK	hisG	ATP phosphoribosyltransferase	2
451	4	4	26.16	19.19	19.19	D7AIU8_GEOSK	infC	Translation initiation factor IF-3	2
452	4	4	27.98	14.88	14.88	D7AI64_GEOSK	KN400_1257	NosL family protein	2
453	4	4	13.85	10.46	10.46	D7AHZ3_GEOSK	KN400_1186	Uncharacterized protein	2
454	4	4	36.94	17.2	17.2	D7AHY6_GEOSK	KN400_1179	Flavodoxin, putative	2
455	4	4	25.1	21.05	21.05	D7AHK9_GEOSK	KN400_1052	Probable transcriptional regulatory protein KN400_1052	3
456	4	4	5.539	3.892	3.892	D7AGD4_GEOSK	tkt	Transketolase	2
457	4	4	35.23	35.23	35.23	D7AFW8_GEOSK	rps	30S ribosomal protein S16	2
458	4	4	24.38	18.91	18.91	D7AFP7_GEOSK	KN400_0548	SAM-dependent methyltransferase, putative	2
459	4	4	9.557	7.226	7.226	D7AEP2_GEOSK	hisD	Histidinol dehydrogenase	2
460	4	4	28.64	28.64	28.64	D7AE08_GEOSK	cbiC	Cobalt-precorrin-8X methylmutase	3

461	4	4	5.493	4.039	4.039	D7ADN9_GEOSK	cbcY	Cytochrome c, 9 heme-binding sites, and cytochrome b	2
462	4	4	56.94	56.94	26.39	D7ADG4_GEOSK	KN400_0171	Flavin and coenzyme A sequestration protein dodecin	2
463	4	4	35.59	35.59	35.59	D7AMS2_GEOSK	rpmD	50S ribosomal protein L30	3
464	4	4	6.951	6.951	6.951	D7AMC9_GEOSK	mleA	Malate oxidoreductase, NAD-dependent	2
465	4	4	18.02	18.02	18.02	D7ALQ5_GEOSK	KN400_2682	Cytochrome c, 1 heme-binding site	2
466	4	4	14.53	14.53	14.53	D7ALG0_GEOSK	KN400_2587	NAD-dependent nucleoside diphosphate-sugar epimerase/dehydratase	2
467	4	4	24.6	24.6	24.6	D7ALD9_GEOSK	KN400_2181	Endoribonuclease L-PSP	2
468	4	4	18.57	18.57	18.57	D7AKP9_GEOSK	KN400_2463	Rhodanese homology domain superfamily protein	2
469	4	4	9.577	9.577	9.577	D7AKL4_GEOSK	KN400_2043	Prolidase family protein	2
470	4	4	31.25	31.25	31.25	D7AKK7_GEOSK	KN400_2036	Uncharacterized protein	2
471	4	4	19.23	19.23	19.23	D7AJW7_GEOSK	KN400_1909	Phosphotransferase system, mannose-type, protein IIA	2
472	4	4	40.58	40.58	40.58	D7AJQ9_GEOSK	KN400_1851	Uncharacterized protein	2
473	4	4	17.23	17.23	17.23	D7AJM6_GEOSK	rph	Ribonuclease PH	2
474	4	4	15.67	15.67	15.67	D7AJ44_GEOSK	KN400_1636	Rossmann fold nucleotide-binding protein	2
475	4	4	15.85	15.85	15.85	D7AJ33_GEOSK	fabG-2	3-oxoacyl-(Acyl carrier protein) reductase	2
476	4	4	80	80	80	D7AI59_GEOSK	KN400_1252	Uncharacterized protein	2
477	4	4	6.737	6.737	6.737	D7AHT4_GEOSK	hpnJ	Radical SAM domain iron-sulfur cluster-binding oxidoreductase with cobalamin-binding-like domain	2
478	4	4	22.5	22.5	22.5	D7AHB5_GEOSK	KN400_0958	Uncharacterized protein	2
479	4	4	23.89	23.89	23.89	D7AGE9_GEOSK	phnA	Phosphonoacetate hydrolase	2
480	4	4	22.55	22.55	22.55	D7AG46_GEOSK	KN400_3279	Cytochrome c, 1 heme-binding site	2
481	4	4	21.3	21.3	21.3	D7AFT9_GEOSK	purE-1	N5-carboxyaminoimidazole ribonucleotide mutase	2
482	4	4	65.15	65.15	65.15	D7AFQ8_GEOSK	KN400_0559	Cold shock DNA/RNA-binding protein	3
483	4	4	17.47	17.47	17.47	D7AE81_GEOSK	atpB	ATP synthase subunit a	2
484	4	4	29.25	29.25	29.25	D7ADR4_GEOSK	KN400_2848	Cupin superfamily barrel domain protein	2
485	4	4	46.4	46.4	46.4	D7ADD9_GEOSK	KN400_0146	Uncharacterized protein	2
486	3.78	3.78	29.02	13.99	13.99	D7AGN7_GEOSK	KN400_0752	Flavodoxin, putative	2
487	3.75	3.75	28.91	14.84	14.84	D7AG82_GEOSK	KN400_3315	TIM barrel protein, AP endonuclease family 2/xylose isomerase-like family	2
488	3.62	3.62	23.64	8.909	6	D7ADJ7_GEOSK	KN400_0204	Acyl-CoA synthetase, AMP-forming	2
489	3.49	3.49	13.98	13.98	13.98	D7AI98_GEOSK	ispB	Octaprenyl diphosphate synthase	2
490	3.43	3.43	37.04	19.58	19.58	D7ADM4_GEOSK	KN400_0231	Flavoredoxin	2
491	3.42	3.42	24.48	24.48	7.67	D7AET4_GEOSK	aroG-2	3-deoxy-D-arabino-heptulosonate 7-phosphate synthase	2
492	3.39	3.39	13.08	13.08	13.08	D7AM94_GEOSK	KN400_2219	Uncharacterized protein	2

493	3.34	3.34	56	45.6	45.6	D7AIW4_GEOSK	hisI	Phosphoribosyl-AMP cyclohydrolase	3
494	3.3	3.3	15.15	6.061	6.061	D7AG80_GEOSK	selA	L-seryl-tRNA(Sec) selenium transferase	2
495	3.28	3.28	33.52	27.37	27.37	D7ALV6_GEOSK	yrdA	Uncharacterized protein	2
496	3.2	3.2	31.72	8.621	8.621	D7ADI3_GEOSK	folD-1	Bifunctional protein FolD	2
497	3.14	3.14	14.62	10.85	10.85	D7AEP3_GEOSK	hisGS	ATP phosphoribosyltransferase	2
498	3.13	3.13	21.97	21.21	15.91	D7AE93_GEOSK	nuoI-1	NADH-quinone oxidoreductase subunit I	2
499	3.09	3.09	17.75	14.13	14.13	D7AKD3_GEOSK	nadC	Quinolinate phosphoribosyltransferase, decarboxylating	3
500	2.95	2.95	26.59	8.614	8.614	D7AKS5_GEOSK	KN400_2489	Polysaccharide deacetylase domain protein	2
501	2.95	2.95	9.357	9.357	9.357	D7AFD1_GEOSK	gpmI	2,3-bisphosphoglycerate-independent phosphoglycerate mutase	2
502	2.86	2.86	14.24	14.24	14.24	D7AHG5_GEOSK	aguA	Agmatine deiminase, putative	3
503	2.86	2.86	28.34	28.34	15.51	D7AHE0_GEOSK	KN400_0983	Amidohydrolase, YcaC-related	2
504	2.84	2.84	44.68	32.98	32.98	D7AL00_GEOSK	KN400_2564	Helix-turn-helix transcriptional regulator, ArsR family	2
505	2.83	2.84	30.91	26.67	26.67	D7AG63_GEOSK	KN400_3296	Uncharacterized protein	2
506	2.82	2.82	26.54	21.8	13.27	D7AMT4_GEOSK	rpsC	30S ribosomal protein S3	2
507	2.69	2.69	48.09	48.09	48.09	D7AMR5_GEOSK	rpsK	30S ribosomal protein S11	3
508	2.68	2.69	15.94	12.56	12.56	D7AEY0_GEOSK	KN400_0415	Menaquinone biosynthesis decarboxylase, putative	2
509	2.63	2.63	31.71	31.71	31.71	D7AI72_GEOSK	KN400_1265	Response regulator, putative	2
510	2.58	2.58	30.59	15.98	15.98	D7ADK0_GEOSK	KN400_0207	UPF0502 protein KN400_0207	2
511	2.55	2.55	13.37	3.429	3.429	D7AM59_GEOSK	alaS	Alanine--tRNA ligase	2
512	2.55	2.55	25.88	25.88	25.88	D7ADK9_GEOSK	acp	Acyl carrier protein	2
513	2.49	2.49	14.29	14.29	14.29	D7AMJ7_GEOSK	trpC	Indole-3-glycerol phosphate synthase	2
514	2.44	2.44	9.742	9.742	9.742	D7AK96_GEOSK	KN400_1925	ABC transporter, periplasmic substrate-binding protein, MCE domain-containing	2
515	2.42	2.42	27.54	15.22	15.22	D7AJC2_GEOSK	nusB	N utilization substance protein B homolog	2
516	2.38	2.38	27.64	27.64	27.64	D7AHT9_GEOSK	KN400_1132	Glutaredoxin family protein	2
517	2.23	2.23	8.807	8.807	8.807	D7AE18_GEOSK	cobT	Nicotinate-nucleotide--dimethylbenzimidazole phosphoribosyltransferase	2
518	2.22	2.22	18.15	14.65	14.65	D7AFY6_GEOSK	prsA	Ribose-phosphate pyrophosphokinase	2
519	2.18	2.18	15.93	15.93	15.93	D7AKM2_GEOSK	pil	Type IV pilus assembly lipoprotein PilP	2
520	2.15	2.15	18.92	7.278	5.822	D7AFQ6_GEOSK	glyS	Glycine--tRNA ligase beta subunit	2
521	2.14	2.15	31.65	11.93	6.422	D7AKA5_GEOSK	psd	Phosphatidylserine decarboxylase proenzyme	1
522	2.13	2.13	11.5	2.966	1.029	D7AI33_GEOSK	KN400_1226	Multicopper oxidase with phosphopantotheine attachment site	1
523	2.09	2.09	29.1	17.46	17.46	D7AL67_GEOSK	gmhA	Phosphoheptose isomerase	2
524	2.08	2.08	25.5	25.5	25.5	D7AH05_GEOSK	KN400_0846	Cell division protein DivIVA, putative	2
525	2.05	2.05	36.77	25.81	25.81	D7AI65_GEOSK	KN400_1258	Cytochrome c, 1 heme-binding site	2
526	2.05	2.05	8.936	8.936	2.553	D7AFS6_GEOSK	KN400_0577	Sigma-54-dependent transcriptional response regulator	1

527	2.05	2.05	18	11.43	7.429	D7AEP1_GEOSK	hisC	Histidinol-phosphate aminotransferase	1
528	2.04	2.04	6.689	4.849	3.344	D7AF54_GEOSK	typA	Translation-regulating membrane GTPase TypA	1
529	2.04	2.04	8.092	8.092	3.468	D7AMV8_GEOSK	argC	N-acetyl-gamma-glutamyl-phosphate reductase	1
530	2.02	2.02	15.89	4.277	2.444	D7AMK0_GEOSK	trpE	Anthranilate synthase, catalytic subunit	1
531	2.02	2.02	9.5	8	3.25	D7ALL6_GEOSK	acrA	Efflux pump, RND family, membrane fusion lipoprotein	1
532	2.02	2.02	15.06	5.176	2.588	D7AKU7_GEOSK	KN400_2511	Uncharacterized protein	1
533	2.02	2.02	22.58	13.82	5.53	D7AM35_GEOSK	KN400_0100	Uncharacterized protein	1
534	2.02	2.02	13.22	10.66	4.478	D7AI31_GEOSK	KN400_1224	Sigma-54-dependent transcriptional response regulator	1
535	2.02	2.02	11.49	5.583	3.12	D7ADN5_GEOSK	glmS	Glutamine--fructose-6-phosphate aminotransferase [isomerizing]	1
536	2.02	2.02	6.439	6.439	4.167	D7AIM2_GEOSK	KN400_1464	Peptidase lipoprotein, M48 family	1
537	2.02	2.02	16.67	16.67	10.56	D7AHV6_GEOSK	ogt	Methylated-DNA--protein-cysteine methyltransferase	1
538	2.01	2.01	8.568	3.495	1.127	D7AL25_GEOSK	valS	Valine--tRNA ligase	1
539	2.01	2.01	13.07	7.015	7.015	D7AMI9_GEOSK	mcp64H-2	Methyl-accepting chemotaxis sensory transducer, class 40+24H	2
540	2.01	2.01	10.8	6	4	D7AK93_GEOSK	kdsB	3-deoxy-manno-octulosonate cytidylyltransferase	1
541	2.01	2.01	7.455	3.241	1.783	D7AJD0_GEOSK	KN400_1722	TPR domain protein	1
542	2.01	2.01	12.99	6.818	6.818	D7AEU9_GEOSK	cysM	Cysteine synthase B	1
543	2.01	2.01	34.72	21.53	10.42	D7AET7_GEOSK	mosC	Molybdopterin sulfurtransferase MOSC domain protein	1
544	2.01	2.01	7.859	2.161	2.161	D7AEL6_GEOSK	murE	UDP-N-acetylmuramoyl-L-alanyl-D-glutamate--2,6-diaminopimelate ligase	1
545	2.01	2.01	30.32	30.32	6.383	D7AI28_GEOSK	KN400_1221	Uncharacterized protein	1
546	2	4	14.33	8.232	8.232	D7AIV7_GEOSK	rpoS	RNA polymerase sigma factor	3
547	2	2	16.78	5.437	5.437	E1PTD0_GEOSK	KN400_0917	Three rhodanese homology domain protein, selenocysteine-containing	1
548	2	2	11.41	2.791	2.791	D7ALB4_GEOSK	leuS	Leucine--tRNA ligase	2
549	2	2	18.82	7.527	7.527	D7AM99_GEOSK	prfB	Peptide chain release factor 2	1
550	2	2	26.91	3.21	3.21	D7ALM2_GEOSK	moeA	Molybdopterin--molybdenum ligase	1
551	2	2	24.79	9.972	9.972	D7AJU5_GEOSK	vorA	2-oxoacid:ferredoxin oxidoreductase, alpha subunit	1
552	2	2	41.26	17.48	17.48	D7AJJ1_GEOSK	purN	Phosphoribosylglycinamide formyltransferase, folate-dependent	1
553	2	2	12.21	3.117	3.117	D7AHJ3_GEOSK	sucC	Succinyl-CoA ligase [ADP-forming] subunit beta	1
554	2	2	55.8	10.14	10.14	D7AFG2_GEOSK	KN400_3175	Uncharacterized protein	1
555	2	2	11.68	7.009	3.505	D7AFC0_GEOSK	mcp44H	Methyl-accepting chemotaxis sensory transducer, class 44H	1
556	2	2	30.82	10.27	10.27	D7AEN4_GEOSK	yqeY	Uncharacterized protein YqeY	1
557	2	2	19.33	2.731	2.731	D7ADN6_GEOSK	glmU	Bifunctional protein GlmU	1
558	2	2	12.74	3.861	3.861	D7ALW5_GEOSK	KN400_0030	Nitrilase/amidohydrolase superfamily protein, class 5	1

559	2	2	10.76	2.915	2.915	D7AL39_GEOSK	KN400_2081	Zinc protease PmbA, putative	1
560	2	2	3.694	1.741	1.741	D7AL18_GEOSK	pilY1-2	Type IV pilus assembly protein PilY1	1
561	2	2	15.84	5.709	5.709	D7AKW2_GEOSK	mcp40H-14	Methyl-accepting chemotaxis sensory transducer, class 40H	1
562	2	2	15.65	6.803	6.803	D7AH15_GEOSK	KN400_0856	Uncharacterized protein	1
563	2	2	15.38	5.128	5.128	D7AGC0_GEOSK	ltaE	L-threonine aldolase, low-specificity	1
564	2	2	11.47	3.44	3.44	D7AFT1_GEOSK	thiC-1	Phosphomethylpyrimidine synthase	1
565	2	2	6.832	6.832	3.52	D7AF31_GEOSK	aspA	Aspartate ammonia-lyase	1
566	2	2	16.59	7.373	7.373	D7AE16_GEOSK	cobC	Adenosylcobalamin-5'-phosphate phosphatase, putative	1
567	2	2	29.2	8.029	8.029	D7ADY1_GEOSK	KN400_2915	Lipoprotein, putative	1
568	2	2	21.57	10.59	10.59	D7ADH1_GEOSK	KN400_0178	Dehydrogenase molybdenum cofactor insertion protein	1
569	2	2	20.85	6.161	6.161	D7ADE6_GEOSK	KN400_0153	Flavodoxin, putative	1
570	2	2	46.77	19.35	19.35	D7AMT2_GEOSK	rpmC	50S ribosomal protein L29	1
571	2	2	4.032	4.032	4.032	D7AMR8_GEOSK	map	Methionine aminopeptidase	1
572	2	2	9.426	2.664	2.664	D7AMM9_GEOSK	KN400_2738	Cytochrome c, 5 heme-binding sites	1
573	2	2	30.33	9.836	9.836	D7ALZ6_GEOSK	KN400_0061	Uncharacterized protein	1
574	2	2	25.77	8.589	8.589	D7ALM4_GEOSK	moaB	Molybdopterin adenylyltransferase MoaB, putative	1
575	2	2	23.58	8.943	8.943	D7ALC3_GEOSK	cheY40H-2	Response receiver CheY associated with MCPs of class 40H	1
576	2	2	11.43	6.19	6.19	D7AKW6_GEOSK	KN400_2530	Amidohydrolase, YcaC-related	1
577	2	2	5.208	3.125	3.125	D7AKR9_GEOSK	nspC	Carboxynorspermidine/carboxyspermidine decarboxylase	1
578	2	2	6.386	2.903	2.903	D7AKR0_GEOSK	fusA-2	Elongation factor G	1
579	2	2	6.744	4.419	4.419	D7AKN4_GEOSK	omcT	Cytochrome c, 6 heme-binding sites	1
580	2	2	13.87	5.067	5.067	D7AKL7_GEOSK	KN400_2046	TPR domain protein	1
581	2	2	8.447	5.177	5.177	D7AKJ5_GEOSK	KN400_2024	FAD-dependent pyridine nucleotide-disulfide oxidoreductase family protein	1
582	2	2	7.453	3.416	3.416	D7AKE4_GEOSK	KN400_1973	Uncharacterized protein	1
583	2	2	31.54	8.725	8.725	D7AK07_GEOSK	hspA-2	ATP-independent chaperone, alpha-crystallin/Hsp20 family	1
584	2	2	32.61	20.65	20.65	D7AJH9_GEOSK	ihfB-1	Integration host factor, beta subunit	1
585	2	2	18.24	8.784	8.784	D7AJ36_GEOSK	rpiB	Ribose-5-phosphate isomerase B	1
586	2	2	32.31	18.46	18.46	D7AIU9_GEOSK	rpmI	50S ribosomal protein L35	1
587	2	2	6.792	2.83	2.83	D7AI63_GEOSK	KN400_1256	Outer membrane channel, putative	1
588	2	2	10.36	6.306	6.306	D7AI48_GEOSK	lepB	Signal peptidase I	1
589	2	2	29.47	13.68	13.68	D7AHY8_GEOSK	KN400_1181	HesB/YadR/YfhF family protein, selenocysteine-containing	1
590	2	2	15.52	9.483	9.483	D7AHV1_GEOSK	KN400_1144	Uncharacterized protein	1
591	2	2	26.04	26.04	10.06	D7AGV2_GEOSK	def-2	Peptide deformylase	1

592	2	2	7.463	2.985	2.985	D7AG33_GEOSK	KN400_3266	Phosphoglucomutase/phosphomannomutase family protein	1
593	2	2	14	7.333	7.333	D7AFM1_GEOSK	KN400_3234	Ferritin-like domain protein	1
594	2	2	6.114	6.114	2.367	D7AFH6_GEOSK	KN400_3189	Cytochrome c, 7 heme-binding sites	1
595	2	2	23.23	13.13	13.13	D7AFF7_GEOSK	KN400_3170	Ferredoxin, Rieske superfamily	1
596	2	2	42.35	15.29	15.29	D7AFF5_GEOSK	rpmA	50S ribosomal protein L27	1
597	2	2	11.57	7.851	7.851	D7AFC7_GEOSK	KN400_3140	Outer membrane lipoprotein carrier/sorting protein LolA	1
598	2	2	10.29	4.18	4.18	D7AEL9_GEOSK	rsmH	Ribosomal RNA small subunit methyltransferase H	1
599	2	2	15.67	8.209	8.209	D7AEC9_GEOSK	KN400_0350	Uncharacterized protein	1
600	2	2	18.9	5.118	5.118	D7AE53_GEOSK	hypB	Hydrogenase accessory protein HypB	1
601	2	2	18.9	18.9	18.9	D7AE09_GEOSK	cbiX	Sirohydrochlorin cobaltochelatase	2
602	2	2	16.36	16.36	16.36	D7ADJ2_GEOSK	KN400_0199	Cupin superfamily barrel domain protein	1
603	2	2	16.13	16.13	16.13	E1PTE3_GEOSK	pilA-C	Geopilin domain 2 protein	1
604	2	2	12.04	12.04	12.04	D7AMS9_GEOSK	rplX	50S ribosomal protein L24	1
605	2	2	11.32	11.32	11.32	D7AML9_GEOSK	KN400_2728	UPF0145 protein KN400_2728	1
606	2	2	23.19	23.19	23.19	D7AM24_GEOSK	atpC	ATP synthase epsilon chain	1
607	2	2	30.77	30.77	30.77	D7ALY7_GEOSK	KN400_0052	Uncharacterized protein	1
608	2	2	17.74	17.74	17.74	D7ALR0_GEOSK	KN400_2687	Uncharacterized protein	1
609	2	2	1.31	1.31	1.31	D7ALH1_GEOSK	ompC	Multicopper oxidase, manganese oxidase family	1
610	2	2	29.03	29.03	29.03	D7ALG2_GEOSK	KN400_2589	Uncharacterized protein	1
611	2	2	3.324	3.324	3.324	D7ALC6_GEOSK	cheA40H	Sensor histidine kinase CheA associated with MCPs of class 40H	1
612	2	2	13.79	13.79	13.79	D7ALB1_GEOSK	rpsT	30S ribosomal protein S20	2
613	2	2	4.93	4.93	4.93	D7AL42_GEOSK	KN400_2084	Metal-dependent phosphohydrolase, HDD domain-containing	1
614	2	2	8.889	8.889	8.889	D7AL28_GEOSK	KN400_2070	Uncharacterized protein	1
615	2	2	18.87	18.87	18.87	D7AKZ3_GEOSK	yajC	Preprotein translocase, YajC subunit	1
616	2	2	7.534	7.534	7.534	D7AKP6_GEOSK	KN400_2460	Lipoprotein cytochrome c, 1 heme-binding site	1
617	2	2	8.543	8.543	8.543	D7AKM9_GEOSK	KN400_2443	Lipoprotein, putative	1
618	2	2	4.237	4.237	4.237	D7AK44_GEOSK	lpdA-1	Dihydrolipoyl dehydrogenase	1
619	2	2	5.988	5.988	5.988	D7AJX3_GEOSK	lptA	Lipopolysaccharide ABC transporter, periplasmic protein LptA	1
620	2	2	12.77	12.77	12.77	D7AJV1_GEOSK	KN400_1893	Lipoprotein, putative	1
621	2	2	6.704	6.704	6.704	D7AJU3_GEOSK	vorC	2-oxoacid:ferredoxin oxidoreductase, gamma subunit	1
622	2	2	3.521	3.521	3.521	D7AJP3_GEOSK	argS	Arginine--tRNA ligase	1
623	2	2	4.4	4.4	4.4	D7AJE8_GEOSK	queE	7-carboxy-7-deazaguanine synthase	1
624	2	2	4.792	4.792	4.792	D7AJ81_GEOSK	fbp	Fructose-1,6-bisphosphatase class 1	1
625	2	2	19.48	19.48	19.48	D7AJ34_GEOSK	acp	Acyl carrier protein	1
626	2	2	12.71	12.71	12.71	D7AJ19_GEOSK	rbfA	Ribosome-binding factor A	1

627	2	2	22.22	22.22	22.22	D7AIZ3_GEOSK	KN400_1585	Uncharacterized protein	1
628	2	2	6.944	6.944	6.944	D7AIV6_GEOSK	pcm	Protein-L-isoaspartate methyltransferase	1
629	2	2	15.63	15.63	15.63	D7AIQ2_GEOSK	korD	2-oxoglutarate:ferredoxin oxidoreductase, ferredoxin subunit	2
630	2	2	6.939	6.939	6.939	D7AIP7_GEOSK	rlmB	23S rRNA (2'-methyltransferase	1
631	2	2	5.643	5.643	5.643	D7AI05_GEOSK	KN400_1198	Uncharacterized protein	1
632	2	2	13.33	13.33	13.33	D7AHM1_GEOSK	KN400_1064	Phasin superfamily protein	1
633	2	2	5.464	5.464	5.464	D7AHF7_GEOSK	KN400_1000	Uncharacterized protein	1
634	2	2	11.43	11.43	11.43	D7AHF4_GEOSK	KN400_0997	Uncharacterized protein	1
635	2	2	4.297	4.297	4.297	D7AHE7_GEOSK	fabI	Enoyl-[acyl-carrier-protein] reductase [NADH]	1
636	2	2	4.955	4.955	4.955	D7AGZ1_GEOSK	KN400_0832	Transporter, DUF21, CBS domain pair and CorC_HlyC domain-containing, putative	1
637	2	2	16.33	16.33	16.33	D7AGW4_GEOSK	rpmH	50S ribosomal protein L34	1
638	2	2	8.725	8.725	8.725	D7AGT0_GEOSK	KN400_0795	ABC transporter, periplasmic substrate-binding protein, MCE family	1
639	2	2	4.384	4.384	4.384	D7AG97_GEOSK	KN400_3330	Lipoprotein, putative	1
640	2	2	3.873	3.873	3.873	D7AFZ4_GEOSK	omcX	Cytochrome c, 12 heme-binding sites	1
641	2	2	4.762	4.762	4.762	D7AFX7_GEOSK	nadE	NH(3)-dependent NAD(+) synthetase	1
642	2	2	15.48	15.48	15.48	D7AFW6_GEOSK	KN400_0617	Uncharacterized protein	1
643	2	2	8.772	8.772	8.772	D7AFK7_GEOSK	KN400_3220	Thioredoxin-related protein disulfide reductase, putative	1
644	2	2	8.943	8.943	8.943	D7AFH0_GEOSK	KN400_3183	Response regulator, putative	1
645	2	2	11.73	11.73	11.73	D7AEZ8_GEOSK	KN400_0433	3-oxoacyl-(Acyl carrier protein) synthase-related protein	1
646	2	2	9.877	9.877	9.877	D7AEV3_GEOSK	msrA	Peptide methionine sulfoxide reductase MsrA	1
647	2	2	2.433	2.433	2.433	D7AEK6_GEOSK	ftsA	Cell division protein ftsA	1
648	2	2	4.676	4.676	4.676	D7AEK0_GEOSK	nfnB	NADH-dependent ferredoxin:NADP+ oxidoreductase, beta subunit	1
649	2	2	18.37	18.37	18.37	D7AE73_GEOSK	gspG	Type II secretion system major pseudopilin GspG	1
650	2	2	33.33	33.33	33.33	D7ADY0_GEOSK	KN400_2914	Uncharacterized protein	1
651	1.85	2	4.206	4.206	4.206	D7AIF5_GEOSK	ideR	Iron/manganese-dependent transcriptional regulator	1
652	1.85	2	19.63	19.63	19.63	D7AIA5_GEOSK	KN400_1298	RNA-binding protein	1
653	1.85	2	3.673	3.673	3.673	D7AHP9_GEOSK	KN400_1092	GAF domain protein, putative	1
654	1.85	2	19.74	19.74	19.74	D7AFG0_GEOSK	KN400_3173	Uncharacterized protein	1
655	1.85	2	8.718	8.718	8.718	D7AEP0_GEOSK	hisB	Imidazoleglycerol-phosphate dehydratase	1
656	1.82	2	8.974	8.974	8.974	D7ADG9_GEOSK	KN400_0176	Aerobic-type carbon monoxide dehydrogenase, small subunit-like protein	1
657	1.66	1.66	15.75	4.972	4.972	D7AEC2_GEOSK	gcvT	Aminomethyltransferase	1
658	1.66	1.66	8.609	5.96	5.96	D7AJ12_GEOSK	bioA	Adenosylmethionine-8-amino-7-oxononanoate aminotransferase	1

659	1.66	1.66	9.314	9.314	9.314	D7AFC4_GEOSK	cheC44H	Protein phosphoaspartate phosphatase CheC associated with MCPs of class 44H	1
660	1.52	1.52	9.091	2.674	2.674	D7AGY4_GEOSK	acnA	Aconitate hydratase 1	1
661	1.45	1.45	10.43	7.66	2.766	D7AEJ9_GEOSK	nfnA	NADH-dependent ferredoxin:NADP+ oxidoreductase, alpha subunit	1
662	1.43	1.43	19.42	4.796	4.796	D7AEP4_GEOSK	murA	UDP-N-acetylglucosamine 1-carboxyvinyltransferase	1
663	1.43	1.43	16.21	11.07	11.07	D7AEN7_GEOSK	hisF	Imidazole glycerol phosphate synthase subunit HisF	1
664	1.37	1.37	28.35	18.11	5.906	D7AF55_GEOSK	yfiO	Outer membrane protein assembly factor BamD	1
665	1.36	1.36	11.02	3.305	2.203	D7AES3_GEOSK	mrcA	Peptidoglycan transglycosylase and transpeptidase MrcA	1
666	1.35	1.35	21.11	10	10	D7AE07_GEOSK	KN400_2941	Uncharacterized protein	1
667	1.22	1.22	8.209	6.468	6.468	D7AF48_GEOSK	KN400_0483	Efflux pump, RND family, membrane fusion protein	1
668	1.09	1.09	10.11	4.632	4.632	D7AHP1_GEOSK	KN400_1084	Aldehyde dehydrogenase	1
669	1.06	1.06	8.479	1.48	1.48	D7AJV5_GEOSK	nrdJ	Ribonucleoside diphosphate reductase, adenosylcobalamin-dependent	1
670	0.97	0.97	7.838	7.568	7.568	D7AET9_GEOSK	mobA-1	Molybdopterin nucleotidyltransferase and molybdopterin-guanine dinucleotide biosynthesis protein MobB	1
671	0.94	0.94	15.12	9.879	4.032	D7ALS5_GEOSK	glpK	Glycerol kinase	1
672	0.91	0.91	2.381	2.381	2.381	D7AKG3_GEOSK	KN400_1992	Uncharacterized protein	1
673	0.82	0.82	29.13	29.13	29.13	D7ALL8_GEOSK	moaE	Molybdopterin synthase, large subunit	2
674	0.74	0.74	6.832	2.795	2.795	D7AIS2_GEOSK	ribF	Riboflavin kinase and FAD synthetase	1
675	0.62	0.62	15.3	5.97	5.97	D7AJR2_GEOSK	scpA	Chromosome segregation and condensation protein ScpA	1
676	0.61	0.61	2.901	1.527	1.527	D7AHA1_GEOSK	KN400_0944	REVERSED Sensor histidine kinase, HAMP domain-containing	1
677	0.56	0.56	7.857	7.857	7.857	D7AGU0_GEOSK	KN400_0805	Uncharacterized protein	1
678	0.52	0.52	33.69	15.96	15.96	D7AKH9_GEOSK	KN400_2008	Periplasmic polysaccharide biosynthesis/export protein	2
679	0.49	0.49	16.44	16.44	16.44	D7ALW4_GEOSK	KN400_0029	Biopolymer transport membrane proton channel, TolQ-related	2
680	0.47	0.47	13.78	10.6	6.007	D7AFX6_GEOSK	KN400_0627	Nitrilase/amidohydrolase superfamily protein, class 8	1
681	0.45	0.45	21.23	12.57	8.939	D7AMI4_GEOSK	rmlB	dTDP-glucose 4,6-dehydratase	1
682	0.44	0.45	9.677	9.677	9.677	D7AHX3_GEOSK	KN400_1166	Fructose-1,6-bisphosphatase class 1	1
683	0.44	0.44	6.92	6.027	6.027	D7AEC4_GEOSK	gcv	Probable glycine dehydrogenase [decarboxylating] subunit 1	1
684	0.42	0.42	16.73	12.35	12.35	D7AK62_GEOSK	KN400_2412	Metal-dependent hydrolase, beta-lactamase superfamily	2
685	0.4	0.4	1.609	1.609	1.609	D7AE14_GEOSK	thiC-2	REVERSED Phosphomethylpyrimidine synthase	1
686	0.37	0.37	3.497	3.263	3.263	D7AEA7_GEOSK	KN400_0328	REVERSED Peptidoglycan-binding outer membrane protein,	1

687	0.36	0.36	20.85	11.06	4.255	D7AEL5_GEOSK	murF	UDP-N-acetylmuramoyl-tripeptide--D-alanyl-D-alanine ligase	1
688	0.36	0.36	11.36	11.36	11.36	D7ALB3_GEOSK	lptE	Lipopolysaccharide biogenesis outer membrane chaperone lipoprotein LptE, putative	1
689	0.35	0.35	14.38	7.516	7.516	D7AGQ5_GEOSK	KN400_0770	Uncharacterized protein	1
690	0.35	0.35	3.571	3.571	3.571	D7ALE9_GEOSK	wbjB	UDP-N-acetylglucosamine 4,6-dehydratase and UDP-2-acetamido-2,6-dideoxy-alpha-D-xylo-4-hexulose 5-epimerase	1
691	0.31	0.31	13.83	2.128	2.128	D7AHB2_GEOSK	KN400_0955	Uncharacterized protein	1
691	0	0.31	1.163	1.163	1.163	D7ALU4_GEOSK	KN400_0009	Response receiver sensor histidine kinase, PAS domain-containing	1
691	0	0.31	7.895	7.895	7.895	D7AJJ7_GEOSK	xseB	Exodeoxyribonuclease 7 small subunit	1
692	0.27	0.27	10.67	3.698	3.698	D7AI09_GEOSK	KN400_1202	Outer membrane channel, putative	1
693	0.26	0.26	8.631	8.631	8.631	D7ALE5_GEOSK	uge	UDP-galacturonate 4-epimerase	1
694	0.24	0.24	9.74	4.762	4.762	D7AK84_GEOSK	KN400_2434	Magnesium-dependent deoxyribonuclease, TatD family, and radical SAM domain iron-sulfur oxidoreductase	1
695	0.2	0.2	14.04	7.234	7.234	D7ALX7_GEOSK	KN400_0042	Peroxiredoxin-like 2 family protein, selenocysteine-containing	1
696	0.19	0.19	7.22	7.22	7.22	D7AI01_GEOSK	KN400_1194	Response regulator, GspIIEN domain-containing	1
697	0.17	0.17	10.12	4.444	4.444	D7AE51_GEOSK	KN400_0272	Sensor protein, DUF3365, HAMP and PAS domain-containing, heme-binding	1
698	0.16	0.16	17.9	4.859	2.813	D7AEM8_GEOSK	rlmL	23S rRNA (2-N-methyl-G2445)-methyltransferase, putative	1
699	0.16	0.16	5.891	2.946	2.946	D7AG11_GEOSK	shc-1	Squalene cyclase	1
700	0.16	0.16	15.23	15.23	15.23	D7AEU3_GEOSK	KN400_3090	PAS domain protein	1
701	0.15	0.15	13.64	5.024	5.024	D7AK34_GEOSK	aceF	Pyruvate dehydrogenase complex, E2 protein, dihydrolipoamide acetyltransferase	2
702	0.15	0.15	17.35	17.35	17.35	D7ALY9_GEOSK	KN400_0054	Helix-turn-helix transcriptional regulator with cupin domain	1
703	0.14	0.14	26.11	11.33	11.33	D7AJ26_GEOSK	yrdC	tRNA (N6-threonylcarbamyl-A37) modification ATPase	1
704	0.13	0.13	15.38	15.38	15.38	E1PTG5_GEOSK	KN400_3465	Uncharacterized protein	1
705	0.13	0.13	17.5	17.5	17.5	D7AEF0_GEOSK	cheY64H-1	Response receiver CheY associated with MCPs of classes 40H and 40+24H	1
706	0.13	0.13	5.298	5.298	5.298	D7AEU3_GEOSK	KN400_3090	REVERSED PAS domain protein	1
707	0.12	0.12	11.95	2.789	2.789	D7AGB8_GEOSK	KN400_3351	REVERSED Polar amino acid/opine ABC transporter, periplasmic amino acid-binding protein	1
708	0.12	0.12	15.79	8.187	8.187	D7AE12_GEOSK	KN400_2946	REVERSED Uncharacterized protein	1
709	0.09	0.09	85.51	44.93	33.33	D7AF86_GEOSK	KN400_0521	Uncharacterized protein	1
710	0.08	0.08	12.47	3.95	3.95	D7AHE1_GEOSK	gnfM	Nitrogen fixation master sigma-54-dependent transcriptional response regulator	1

711	0.08	0.08	23.16	12.63	12.63	D7AMJ9_GEOSK	trpG	Anthranilate synthase, glutamine amidotransferase subunit	1
712	0.08	0.08	6.78	6.78	6.78	D7ADP7_GEOSK	dksA	RNA polymerase-binding transcription factor DksA	1

Note: N is the rank of the protein relative to the other identified proteins in the list. Unused is a measure of confidence reflecting the total amount of peptides identified unique to the given protein. Total, represents a measure of confidence reflecting the total amount of peptide identified (including those not unique) to the given protein. %cov is the sequence coverage given as the percentage of amino acid sequences in each protein sequence identified with a 50% confidence level (%cov(50)) and with a 95% confidence level (%cov(95)). Gene ID represents the species specific gene identifier for the protein, Gene name indicates the name given to the protein, Description provides a description of the identified protein and peptides 95% represents the number of peptide sequences identified for the protein with a 95% confidence.

Appendix D – BLAST result for putative periplasmic CbiK superfamily protein

Top 5 BLAST results for Putative periplasmic CbiK superfamily protein SO1190

Description	Max score	Total score	Query cover	E value	Identity	Accession
nickel transporter (*Shewanella decolorationis*)	533	533	100%	0	96%	WP_023268286.1
nickel transport complex transmembrane protein NikM (*Shewanella baltica* BA175)	479	479	100%	2.00E-168	88%	YP_006019696.1
nickel transport complex transmembrane protein NikM (*Shewanella putrefaciens*)	475	475	100%	9.00E-167	83%	YP_006010859.1
nickel transporter (*Shewanella putrefaciens*)	474	474	100%	2.00E-166	83%	WP_028761462.1
nickel transporter (*Shewanella algae*)	351	351	93%	6.00E-118	64%	WP_025010276.1

Appendix E – BLAST result for the gene encoding OmaC of *G. sulfurreducens* PCA

Entry	Gene identifier	Description	score	Identity	E value
Q749K4	GSU2732	Cytochrome c (*Geobacter sulfurreducens* strain ATCC 51573 / DSM 12127 / PCA)	1,299	100.00%	11E-180
D7ALP7	KN400_2674	Cytochrome c, 8 heme-binding sites (*Geobacter sulfurreducens* strain DL-1 / KN400)	1,299	100.00%	11E-180
B5EB83	oma	Cytochrome c (*Geobacter bemidjiensis* strain Bem / ATCC BAA-1014 / DSM 16622)	972	72.00%	540E-132
C6E1L4	GM21_0866	Uncharacterized protein (*Geobacter* sp. strain M21)	959	72.00%	51E-129
A5GB57	Gura_0988	Uncharacterized protein (*Geobacter uraniireducens* strain Rf4)	930	70.00%	1.4E-123

Appendix F – Replicate chronoamperometry data for *Shewanella oneidensis* MR-1 anodic biofilms

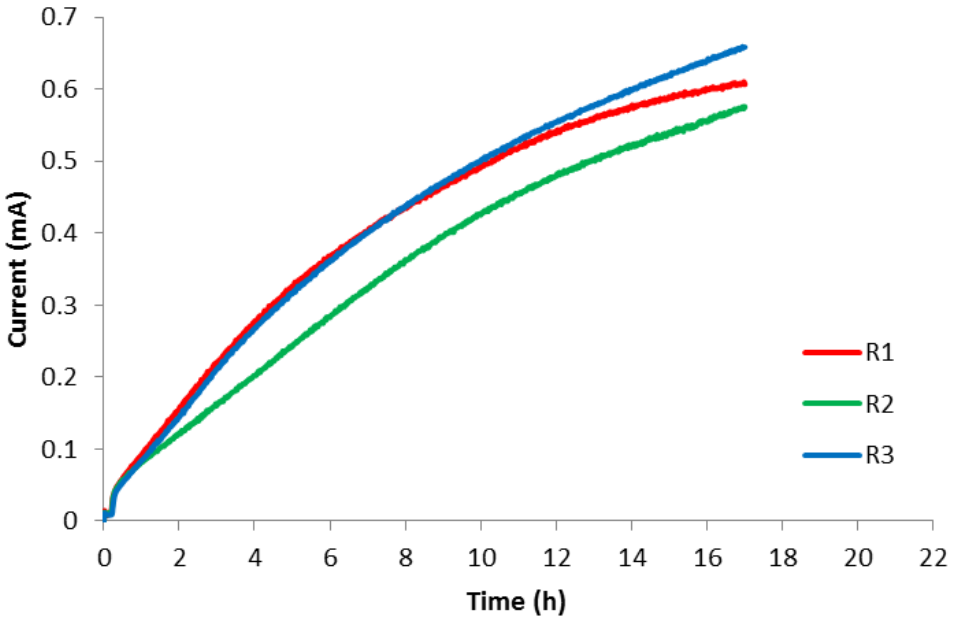

Figure A1 Replicate chronoamperometry profiles for anodic biofilms of *Shewanella oneidensis* MR-1 grown at +0.5 V (Ag/AgCl) used for proteomic analysis

.

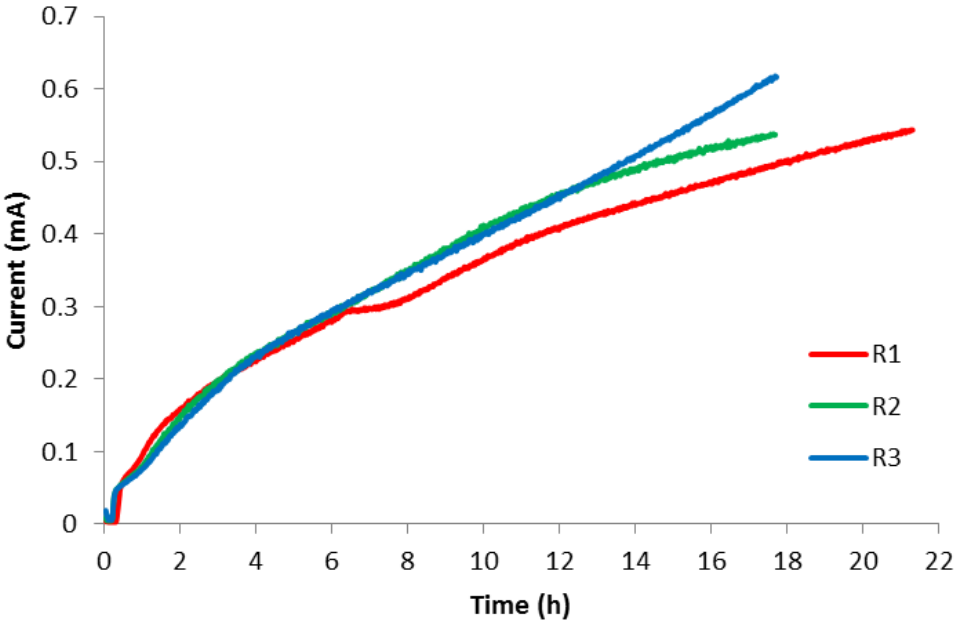

Figure A2 Replicate chronoamperometry profiles for anodic biofilms of *Shewanella oneidensis* MR-1 grown at +0.5 V (Ag/AgCl) used for electrochemical analysis.

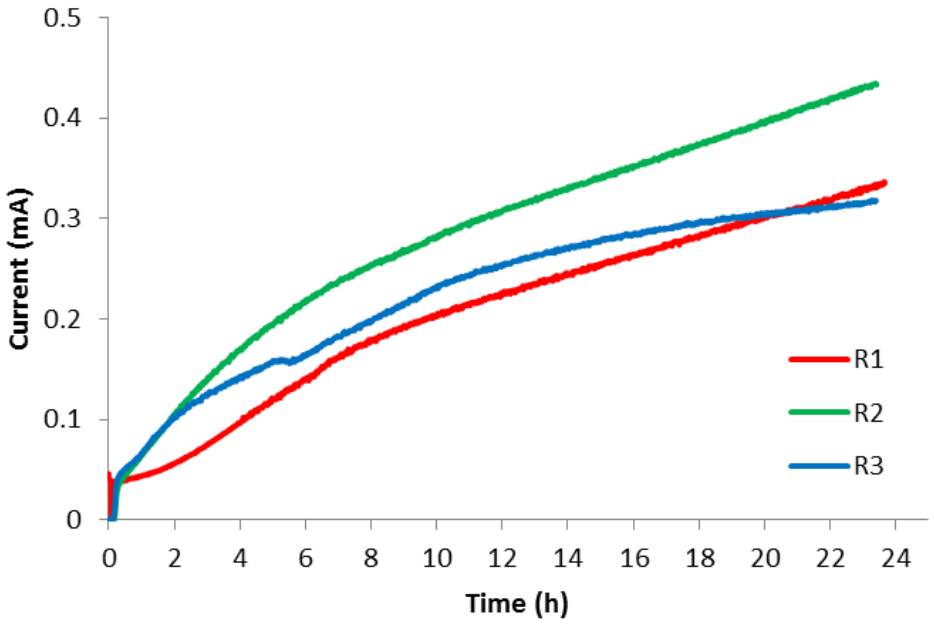

Figure A3 Replicate chronoamperometry profiles for anodic biofilms of *Shewanella oneidensis* MR-1 grown at +0.0 V (Ag/AgCl) used for proteomic analysis.

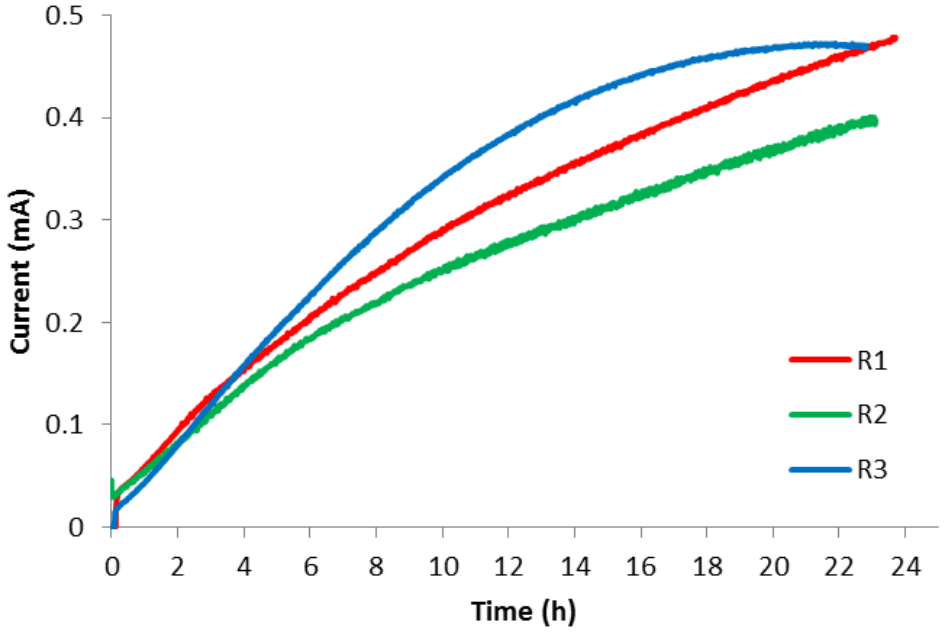

Figure A4 Replicate chronoamperometry profiles for anodic biofilms of *Shewanella oneidensis* MR-1 grown at +0.0 V (Ag/AgCl) used for electrochemical analysis.

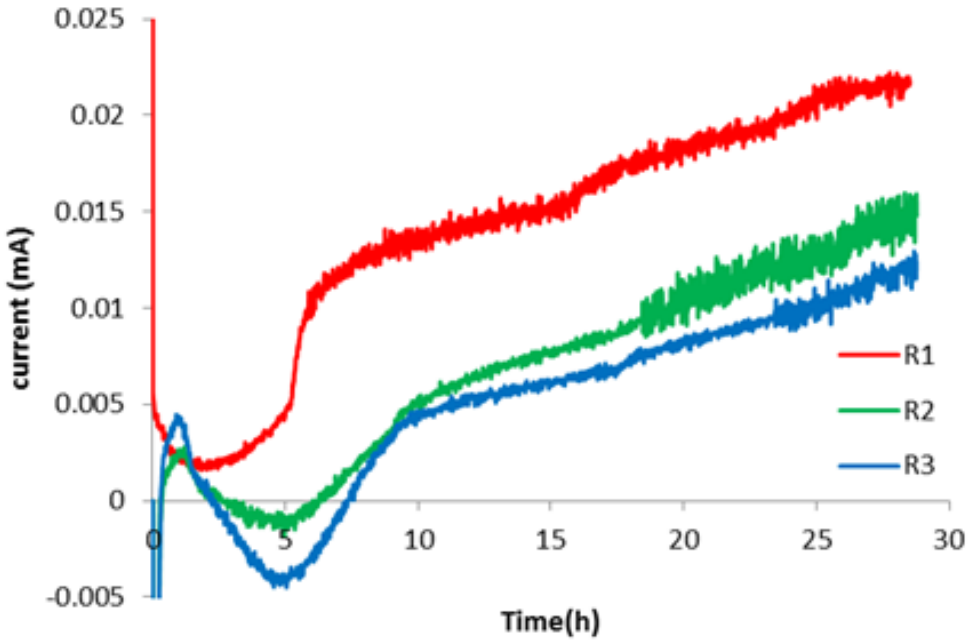

Figure A5 Replicate chronoamperometry profiles for anodic biofilms of *Shewanella oneidensis* MR-1 grown at -0.4 V (Ag/AgCl) used for proteomic analysis.

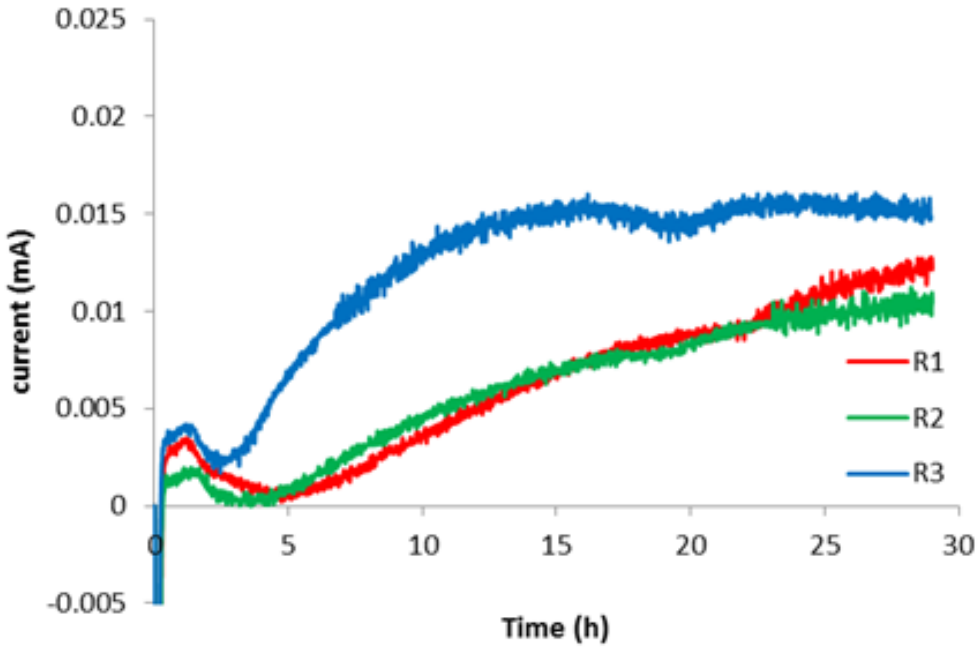

Figure A6 Replicate chronoamperometry profiles for anodic biofilms of *Shewanella oneidensis* MR-1 grown at -0.4 V (Ag/AgCl) used for electrochemical analysis.

Appendix G – Replicate turnover cyclic voltammetry data for *Shewanella oneidensis* MR-1 anodic biofilms

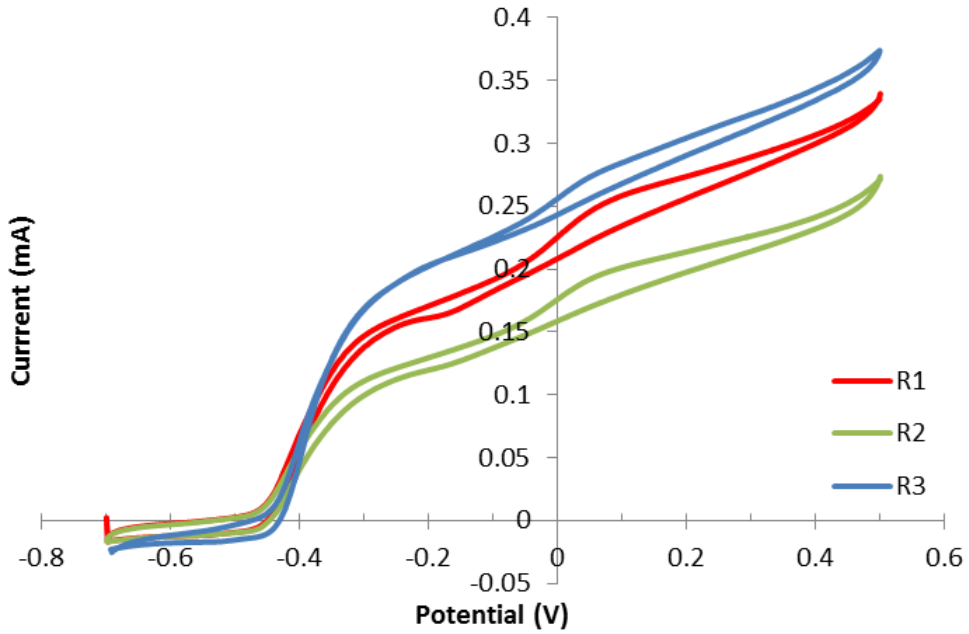

Figure A7 Replicate turnover cyclic voltammetry profiles for anodic biofilms of *Shewanella oneidensis* MR-1 grown at +0.5 V (Ag/AgCl) recordes using a scan rate of $2mVs^{-1}$.

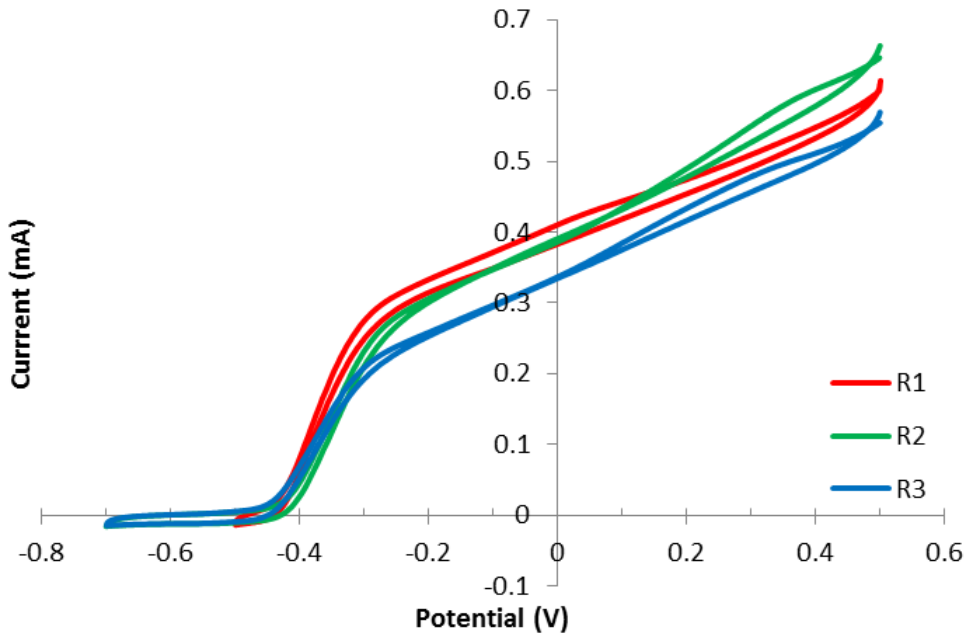

Figure A8 Replicate turnover cyclic voltammetry profiles for anodic biofilms of *Shewanella oneidensis* MR-1 grown at +0.0 V (Ag/AgCl) recordes using a scan rate of $2mVs^{-1}$.

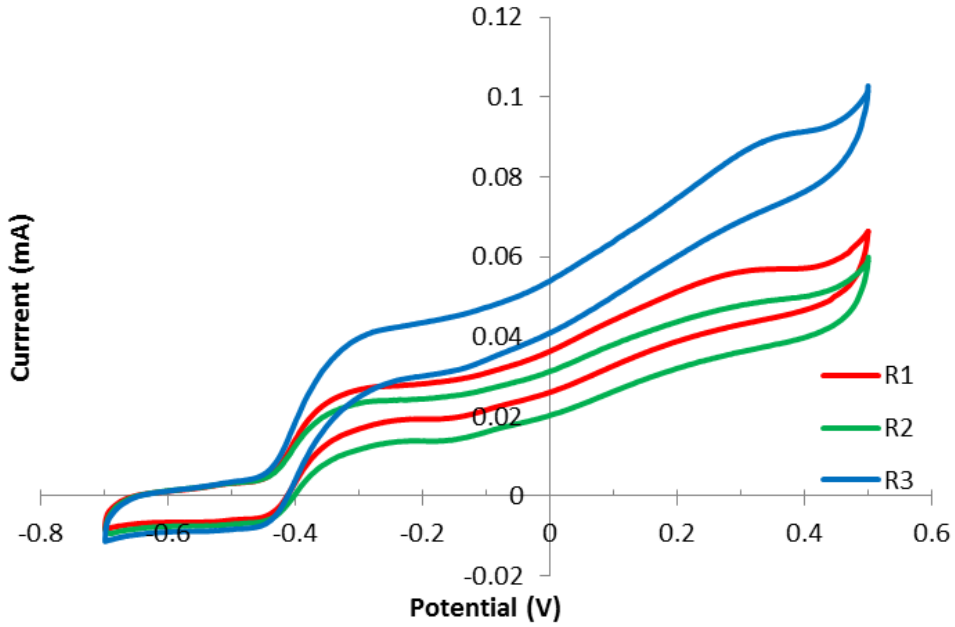

Figure A9 Replicate turnover cyclic voltammetry profiles for anodic biofilms of *Shewanella oneidensis* MR-1 grown at -0.4 V (Ag/AgCl) recordes using a scan rate of $2mVs^{-1}$.

Appendix H – Replicate chronoamperometry data for *Geobacter sulfurreducens* DL-1 anodic biofilms

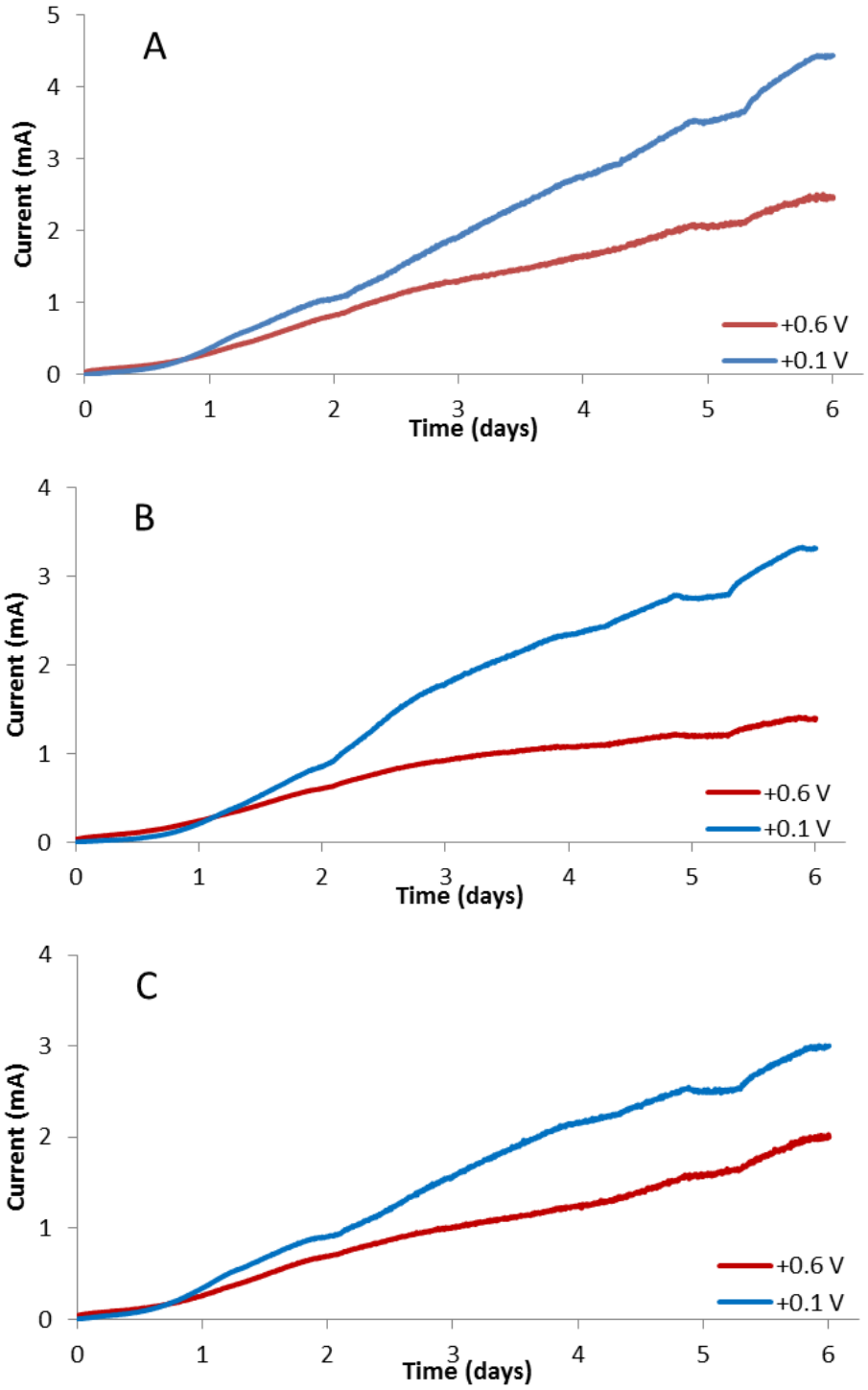

Figure A10 Chronoamperometry profiles of replicate expermients (A, B & C) for anodic biofilms of *Geobacter sulfurreducens* grown at either +0.1 V or +0.6 V (Ag/AgCl) used for proteomic analysis.

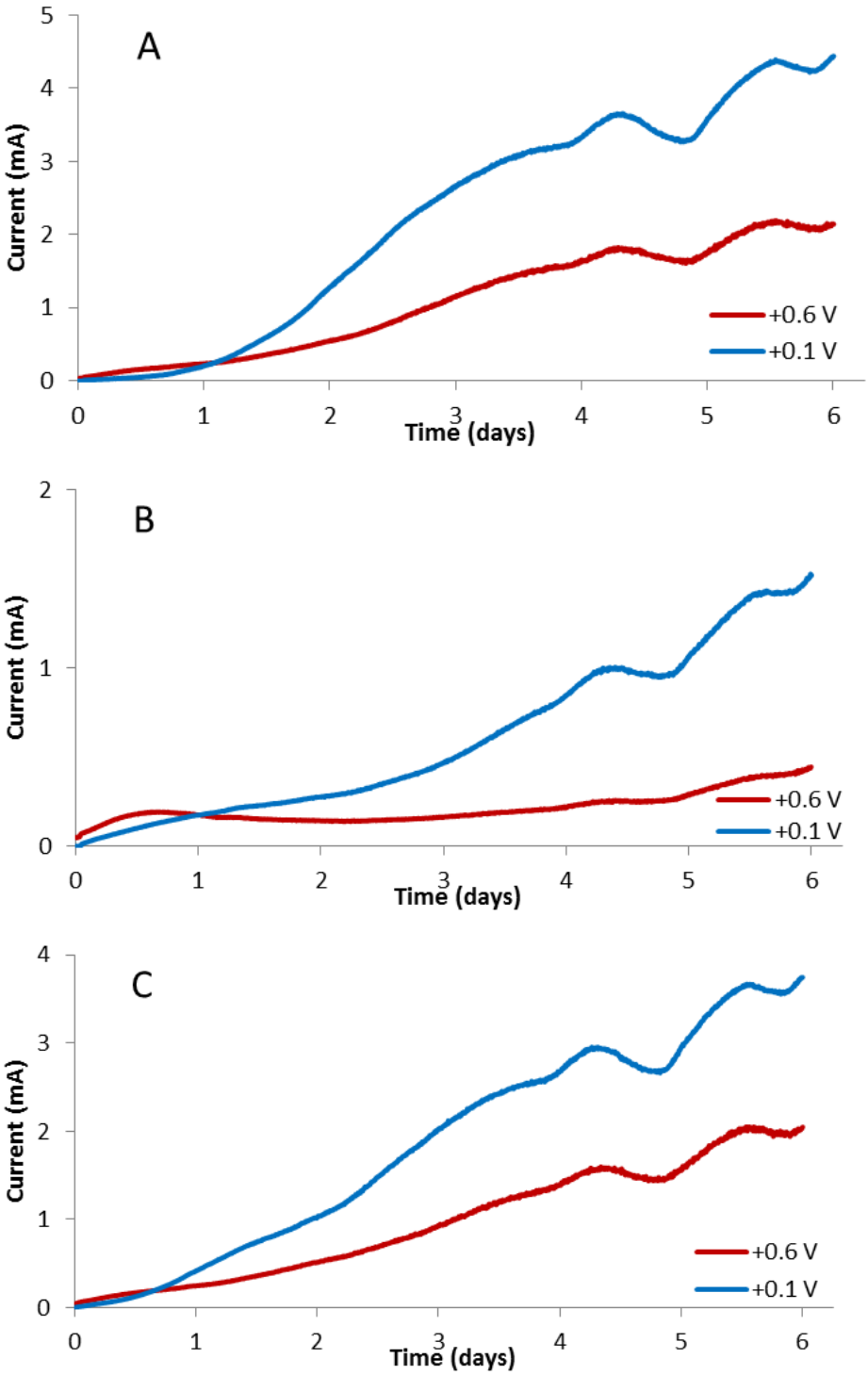

Figure A11 Chronoamperometry profiles of replicate expermients (A, B & C) for anodic biofilms of *Geobacter sulfurreducens* grown at either +0.1 V or +0.6 V (Ag/AgCl) used for electrochemical analysis.

Appendix J – Replicate turnover cyclic voltammetry data for *Geobacter sulfurreducens* DL-1 anodic biofilms

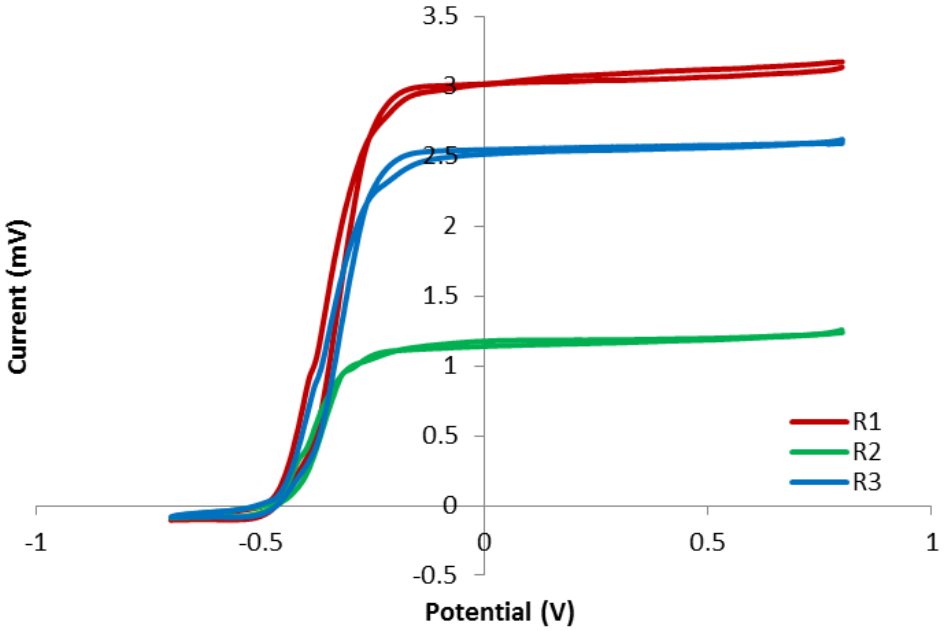

A12 Replicate turnover cyclic voltammetry profiles for anodic biofilms of *Geobacter sulfurreducens* DL-1 grown at +0.1 V (Ag/AgCl) recorded using a scan rate of 1mVs^{-1}.

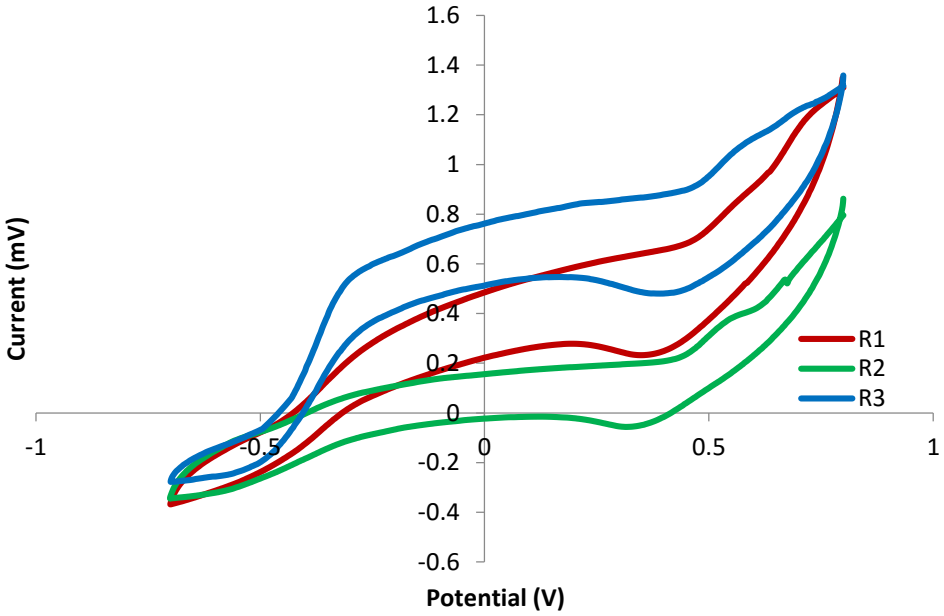

Figure A13 Replicate turnover cyclic voltammetry profiles for anodic biofilms of *Geobacter sulfurreducens* DL-1 grown at +0.6 V (Ag/AgCl) recorded using a scan rate of 1mVs^{-1}.

Appendix K – Replicate non-turnover cyclic voltammetry data for *Geobacter sulfurreducens* DL-1 anodic biofilms

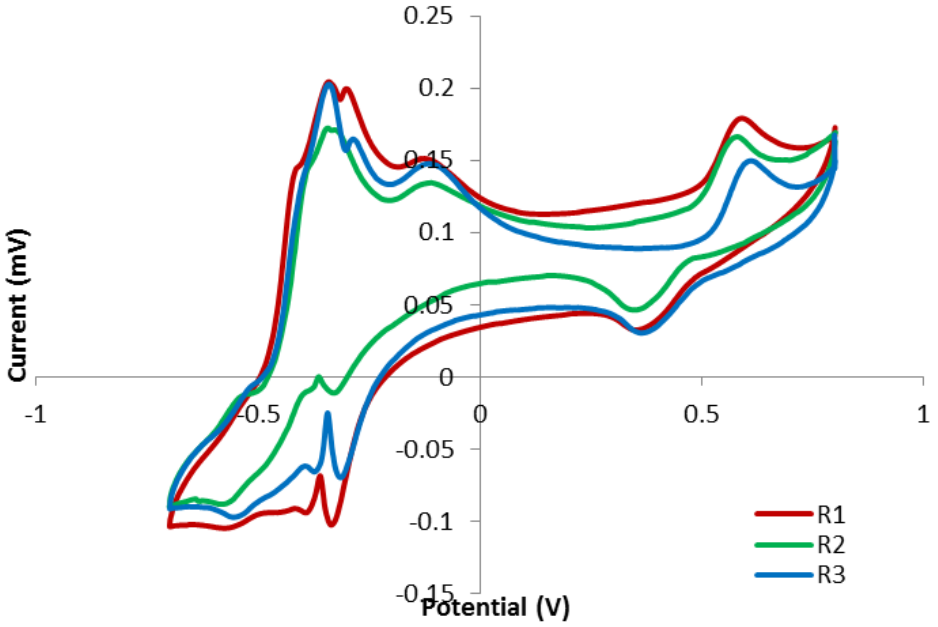

Figure A14 Replicate non-turnover cyclic voltammetry profiles for anodic biofilms of *Geobacter sulfurreducens* DL-1 grown at +0.1 V (Ag/AgCl) recorded using a scan rate of 1mVs^{-1}.

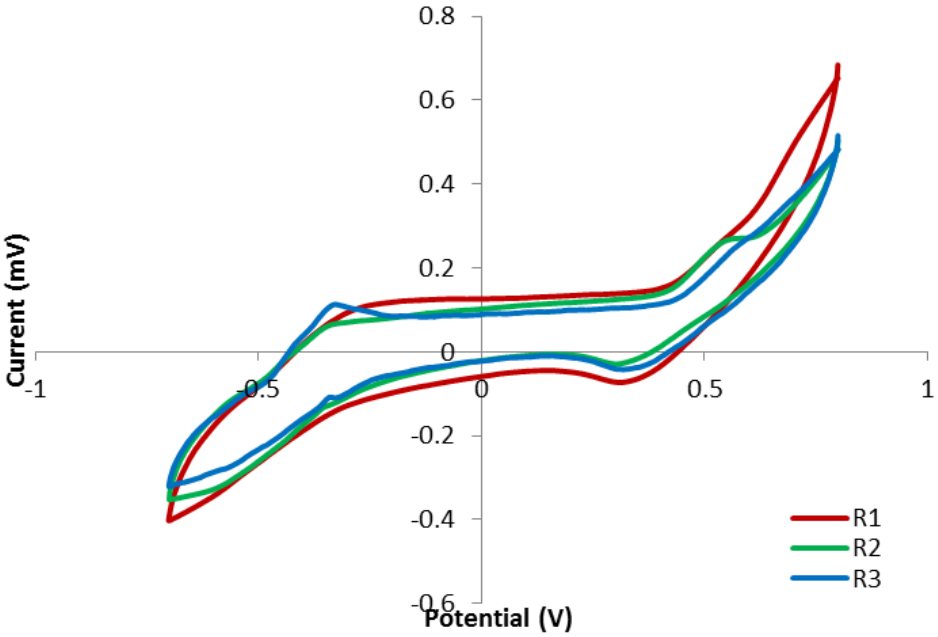

Figure A15 Replicate non-turnover cyclic voltammetry profiles for anodic biofilms of *Geobacter sulfurreducens* DL-1 grown at +0.6 V (Ag/AgCl) recorded using a scan rate of 1mVs^{-1}.